Impact of street trees on urban microclimate and human thermal stress : effect of heatwaves and droughts

Julien Thierry

COLLEGE DOCTORAL PAYS DE LA LOIRE
VEGETAL, ANIMAL, ALIMENT, MER, ENVIRONNEMENT

L'INSTITUT agro Rennes Angers

THESE DE DOCTORAT DE

L'INSTITUT NATIONAL D'ENSEIGNEMENT SUPERIEUR POUR L'AGRICULTURE, L'ALIMENTATION ET L'ENVIRONNEMENT

ECOLE DOCTORALE N° 642
Ecole doctorale Végétal, Animal, Aliment, Mer, Environnement
Spécialité : « Sciences de la Terre et de l'Environnement »

Par
Julien THIERRY

Impact des arbres d'alignement sur le microclimat et le stress thermique humain en ville : effet des vagues de chaleur et des sécheresses

Impact of street trees on urban microclimate and human thermal stress: effect of heatwaves and droughts

Thèse présentée et soutenue à Angers, le 22 mai 2024
Unité de recherche : UP Environnement Physique de la plante Horticole (EPHor)
Thèse N° : D-108_2024-5

Rapporteurs avant soutenance :

Emmanuel BOZONNET	Maître de Conférences HDR, Université de La Rochelle
Thierry AMEGLIO	Directeur de recherche, INRAE

Composition du Jury :

Présidente :	Zahra THOMAS	Professeure, Institut Agro Rennes-Angers
Examinateur.rice.s :	Aude LEMONSU	Directrice de Recherche, CNRM
	Martin SEIDL	Ingénieur de Recherche HDR, École des Ponts ParisTech
Co-dir. de thèse :	Pierre-Emmanuel BOURNET	Professeur, Institut Agro Rennes-Angers
Co-dir. de thèse :	Fabrice RODRIGUEZ	Chercheur IDTPE HDR, Université Gustave Eiffel
Encadrante de thèse :	Sophie HERPIN	Maître de Conférences, Institut Agro Rennes-Angers

Invité.e.s

Encadrante de thèse :	Marie GANTOIS	Ingénieure, Ville de Paris

Titre : Impact des arbres d'alignement sur le microclimat et le stress thermique humain en ville : effet des vagues de chaleur et des sécheresses

Mots clés : Ombrage, Transpiration, Bilan hydrique, Bilan radiatif, Essences d'arbre

Résumé : Les surchauffes urbaines, additionnées aux vagues de chaleur dont la fréquence et l'intensité augmentent en raison du changement climatique, exposent les citadins à un stress thermique croissant. Les arbres d'alignement peuvent permettre d'atténuer ces surchauffes grâce à l'ombrage et la transpiration, deux phénomènes qui peuvent dépendre de leurs caractéristiques morphologiques et physiologiques. En parallèle, les périodes de sécheresse se multiplient et la capacité des arbres d'alignement à croître tout en maintenant des services climatiques importants dans des conditions chaudes et sèches est en jeu. Pour améliorer la compréhension des facteurs influant sur les bénéfices climatiques des arbres, une démarche de recherche basée sur la mesure des interactions le long du continuum sol-arbre-atmosphère dans deux dispositifs expérimentaux complémentaires est proposée. D'un côté, une rue canyon à échelle 1/5ème partiellement végétalisée avec des jeunes pommiers d'ornement (*Malus Coccinella*® 'Courtarou') en pot et irrigués située à Angers (France) a été instrumentée pour quantifier les effets sur le microclimat d'arbres soumis à différentes disponibilités en eau. De l'autre, une campagne de mesures in-situ du microclimat dans et autour de la couronne de 36 arbres d'alignement adultes de 9 essences différentes répartis sur 5 sites dans Paris (France) a été menée. L'analyse croisée de ces deux dispositifs fournit une vue d'ensemble des sources de variabilité des bénéfices climatiques et propose aux aménageurs une meilleure compréhension des liens entre la résistance à la sécheresse des arbres d'alignement et leur pouvoir de réduction du stress thermique humain.

Title: Impact of street trees on urban microclimate and human thermal stress: effect of heatwaves and droughts

Keywords: Radiation interception, Tree transpiration, Water balance, Water restriction, Tree species

Abstract: Cities are characterized by an urban overheating which, combined to more frequent and intense heatwaves caused by climate change, expose the city dwellers to an increasing human thermal stress. Street trees may partially mitigate overheating by means of cast shadows and transpiration, two processes which may depend on their morphological and physiological characteristics. At the same time, periods of severe water shortage are multiplying and the ability of street trees to thrive and maintain significant cooling benefits under heat and drought conditions is crucial. In order to improve the understanding of the factors influencing tree climatic benefits, a methodology based on the monitoring of the interactions along the soil-tree-atmosphere continuum in two complementary experimental facilities was developed. On the one hand, a 1/5 scale canyon street, partially planted with young potted drip-irrigated ornamental apple trees (*Malus Coccinella*® 'Courtarou') located in Angers, France was monitored to quantify the effect of street trees experiencing different water supplies on the microclimate. On the other hand, an in-situ monitoring of the microclimate inside and outside the canopy for 36 mature street trees from 9 different tree species located in 5 sites in Paris, France, was performed. On the basis of a detailed cross-analysis of these two experimental facilities, an integrated assessment of the street trees climatic benefits was proposed to explore the sources of variability of the climatic benefits provided by trees and help stakeholders understand the relationship between drought resistance and human thermal stress mitigation for different tree species.

Remerciements

On s'imagine souvent la thèse comme un exercice assez individuel. Pour ce qui me concerne, j'aurais plutôt tendance à la décrire comme un sport d'équipe car le travail présenté dans ce manuscrit n'aurait en aucun cas pu voir le jour sans l'aide plus ou moins directe de nombreuses personnes que j'aimerais ici remercier chaleureusement.

Mais tout d'abord, quelques rappels concernant la genèse du projet. J'ai été recruté début 2020 par Pierre-Emmanuel Bournet et Sophie Herpin (UP EPHor / Institut Agro Rennes-Angers) rapidement rejoints par Fabrice Rodriguez (LEE / Université Gustave Eiffel) pour étudier le modèle de rue canyon à échelle réduite décrit dans ce manuscrit. Cette expérimentation faisait déjà l'objet d'une thèse en cours, menée par Souleymane Mballo, dont l'objectif était de quantifier et modéliser numériquement les bénéfices climatiques d'arbres d'alignement en confort hydrique. L'objectif de mon projet était de venir adapter cette étude à des arbres soumis à une restriction hydrique. Lors de mon recrutement, ce projet de thèse n'était pas encore financé, c'est pourquoi nous avons candidaté à l'appel à projet lancé courant mars 2020 par la Ville de Paris visant à établir des conventions de recherche Cifre entre ses différentes directions et des laboratoires de recherche. Nous sommes alors entrés en contact avec la Division Expertises Sol et Végétal (DESV / STVA / DEVE) de la Ville de Paris par l'intermédiaire de Mathilde Renard, en charge de cette division, Malorie Clair et Guillaume Debord. La DESV menait à cette époque, depuis déjà deux ans, l'étude Arbres et Climat, également décrite dans ce manuscrit, visant à étudier la pérennité des services climatiques rendus par les arbres dans un contexte de changement climatique. Il est vite apparu que des liens forts existaient entre cette étude et le projet de rue canyon à échelle réduite de l'Institut Agro Rennes-Angers. Le présent projet de thèse a donc été adapté pour inclure ces deux études et s'appuyer sur leur complémentarité pour répondre aux questionnements scientifiques soulevés ici. Accepté par la Ville de Paris à l'automne 2020 puis par l'ANRT, qui gère les conventions Cifre, ce projet a donc pu démarrer début mars 2021 et s'est déroulé sereinement grâce à l'implication de toutes les personnes citées jusqu'ici auxquelles il nous faut ajouter Marie Gantois et Christelle Angeniol qui ont respectivement pris la suite des fonctions de Mathilde Renard et Malorie Clair fin 2021/début 2022.

Vous l'aurez donc compris, mes remerciements les plus sincères s'adressent donc en premier lieu à Pierre-Emmanuel Bournet et Fabrice Rodriguez qui ont co-dirigé cette thèse, Sophie Herpin qui l'a encadrée scientifiquement et techniquement, Mathilde Renard et Marie Gantois qui l'ont supervisée pour le compte de la DESV. Leur écoute, leur disponibilité sans faille, leurs commentaires et conseils toujours constructifs, leur soutien et leur bienveillance m'ont permis de travailler dans une ambiance sereine et motivante.

De plus, les deux expérimentations sur lesquelles repose ce projet ont bénéficié du travail assidu de nombreuses personnes.

Pour la rue canyon d'Angers, je pense d'abord à Souleymane Mballo dont le travail a permis de préparer idéalement mes campagnes de mesure, Dominique Lemesle et Lydia Brialix qui ont porté l'installation et la maintenance de l'ensemble du dispositif, Sabine Demotes-Mainard et Dorine Canonne qui ont grandement contribué à la réflexion, à l'acquisition des

données et aux analyses mais aussi Patrice Cannavo et Marc Saudreau pour leur appui scientifique ainsi que Yvette Barraud-Roussel et les membres de l'IRHS qui ont largement contribué aux mesures : Camille Lebras, Lydie Ledroit, Bénédicte Dubuc, Denis Cesbron, Maxime Brindeau. Le personnel de la plateforme PHENOTIC a également fourni un appui technique nécessaire au bon fonctionnement de l'installation. De plus, Loli Maturana et Rachel Levi, dans le cadre de leur stage de M1 ont toutes deux largement contribué aux campagnes de mesures menées au cours des été 2021 et 2022 et leur travail a directement servi à la présentation de premiers résultats dans le cadre d'un congrès international ainsi qu'à la rédaction d'un article scientifique soumis dans une revue à comité de lecture. Travailler avec vous tou.te.s fut un réel plaisir et pour tout cela, je vous adresse mes plus chaleureux remerciements.

Du côté de l'étude Arbres et Climat, je tiens à remercier vivement Malorie Clair, Guillaume Debord et Christelle Angeniol qui ont largement participé à l'étude tant dans sa mise au point et dans sa gestion que dans les réflexions, Guillaume s'étant également beaucoup investi pour les opérations de montage, maintenance et démontage des capteurs en collaboration avec le personnel du SAB de la Ville de Paris. Jéromine Grandjean et Virginie Comtesse ont également apporté leur pierre à l'édifice en se rendant disponible de longues heures lors d'une campagne de mesures menée sur l'avenue de Flandre en juin 2021. Travailler avec vous tou.te.s fut un grand plaisir et je tiens à vous remercier pour votre aide précieuse.

Ce projet a également profité de nombreux échanges éminemment intéressants avec de nombreuses personnes. Je pense en premier lieu aux membres de mon Comité de Suivi de Thèse que je remercie grandement pour leur temps et leurs conseils : Katia Chancibault, Hervé Cochard, Martin Hendel et Marc Saudreau. Je pense également aux nombreuses personnes ayant participé aux conseils scientifiques annuels dédiés à l'étude Arbres et Climat et qui, de par leurs avis et conseils, ont permis de faire murir les réflexions et analyses liées à cette étude. Enfin, je pense aux membres du jury de thèse qui ont accepté d'évaluer mon travail à travers le présent manuscrit ainsi qu'au cours de ma soutenance le 22 mai 2024 : Emmanuel Bozonnet et Thierry Améglio en tant que rapporteurs ; Zahra Thomas, Aude Lemonsu et Martin Seidl en tant qu'examinateur.rice.s. A tou.te.s, je vous adresse un grand merci.

Je souhaite remercier également les différents organismes ayant contribué au financement de ce projet : l'ANRT via la convention Cifre dont j'ai bénéficié, la Ville de Paris, mon employeur, la région Pays de la Loire, Angers Loire Métropole et le Fond Européen de Développement Régional via le programme régional "Objectif Végétal, Recherche, Formation et Innovation en Pays de la Loire" ainsi que l'IRSTV qui a pris en charge une partie des frais liés à ma participation au colloque ICUC11 et m'a permis de terminer sereinement cette thèse en m'embauchant pour deux mois au cours du printemps 2024.

Je souhaite également remercier Christine Durand de l'UP EPHor ainsi que les membres de la DESV et du STVA pour leur appui concernant les différentes démarches administratives liées à la thèse. Aussi, je souhaite remercier Etienne Chantoiseau et Pierre-Emmanuel Bournet qui m'ont accordé leur confiance et mon permis d'assurer au total une cinquantaine d'heures de travaux dirigés grâce auxquels j'ai pu découvrir l'enseignement.

Pour mener à bien cette thèse, j'ai eu la chance d'évoluer dans une ambiance sereine et chaleureuse à Angers comme à Paris que les collègues de l'unité EPHor et de la DESV ont grandement contribué à créer. Je souhaite les remercier tou.te.s chaleureusement pour leur accueil m'ayant permis de me sentir très rapidement bien intégré dans ces deux environnements nouveaux pour moi. J'ai également une pensée particulière pour le personnel du laboratoire d'agronomie de la DESV avec qui j'ai pu travailler en janvier et février 2021 en attendant de

pouvoir démarrer la thèse. Je tiens à tou.te.s les remercier pour cette petite parenthèse chaleureuse qu'iels m'ont offert et qui m'a permis de me sentir très vite inclus à la DESV et je remercie vivement Mathilde Renard, François Nold et Catherine Chabanne d'avoir pu me permettre d'intégrer cette équipe.

Pour travailler dans de bonnes conditions, il faut aussi réussir à préserver un équilibre pro/perso convenable. Et ça, je n'aurais pas réussi à le faire sans l'aide de nombreuses personnes. La liste est longue et comme je les vois venir je vais faire attention à bien respecter l'ordre alphabétique ;) Tout d'abord, je dois un immense merci à la tribu de doctorant.e.s et stagiaires que j'ai eu la chance de rencontrer à EPHor et qui ont contribué à y créer un environnement de travail d'une incroyable légèreté. Plus que des collègues qui m'ont apporté une aide et un soutien précieux, iels sont rapidement devenu.e.s des ami.e.s qui de par leur écoute, leur bonne humeur, leur énergie, leurs blagues plus ou moins drôles, leur simplicité et leurs bizarreries respectives (qui sont légion) m'ont fait passer 3 merveilleuses années au cours desquelles je n'ai pas vu le temps passer. Beaucoup de souvenirs et qui n'ont pas forcément leur place ici mais TMTC comme qui dirait : Alice, Antoine, Claire, Dorine, Jeanne, Juliette, Loli, Mélanie, Rachel, Souleymane, Stan, Toky et Tom, merci du fond du cœur à vous tou.te.s.

Ensuite, je dois dire que je n'aurais pas pu traverser cette thèse sans l'inlassable acharnement de mes merveilleux colocataires à faire de notre maison un espace impropice à la concentration mais incroyablement chaleureux, bienveillant, festif et réconfortant. Merci du fond du cœur à vous la dreamteam du 16RDR : Antho, Bertille, Louis, Megane, Mélanie, Paul et Sophie (je vous vois venir vous aussi, c'est dans l'ordre alphabétique, vous êtes tou.te.s mes préféré.e.s de toute façon + PS : big up à Raisin le bébouchat) mais aussi à la nouvelle fournée qui a pris le relai avec brio : Alicia, Claire-Marie, Gwennaël et Yoann. Grâce à vous tou.te.s, je me suis très vite épanoui à Angers.

J'ai aussi eu la chance d'être bien entouré à Angers comme ailleurs grâce à Anne, Baptiste, Faustine, mais aussi grâce aux acolytes de GEn avec notamment Clément, Gladys, Laura, Noé, Simon, ainsi que par les belfortains Bouth, Dudu, Maxime et Tristan qui m'ont notamment souvent hébergé lors de mes passages à Paris puis Julie, Kathleen, Lucie et Marie. Profiter avec vous, réfléchir avec vous au monde qui nous entoure et au sens de nos actions, ça n'a l'air de rien mais cela m'a permis d'avancer, de me construire, et cela a eu un impact non négligeable, j'en suis sûr, sur cette thèse.

Iels ne s'attendent peut-être pas à se retrouver ici, mais j'ai une pensée particulière pour mes ancien.ne.s collègues d'EODD que j'ai laissé.e.s à Lyon, non sans tristesse, pour démarrer cette thèse. Sans le savoir, iels m'ont appris énormément de choses sans lesquelles je n'aurais clairement pas abordé cette thèse de la même manière. Pour tout ce que vous m'avez apporté, je vous remercie du fond du cœur.

Enfin, je tiens à clore ces remerciements en pensant à mes parents et à mon frère qui n'ont jamais cessé de me soutenir, de m'encourager, de m'exprimer leur fierté et de donner du sens à mon travail.

Contents

List of figures

List of tables

Abbreviations

a.g.l.	: above ground level	m
AH	: air Absolute Humidity	$g_{water}.kg_{dry\ air}^{-1}$
DAmp	: Daily Amplitude of stem diameter variation	mm
DBH	: Diameter at Breast Height	cm
DG	: Daily Growth of stem diameter	mm
DNV	: Daily Net Variation of stem diameter	mm
ET_{ref}	: Daily accumulated Reference Evapotranspiration	$mm.day^{-1}$
ETPMON	: Daily accumulated Reference Evapotranspiration calculated by Météo-France	$mm.day^{-1}$
FFM	: Daily average wind speed measured by Météo-France	$m.s^{-1}$
GLOT	: Daily integral of the downward global radiation measured by Météo-France	$MJ.m^{-2}$
INST	: Daily insolation duration measured by Météo-France	Hours
LAI	: Leaf Area Index	$m^2.m^{-2}$
LW	: Long Wavelength radiation	$W.m^{-2}$
↓LW	: Downward Long Wavelength radiation	$W.m^{-2}$
↑LW	: Upward Long Wavelength radiation	$W.m^{-2}$
MDS	: Maximum Daily Shrinkage of stem diameter	mm
MDER	: Maximum Diameter Ever Recorded for a stem	mm
PAR	: Photosynthetically Active Radiation	$W.m^{-2}$
NR-AWS	: Non-Readily Available Water Storage	%
PCA	: Principal Component Analysis	-
pt%	: Points of %	-
R-AWS	: Readily Available Water Storage	%
RH	: air Relative Humidity	%

RMSE	: Root Mean Square Error	-
RR	: Daily accumulated rainfall measured by Météo-France	$mm.day^{-1}$
RSCS	: Reduced Scale Canyon Street	-
SVF	: Sky View Factor	-
SW	: Short Wavelength radiation	$W.m^{-2}$
↓SW	: Downward Short Wavelength radiation	$W.m^{-2}$
↑SW	: Upward Short Wavelength radiation	$W.m^{-2}$
TAWS	: Total Available Water Storage	%
T&C	: Trees & Climat study	-
T_a	: Air temperature	°C
T_g	: Globe temperature	°C
T_{leaf}	: Leaf surface temperature	°C
T_{mrt}	: Mean radiant temperature	°C
TM	: Daily average air temperature measured by Météo-France	°C
TN	: Daily minimum air temperature measured by Météo-France	°C
TX	: Daily maximum air temperature measured by Météo-France	°C
UHI	: Urban Heat Island	-
UTCI	: Universal Thermal Climate Index	°C
VPD	: Vapor Pressure Deficit	kPa
VWC	: Volumetric Water Content	%
WR	: Water-Restricted	-
WS	: Wind Speed	$m.s^{-1}$
WW	: Well-Watered	-
Ψ_{soil}	: Soil water potential	MPa

Glossary

Climatic benefits: There is no common definition of the climatic benefits provided by street trees. The term “benefit” induces an enhancement of a given parameter which in the present case is the human thermal stress. In the present study, the climatic benefits of street trees will then be considered as the ability of trees to reduce human thermal stress approached through the calculation of the Universal Thermal Climate Index (UTCI). They will be assessed through the air temperature and UTCI differences between the area influenced by a tree and a reference non-treed area. Both air temperature and UTCI differences will then be the main resulting variables of the present study. However, air temperature and UTCI at a given location result from various thermal transfers with the surrounding environment which is why different other “observation variables” will also be assessed such as absolute humidity, mean radiant temperature, short and long wavelength radiation, surface temperature, etc.

Météo-France: Météo-France is the French meteorological institute which operates two weather stations close to the two experimental facilities studied in the present PhD project. The first one, called “Angers-Beaucouzé” (station n°49020001) is located 400 m west from the reduced scale canyon street of Angers. The second one called “Paris-Montsouris” (station n°75114001) is located in the Montsouris park right at the south frontier of Paris and is located from 2.8 to 8 km away from the studied trees depending on the considered site. Both stations provide reference measurements of the daily accumulated rainfall (RR), daily minimum, average and maximum air temperature (TN, TM, TX), daily accumulated reference evapotranspiration (ETPMON), daily insolation duration (INST), daily integral of the downward global radiation (GLOT) and daily average wind speed (FFM).

Tree morphology: Tree morphology generally corresponds to the physical structure and the external form of the trees. In the present study, the analysis of tree morphology will cover the characterization of the foliage (mainly the total leaf area and the leaf area density -LAI-) and of the crown dimensions (volume, projected area, height, etc.).

Tree physiology: Tree physiology studies the fundamental processes involved in the tree development among which photosynthesis, respiration and transpiration. In the present study, the analysis of tree physiology will focus on tree growth through the measurement of the evolution of tree stem diameter as well as on tree transpiration through direct calculation or through the evaluation of related variables such as stomatal conductance and leaf temperature.

Chapter

1. Introduction

1.1. Context and stakes

1.1.1. Ongoing climate change

Among the multiple effects of the ongoing climate change, the increase of the global average air temperature near the surface of the globe is probably one of the most documented. At the global scale it was reported to be on average 1.09 °C higher in 2011-2020 compared with 1850-1900 with larger increases over land than over the ocean (IPCC, 2023). The decade 2011-2020 was also the hottest one since the beginning of the meteorological records in 1850 (Météo-France, 2020). Although a strong annual variability of the average global air temperature close to the earth's surface does exist, the general increasing trend has been well described and it is considered that global air temperature near the surface of the globe is currently increasing at a rate of +0.2 °C.decade^{-1} approximately. In Paris, France, the 7 hottest years since 1900 were recorded between 2011 and 2020, 2020 being the hottest one ever recorded. The annual average air temperature was 0.8 °C higher during the period 1976-2005 compared to the period 1901-1930 (Agence Parisienne du Climat and Météo-France, 2022) and another 0.5 °C increase (from 12.4 °C to 12.9 °C) was reported when comparing the 30-year periods 1981-2010 and 1991-2020 (Météo-France, 2021). According to multiple forecasts, this trend will very likely continue in the future (IPCC, 2023). A larger overview of the possible effect of climate change on city climate worldwide was proposed by Bastin et al. (2019) who assessed the evolution of the climate of a large sample of cities around the world by 2050. Their work was meant to provide visual understanding of the effect of climate change with the aim of raising awareness and motivating action. They concluded that most of the cities from the northern hemisphere are very likely to experience warmer conditions corresponding to a climate that is found nowadays on average 1 000 km south which represents a shift of around 20 km.year^{-1} southward.

Climate change also comes with a multiplication and an intensification of extreme climatic events such as heatwaves which has been observed in all regions of the world (IPCC, 2023) and was studied locally by different works. Kuglitsch et al. (2010) focused on the eastern Mediterranean region and highlighted a significant increase of heatwave intensity, length and number between 1960 and 2006. In France, a strong increase of both the frequency and the intensity of heatwaves was reported by the French meteorological institute, Météo-France (2022a). Indeed, 9 heatwaves were recorded during the 1947-1989 period and 37 during the 1989-2022 period. The average annual duration of heatwaves was 1.7 days.year^{-1} before 1989 whereas it reached 7.95 days.year^{-1} since 2000 (Météo-France, 2022a). Unfortunately, the frequency of heatwaves is expected to keep increasing during the next decades. In Paris, during the 1971-2005 period, the probability for a heatwave to occur around mid-July was approximately 13 % while it is expected to range between 32 % and 68 % at the end of the 21st century (2071-2100) (Agence Parisienne du Climat and Météo-France, 2022).

The modification of the availability of water in the soil is another expected consequence of climate change. Although the evolution of the quantity and the temporal and spatial distribution of rainfall appears to be hard to predict, a reduction of the water availability in the soils is expected (IPCC, 2023). Indeed, the increasing average air temperature comes with a higher vapor pressure deficit which enhances water evaporation. Thereby, the soils dry faster from the direct evaporation and the plants also have to transpire more, which means more uptake of the water contained into the soils. In metropolitan France, the annual rainfall has remained quite stable since 1960 when averaged over the entire metropolitan territory. However, strong seasonal and geographical contrasts exist and tend to increase. When comparing the 1981-2010 and the 1991-2020 periods, an average increase of the soil moisture was reported in winter while an average decrease was noticed in spring, summer and autumn for part of the territory (Météo-France, 2023). From 2017 to 2020, 30 % of the metropolitan France territory was subjected to water use restriction every year (Météo-France, 2023). These tendencies are also expected to continue in the near future. In the French region Pays de la Loire, where one of the experimental facilities of the present work is located, the water flow of the rivers could decrease by 30 to 60 % by 2050 and the volume of water contained in the underground reservoirs by 30 % (CESER Pays de la Loire, 2016). Also, the models assessing the evolution of rainfall in the western Europe region generally forecast an increase of the rainfall in northern Europe and a decrease in southern Europe. The limit between both zones is still very variable from one model to the next one but it could probably cross the France metropolitan territory (Agence Parisienne du Climat and Météo-France, 2022).

1.1.2. Urbanisation

The world's population has been rising quickly and continuously across the 20th century from 2.5 billion in 1950 to approximately 8 billion at the end of 2022 (United Nations Department of Economic and Social Affairs, Population Division, 2022; Ritchie et al., 2023). This increase was partly caused by the increasing life expectancy which rose by almost 9 years from 1990 to 2019 to reach 72.8 years on average. Although the global population growth rate fell under 1 %.year^{-1} in 2020 for the first time since 1950, the world's population is still projected to reach 8.5 billion by 2030, 9.7 billion by 2050 and 10.4 billion by 2100, partly because life expectancy is expected to keep increasing until reaching 77.2 years by 2050 (United Nations Department of Economic and Social Affairs, Population Division, 2022).

At the same time the number of people living in cities has been increasing since the beginning of the 20th century. While 30 % of the world's population was living in cities in 1950, this ratio increased to 55 % in 2018. Important contrasts exist between continents, 74 % of the European continent's population being urban versus 43 % in the African continent. Around half of the city dwellers live in cities hosting less than 500,000 inhabitants and around 12.5 % live in megacities hosting more than 10 million inhabitants. The number of urban dwellers is expected to keep rising in all regions of the world to reach 68 % of the total population by 2050 with larger growth rates in Africa and Asia (United Nations Department of Economic and Social Affairs, 2018).

To cope with the growth of their population, cities are expanding and the natural environment surrounding them is progressively being replaced by a human-made environment which comes with very different characteristics. Human activities generally spread wasted energy in the form of heat, they cause the emission of various pollutants, among which greenhouse gases, and they need space. Thus, the natural soils which store water and host vegetation as well as a wide part of the globe's fauna are progressively being replaced by anthropogenic surfaces generally made of mineral and impervious materials. In France, the total amount of human-made surfaces has increased on average by 1.5 % each year at the metropolitan territory scale between 1981 and 2012, which is three times faster than the growth rate of the French population over the same period (on average +0.5 %.year^{-1}). In 2018, it was then estimated that 6.7 % of the French metropolitan territory was already covered with human-made surfaces (Bouvard et al., 2018; Comité pour l'économie verte, 2019). Such surfaces induce a modification of the matter and energy balances and various resulting effects among

which the modification of the water cycle at the local scale and the creation of a microclimate proper to the urban environment mainly characterized by an overheating phenomenon.

1.1.3. Urban overheating

At the beginning of the 19th century, Howard (1833) compared the air temperature measured in the urban area of London to the one measured in its surrounding countryside and found out that London's city center was warmer. During the following decades, similar observations were reported in other European cities (Mestayer and Anquetin, 1995) such as Paris where Emilien Renou reported an approximately 1 °C overheating compared to the countryside (Landsberg, 1981). This phenomenon, called Urban Heat Island (UHI), began to be widely studied mainly after the pioneering work of Oke (1978). Descriptions of the different mechanisms causing the urban overheating were proposed and many works studied the overheating in various cities. In France, air temperature differences between cities and their surrounding countryside were found to reach 10 °C in Paris (Cantat, 2004) or 7 °C in Rennes (Dubreuil et al., 2020) in conditions of clear sky and low-wind days. The UHI intensity was also related to the city size by Oke (1973) who compared the climatic data of cities of different sizes in Quebec, Canada. Akbari et al. (1992) showed that maximum urban temperatures increased by approximately 2.5 °C between 1920 and 1997 by analyzing measurements carried out in Los Angeles and other Californian cities. They also reported that the city centers were generally cooler by around 0.5 °C than the surrounding countryside before 1940. Afterwards, the temperature in these cities rose at a rate of around +0.4 °C.decade^{-1} between 1940 and 1990.

1.1.4. Human thermal stress and health

The combination of the already existing urban overheating and the multiplication and intensification of heatwaves is particularly worrying in cities as it exposes the human body to an increasing thermal stress as highlighted in Poland by Kuchcik (2021). The author studied the evolution of cold stress and heat stress in various cities of Poland over the 1975-2014 period and showed that most of the cities experienced a clear statistically significant decrease in cold stress days and an increase in thermal heat stress days.

Such thermal stress exposure may have various effects on human well-being. Numerous studies reported that heat exposure could have a negative impact on work productivity (Zander et al., 2015). Others assessed this effect from a larger point of view by studying the impact of

heatwaves on economic indicators such as growth domestic product (Callahan and Mankin, 2022).

But more importantly, it is known that heat exposure is very likely to cause sanitary issues (IPCC, 2023). Heat-related deaths have been reported since the beginning of the 20th century in the USA. Since then, multiple works have highlighted the increasing mortality during heatwaves as reported by Basu and Samet (2002) and Brooke Anderson and Bell (2011) who reviewed the epidemiologic evidence of the relationship existing between heat exposure and hospitalizations and death. Hajat et al. (2002), for instance, studied the daily data of air temperature and mortality with all the causes of death referenced in the greater London (United Kingdom) area during a 21-year period from 1976 to 1996. They tried to determine the threshold of air temperature above which an excess death rate was highlighted and they reported a linear positive relationship between excess deaths and air temperature when the daily average air temperature exceeds 19 °C. They also underlined the more important influence of daily minimum air temperature compared to daily maximum air temperature.

In Europe, the long and intense heatwave of summer 2003 caused an abnormally high death rate in most countries. Approximately 35,000 dead were attributed to the heatwave in the entire continent (Wright et al., 2005) and 15,000 in France. As already reported by previous studies (Basu and Samet, 2002), the mortality risk appeared to be higher in cities where the UHI intensifies the overheating especially at night (Laaidi, 2012; Kuchcik, 2021). Indeed, due to the low night-time cooling of the streets' surfaces, the outdoor air temperature remains high at night. As a consequence, the night-time air temperature inside the buildings also remains high because of the inertia of the building materials and the difficulty to efficiently ventilate the dwellings which prevents the human organisms to rest correctly. Wright et al. (2005) highlighted this phenomenon by measuring the indoor air temperature in 9 dwellings in England during the August 2003 heatwave. In Paris, the study of a sample of 482 elderly (more than 65 years old) persons during the August 2003 heatwave reported that living in a warmer district could double the mortality risk (Laaidi, 2012).

Although persons with pre-existing pathologies such as cardiovascular or respiratory diseases are more exposed to heat-related injuries, the risk also appears to highly depend on socio-economic factors. Various studies highlighted that the death risk was higher for elderly, infants or low socio-economic status persons (Basu and Samet, 2002). However, heat may sometimes not be identified or listed among the causes of death, which is the reason why the real consequences of heat related injuries are likely to be underestimated (Basu and Samet, 2002).

Given the clear sanitary issues caused by heat exposure, it rapidly became a high priority concern for policymakers to launch observation programs and awareness campaigns during summer to alert and prevent sanitary issues while looking for solutions to mitigate and also to adapt to urban overheating.

1.1.5. Passive cooling strategies

Thereby, finding ways to cool down the existing cities and to build new cities which guarantee human thermal comfort is at stake. However, it is very important to find solutions which induce low energy consumption in order to cope with the national and international objectives aiming at reducing the greenhouse gas emissions. Indeed, the French national electricity network operator is already planning an increase of the electricity consumption especially due to the growing use of air conditioning to limit human thermal stress increase in summer and especially during heatwaves (RTE, 2021).

Different promising strategies to mitigate the urban climate exist. They rely on a wise selection of surface materials, on the creation of shaded areas or on the use of water and vegetation.

1.1.5.1. Materials

Urban surface materials are generally characterized by a low albedo and a high inertia. Thereby, they can reach very high temperatures when exposed to the sun and cannot cool down efficiently at night. Doulos et al., (2004) conducted a detailed assessment of the surface temperature of 93 materials used for pavement in urban areas with infrared thermal imagery and reported for instance up to 22.5 °C surface temperature difference around noon between tiles made of marble and others made of asphalt. They also assessed the effect of different colors and textures and reported for instance that rough surfaces showed higher surface temperatures compared to smooth ones.

Various works proposed to increase the albedo of the urban surfaces to reduce the amount of energy they store and thus reduce their temperature and emitted long wavelength radiation (Santamouris and Asimakopoulos, 1996; Ringenbach, 2004; Bouyer, 2009; Castellani, 2021; Bamdad, 2023; Carlosena et al., 2023). Some ancient buildings built by Mediterranean cultures such as Greece or North Africa communities widely used this technique and painted their buildings white to prevent their streets and dwellings from overheating. Multiple works evaluated the effect of increasing the albedo of the facades and roofs at city

scale on the cooling energy consumptions (Akbari et al., 1992) or on air temperature (Taha, 1997). Taha for instance reported that decreases of air temperature from 2 to 4 °C could be expected when increasing the global albedo of a city from 0.25 to 0.4.

However, the evaluation of the long-term impact of such high albedo material needs to take into account the progressive decrease of their albedo mainly caused by the progressive accumulation of all kinds of dirt brought by the wind and the rain (Bozonnet et al., 2006; Bouyer, 2009). Also, increasing the surface albedo may come with drawbacks as it may increase the amount of radiation reflected to the pedestrians which is likely to cause glare and will impact their energy balance which may increase human thermal stress during hot days.

Finally, the materials found in the urban environment are most of the time not permeable to water which prevents rainwater to be stored into the soil and by that means limits the direct evaporation of water from the soil. Yet, the resulting latent heat flux could be very useful to cool down the urban surfaces which is why using more pervious materials is also of high interest (FISRWG, 1998).

1.1.5.2. Creation of cast shadows

Urban overheating as well as human thermal stress are highly driven by the incoming solar radiation. Creating shaded areas therefore appears to be an efficient way to cope with both issues. Some authors compared different urban geometries in order to provide guidelines on the best practices to adopt. Ali-Toudert and Mayer (2006) used numerical simulation to highlight the impact of street orientation and aspect ratio (height of the buildings divided by the width of the street) on human thermal stress and they (2007) evaluated the advantages of designing shaded galleries on the sides of the street to provide more comfortable zones for pedestrians.

Other works proposed for instance to stretch sails between the buildings to create cast shadows (Elgheznawy and Eltarabily, 2021; Garcia-Nevado et al., 2021; Zhao et al., 2024). Although such solutions may reduce the amount of solar radiation entering the streets during daytime, they may also overheat by intercepting part of the solar radiation and may be responsible for important longwave radiation emissions onto the street's surfaces. At night, such sails may also limit the radiation exchanges which the street needs to cool down.

1.1.5.3. Watering of the street's surfaces

It was already mentioned hereinabove that the impervious materials used in cities limit the latent heat flux resulting from the direct evaporation of the water contained in the soil. In

response to this issue, some studies proposed to water the pavement of the streets in summer in order to create a latent heat flux which would cool down the pavement. Hendel (2015) reported for instance up to 0.79 °C lower air temperature, 2.39 °C lower mean radiant temperature and 1.03 °C lower UTCI (Universal Thermal Climate Index) at 1.5 m above ground level (a.g.l.) in the late afternoon in a pavement-watered street compared to a control one.

However, such solutions obviously should not be competing with other uses of water and especially not rely on the use of drinking water. It should only be considered if associated with a wise management of the rainwater or for instance with the use of recycled water.

1.1.5.4. Vegetation

The greening of urban areas has been raising an increasing interest during the last decades (Akbari et al., 1992; Bowler et al., 2010; Jamei et al., 2016) as it may provide interesting cooling benefits through the shadows cast by the plants and the water they transpire.

1.1.5.4.1. Lawns

Grass covers, although they cannot cast shadows on other street surfaces, are characterized by a higher albedo (approximately 0.25 to 0.3) compared to typical asphalt surfaces (0.05 to 0.20) (Akbari et al., 1992) and can transpire water contained into the soil, which enables them to keep their temperature low even during warm and sunny days. Armson et al. (2012), for instance, measured a ground surface temperature up to 24 °C lower with a grass cover compared to a concrete cover during a sunny day. Different works reviewed by Bowler et al. (2010) also reported lower air temperatures above grass covers compared to classic concrete paving. However, the impact of grass covers on the human thermal stress is limited as it does not provide shaded areas for the pedestrians, which are still directly exposed to sunlight.

1.1.5.4.2. Green roofs and facades

Multiple systems exist to integrate vegetation on buildings' facades and roofs (Fleck et al., 2022). They all come with different advantages and drawbacks but still, they prevent the vegetated surfaces from overheating as the plants intercept the incoming solar radiation and transpire water to cool down (Convertino et al., 2021). The efficiency of the green roofs and facades may obviously vary depending on the type of vegetation and its density.

Such a system may be very interesting for facades as the vegetated facades will reflect less solar radiation to other buildings or other parts of the street and emit less long wavelength radiation fluxes at night compared to classical urban facades (Alsaad et al., 2022).

It may also be very interesting for roofs as it may also provide a good thermal insulation and a storage for the retention of rainwater. Such a storage would be useful to reduce the water runoff to the waste water network and provide water for the transpiration of the plants composing the green roof. Green roofs however have no influence on the human thermal stress outside at the pedestrian level.

1.1.5.4.3. Urban parks

The cooling potential of urban parks has recently raised an increasing interest as they may provide cooler air temperatures compared with other urban places (Liu et al., 2023). Bowler et al. (2010) reviewed various field surveys carried out in multiple sites to draw a general trend. They concluded on an average 0.94 °C reduction of air temperature over daytime (26 studied sites from 16 different studies) and an average 1.15 °C reduction at night (12 sites from 7 different studies). Obviously, the cooling potential of the parks may depend on various factors such as the size of the park or the type of vegetation and different temporal trends and different levels of spatial heterogeneity may be found when comparing different parks (Liu et al., 2023).

However, urban parks generally represent a small part of the city surfaces and their influence on the microclimate is quite local. Their effect on the surrounding streets depends on various factors such as wind speed and direction (Bernard et al., 2022) and other solutions are needed to provide cooling benefits directly inside the streets.

1.1.5.4.4. Street trees

Street trees offer a very interesting solution to mitigate overheating as well as human thermal stress inside the streets. Their foliage intercepts part of the solar radiation which would otherwise reach the surrounding surfaces and street furniture. Thus, the shadows cast by the trees prevent part of the incoming solar energy from being stored in the urban environment but also to directly reach the pedestrians, which helps reduce their thermal stress. Such cast shadows may depend on the morphological characteristics of the considered trees: crown projected area, foliage density, etc. Trees also transpire water through their leaves, and the evaporation of this water uptakes energy contained at the leaf surface and in the surrounding atmosphere which are locally cooled down. Trees can then help cool down the air inside the streets, which has been

heated by the surrounding hot surfaces. Deciduous trees also have the advantage to lose their leaves in winter, which enables the street surfaces to be heated by the winter sun, making it possible to lower the energy consumption for heating of buildings. A variety of diurnal air temperature reductions beneath tree canopy compared to reference open areas can also be found in the literature, ranging from 0.7 °C (Souch and Souch, 1993) to more than 5 °C (Vailshery et al., 2013).

Trees, and especially street trees, therefore appear to be an interesting solution as they provide a direct effect on both human thermal stress as well as urban overheating very close to the city dwellers. Street trees are therefore the subject of the present work.

1.1.5.4.5. Ecosystem services provided by urban vegetation

Moreover, compared with the other cooling strategies listed hereinabove, vegetation, and especially street trees, provides cities with a wide range of ecosystem services (AURAV, 2020) defined as the "goods and services that humans can obtain from the ecosystems, directly or indirectly, to ensure their well-being" (CEREMA, 2023):

- Vegetation plays an important role in the water cycle and can be very useful for rainwater management in cities to reduce run-off and flood risk.
- They absorb CO_2 which is a key element of their photosynthetic metabolism. Then, they form an interesting carbon stock storing part of the CO_2 emitted by human activities.
- Their important leaf area may intercept part of the pollutants released in the urban environment.
- They host various animal species in their roots, bark, trunk and their leaves, litter, and fruits also are food for various animal species.
- They enhance human well-being.

Obviously, the intensity of such ecosystem services may vary a lot depending on the type of vegetation and especially the considered tree species, their phenology, the density of trees, their age, their physiological status, their location inside the urban environment.

1.1.6. Water availability for street trees

Water is essential for plants. They use it to carry minerals from the ground to their leaves through their vessels where an important part of this water is transpired and spread out into the surrounding atmosphere as water vapor. The lack of water may have various consequences on the processes involved in plant growth and therefore on the plant physiology and morphology. Such consequences may include transpiration reduction or stop, leaf withering or loss and even plant death and are obviously very likely to impact the cooling benefits they provide.

However, the multiplication and intensification of drought spells induced by the ongoing climate change and described previously expose plants to longer and more frequent periods of water scarcity. In the meantime, the increasing average air temperature leads them to transpire greater quantities of water which speeds up soil drying. Moreover, in cities, the need for heat mitigation drives important greening projects which means that more plants will have to compete for a rarifying water resource. Also, urban trees may have to deal with low water resources as the volume of soil they can prospect is low and their plantation pits are generally partly sealed which is likely to reduce the amount of rainwater flowing into the pits.

In this context, it appears crucial to understand if and how street trees are able to resist the changing climatic conditions. In the meantime, they are expected to provide efficient cooling benefits to help cities withstand the forthcoming heatwaves and their ability to do so in such harsh conditions is at stake.

1.1.7. Public policies and technical answers

Stakeholders and policy makers are progressively taking into account the dangers coming with climate change. To cope with these issues, they generally try to evaluate the consequences of climate change at different scales (country, region, city) depending on the territory they manage and then to launch action plans to reduce their contribution to climate change and prepare for adaptation.

In France, the French ministry of ecology ordered for instance a report from the "Direction Générale de l'Energie et du Climat", aiming at downscaling the IPCC scenarios at a regional scale for French territory and proposing actions to adapt France to the future climate (Ouzeau et al., 2014). Similar initiatives can also be found at city scale. The city of Paris, in collaboration with the French meteorological institute, Météo-France, launched in 2007 an interdisciplinary study aiming at assessing the impact of global climate change at the Parisian

scale and evaluating the potential of different adaptation scenarios based on the use of reflective materials, vegetation and pavement watering (CSTB and Météo France, 2012). In 2007, the city of Paris published its first "Climate Action Plan" (City of Paris, 2018; Ville de Paris, 2024a) in which urban greening was considered as a key adaptation solution, especially regarding the overheating mitigation. In this context, the green spaces department of the city of Paris launched in 2018 the "Trees and Climate" study in order to assess the ability of Parisian street trees to thrive in spite of the changing climate and the harsh urban conditions while providing efficient cooling benefits.

These actions were also accompanied by other structural plans dedicated to specific topics such as the "Tree plan" launched in 2021 by the green spaces department of the city of Paris. This plan was meant to increase the knowledge about the Parisian population of trees and its protection, to improve the tree species selection process and to enhance the plantation of a large number of new trees in Paris. In this frame, a wide comparison of the ecosystem services provided by more than a hundred tree species, mainly originated from the Parisian region, was ordered by the green spaces department of the city of Paris (CEREMA, 2023). In 2023, the tree plantation strategy of Paris was also strengthened by the publication of a "Tree species guide" (Ville de Paris, 2023) aiming at adapting the choice of the new planted species to the current environmental and sanitary stakes. More precisely, it was meant to increase knowledge about the tree species currently present in Paris and the one expected to be able to fit in the future Parisian urban environment and provide guidelines for tree species selection for new projects.

1.2. Problematic

In this context, it appears crucial to understand more precisely the impact of the extreme climatic events such as heatwaves and droughts on the development of urban trees and to evaluate their ability to resist to such conditions and to keep mitigating urban overheating. Such understanding is indeed essential to properly evaluate the potential of urban trees as a cooling strategy in the future climate. Moreover, stakeholders and urban planners are looking for advices regarding the selection of tree species adapted to the future climates and providing interesting ecosystem services among which overheating mitigation. Then, the present work proposes to focus on the following problematic:

"How are street trees able to provide efficient cooling benefits in a context of water restriction while preserving their development?"

The present work relies on the following hypothesis: street trees experiencing a moderate water restriction can maintain a good development and growth and keep providing significant climatic benefits.

To answer to the problematic, the present work deals with the following sub-questions:

- What is the impact of a water restriction on the climatic benefits provided by street trees?
- What are the respective contributions of cast shadows and tree transpiration to the climatic benefits provided by street trees experiencing both well-watered and water-restricted conditions?
- How are the climatic benefits related to morphological characteristics and or physiological behaviors of the trees? Are there differences between tree species?

In **chapter 2**, the different phenomena at stake are presented in order to understand the physical basis of the urban overheating and the interactions between trees and their surrounding environment. The general processes involved in the tree growth are also described in order to explain how they can be impacted by heat and drought stress. Then, this chapter reviews the literature concerning the quantification of the climatic benefits and the effects of heat and drought stress on both the climatic benefits and the tree growth related processes. Finally, this chapter explains the structure of the work proposed in the present manuscript and presents the two complementary experimental facilities that are used. **Chapter 3** proposes to assess the impact of a water restriction on the summer climatic benefits of trees inside an outdoor canyon street scale model located in Angers, France. It describes the research methodology and then presents the results obtained. **Chapter 4** proposes to assess the summer climatic benefits provided by mature street trees from 9 different species in 5 sites in Paris, France. This chapter describes the methodology and presents the results. **Chapter 5** proposes a wide discussion of the results obtained in chapter 3 and 4. It takes a step back in order to draw a general overview of the climatic benefits provided by the trees especially analyzing the complementarity of the two experimental approaches. Finally, **chapter 6** will summarize the main conclusions of this work in the frame of the problematic stated hereinabove and discuss a few perspectives.

The work described in the present manuscript was shared with the scientific community and society through multiple publications and presentations which are listed in section 7.3.

Chapter

2. Scientific background

In this chapter, the different physical and biophysical processes at stake are first described. Then, the state of the art concerning the climatic benefits provided by street trees is proposed. Finally, the lacks of the literature are summarized in order to highlight the scientific questions which still need to be answered and detail the objectives and the structure of the present work.

2.1. Description of the phenomena and processes at stake

2.1.1. Urban climate and overheating

2.1.1.1. Spatio-temporal scales

The study of the earth's climate aims at providing a representation of the status of the atmosphere over a given region during a given period of time. It involves the assessment of multiple meteorological variables such as air temperature, rainfall or wind speed and direction at different spatio-temporal scales. Indeed, the sun radiation being the main energy flow reaching the earth's atmosphere and surface, the meteorological variables are subject to spatial and temporal variabilities mainly induced by the rotation of the earth on its own axis (daily variability), the varying relative position of the earth and the sun (seasonal variability), the latitude of the considered region and the inertia of the different earth components (ground, oceans, atmosphere). Three main spatial scales are generally considered, although some intermediate scales have also been defined in the literature to meet specific needs (Bouyer, 2009) as illustrated in Figure 1:

- The macro-scale (also called global scale) aims at assessing the general mass flows occurring in the atmosphere across large land areas such as continents. It is generally associated with a spatial resolution of hundreds of km, a temporal resolution of a few years and used to forecast the evolutions of the earth's climate.
- The meso-scale is used to study the regional climate as it focuses on the aerodynamic, physic and chemical interactions between the global climate and the regional particularities such as the presence of urban areas. It is generally associated with a spatial resolution of tens of kilometers, a temporal resolution of a few days and used to forecast weather for the next coming days.
- The micro-scale is used to study very local particularities. It is for instance well adapted to the rugosity and heterogeneity of the urban environment. It is generally associated with a spatial resolution of a few meters, a temporal resolution of an hour or less and used to evaluate air quality or human thermal comfort at the street scale for instance.

Different vertical scales have also been defined to take into account different boundary layers that develop above the earth's surface, which are characterized by varying respective contributions of global earth mechanisms and local specificities (roughness, topography, human constructions) to the observed phenomena (Bouyer, 2009).

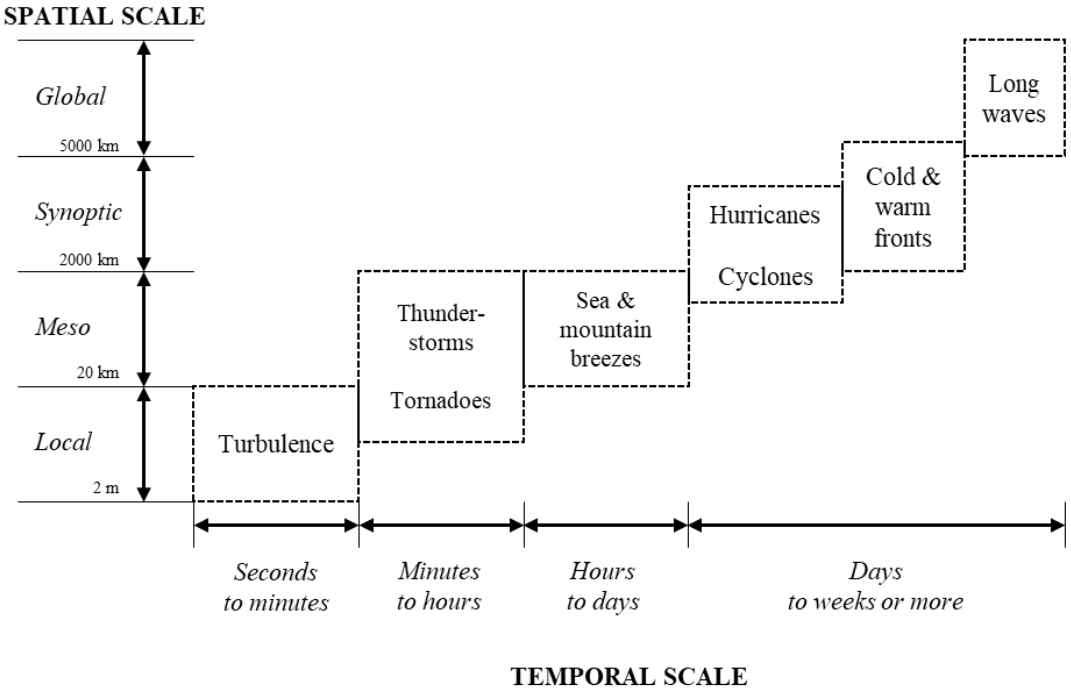

Figure 1: Spatio-temporal scales of the different atmospheric movements adapted from Bozonnet (2005) after Lyndon State College (http://apollo.lsc.vsc.edu/).

The phenomena studied in the present work will be assessed at the micro-scale as the climatic benefits provided by street trees are very likely to be influenced by the high heterogeneity of the urban environment. The micro-scale is generally associated with a thin boundary layer, called urban canopy layer, which height is generally considered equal to the average building height. In this urban canopy layer, the rugosity of the urban forms creates important vortices in the atmospheric mass flows. Moreover, the high heterogeneity of materials, the presence of sources and sinks of heat and humidity are very complex to take into account as they may locally modify the wind flow. Also, the thermal effects caused by contrasted solar exposures (due to heterogeneity of cast shadows) may also disturb wind flow with natural convection cells. At this scale, the interesting mechanisms have to be studied at a very low time-step (no more than 1 hour) because the temporal variability of the climatic variables is very high.

2.1.1.2. Energy balance of an urban versus a rural surface

The urban environment and the countryside both show very contrasted characteristics which induce different mass and energy balances. Such balances have been compared in various works in order to understand the local climate differences observed between both environments and the factors inducing them.

First, such balances are mainly influenced by the sun which is the main source of energy reaching the earth's atmosphere and surfaces. The sun, just as every material body with a temperature greater than 0 K, emits energy in the form of radiation. The radiation transfers have been described by different laws which were first established for blackbodies (i.e. hypothetical bodies able to absorb and emit back all the radiation they receive whatever be the wavelength of the radiation with null reflection and transmission) and were then adapted to real bodies by taking into account their emissivity. Stefan-Boltzmann's law (equation (1)) states that the amount of energy emitted by a given body through radiation only depends on its temperature.

$$M_T = \varepsilon \sigma T^4 \quad (1)$$

With M_T the amount of energy emitted ($W.m^{-2}$), ε the emissivity of the considered real body, σ the Stefan-Boltzmann constant ($5.67*10^{-8}$ $W.m^{-2}.K^{-1}$) and T, the temperature of the considered body (K).

This radiative energy is emitted through a wide range of wavelengths and the amount of energy emitted varies for each wavelength. Moreover, Planck's law states that the distribution of emitted radiation in terms of both wavelength and amount of energy depends on the temperature of the considered body (Figure 2), especially this distribution has a maximum value

which depends on the temperature of the considered body. The wavelength associated with the maximum amount of energy emitted is actually inversely proportional to the temperature of the body as stated by Wien's law (equation (2)). The higher the temperature of the body, the lower the wavelength associated with the maximum of energy emitted.

$$\lambda_{max} = \frac{2898}{T} \quad (2)$$

With λ_{max} the wavelength of the maximum amount of energy emitted by a black body (µm) and T the temperature of the considered black body (K).

The surface temperature of the sun ranges between 5000 K and 6000 K which is why the wavelength of its maximum energy radiated is close to 0.56 µm (Ling et al., 2016) which is located in the visible part of the electromagnetic spectrum (approximately 0.38 to 0.76 µm (Bouyer, 2009)). Figure 2 shows that an important part of the radiation emitted by the sun is emitted through wavelengths lower than 0.38 µm (ultraviolet) and higher than 0.76 µm (infrared) but most of the concerned wavelengths are lower than 3 µm. Indeed, the high temperature bodies emit most of their radiation through short wavelength radiation (SW) i.e. between 0.3 and 3 µm. The low temperature bodies (e.g.. earth's atmosphere and soil, plants and all other objects found at the earth's surface) also emit radiation but through long wavelength radiation (LW) i.e. between 3 and 100 µm.

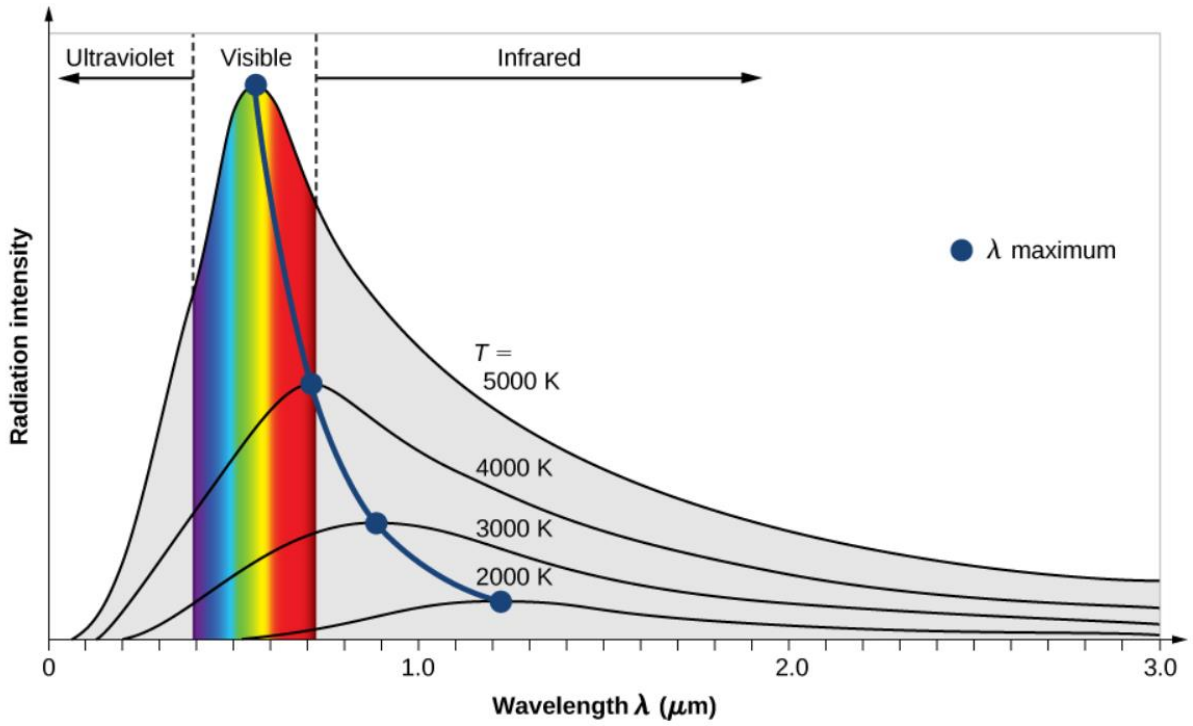

Figure 2 : Intensity of the blackbody radiation versus the wavelength of the emitted radiation depending on the blackbody's temperature (Ling et al., 2016).

When reaching the atmosphere of the earth, the sun radiation is divided into multiple fluxes (Figure 3). Part of this radiative energy is directly reflected to the space on top of the atmosphere, part of it is absorbed by the particles composing the atmosphere which contributes to warming the atmosphere, part of it is diffused in many directions and may then reach the different earth's surfaces while the rest (the greatest part) directly reaches the earth's surface. The earth's surface will reflect part of this radiation and absorb the remaining part which will increase its temperature.

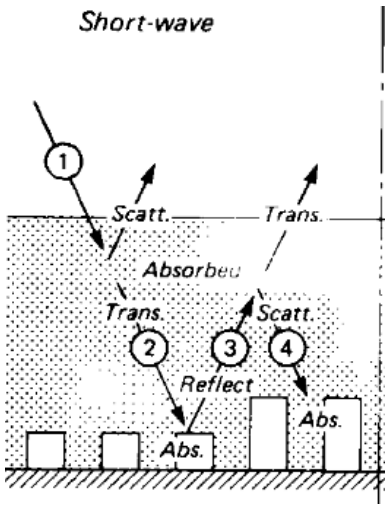

Figure 3 : Different radiation fluxes induced by a SW flux emitted by the sun and reaching the earth's atmosphere and surface (Oke, 1988).

To introduce the energy balance at the earth surface, Oke (1987) and Grimmond (1992) proposed to consider a hypothetical volume composed of a layer of atmosphere on top of a layer of soil and enabling to summarize the different energy inputs and outputs that can be expressed for a non-urban area as presented in equation (3). The considered volume receives and reflects SW and emits LW which, when combined together, form a net all-wave radiation flux called Q*. Heat can be stored in the volume depending on the thermal capacity of the materials it is made of and the variation of the amount of heat stored is called ΔQS. The different surfaces contained inside the volume may release sensible heat through conduction and convection which induces a flux called Q_H. They may also release latent heat through the eventual evaporation of water which induces a flux called Q_E. Finally, heat can be advected in and out the considered volume through eventual air flows from or towards the surrounding environment which induces a flux called ΔQ_A. All these fluxes can be expressed for instance in $W.m^{-2}$.

$$Q^* = Q_H + Q_E + \Delta Q_S + \Delta Q_A \quad (3)$$

Obviously, such heat transfers are very likely to vary with the characteristics of the considered surface which is why the different terms of the energy balance vary comparing an urban surface and a rural one when exposed to the same incoming solar radiation.

2.1.1.2.1. Materials

The urban surfaces (ground and building facades) are usually made of low albedo[1] mineral materials which store most of the radiative energy they receive instead of reflecting it inducing an increase of their temperature (Akbari et al., 1992). Conversely, the materials found in the countryside reflect more radiative energy to the surrounding environment and their temperature remains low. Indeed, albedo is considered to range approximately from 0.05 to 0.20 for typical asphalt surfaces, from 0.1 to 0.35 for concrete and from 0.25 to 0.3 for lawns (Akbari et al., 1992).

Urban materials are also generally denser and characterized by a high inertia which means that the energy they store during the day is mainly released at night into the urban environment (Bouyer, 2009). The temperature of the urban surfaces directly affects the air temperature through natural convection. Considering the energy balance presented previously in equation (3), the lower albedo and higher inertia of the urban materials is likely to induce high surface temperatures in cities under sunny conditions leading to important energy transfers from the surfaces to the surrounding environment through convection (sensible heat term, Q_H) and through the emission of LW radiation (net all-wave radiation term, Q^*). The net heat storage term (ΔQ_S) which represents the amount of energy stored in the urban surfaces is also likely to increase if the considered surfaces cannot lose all the energy the received from the sun.

2.1.1.2.2. Effect of the urban geometry on radiation transfers

The city centers are generally densely built and most of the urban outdoor ground surfaces are narrow and surrounded by high buildings which leads to a reduced sky view factor[2] (SVF) compared to the rural environment. In cities, streets are generally bordered by buildings on both sides, they are thus called canyon streets and they can be characterized by their aspect ratio generally defined as the height of the buildings divided by the width of the street. The higher the aspect ratio, the lower the SVF. Both SVF and aspect ratio are geometrical notions

[1] The albedo of a surface is the ratio between the SW fluxes reflected by the surface and the incident SW on the surface. The higher the albedo, the higher the amount of reflected SW.

[2] The sky view factor (SVF) is calculated at a given location as the ratio between the area of sky visible from this location and the theoretical area of sky visible without any surrounding object masking the sky. The higher the sky view factor, the lower the amount of surrounding objects masking the sky.

highly related to the SW and LW exchanges of a given surface. Indeed, low aspect ratio and high SVF (which generally characterizes rural environments) come with a high amount of incident SW but also a high amount of SW reflected to the sky. Conversely, high aspect ratio and low SVF (which generally characterizes urban environments) may come with a lower incident SW due to the shadows cast by the surrounding buildings (Du et al., 2020), but also with a lower amount of SW reflected to the sky. Indeed, the sunrays entering the urban rugosity (e.g. a canyon street) are subject to multiple reflections on the urban surfaces and most of them will reach multiple times the different urban surfaces before being redirected to the sky. This phenomenon, called radiative trapping, induces a high absorption of the incident sunrays into the urban surfaces (Figure 4) (Bouyer, 2009). The intensity of the radiative trapping has often been related to the aspect ratio of the considered street and it appears that a threshold exists. When the aspect ratio is lower than this threshold, the radiative trapping intensity increases with the increasing aspect ratio. However, when the aspect ratio is higher than this threshold, greater aspect ratio leads to lower radiative trapping as the shadows cast by the surrounding buildings strongly reduce the amount of radiation entering the street.

Some works characterized the impact of this phenomenon on the resulting net radiation transfers through the calculation of a global albedo at the district or even the city scale as reviewed by Bozonnet et al. (2006). Average albedo values for 12 cities around the world were for instance reported by Taha (1997). Although the global albedo of an urban surface depends on the solar angle and is therefore subject to seasonal variations, it appears that the increasing roughness, irregularities and the heterogeneity of the building heights decrease the global albedo, especially in winter. Aida (1982) experimentally modeled 3 urban geometries (canyon street North-South and East-West oriented and regularly scattered buildings) with cubic concrete blocks to compare them to a flat surface. They reported up to 20 % higher solar radiation absorption for the regularly scattered building configuration compared to the flat surface. Both North-South and East-West oriented canyon streets provided comparable results with a higher absorption compared to the flat surface but lower compared to the regularly scattered buildings. They also found that the taller models (higher buildings) showed smaller albedo values (more radiation absorbed). The height of the buildings also impacts the respective contributions of the optical properties of the roofs, ground and facades to the global albedo. The roofs' contribution increases with the average buildings' height while that of the facades and ground decreases and vice versa.

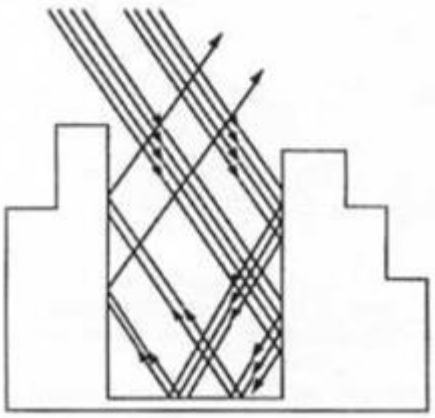

Figure 4: Drawing of the radiative trapping phenomenon adapted by Ringenbach (2004).

Aspect ratio and SVF also highly influence the LW transfers. In a rural environment, the surfaces generally have a high SVF meaning that most of their radiation exchanges will involve the sky. At night, the sky temperature is very low and the net radiation transfer between the sky and the rural surfaces has a high absolute value which enables the rural surfaces to lose an important part of their energy through radiation emitted to the sky. In cities, the SVF is much lower and most of the radiation exchanges occur with other urban surfaces having a close temperature. The net radiation exchanges are then quite low even at night and the urban surfaces are not able to cool down as efficiently as the rural ones through radiative transfers.

Considering the energy balance presented previously in equation (3), the lower SVF of the urban configuration directly impacts the net all-wave radiation term (Q^*) by reducing the amount of SW reflected to the sky and the amount of LW emitted to the sky. This induces indirect effects on the other terms of the energy balance.

2.1.1.2.3. Effect of the urban geometry on the wind flow

Wind refers to the flow of air occurring in the earth's atmosphere to balance the pressure gradients and the Coriolis force. Wind speed and direction are subject to a very high spatial and temporal variability. Moreover, although the wind profile may remain constant on a horizontal plane when considering wide homogeneous open areas free from obstacles, the urban geometry and volumetry (forms of the buildings and orientation of the streets) create an important roughness which affects both wind speed and direction. Many works have studied the effect of different urban morphologies, textures, roughness on the air flow as reviewed by Bozonnet et al. (2006). Gandemer and Guyot (1976), for instance, described the effect of different classic urban configurations on the wind flow (pipe effect, Venturi effect, bypass effect, Wise effect). Multiple works took place in canyon streets. Oke (1987) studied the case of a perpendicular

incoming wind and reported different air flows depending on the aspect ratio of the considered canyon street. Studies assessing the concentration of pollutants showed that a whirling wind flow could form close to the sidewalks on each side of the street when considering canyon streets with higher aspect ratio and a perpendicular incoming wind. As a consequence, an accumulation of pollutants and small particles close to the ground was reported (Burton, 2016).

Considering the urban overheating mitigation, wind is generally a good ally as it increases the convective heat transfers between the surfaces and the atmosphere. However, the average wind speed is strongly reduced by the urban roughness which induces a reduction of the amount of energy lost through convection in cities compared to rural areas (Plate and Kiefer, 2001; Bouyer, 2009) which may impact both the sensible heat term (Q_H) and the latent heat term (Q_E) of the energy balance (equation (3)). Then, urban overheating is likely to be higher under low-wind conditions. Also, a lower wind speed induces lower heat loss through convection for the human body which can decrease human thermal stress in winter but increase it in summer.

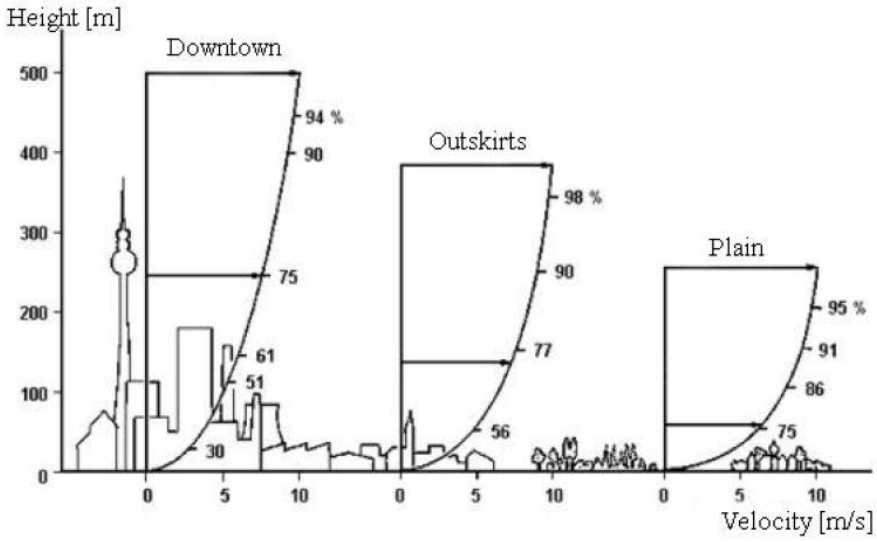

Figure 5: Vertical profile of wind speed above 3 different land use configurations (Hudișteanu et al., 2018).

2.1.1.2.4. Evapotranspiration in urban areas

The earth's surfaces may also release part of their energy through the latent heat flux associated with the evaporation of water. Indeed, the phase change from liquid water to water vapor consumes a high amount of energy which is uptaken from the surrounding surfaces and atmosphere. The water can evaporate directly from the soil surface, the lakes and rivers or when transpired by vegetation. The term "evapotranspiration" refers to all these different processes. Evapotranspiration in a given area depends on the daily climatic conditions as well as on the

type of vegetation found in this area and the water content of the soil. It is generally approached by the calculation of the reference evapotranspiration (ET_{ref}), a standardized value which can then be adjusted with a crop coefficient taking into account the type of plant and its development stage, and a water availability coefficient. ET_{ref} corresponds to the evapotranspiration of a 1 m² reference surface of 0.12 m high well-watered grass crop fully exposed to sunlight radiation and with an albedo of 0.23. It can be calculated with different techniques among which the use of the Penman-Monteith (equation (4)) (FAO et al., 2006):

$$ET_{ref} = \frac{0.408\Delta(R_n - G) + \gamma \frac{900}{T + 273} u_2 (e_s - e_a)}{\Delta + \gamma(1 + 0.34u_2)} \quad (4)$$

ET_{ref} is the reference evapotranspiration in $mm.day^{-1}$, Δ is the slope of the water vapor saturation curve in $kPa.°C^{-1}$, Rn is the daily net radiation in $MJ.m^{-2}.day^{-1}$ measured at 2 m a.g.l., G is the conductive heat flux density in the ground in $MJ.m^{-2}.day^{-1}$ usually considered null on a daily time step, γ is the psychrometric constant in $kPa.°C^{-1}$ (0.066 $kPa.°C^{-1}$), T is the daily mean air temperature measured at 2 m a.g.l. in °C, u_2 is the daily mean wind speed measured at 2 m a.g.l. in $m.s^{-1}$, e_s is the daily mean water vapor saturation pressure in kPa and e_a is the daily mean water vapor pressure in kPa. Δ, e_s and e_a can be calculated with the equations proposed by FAO et al. (2006).

Unlike rural environments, cities are generally characterized by very few open water surfaces and vegetated areas and most of the natural soils have been replaced by human-made surfaces mainly composed of mineral materials (Arnold and Gibbons, 1996). In addition to having a low albedo and a high inertia, as explained hereinabove, such materials are generally impervious and do not enable water to infiltrate (Figure 6). Although part of the rainwater fallen onto the ground may evaporate right after the rainfall event, the major part runs off and is drained to the stormwater evacuation system. This may enhance the convective heat transfer from the ground surface to the water but it mainly prevents the water from being stored into the soil and evaporated later directly from the soil surface or after being transpired by vegetation when the reference evapotranspiration further increases. Thus, the global latent heat flux (Q_E) of the urban surfaces is much lower than the one of the rural environment.

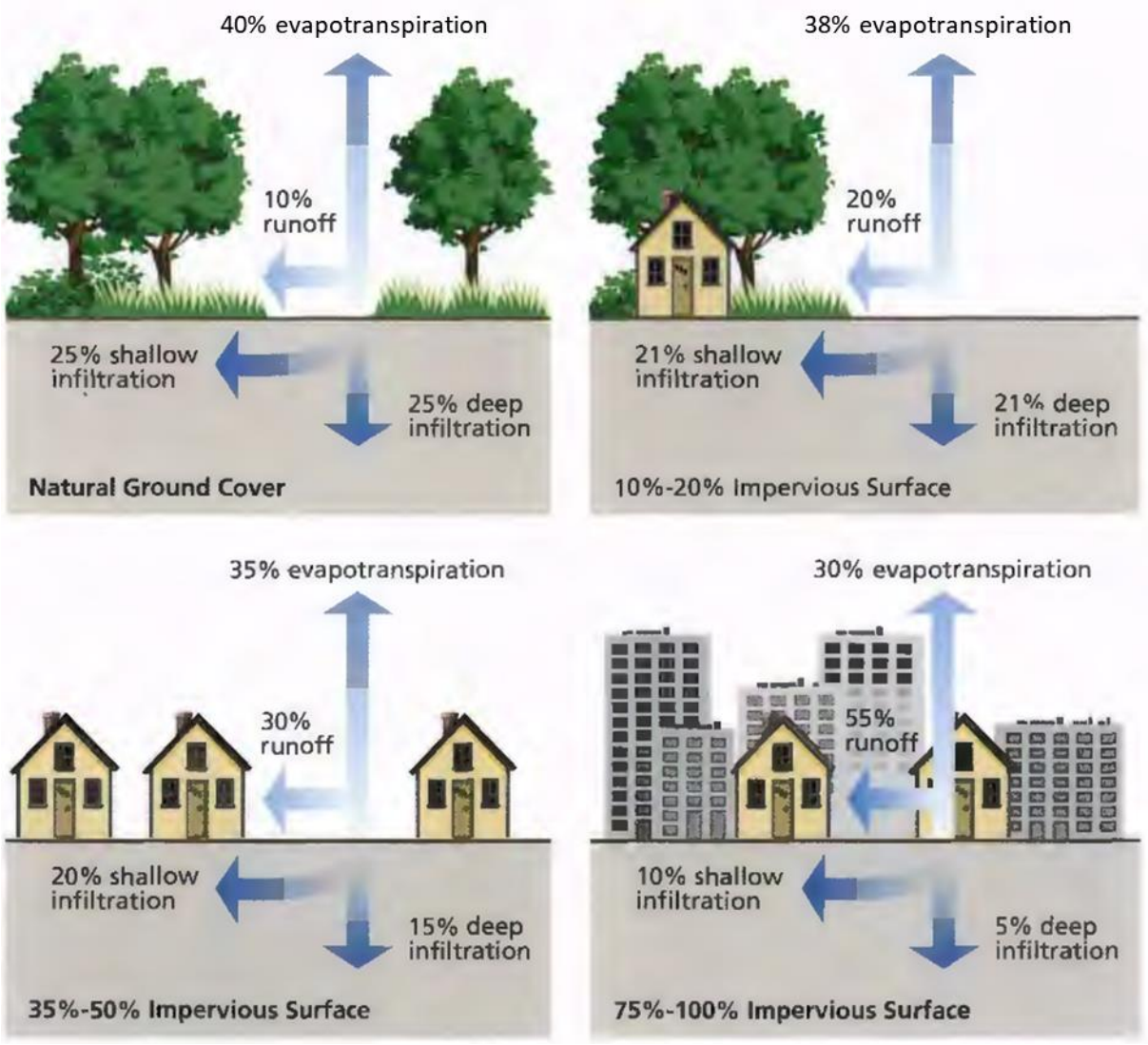

Figure 6 : Relationship between impervious cover and surface runoff (FISRWG, 1998).

Evapotranspiration corresponds to the amount of water evaporated to form the latent heat flux Q_E presented hereinabove and is therefore involved in both the energy balance expressed hereinabove in equation (3) and the water balance which is detailed hereinafter in equation (5) and illustrated in Figure 7 for the same considered volume as proposed by Grimmond and Oke (1991).

$$P + I + F = E + r + \Delta S + \Delta A \quad (5)$$

With P the rainfall, I the piped water supply, F the water released by the anthropogenic activities, E the evapotranspiration, r the runoff of water in the soil, ΔS the net change in water storage in the soil and ΔA the net moisture advection in the atmosphere. All fluxes of water can be expressed for instance in $mm.hr^{-1}$.

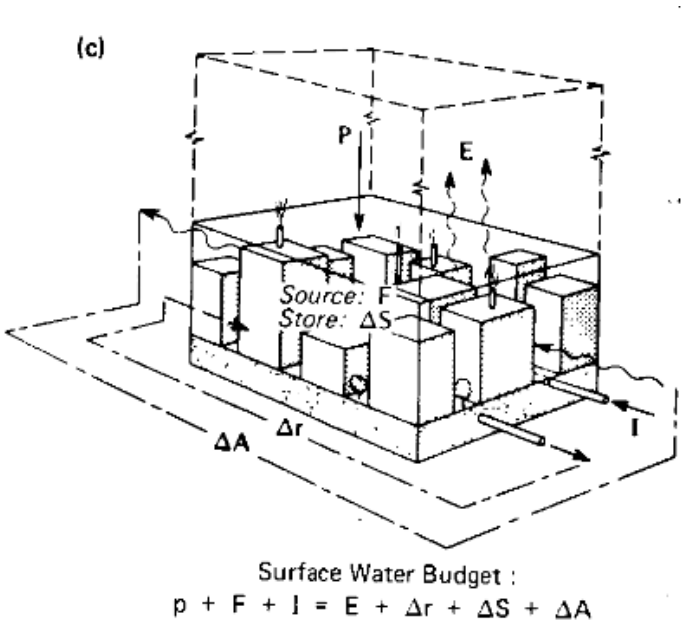

Figure 7: Water balance established on top of an urban volume proposed by Oke (1988).

2.1.1.2.5. Anthropogenic heat

Cities host a high density of human activities which release a lot of energy in the form of heat among which building air conditioning, transport or industry (Akbari et al., 1992; Bouyer, 2009). Fan and Sailor (2005) modeled the amount of waste energy released in the form of heat by human activities in urban environments and reported that, in the case of the city of Philadelphia, it could play an important role in the formation of the UHI, mainly at night and during winter. Simulations for winter suggested a 2 to 3 °C contribution to the night-time UHI. Grimmond (1992) also modeled it for a suburban area of Vancouver, Canada, and reported that it contributes to approximately 10 % of the energy balance over an entire day during winter until April. It could then only be considered negligible when studying daytime hours (lower heat load) or non-wintertime period. Although the anthropogenic heat flux is generally considered lower than 100 $W.m^{-2}$ (as a comparison, incoming solar radiation can reach for instance 1000 $W.m^{-2}$ during daytime in summer in France), it can vary a lot according to the urban density (Bozonnet et al., 2006) but also depending on the heating and cooling loads of the different regions of the world. Human activities also cause a higher concentration of pollutants and particles which may reduce the transparency of the urban atmosphere which is then likely to absorb a higher amount of solar radiation and overheat.

Thus, when considering the urban environment, a new term (Q_F) which represents the anthropogenic heat flux, has to be integrated to the energy balance presented earlier (equation

(3)) on the left side of the equation corresponding to the inputs (see equation (6)). An illustration of a theoretical urban volume considered for this energy balance is proposed in Figure 8.

$$Q^* + Q_F = Q_H + Q_E + \Delta Q_S + \Delta Q_A \quad (6)$$

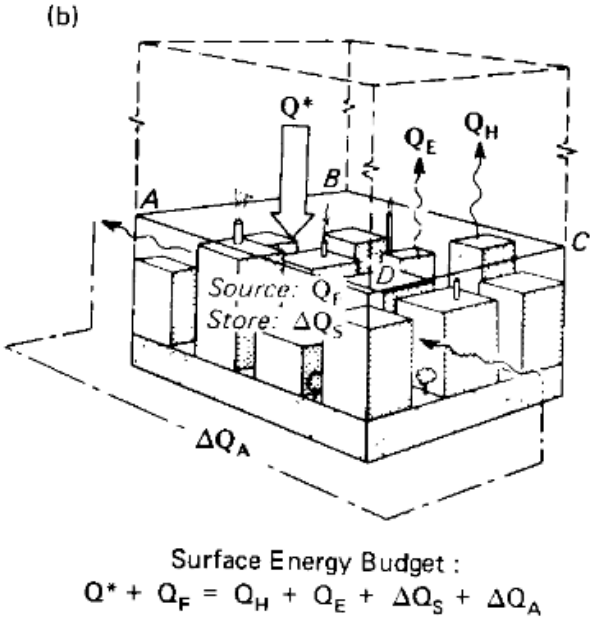

Figure 8: Energy balance established on top of an urban volume proposed by Oke (1988).

2.1.1.2.6. Resulting urban overheating

To illustrate the modification of the energy balance induced by the urban environment, Sass (n.d.) proposed an estimation of the different terms for a typical summer day in Houston, Texas, USA (Figure 9).

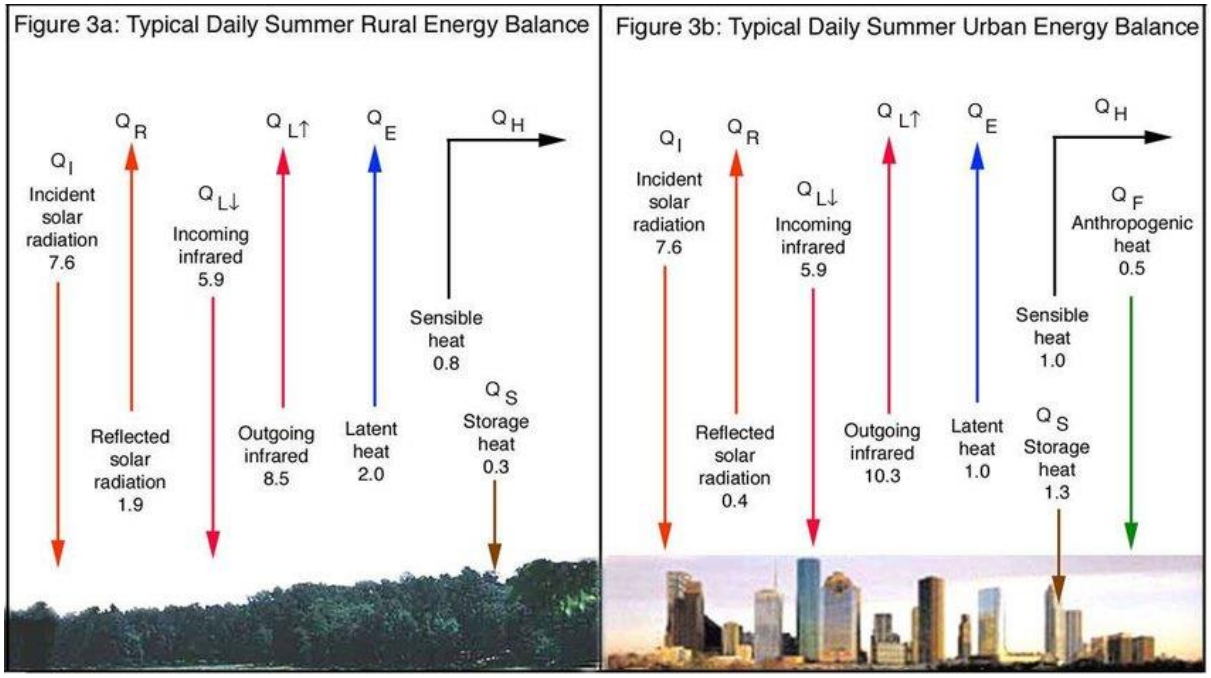

Figure 9 : Typical daily summer energy balance of a rural and an urban surface for Houston, Texas, USA, expressed in $MJ.day^{-1}.m^{-2}$ proposed by Sass (n.d.).

The different phenomena described in the previous sections result in higher surface temperature and higher air temperatures in the urban environment compared to rural areas. As a consequence, the air temperature inside the buildings is likely to increase which may admittedly induce a reduction of the heating loads in winter but an increase of the cooling loads in summer.

Although the overheating phenomenon can be studied at the entire city scale, it is clear that the phenomena described hereinabove have direct implications at street scale. They may also highly depend on the heterogeneity of the urban environment. Streets made of different materials, with different sky view factors, orientations or amounts of vegetation will indeed induce contrasted overheating and levels of human thermal stress (Chen et al., 2022). Therefore, focusing on the street scale appears to be very adapted to evaluate the effect of various solutions, among which the use of vegetation, on the overheating mitigation.

2.1.1.2.7. Heatwaves and droughts

Heatwaves and droughts are two climatic events, of which distribution around the world is highly heterogeneous. However, the ongoing climate change appears to increase both their frequency and intensity, which is likely to intensify even more the urban overheating. Heatwaves come with extreme air temperature which might induce a low temperature gradient between the air and the surfaces reducing the potential cooling of the urban surfaces through sensible heat flux. Droughts reduce the water availability which limits the potential latent heat flux that the urban surfaces need to cool down.

A heatwave corresponds to an abnormally high air temperature measured during a few successive days, however, there is no universal definition of this phenomenon. The thresholds of air temperature and duration of the event vary in the different regions of the world and for the different considered applications (Météo-France, 2022a). In France, the French meteorological institute, in collaboration with the French ministry of health generally monitors the moving averages of the daily minimum and maximum air temperatures calculated over 3 days during the European summer (i.e. from June 1st to August 31st). Also, a national thermal indicator was defined to characterize heatwaves. It is calculated as the average of the daily mean air temperature measured in 30 weather stations homogeneously scattered across the metropolitan territory (Météo-France, 2022a). A hot event is called a heatwave when this indicator exceeds 25.3 °C during one single day or 23.4 °C during 3 days or more. The heatwave is considered finished when this indicator decreases under 22.4 °C during one single day or under 23.4 °C during 2 consecutive days. However, the French metropolitan territory is composed of a variety of climates and heatwaves may sometimes only concern part of the territory. In order to provide the population of each French region with recommendations to prevent heat-related injuries (Vachon, 2015), the French meteorological institute defined alert thresholds on the basis of 30 years of meteorological data cross-analysed with mortality data for each French department (Les Décodeurs, 2016). A day is then considered as forming part of a heatwave in Paris if the maximal temperature exceeds 31 °C and the minimal temperature exceeds 21 °C. In Angers, the maximal and minimal temperatures must exceed respectively 34 °C and 19 °C.

Other methods to identify heatwaves and characterize their intensity, number and length can be found in the literature. Kuglitsch et al. (2010), for instance, defined temperature thresholds on the basis of the daily maximum and minimum air temperatures to estimate the beginning and the end of a heatwave. For each day from June to September, a daily threshold for minimal/maximal air temperature was defined as the 95° percentile of the minimal/maximal

air temperature measured on a sample of 15 days centered on the considered day over the 1969-1998 period. Then, they defined heatwaves as periods of 3 or more consecutive days with minimal and maximal temperatures exceeding this threshold. For the hot days, the difference between the maximal and minimal temperatures and their respective thresholds is then used to quantify the intensity of the heatwave.

Droughts may concern the atmosphere, the soil or the rivers and lakes. Thereby, different types of dry events may be defined (Agence Parisienne du Climat and Météo-France, 2022; Météo-France, 2023):

- The meteorological drought refers to the absence of rainfall during an abnormally long period of time.
- The agricultural drought refers to a water deficit in the superficial layer of the soil (1 or 2 m deep) which is likely to alter the development of vegetation. The superficial soil moisture depends on the rainfall, the direct evaporation of water at the soil surface and the transpiration rate of the plants. It is then very related to the air temperature and relative humidity, wind speed as well as the nature of the soil (texture) and the type of plants.
- Hydrologic drought refers to an abnormally low level of water in the lakes and the underground water reservoirs and low water flow of the rivers.

2.1.1.2.8. Human thermal stress

Heat has long been known to impact human physiology. Thus, various studies have first addressed the impact of heat on labor productivity (Marigo et al., 2023) as well as its potential dangers on human health. This is the reason why the human thermal stress (or comfort) notion was introduced in order to quantify the thermal sensation experienced by a human body. However, the assessment of human thermal stress is quite complex. Indeed, it is associated with a subjective perception and different people may feel more or less comfortable in a same given thermal environment, and both qualitative and quantitative factors influence this perception. Indeed, the people's dressing, their level of physical activity, or their thermal history at the moment of the assessment may highly influence their expectations as well as their thermal sensation (De Dear et al., 1998). As a consequence, multiple definitions of human thermal comfort exist and Migliari et al. (2022) summarized the two main ones:

- "From a quantitative and thermophysiological point of view, thermal comfort is defined as the condition of thermal neutrality, which corresponds to the dissipation

of heat surplus generated by metabolism. This process can be studied analytically through heat balance formulas.

- From a qualitative and psychological point of view, thermal comfort is defined as the mind state that expresses the satisfaction with the thermal environment, which can be investigated empirically via questionnaires (ASHRAE, 2020)."

Therefore, it appears important to accurately quantify human thermal stress in order to be able to compare different thermal environments on a common basis. The different meteorological variables used to describe the climate appeared to bring only incomplete information when considered separately. Therefore, indices taking into account the complete energy transfers between a human body and its surrounding environment were developed and proposed in the literature. Indeed, the human body has a thermo-regulation mechanism which is based on sensible heat exchanges through conduction, convection and radiation, latent and sensible heat through respiration and latent heat through transpiration. However, tens of different indices relying on different sets of meteorological variables and different physiological models can now be found in the literature. Migliari et al. (2022) identified and described the most commonly used thermal comfort indices, especially those that can be calculated with available numerical models. They also proposed a methodology to compare them and select the most adapted ones depending on the context and the objectives. While testing their methodology, they reported that two indices could be appropriate for the outdoor human thermal comfort assessment in the Parisian case study: the Physiological Equivalent Temperature (PET) (Höppe, 1990) and the Universal Thermal Climate Index (UTCI) (Bröde et al., 2012, 2010). Both were found to bring very comparable results and to be strongly correlated even in very contrasted climates. Zare et al. (2018) analyzed a 1 year data set collected in Kerman, Iran (BSk arid climate) whereas Matzarakis et al. (2015) used ten years of hourly data acquired in Freiburg, Germany (Cfb temperate oceanic climate). UTCI appeared to perform slightly better for warm and humid environments, maybe because of its more accurate thermo-physiological model (Fiala multi-node model) (Staiger et al., 2019). The UTCI therefore appears to be a very good solution for the assessment of outdoor human thermal stress in cities.

The calculation of the UTCI is based on a polynomial regression taking into account the detailed thermophysiological UTCI-Fiala model (Fiala et al., 2012) coupled with a clothing model (Havenith et al., 2012). The concept of UTCI is described in Figure 10.

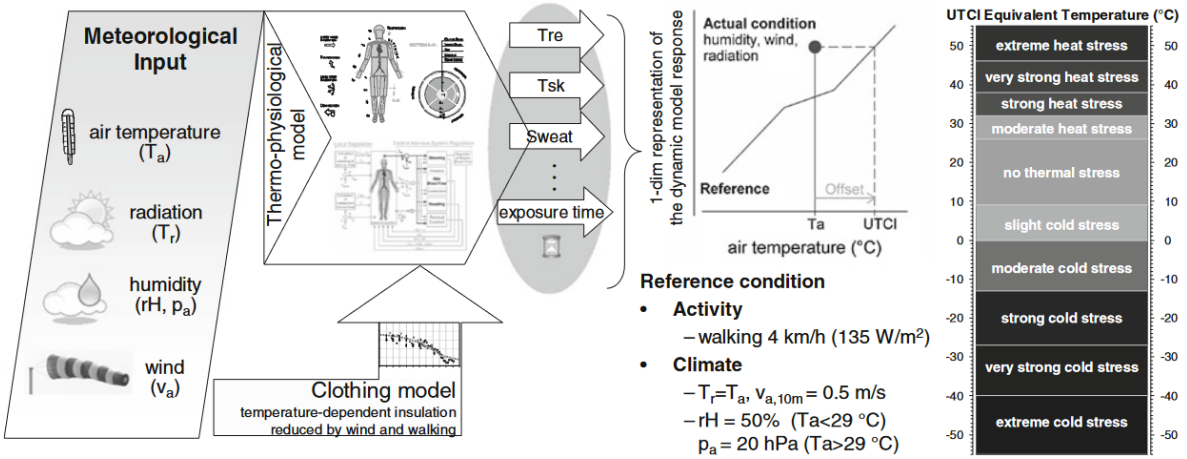

Figure 10: Concept of UTCI proposed by Bröde et al. (2012).

Finally, one of the main interests of the human thermal stress indices is that they enable to study the respective impacts of the different climatic variables on the human thermal stress. In this way, they form useful tools to help urban planners adapt their strategy to improve climate conditions in cities. Bröde et al. (2012) run a sensitivity analysis of the UTCI regarding humidity, wind speed and radiation and they reported among others a strong effect of the all-wave radiation. A 0.27 °C increase of the UTCI was reported for every 1 °C increase of the T_{mrt} - T_a difference whatever be the considered air temperature between 20 °C and 50 °C.

2.1.2. Trees in the soil-plant-atmosphere continuum

Plants, among which trees, are composed of three organs enabling them to run multiple interactions with their surrounding environment: leaf, stem, and root. Such interactions are closely related to their metabolism.

One of the main characteristics of trees is that they are autotrophic organisms which means that they produce their own biomass to create new tissues and grow. To do so, they rely on a process called photosynthesis, a biological process using radiation energy to drive energy-requiring cellular processes (Blankenship, 2021). Photosynthesis requires light energy, carbon dioxide and water as inputs and results in the production of glucose, dioxygen and water. It then directly depends on the supply of radiation energy, water and carbon dioxide (Stirbet et al., 2020).

Photosynthesis comes with a closely related process called transpiration. Indeed, the photosynthetic reaction requires water which is uptaken in the soil through the roots of the trees and releases water vapor through the leaves.

Plants perform at the same time a cellular respiration occurring during both daytime and night-time and uses dioxygene to convert the glucose produced by the photosynthesis to energy used for all the energy-requiring processes occurring in the cells. The radiation energy that was transformed and stored in the form of glucose through photosynthesis is then used for the growth and other life processes of the plant through respiration (Whiting et al., 2023).

2.1.2.1. Leaves and radiation interception

The photosynthesis may be performed by different pigments which are able to convert radiation energy into chemical energy useful for biochemical processes. Chlorophyll, the most widespread pigment, absorbs radiation in the visible spectra. This pigment is mainly found in the leaves of the plants which are thus the heart of the photosynthetic activity. Tree leaves are composed of different layers (Figure 11). The central one is called mesophyll and contains various types of cells among which the ones performing photosynthesis which are called chloroplasts for trees relying on chlorophyll to perform photosynthesis. The mesophyll is held in between two layers of epidermis aiming at protecting it from mechanical injuries, water loss or infection. The epidermis is covered with a layer of wax called cuticle also preventing water loss. Leaves are also crossed by veins that connect the mesophyll to the rest of the tree.

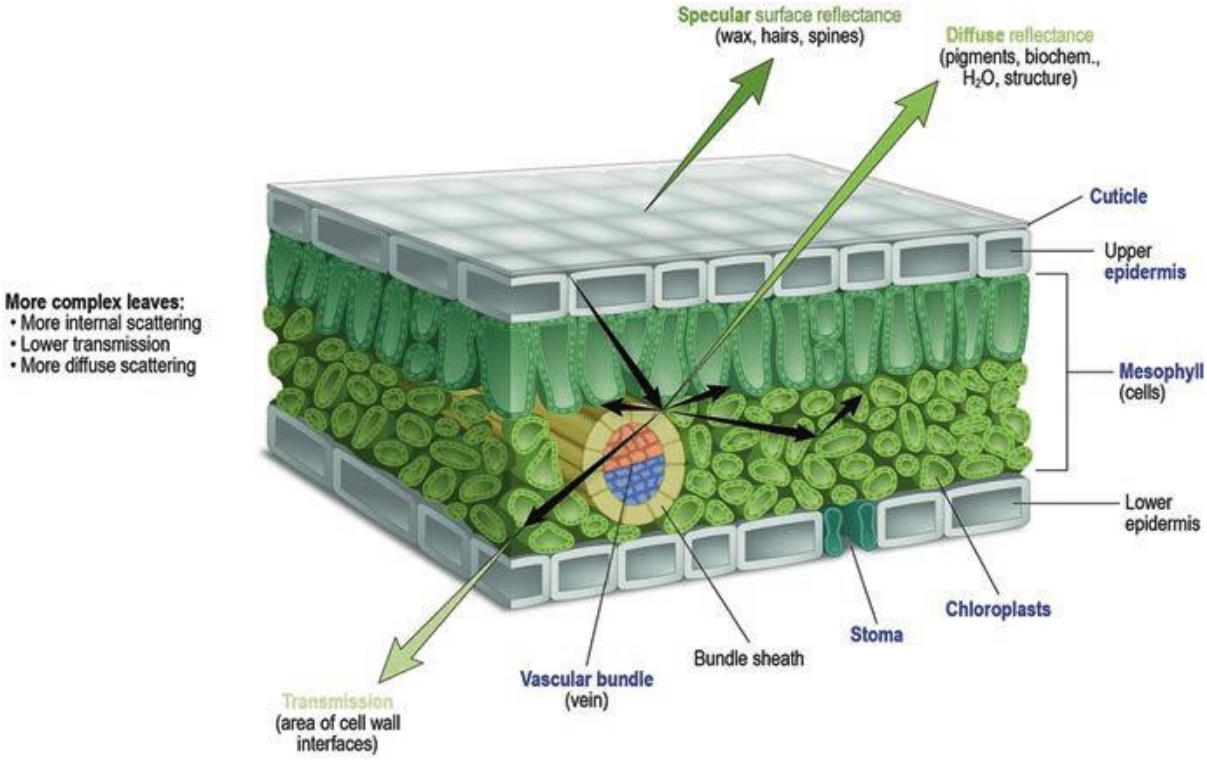

Figure 11: Internal structure of a tree leaf and its interaction with the incident radiation (Serbin and Townsend, 2020).

Thereby, the entire foliage developed by the trees (also called tree crown) aims at receiving the appropriate amount of radiation to enhance photosynthesis. Trees therefore need to maximize both their leaf surface and the solar exposure of their foliage. Although part of the incoming radiation may be transmitted through the tissues of the leaf, the rest is absorbed by the chloroplasts or directly reflected at the surface of the leaf (Figure 11) which means that the amount of radiation received under a tree crown is lower than the one received on top of the tree. Trees therefore reduce the amount of radiation reaching their close surrounding environment creating cast shadows meaning that trees may then have a direct impact on the energy balance of their surrounding environment. However, radiation interception provided by trees is likely to depend on various parameters:

- The shadow cast by the tree is directly influenced by simple geometrical considerations which do not depend on the tree characteristics. Indeed, for a given tree, the area and the location of the cast shadow varies throughout the day according to the position of the sun in the sky (Figure 12). The area of the cast shadow will then vary from one day to the next one and no shadow is cast at night.
- The shadow cast by the tree is directly influenced by morphological characteristics as contrasted morphologies may result in contrasted amounts of radiation

intercepted. First, the leaves may be quite diverse in terms of size, shape, inclination respect to the horizontal plane and optical characteristics depending on the considered tree species. Tree crowns may also have contrasted shapes and total leaf surfaces which induces contrasted leaf densities. Different studies reported higher radiation interception rates for trees with higher foliage density (Armson et al., 2013; Rahman et al., 2020). Trees may also have contrasted heights and horizontal developments influencing the dimension of the shadow they cast as illustrated in Figure 12.

- The shadow cast by the tree is indirectly influenced by physiological processes as such processes may impact tree morphology. The total leaf area of trees varies throughout their life and, when considering deciduous trees, throughout their annual vegetative cycle as they lose their entire foliage from autumn to spring. Then biotic and abiotic factors may induce physiological responses influencing the dynamic of the vegetative growth as well as the traits of the leaves. For instance, it is easy to notice that the light access influences leaves' characteristics as lower canopy leaves generally tend to be smaller and provide a lower photosynthetic rate compared to leaves well exposed to sunlight on top of the canopy (Serbin and Townsend, 2020).

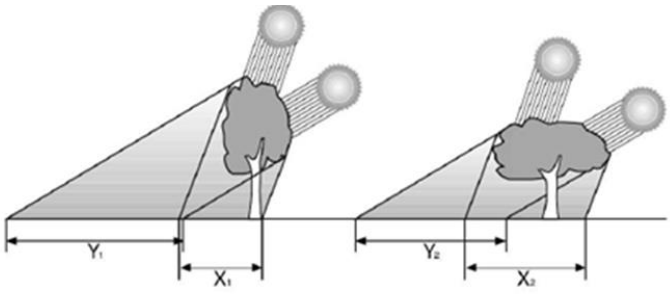

Figure 12: Theoretical influence of the position of the sun, crown shape and tree height on the shadows cast by trees (Bouyer, 2009). X: length of the cast shadow for a low solar angle, Y: length of the cast shadow for a high solar angle.

The intensity of the radiation interception may also depend on the considered wavelength. Indeed, only part of the entire range of wavelengths emitted by the sun is useful for photosynthesis. The entire visible range (0.4-0.7 μm) highly contributes to photosynthesis and is generally called photosynthetically active radiation (PAR) (Figure 13). Part of the near infrared (up to 1 μm) also contributes to photosynthesis but most organisms cannot use the wavelengths greater than 0.7 μm and no organism able to use wavelengths greater than 1 μm has been discovered so far, probably because infrared light has a lower energy content and is then less efficient for the supply of the photosynthesis (Blankenship, 2021). Thus, although

most tree species may provide a high interception of the radiation associated to the visible spectra (associated to a high amount of energy), their interception in the close infrared may differ resulting in varying qualities of radiation transferred under the tree canopies.

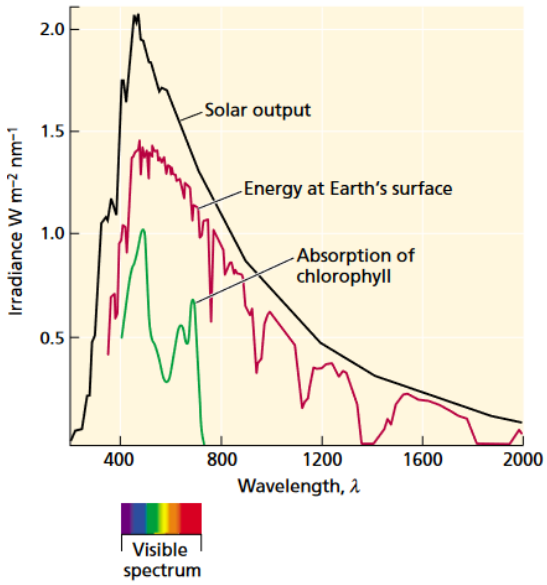

Figure 13: Solar irradiance spectra (wavelength in nm) emitted by the sun and received above the earth's atmosphere (black line) as well as at the earth's surface after being partly absorbed by the molecules of the atmosphere (red line) and absorbed by chlorophyll pigments (green line) (Taiz and Zeiger, 2002).

The photosynthesis process, which mainly occurs in the leaves, also implies gas exchanges between the plant and its surrounding atmosphere. Therefore, leaves are also composed of small orifices called stomata which can be found on either one (generally the downfacing side) or both sides of the leaves where such gas exchanges can happen (Taiz and Zeiger, 2002). The number of stomata per unit of leaf area may vary for different tree species. These stomata are used for the carbon dioxide and dioxygene exchanges involved in the photosynthetic process as well as the water vapor release induced by the transpiration. Stomata may be more or less open. The opening of stomata is managed by specific cells called guard cells and can be quantified through the measurement of the stomatal conductance. The higher the conductance, the more open the stomata. Stomatal conductance is highly driven by different factors such as the vapor pressure deficit of the atmosphere surrounding the leaf, the leaf temperature and the radiation reaching the leaf. The effect of such factors will be presented more accurately later on in section 2.1.2.4.

2.1.2.2. Roots

The interface between the trees and the soil is ensured by a network of roots which have different functionalities. They are supposed to anchor the entire tree in the soil in order to ensure that it is able to develop its aerial organs (trunk, branches and leaves) while enabling the tree to stand and resist strong winds for instance. Then, the roots are supposed to uptake in the soil the water which is essential for the photosynthetic metabolism. To do so, roots bear root hairs, microscopic extensions of their epidermal cells, which highly increase the surface area of the root system and therefore the interface between the roots and soil particles (Figure 14).

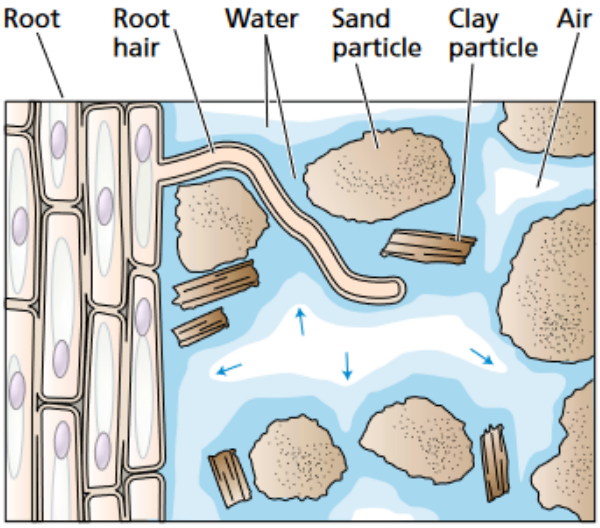

Figure 14: Drawing of a root and a root hair in contact with soil particles (Taiz and Zeiger, 2002).

By that means, roots also enable the trees to absorb nutrients and minerals contained in the soil which play a key role in their metabolism. Such nutrients, among which phosphorus or potassium are uptaken in the form of inorganic ions in solution in the soil water. They are then transported to different parts of the plant where they are involved in multiple biological functions such as the formation of organic compounds used for plant structure, energy storage or electron transfer reactions.

Different types of roots organization may exist (Atger, 2015; Syndicat intercommunal de la vallée de l'Orge Aval, n.d.) and are likely to depend on the depth and texture of the soil. It is also generally admitted that soils which are too compact may be less suitable for root growth while soils which are too loose may not offer a sufficiently strong anchorage for high trees.

2.1.2.3. Trunk and branches

Between these underground and overground compartments, the trees are composed of stems. The main one, also called the trunk, starts from the soil, is directly connected to the root system and bears all the other stems which are called branches and bear the foliage of the tree. The stems are also often called axes and are given an order which represents their location in the tree architecture. The trunk is the only axis of order 1 as it bears all the branches. The branches directly born by the trunk are axes of order 2, and so on. The stems are composed of the following elements (from the edge to the center) as illustrated in Figure 15:

- The bark which is meant to protect the other elements from the outside environment and from eventual damages.
- The phloem, a network of vessels aiming at transporting the products of the photosynthesis, also called elaborated sap, from the leaves to the different organs of the tree.
- The cambium which is where the radial growth of the stem takes place. The cambium is the zone between the phloem and xylem where the tissues of both the phloem (towards the edge of the stem) and xylem (towards the center of the stem) are created.
- The xylem, a network of vessels aiming at transporting the water which is uptaken from the soil, also called raw sap, through the roots up to the leaves where it is used by the photosynthesis process. A new ring of xylem vessels is created every growing season and actually in use. The xylem rings of the previous growing seasons turn into wood and form the rigid structure of the stem and of the entire tree.

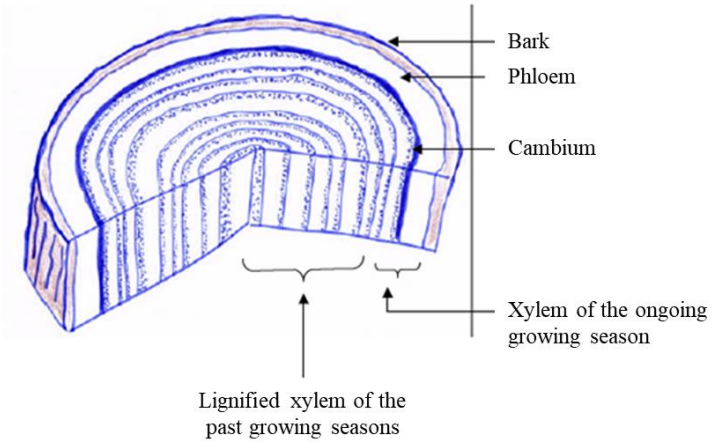

Figure 15: Cross-section of the trunk of a tree adapted from Syndicat intercommunal de la vallée de l'Orge Aval (n.d.).

2.1.2.4. Water fluxes and transpiration

Water plays an essential role in the life of plants, especially as it is involved in the photosynthetic process. The amount of water required is very important as it has been estimated that the formation of 1 g of organic matter by a plant may require up to 500 g of water (Taiz and Zeiger, 2002). Water is also vital for the plant cells as it creates an internal hydrostatic pressure, called turgor pressure which is essential for the rigidity and mechanical stability of the trees' tissues. Turgor pressure is also essential for many physiological processes such as cell enlargement, gas exchanges in the leaves, transport in the phloem and multiple transport processes across membranes (Taiz and Zeiger, 2002).

Trees are composed of an entire hydraulic system enabling to drive the water extracted from the soil from the roots up to the leaves where photosynthesis occurs. This hydraulic system therefore connects the water in the soil to the water in the atmosphere which are both exposed to contrasted tensions.

In the soil, the water is withheld into the porosity of the particles at a certain water potential (Ψ_{soil}, expressed as a pressure) which depends on the water availability. In the leaves, the water brought by the stem is directly exposed to the outside atmosphere when the stomata are open. The atmosphere contains water in the form of water vapor but is generally not saturated which means that it can still receive some more water. The water content of the atmosphere is characterized by the relative humidity as well as the vapor pressure deficit (VPD) (also expressed as a pressure). The water potential in the atmosphere (i.e. VPD) is generally much lower than the water potential in the soil, thus, a strong gradient exists between the soil and the atmosphere (water potential is decreasing when traveling from the roots to the leaves) which constitutes the driving force enabling the water taken in the soil to travel up the long-distance ascending transport system formed by the tree (Figure 16). Water moves towards regions of low water potential and purely in response to physical forces.

The amount of water in the soil that a tree is able to collect is called the Total Available Water Storage (TAWS) and is defined by two soil volumetric water content (VWC) limits called field capacity and permanent wilting point. The field capacity is related to the texture of the soil and is generally associated to a water matric potential of approximately -0.033 MPa (Cassel and Nielsen, 1986; Bouthier et al., 2022). The permanent wilting point, depends on the soil texture but may also strongly rely on the considered plant. Then, the TAWS is generally divided into a Readily AWS (R-AWS), where the plant is supposed to experience a comfortable access to water, and a Non-Readily AWS (NR-AWS) where pumping water may be more

difficult for the plant which is likely to experience hydric stress. The location of the threshold delimiting the R-AWS and the NR-AWS may vary depending on the considered tree species. As an example, R-AWS corresponds to approximately 50 % of the TAWS for apple trees while it could reach 70 % of the TAWS for conifer trees (FAO et al., 2006).

Then, the water brought by the stem to the stomata evaporates into the atmosphere and progressively spreads outside of the leaves through the stomata while new water is being brought from the stem.

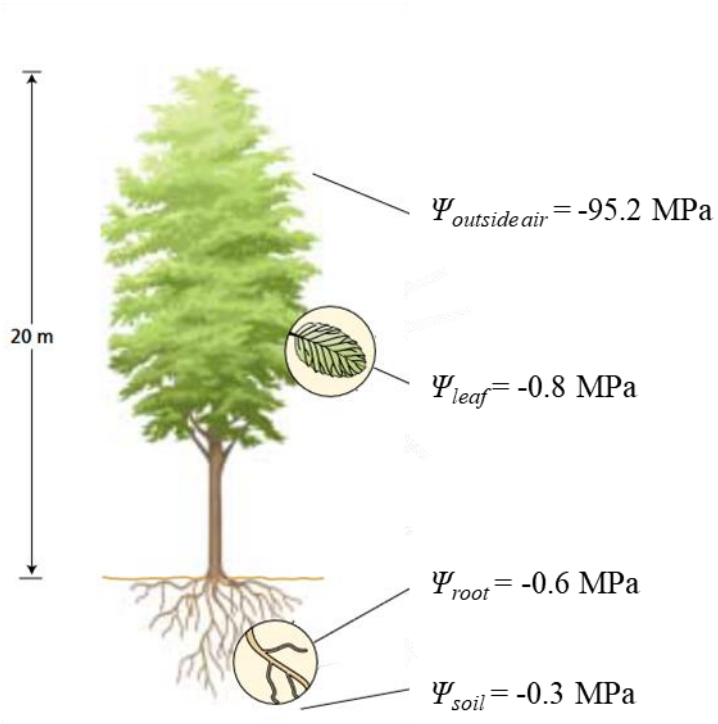

Figure 16 : Representative overview of the water potential at various points in the transport pathway from the soil through the plant to the atmosphere (adapted from Taiz and Zeiger (2002)).

The release of water into the atmosphere through the leaves is called transpiration and has another main interest: it is involved in the thermal balance of the leaves. The evaporation of the water contained in the stomata is an endothermic transformation uptaking energy contained in the surrounding atmosphere which contributes to cooling down its temperature. Therefore, transpiration is a way to dissipate the heat gained by the leaves when exposed to sunlight. Although the leaves can also dissipate part of this energy through sensible heat fluxes (emission of LW and convection with the surrounding atmosphere), the evaporation of water in the stomata of the leaves is responsible for an important latent heat flux especially as the amount of water transpired is very important. Indeed, it is generally admitted that more than 90

% of the water extracted from the ground is transpired (Taiz and Zeiger, 2002). If transpiration is stopped while the leaves are still exposed to sunlight, leaves are then very likely to warm up.

The transpiration rate of trees may be impacted by various factors. First, the total leaf area born by a tree is adjusted to maximize photosynthesis but an increasing amount of leaves also increases the gas exchanges with the surrounding atmosphere which enhances transpiration. Rahman et al. (2015) for instance, found higher transpiration rates for tree species with higher foliage density. Also, transpiration may be highly variable over a single day as it is ruled by the stomata opening. Rahman et al. (2015) also highlighted the link between stomatal conductance and transpiration. Indeed, transpiration is by nature tightly related to photosynthesis which is why it is generally low or null at night. During night-time, the photosynthetic activity is not possible as there is no radiation and there is no use to uptake carbon dioxide from the atmosphere nor to cool down the leaves. Stomata are then generally closed which at the same time prevents useless loss of water. However, some studies reported non-null night-time transpiration for various tree species. Although the night-time transpiration was low compared to the daytime one, it was not negligible. Vialet-Chabrand (2013) reported high stomatal conductance even at night for multiple species and noted a high intra and inter-specific variability. VPD, temperature and wind speed were supposed to be the main drivers of tree transpiration at night.

During the day, the stomata opening is ruled by different factors which were ranked by decreasing magnitude by Vialet-Chabrand (2013) as follows: leaf water potential, VPD and radiation. When leaf water potential strongly decreases, the stomata may remain closed even during daytime or they may close earlier than usual which directly limits or stops the transpiration rate. Water availability is then the main limiting factor. When stomata are open, the transpiration rate is then mainly influenced by the meteorological conditions among which VPD is one of the main drivers. The VPD characterizes the dryness of the atmosphere. An increase of the VPD expresses a dryer atmosphere which induces a higher vapor pressure gradient between the atmosphere and the leaves and induces a higher transpiration rate. Then, the amount of radiation received by the leaves is the second driver of tree transpiration especially as it increases the leaf temperature and enhances the need for water evaporation for the leaf cooling. Litvak et al. (2017) performed continuous measurement of the daily tree transpiration of well-watered trees from 14 different tree species during 2 years and highlighted the proportionality between tree transpiration and ET_{ref}, incoming solar radiation, and VPD.

Climatic conditions are highly variable even during a single day. The amount of radiation received by the leaves is highly driven by the sun's cycle but also highly depends on

the cloud cover which may be highly variable and induces very quick changes of incoming radiation. Leaves may then be exposed to important direct radiation coming from the sun and then shaded by clouds from an instant to the next one. They are then permanently adjusting their stomatal conductance to fit to the changing conditions. The stomatal conductance is therefore almost continuously varying especially as its time response is not negligible.

Tree transpiration can be assessed by using different techniques (Rahman and Ennos, 2016). It is first possible to assess the transpiration at the leaf scale by using the Fick's law, described in equation (7), as performed by Rahman et al. (2015). The entire tree transpiration can then be estimated by multiplying this value by the total leaf area of the tree but the representativeness of the stomatal conductance measurement carried out on a sample of leaves may be discussed as leaves with contrasted irradiance may have very different stomatal conductance.

$$E = g_{Vtotal} . \frac{(e_{leaf} - e_a)}{P_a} \quad (7)$$

With E, the transpiration rate ($mmol.m^{-2}.s^{-1}$), g_{Vtotal} the stomatal conductance ($mmol.m^{-2}.s^{-1}$), e_{leaf} the vapor pressure inside the leaf which can be considered equal to the saturation vapor pressure at the leaf temperature (Pa), e_a the vapor pressure of the atmosphere (Pa) and P_a the atmospheric pressure (Pa).

To estimate the transpiration at the tree scale, some authors proposed to perform sap flow measurements (Burgess and Dawson, 2008) such as Caspari et al. (1993) who used the heat pulse method consisting in the insertion of two pins inside the tree trunk, one being heated and the second one measuring the evolution of temperature. If the area of the water conductive tissues has been previously estimated, for instance after sampling the core of the tree trunk, the entire water fluxes and therefore the transpiration can then be estimated. Other works performed water balances on the soil compartment for instance with continuous weighing of the studied trees (Caspari et al., 1993) or by using lysimeters. Finally, FAO et al. (2006) propose a more energy-based approach by computing ET_{ref}, for instance with the Penman-Monteith equation, and to adjust it with a crop coefficient (provided by the FAO for different types of plants) and a water availability coefficient. These coefficients also take into account the development stage of the crops, however, this technique is better suited in an agricultural context for irrigation scheduling and appears not to be well adapted to urban plants and urban trees especially as the foliage development of the urban trees may be highly influenced by the urban geometry and the trimming rules which means that their dimensions are likely to be different to what they would be in a natural context (Litvak et al., 2017).

2.1.2.5. Growth & phenology

The growth dynamic of trees is generally composed of different phases. Considering deciduous broadleaved trees which are commonly found in temperate climate cities, the growth process starts in spring with the formation of leaves which enable the photosynthetic process to start. The growth rate increases and reaches its maximum value during summer before slowing down and stopping in autumn (AURAV, 2020). At this time of the year, deciduous trees lose their leaves to prevent frost-induced injuries and also because winter, besides being characterized by low temperatures, also comes with less solar radiation.

The phenology of the trees may depend on the considered tree species as well as on the climatic conditions. Indeed, a warmer end of winter or spring may for instance lead to an earlier formation of the leaves. The ongoing climate change, which comes with warmer winters, therefore already affects the phenology of trees. The more frequent warm springs induce for instance an earlier start of the growth of trees while frost is still likely to occur which endangers the trees.

Focusing on the stems, the growth is composed of two phases. The first one, called primary growth, concerns the elongation of the axes. The second one, called secondary growth, concerns the radial growth, i.e., thickening of the stems. This radial growth takes place in the cambium area of the stems, as previously explained in section 2.1.2.3, where both the xylem and phloem vessels are created. Every year, new xylem vessels are created to transport raw sap (i.e. water uptaken in the soil). Only the vessels of the current year are used for transportation. Vessels of the previous years turn into wood and are not in use anymore. Therefore, when cutting a tree stem along its section, concentric rings formed by the yearly xylem vessels can easily be noticed and distinguished because the tree produces wood with varying color all year long (the color is lighter during spring and darker during fall which makes it easy to distinguish the different rings). Each ring is associated with one year of vegetative growth, which makes it possible to evaluate the stem age by counting the number of rings. When considering the tree trunk, it is then possible to evaluate the age of the entire tree and also to estimate the growth rate of the trees by dividing the total radius by the number of rings. However, a non-negligible variability may exist between individuals. In Paris, a dendrochronological study carried out by Renard (2020) in 2019 focused on core samplings of 80 *Tilia spp.* trees and reported that younger trees had higher growth rates than older ones. They also showed that diameter at breast height (DBH), which is often measured to estimate the age of trees, could provide wrong estimations as trees of the same age (determined by counting the number of rings inside their trunk) could have very contrasted DBH. Many factors may influence the growth rate of trees

and some studies have tried to relate the dendrochronological analysis to the variability of the yearly climatic conditions.

2.1.2.6. Stem Diameter Variation

Dendrochronology is an invasive technique and it can only provide analysis at a yearly time step. To overtake these issues, other growth monitoring techniques such as the measurement of stem diameter were developed, some of them, like microdendrometers (Adam et al., n.d.), enabling to monitor the stem diameter at a very low time step (e.g. 10 minutes) with a high precision (0.5 μm). Figure 17a illustrates the evolution of a stem diameter during an entire year monitored with a microdendrometer. The different phases of tree growth described in the previous section can easily be noticed. During winter (i.e. from November to February considering the northern hemisphere), the diameter of the axis remains stable because the tree is in the dormancy phase. Between the end of winter and the beginning of spring, new leaves develop on the tree branches enabling the pressure gradient inside the tree to come back and the photosynthetic activity to start again. The growth of the axis diameter starts and lasts until autumn. In this season, while air temperature and daily insolation start to decrease, leaves start to fall and starch formed in the tissues is progressively turned into soluble sugar which provides the tree with resistance to frost.

When zooming on the diameter variation, daily oscillations of the diameter of the stem can easily be noticed (Figure 17b). It is considered that they are caused by different processes occurring at the same time (Daudet et al., 2005):

- The water transport inside the vessels induces a variation of the water content of the tissues which takes the form of a reversible swelling and shrinkage of living and dead tissues.
- The formation of new xylem and phloem tissues which induces an irreversible growth.
- The dilatation of the tissues due to the temperature variations.

When the trees are in dormancy, the water fluxes as well as the formation of new tissues are stopped. The eventual variations of axis diameter are then likely to be caused by the dilatation of the trees' tissues due to the daily variations of air temperature. Starting from spring and the formation of new leaves, the irreversible growth starts again and can be noticed through the general increase of the stem diameter. The water fluxes also start again and induce strong daily variations of the stems' diameter. During daytime, the amount of water transpired by the

trees may be higher than the amount absorbed from the ground. In this case, the tree uses water contained in its own stock (i.e. the water contained in its tissues) to keep transpiring which induces a shrinkage of its tissues and a reduction of the stems' diameter. During night-time, while the transpiration is low or null, the water absorbed by the roots can be used to refill the tissues of the trees which induces an inflation of their axes (Dietrich et al., 2018).

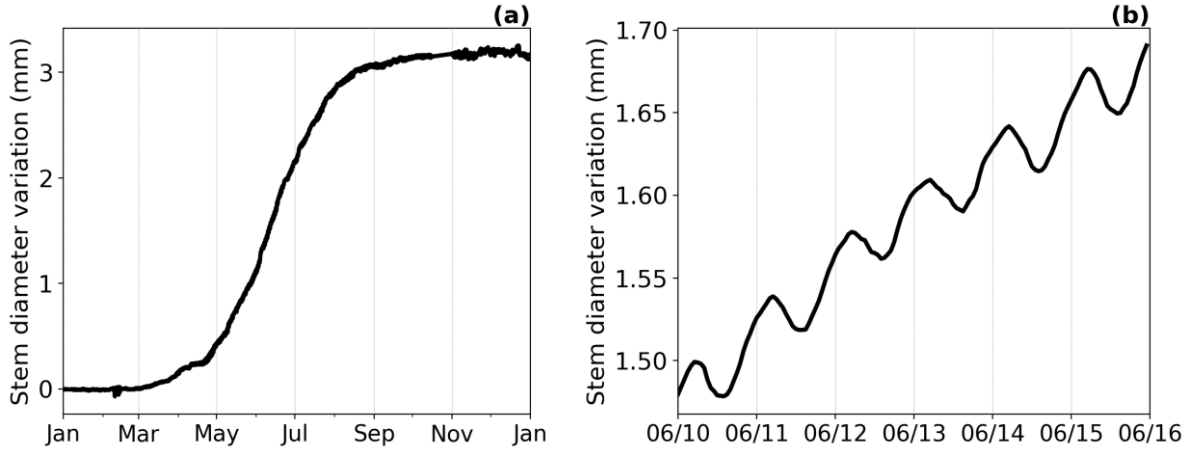

Figure 17 : Typical stem diameter variation of a tree (a) over an entire growing season and (b) over a few summer days.

Different sources of variability may however influence the stem diameter variations. First, some studies tried to investigate the variability that may exist between the different stems of a same tree. Most of them reported similar temporal patterns of stem diameter variation when comparing different locations on the trunk and different branches (Ueda et al., 1996; Daudet et al., 2005; Corell et al., 2014). Some works highlighted a faster growth and higher daily amplitudes close to the basis of the trunk (Daudet et al., 2005). Others reported temporal delay when comparing the maxima and minima for different parts of the trees (Dobbs and Scott, 1971; Ueda et al., 1996), including branches, which appeared to be linked to the respective solar exposure of each branch. Burgess and Dawson (2008) observed that daily maximal values were reached in the morning for East-facing branches and in the afternoon for West-facing branches. This is consistent with the fact that branches having a high exposure are characterized by a high stomatal conductance and important water fluxes.

The age and the species of the considered trees may also induce variability of the stem diameter variations, especially as the proportion of dry and wet tissues may vary (Taiz and Zeiger, 2002), however, it is not clear how the different types of tissues of the stem contribute to the overall stem diameter variation (De Swaef et al., 2015; Dietrich et al., 2018). In this way, the comparison of the absolute stem diameter variations of different individuals is not trivial. Therefore, some works proposed to compute normalized diameter variations for instance by

dividing the absolute variations by the overall maximum diameter measured during the measurement period (Dietrich et al., 2018).

Nonetheless, stem diameter variations are considered as a good indicator for the monitoring of the tree growth and water fluxes and have also been used to schedule irrigation events and monitor the response of trees to external stress such as decreasing water availability (De Swaef et al., 2015).

2.1.2.7. Trees in cities

Cities are very different from the natural environment of trees. Thereby, urban trees and especially alignment trees generally have to face multiple obstacles that may affect their health and development.

Street trees are most of the time planted in low volume pits (generally around 10 m^3 (Bonnardot, 2020)) especially because urban soils already host a lot of networks for gas, water, electricity, etc. Combined with the generally high density of the urban soils which have to bear the weight of multiple human constructions, the development of the root system is constrained which limits the anchorage of the trees in the soil as well as the volume of soil they can prospect to find water. In addition, tree pits are generally sealed with metal railings, stabilized soils or pavement and their open surface is generally small which limits the amount of rainfall entering the pits (Fini et al., 2022). Street trees therefore may have to face low water availability because rainwater is their main source of water as they are generally not irrigated except in some cities like Paris during the first three years following their plantation to ensure a good adaptation to their new environment.

A low development of the root system is also likely to limit the development of their aerial organs which, in cities, is also constrained by the surrounding buildings. The tree crowns have to fit in a limited aerial volume and are generally regularly pruned by the cities' green spaces services to avoid branches falling or branches hitting some building or other human construction (AURAV, 2020). The effect of soil sealing on the development of trees was evaluated in different works such as the one of Yu et al. (2018) who reported that highly sealed conditions led to significantly lower leaf area and a higher exposure to water stress compared to trees grown in unsealed soils such as parks. Renard (2020) highlighted a higher growth rate for trees planted in vegetated tree pits and in pits sealed with stabilized soil compared with trees planted in pits sealed with concrete for *Tilia spp.* grown in Paris, France.

The surrounding buildings also reduce the amount of solar radiation reaching the tree crowns which is likely to limit their photosynthesis activity. Higher growth rates was for instance observed by Angeniol and Dianoux (2023) and Renard (2020) comparing *Tilia spp*. and *Platanus x hispanica* grown in parks and in streets in Paris.

In cities, trees are also exposed to high pollutants concentration and it has been reported that a repeated exposure to pollutants may lead to partial leaf necrosis, leaf color loss, defoliation or general weakening of the tree (Syndicat intercommunal de la vallée de l'Orge Aval, n.d.).

The selection of trees for urban plantation is therefore very complex, especially because it is generally supervised by various services of the same city council which may have different goals. Not only do the selected trees have to resist the hard urban conditions, they have to comply with multiple other criteria among which the absence of production of toxic fruits or fruits that could easily get the street surfaces dirty, the absence of production of allergen substances or aesthetics considerations, especially in historical districts.

2.1.2.8. Water and heat stress

The description of the metabolism of trees proposed in the previous sections highlighted the crucial role of water. Thereby, the lack of water has long been known to be one of the main limiting factors of plants growth and development. It is also known to endanger plant's health and is therefore very likely to impact the climatic benefits provided by urban trees.

When soil moisture decreases, Ψ_{soil} also decreases towards more negative values. Such a decrease was for instance accurately reported by some works who measured Ψ_{soil} at different depths for *Prunus dulcis* (Nortes et al., 2005). In order to maintain the water potential gradient which is necessary to drive the water through their stems, the trees have to progressively dry their tissues to decrease their water potential. Several works studied the evolution of the stem water potential of trees experiencing a water deficit. Ebel et al. (1995a, 2001), Girona et al. (2010) and Osroosh et al. (2016) all studied apple trees (*Malus domestica*) and found very consistent values ranging from - 0.8 MPa to - 1 MPa for control well-watered trees, from - 1.5 MPa to - 2 MPa for the same trees experiencing a moderate water stress and from - 2 MPa to - 2.8 MPa for trees experiencing a severe water stress. Ebel et al. (1993) also measured the leaf water potential for *Malus domestica* experiencing contrasted access to water. They measured - 1.5 MPa for well-watered trees and - 2.5 MPa for water stressed trees. Rapoport et al. (2004)

studied *Olea europea* and measured a - 1 MPa leaf water potential for well-watered trees and - 3.1 MPa for water-stressed trees.

However, trees can only decrease the water potential of their tissues down to a lower limit called the permanent wilting point. Below this point, water is still present in the soil but it is held too tightly in the porosity of the soil and trees cannot apply a sufficient suction to uptake it. Indeed, the high tensions applied to the water contained in the xylem may lead to the formation of gas bubbles, a phenomenon called cavitation. Such bubbles break the conductivity of the water column which prevents the water from flowing in the xylem. This phenomenon, called embolism, may cause the dehydration and death of the tree (Taiz and Zeiger, 2002). The water potential therefore forms a useful indicator of the water stress experienced by the trees especially as it influences different processes such as cell growth and photosynthesis (Taiz and Zeiger, 2002).

In order to cope with droughts, trees can adopt different responses (Cochard and Granier, 1999; Lecoeur, 2007; Brendel and Cochard, 2011). First, they may reduce their stomatal conductance which limits the loss of water through transpiration and the decrease of the leaf water potential. However, the stop of transpiration is likely to lead to leaf overheating and stomatal closure also prevents the CO_2 intake from occurring, which stops the photosynthetic process. Significant decreases of stomatal conductance were reported during a dry period for different tree species (Caspari et al., 1993; Konarska et al., 2016). Some studies even observed correlations between stomatal conductance and stem water potential for apple trees (Ebel et al., 1995b; Naor, 2000). However, a high variability of the stomatal response may exist within and between tree species.

The decreasing water content in the trees may also lead to a decrease of the turgor pressure which gives rigidity to the trees' tissues. Such a turgor pressure loss may first induce the wilting of the leaves which may slightly reduce their solar exposure, heat stress and water loss through transpiration and then to leaf fall which leads to a reduction of the total leaf surface of the tree. Such phenomena are easily observable during summer droughts. In Paris, France, a significant leaf loss was observed during the dry summer of 2022 for both *Platanus* and *Aesculus* trees starting from August, which is one month earlier than during a regular summer (AFP, 2022). The loss of turgor pressure may also affect other physiological processes such as cell division and enlargement, two mechanisms which are necessary for stem elongation, leaf formation and expansion (Taiz and Zeiger, 2002). Both the growth rate and the overall aerial morphology of the trees may then be impacted. The smaller resulting leaf area induces lower transpiration need, which slows down the decrease of the soil water stock.

The water stress may also induce an adaptation of the root system. As the soil dries, roots are likely to extend deeper and far from the trunk to prospect for wetter zones (Taiz and Zeiger, 2002).

Water stress can then have strong impacts on both plant physiology and morphology characterized by contrasted temporal responses (Brendel and Cochard, 2011). The stomatal closure can be noticed from one day to the next one (Zweifel et al., 2007) whereas morphological adjustments may take several weeks. These different mechanisms may also be combined and form part of larger strategies to resist drought. When comparing the behavior of different trees experiencing droughts, it has been reported that two main strategies may exist (Dervishi et al., 2023):

- Drought stress avoidance (isohydric species): the trees close their stomata quickly when the water deficit appears in order to limit the drying of their tissues.
- Drought stress tolerance (anisohydric species): the trees maintain their stomata open to keep biomass production running but this may lead to the drying of the tissues as the trees keep transpiring. Some adaptations may be needed such as reduction of the leaf area or osmotic adjustments aiming at avoiding excessive turgor pressure loss. This strategy may expose the trees to an important decrease of their stem water potential, which may lead to cavitation and embolism.

The different strategies and mechanisms described hereinabove naturally have a strong impact on tree transpiration which has already been reported in the literature as reviewed in the next section. The regulation of the transpiration and the leaf surface temperature is also related to another potential abiotic stress threatening the trees: heat stress. Indeed, most of the hydrated trees tissues, among which leaves, cannot survive when exposed to temperatures higher than 45 °C (Taiz and Zeiger, 2002). Yet, the intensification of heatwaves increases the exposure of trees to air temperatures higher than 40 °C. If such periods are combined with low water availability and reduction of transpiration, leaf surface temperature is likely to rise up to extreme values endangering the tissues. Visual damages have been reported on leaves when trees were exposed to very high temperatures.

2.2. Literature review

Many works already studied the influence of street trees on different climatic variables and different approaches have been used to cope with the high diversity of existing urban configurations and study the high number of variables which is involved.

Some studies quantified their radiation interception and reported from 55 % to 90 % interception of the incident solar radiation (Heisler, 1986; Kotzen, 2003; Shahidan et al., 2010; Konarska et al., 2014; Rahman et al., 2020). As a consequence, important surface temperature reductions ranging approximately from 9 °C to 20 °C were measured comparing shaded and non-shaded surfaces for different tree species (Kotzen, 2003; Armson et al., 2012, 2013; Rahman et al., 2020). Yet, this wide range of surface temperature reduction may come from the fact that the studied surfaces may be composed by different materials which behave differently when exposed to the sun (Rahman et al., 2020).

Thereby, the trees induce a reduction of the radiation fluxes in their shade which was highlighted by the measurement of diurnal reductions of globe temperature (Rahman and Ennos, 2016). Armson et al. (2012) found from 5 °C to 7 °C reduction and Armson et al. (2013) reported an average 4 °C reduction comparing 5 different tree species. As a consequence, mean radiant temperature is also strongly reduced in the shade of trees as highlighted by Rahman and Ennos (2016) in their review which reported T_{mrt} reductions averaging 25 °C.

Some studies compared different tree species and tried to related the differences of climatic benefits they observed to morphological characteristics of the trees. A significant influence of the Leaf Area Index (LAI) on the interception of incident solar radiation was found by Shahidan et al. (2010) who compared two tree species while Armson et al. (2013) reported a positive correlation between LAI and surface temperature reduction by comparing for instance 5 tree species. Gillner et al. (2015) compared 6 urban tree species and reported that high leaf area densities and high rate of transpiration were associated with higher air temperature reduction. Rahman et al. (2020), in their review, identified crown density as having the main effect on the climatic benefits provided by the trees. Indeed, they reported that the surface temperature in the shade of trees decreased almost linearly with increasing crown density. Higher LAI was also found to be related to higher transpiration rates by Rahman et al. (2015) although transpiration may be highly variable over a single day as it is ruled by the stomata opening. However, a general lack of data concerning the morphology of urban trees was pointed out (Musy, 2014; Rahman and Ennos, 2016; Rahman et al., 2020) especially as such

information are often difficult to obtain which means that further assessments of the influence of morphological characteristics on the climatic benefits are required.

A variety of diurnal air temperature reductions beneath tree canopy compared to reference open areas can also be found in the literature (Rahman and Ennos, 2016), ranging from 0.7 °C (Souch and Souch, 1993) to more than 5 °C (Vailshery et al., 2013). Coutts et al. (2016), for instance, compared 3 canyon streets with different tree coverage and reported a maximum air temperature reduction reaching 1.5 C. They also assessed human thermal stress through the calculation of UTCI and reported a strong reduction of the heat stress from the very strong heat stress category (UTCI > 38 °C) to the strong heat stress category (UTCI > 32 °C) in a treed street compared to a non-treed one. This UTCI reduction was observed at different times over daytime depending on the respective positions of the trees and weather stations. They attributed this human thermal stress decrease to a large reduction of mean radiant temperature as they reported higher mean radiant temperature in the streets containing fewer trees during the day. Conversely, they found out that mean radiant temperature was lower in the studied open street compared to the treed street at night. Such observations suggested that the presence of trees decreased the SVF and by the way the nocturnal cooling of the treed street through LW fluxes. Some works also pointed out that the effect of street trees on air temperature and human thermal stress was very localized and was decreased in narrow and deep canyons due to the shadows already cast by the surrounding buildings (Musy, 2014; Coutts et al., 2016). Their observations therefore suggested a strong spatial and temporal variability of the climatic benefits.

The assessment of the dynamic and the spatial extent of the climatic benefits of street trees would require both continuous monitoring and a high density of sensors but very few studies can afford it especially in real urban conditions. Rahman and Ennos (2016) indeed pointed out the dynamic of evapotranspirational cooling over a single day or over a year remained unexplored and that more data should be acquired to understand the influence of the tree coverage, of the position of the trees in the streets, and of weather on their cooling potential. Then, although radiation interception is sometimes considered as the most important factor for human thermal stress reduction, Rahman et al. (2020) pointed out in their review that available studies generally focused either on radiation interception quantification or on transpiration quantification and that a detailed comparison of the contribution of both mechanisms is still needed. The use of experimental reduced scale models may offer a practical solution to these issues. Although the transposition of the results at full-scale is a critical point, reduced scale models are more convenient to perform continual monitoring and allow to control more

parameters such as building heights and surface materials (Hang and Chen, 2022). Herpin et al. (2022) for instance, measured an average air temperature reduction of 2 °C and an average UTCI reduction of 5.3 °C under well-watered trees compared to a non-vegetated zone for 120 studied days with a large panel of weather conditions in a 1/5 scale north-south oriented canyon street. This same experimental device also enabled to estimate that the shade cover effect was responsible for 74 % of the cooling benefits of trees and transpiration for the remaining 26 % (Mballo et al., 2021), in well-watered conditions.

In the meantime, various works have also tried to provide urban planners with recommendations on how to design efficient vegetated areas. Different tools have been developed to simulate the impact of trees on the urban microclimate (Musy, 2014) and to guide urban planning, for example by comparing the effect of different greening scenarios. They generally compared varying tree planting densities (Aboelata, 2020; Aboelata and Sodoudi, 2020; Ouyang et al., 2020; Teshnehdel et al., 2020; Geletič et al., 2022; Gholami et al., 2023; Wang et al., 2022) or tree morphological variables (height, crown projected area, leaf area index) (Meili et al., 2021; H. Liu et al., 2022; T. Chen et al., 2023; Ge et al., 2023) to provide urban planners with advices on the best strategies to design urban green areas. However, these modeling tools mostly consider well-watered vegetation. This is a direct consequence of the lack of experimental data regarding the climatic benefits of street trees under low water availability conditions. Indeed, most studies did not control or did not have any information about the soil moisture or the water status of the trees and most of them pointed out that further works should take into account water stress for a comprehensive estimation of the climatic benefits of street trees. This aspect is crucial especially as street trees are very likely to experience critical soil water potential during multiple months each year as highlighted by Schütt et al. (2022) who monitored the soil water potential inside the tree pits of 17 street trees in 2018-2019.

The effects of the lack of water on the evolution of transpiration and of the related physiological processes have been assessed but the effects on the radiation interception and on the climatic benefits, especially in terms of human thermal stress mitigation, remain widely unexplored.

More precisely, some studies reported correlations between stomatal conductance and stem water potential (Ebel et al., 1995b; Naor, 2000) and other works observed significant decrease of stomatal conductance (i.e. stomatal closure) during dry periods (Caspari et al., 1993; Konarska et al., 2016). Caspari et al. (1993) measured a 25 % to 35 % reduction of tree transpiration comparing trees grown in a soil maintained at 100 % and 50 % of its water holding

capacity for 40 days. Chen et al. (2011) monitored the transpiration of multiple trees and soil water content up to 1 m depth in an urban park during 15 months. Though they could highlight the dominant influence of the vapour pressure deficit (VPD) on transpiration, they could not observe any correlation of the transpiration with soil moisture content especially because they could not measure the water availability in the soil deeper than 1 m under ground level. Litvak et al. (2017) also performed continuous measurement of the daily tree transpiration from 14 different tree species during 2 years and highlighted the proportionality between tree transpiration and ET_{ref}, incoming solar radiation, and VPD but they only considered well-watered trees. Rahman et al. (2011), by comparing urban trees grown in different types of soils with different soil compaction, highlighted a 50 % reduction of tree transpiration during a spring drought. They also reported that trees growing in the less compacted soil had a less negative leaf water potential, a higher stomatal conductance and therefore higher transpiration.

Water stress also appeared to impact the stem diameter variations as this indicator reflects the reversible shrinkage and swelling of tissues caused by water fluxes (Daudet et al., 2005; Nortes et al., 2005; De Swaef et al., 2015; Dietrich et al., 2018). When the amount of water taken from the soil is not sufficient, the plant may use part of the water stored in its tissues to keep transpiring which may lead to the drying of the tissues (Adam et al., n.d.). It is not yet clear how much of the daily transpiration can be attributed to the internally stored water, but various works have already shown that the drying of the tissues of the stems may lead to stem shrinkage. Moreover, Dietrich et al. (2018), calculated the daily maximum shrinkage as the difference between the maximum diameter ever recorded and the daily minimum diameter and reported a very good correlation between this indicator and the leaf water potential for 6 tree species. Stem diameter variation therefore appears to be a good indicator of the water stress experienced by the trees. Améglio and Archer (1996) monitored tree transpiration, sap flow, soil and stem water potential and stem diameter variation for young *Juglans regia*. They compared a tree with high water availability in the soil (irrigated every day) and a tree with decreasing soil water content (not irrigated). They highlighted the decreasing soil and stem water potential which led to a quick decrease (approximately 4 days needed) of the sap flows and a very quick stop of radial stem growth (second to third day of the experiment). At the same time, the daily amplitudes of stem diameter variations increased for the non-irrigated tree which was attributed to a greater use of the water contained inside the tissues of the non-irrigated tree.

In addition, some authors investigated the effect of the lack of water on the leaf surface temperature. Alderfasi and Nielsen (2001) measured significantly different canopy temperatures for irrigated and non-irrigated wheat through infrared thermometer and Gräf et al.

(2021) reported canopies from 6 °C to 8 °C higher for water-stressed plants compared to well-watered ones from 4 species. Given that transpiration enables the plant to cool down its foliage, leaf surface temperature may give useful information about the transpiration status of the plant and also about the complete radiation balance of the plant. In this way, leaf surface temperature is used in the literature as an indicator of plants water stress, for instance under the form of the crop water stress index (CWSI), a tool which has been developed among others for crop management (agriculture) to schedule irrigation (Jackson et al., 1981).

Finally, the impact of heatwaves on plants appears to have been mainly studied in the frame of crop productivity. Among the studies investigating the effect of heatwaves on plant growth reviewed by Teskey et al. (2015) only three focused on trees and highlighted a reduction of the growth of the studied trees. Teskey et al. (2015) synthesized their results which showed that both the temperature and the duration of the exposure are involved in the proportion of leaves damaged. They also summarized the other known effects of heat stress on trees at the cellular, leaf and whole plant scale. A noticeable variability may exist between species, for instance heat stress may enhance or limit stomatal conductance and transpiration depending on the considered species. But it appears that for all the studied tree species, heat stress reduces photosynthesis and therefore growth and leaf area development while increasing the leaf loss and mortality rate. The authors also reported that heat stress resistance is subject to an inter-specific variability and that trees may be able to acclimatize after multiple expositions to heat stress. It also appears that a given air temperature can have various impacts depending on the moment when they occur during the vegetative growth. More recently, Esperon-Rodriguez et al. (2021) reported a decrease of stomatal conductance while air temperature and VPD were increasing during heatwaves. However, although some of the works cited hereinabove studied the climatic benefits of trees during heatwaves, they did not really isolate the effect of the heatwaves on such benefits.

2.3. Conclusion and objectives

In the frame of the problematic presented previously in chapter 1, the different phenomena described hereinabove in section 2.1, can be summarized as proposed in Figure 18. The present work aims at investigating the climatic benefits provided by street trees but it was highlighted hereinabove that various different strategies have been proposed in the literature to quantify such benefits and that no common definition of these benefits has emerged. In the present work, the assessment of the climatic benefits provided by street trees will include the evaluation of their effect on different microclimate variables (T_a, T_{mrt}, AH, etc.) as well as their ability to reduce human thermal stress.

The climatic benefits provided by street trees are characterized by many sources of variability, first because the ever-changing meteorological conditions have a direct impact on the human thermal stress but may also influence cast shadow and transpiration, the two processes responsible for the climatic benefits. Cast shadows and transpiration are direct consequences of the tree morphology generally considered as the physical structure and the external form of the tree, and its physiological behavior which covers the processes involved in the tree development such as photosynthesis, respiration and transpiration. Finally, the availability of water in the soil, which varies according to the meteorological conditions, influences the physiological processes of the trees and in the end their morphological characteristics.

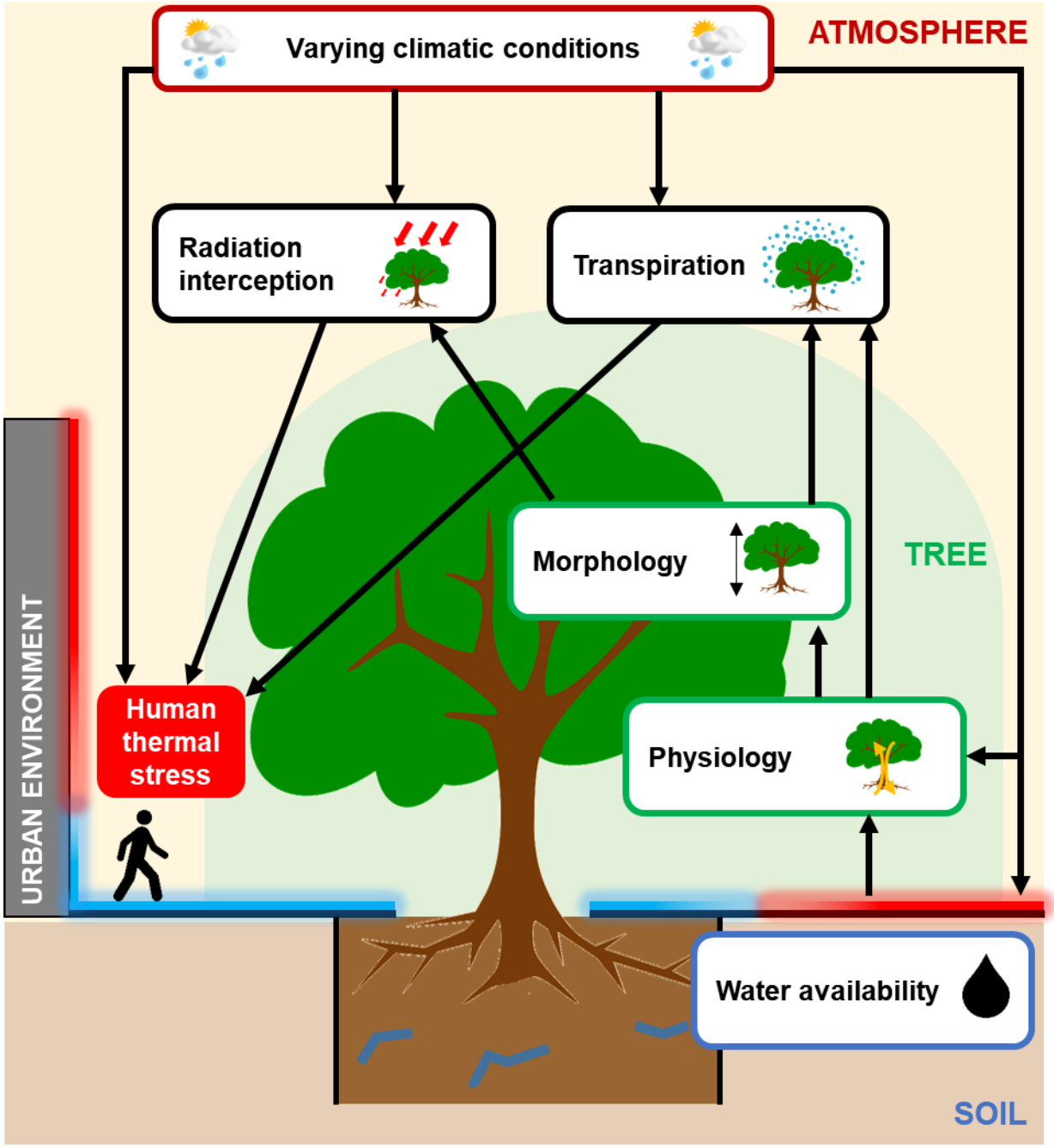

Figure 18: General drawing of the processes involved in the climatic benefits provided by trees in the urban environment.

2.3.1. Scientific knowledge lacking in the literature

The literature review proposed in section 2.2 shows that numerous works have already focused on the interactions existing between trees and their surrounding environment (soil and atmosphere) including in the urban context. Especially, many studies proposed some evaluations of the climatic benefits provided by urban trees but the complete understanding of these benefits is not easy regarding the high number of variables involved, the high heterogeneity of the urban configurations and the important diversity of tree morphologies and physiological responses.

For most of the studies, only part of the variables of interest are measured. It is then generally not possible to estimate the respective contributions of cast shadows and transpiration to the climatic benefits or to evaluate at the same time the effect of the trees on the street energy balance and on human thermal stress. The density of sensors is generally low and few studies could perform long-term (days, week or years) continuous monitoring with a small time step (e.g. 1 hour). Thus, the assessment of the spatial extent as well as of the daily variability of the climatic benefits is not easy.

A few works have tried to compare trees from different species at the same time and to relate the effect of trees mainly to their LAI. However, more data is still needed to understand the influence of the morphological characteristics of urban trees on the climatic benefits they provide.

Finally, although the effect of water stress and heat stress on plant physiology including trees have been widely studied, the morphological and physiological consequences of these abiotic stresses on the climatic benefits provided by the trees remain widely unexplored. Indeed, the major part of the studies assessing the climatic benefits provided by trees neither control the water availability for the trees nor monitor it.

2.3.2. Objectives and structure of the present work

In order to increase the knowledge about the climatic benefits provided by street trees and provide new answers to the lacks identified in the literature, the present project focuses on the following objectives:

- **Evaluate the sources of variability of the climatic benefits provided by urban trees.**
- **Quantify the impact of heatwaves and droughts on the physiology and morphology of urban trees.**
- **Quantify the impact of heatwaves and droughts on the climatic benefits provided by urban trees.**

To achieve these objectives, the present project proposes an original methodology relying on two complementary experimental facilities, both based on the long-term monitoring of the influence of trees on the urban microclimate with measurements along the soil-plant-atmosphere continuum. On the one hand, a 1/5 scale canyon street ("reduced scale canyon street" also called "RSCS"), partially planted with young potted drip-irrigated ornamental apple trees (*Malus Coccinella*® 'Courtarou') located in Angers, France is monitored to quantify the effect of street trees experiencing different water supplies on the microclimate. With this facility, well-watered trees and water-restricted trees grown in the same controlled conditions can be monitored at the same time with a high density of sensors. On the other hand, an in-situ monitoring of the microclimate inside and outside the canopy of 36 mature street trees from 9 different tree species located in 5 sites in Paris was performed from 2019 to 2022 ("Trees & Climate" study also called "T&C"). With this facility, the summer behavior and climatic benefits provided by multiple tree species experiencing real urban conditions and water availability can be assessed.

In the frame of this research methodology, the climatic benefits of street trees will then be understood as the ability of trees to reduce human thermal stress which will be quantified through the calculation of the Universal Thermal Climate Index (UTCI). Yet, human thermal stress is influenced by various thermal transfers occurring between the considered human body and its surrounding environment. Therefore, the effect of trees on different "observation variables" will be assessed among which air temperature (T_a), mean radiant temperature (T_{mrt}), surface temperature, absolute humidity (AH) or short and long wavelength radiation (SW and LW). The analysis of tree morphology will cover the characterization of the foliage (mainly the total leaf area and the leaf area density -LAI-) and the crown dimensions (volume, projected

area, height, etc.). The analysis of tree physiology will focus on tree growth through the measurement of the evolution of tree stem diameter as well as on tree transpiration calculated through a water balance or approached by related variables such as stomatal conductance and leaf temperature. Different abbreviations will be used to call the multiple parameters studied on this work, their meanings have been summarized at the beginning of the present manuscript.

Due to their respective characteristics, both facilities bring different insights of the studied climatic benefits. Table 1 presents their respective contributions to the three main objectives listed hereinabove which are also split in multiple sub-objectives.

Table 1: Main characteristics of the two experimental facilities and their respective contributions to the three main objectives of the project.

Scientific questions and objectives	Reduced scale canyon street (RSCS) ***Reduced scale model*** ***Controlled and measured water availability*** ***1 tree species*** ***8-week campaign***	Trees & Climate (T&C) ***Full scale in-situ*** ***Uncontrolled but partially measured water availability*** ***9 tree species on 5 sites*** ***4-year monitoring***
[1.] Exploring the variability of the climatic benefits		
Spatial distribution	X	
Temporal variability	X	X
Varying climatic conditions	X	X
Respective contributions of transpiration and cast shadows	X	
Morphological characteristics		X
[2.] Impact of heatwaves and droughts on tree physiology and morphology		
Effect on stomatal conductance	X	
Effect on transpiration	X	
Effect on leaf temperature	X	
Effect on stem diameter variations	X	X
Effect on leaf area density	X	
[3.] Impact of heatwaves and droughts on the climatic benefits		
Effect on absolute humidity	X	
Effect on radiation interception	X	
Effect on surface temperature	X	
Effect on radiation balance	X	
Effect on air temperature	X	X
Effect on UTCI	X	X

Chapter

3. Impact of a water restriction on the summer climatic benefits of trees inside an outdoor canyon street scale model

The reduced scale treed canyon street (RSCS) of Angers was progressively built starting from 2018 in order to evaluate the influence of a typical urban environment on the microclimate and the influence of alignment trees on the urban microclimate. It was designed as a simplified street with a few controlled parameters enabling first to easily control the water availability of the studied trees and then to provide a detailed and well described data set useful for modelling purposes. First monitoring campaigns of the microclimate inside and outside the street were performed in 2019 and 2020 in the frame of a previous PhD project (Mballo, 2022). These campaigns aimed at studying the climatic benefits provided by street trees experiencing well-watered conditions and simulating the experimental results through a computational fluid dynamics approach.

In the frame of the present PhD project, two measurement campaigns were then performed in 2021 and 2022. They aimed especially at evaluating the influence of a water restriction on the climatic benefits provided by the studied trees. The 2021 campaign, which lasted 10 days, was used to test and adapt the water restriction protocol and to provide first results which were presented in an international congress (Thierry et al., 2022). The 2022 campaign offered stronger results and especially the possibility to run an 8-week long water restriction period during a dry and warm summer. Summer 2022 was indeed drier (45 mm total rainfall in July and August) than summer 2021 (73.2 mm) while being hotter as the daily maximum T_a was 29.2 °C and 29.4 °C on average in July and August 2022 while it was 24.4 °C and 23.5 °C on average during July and August 2021.

Section 3.1 focuses on the effect of a water restriction on tree transpiration, radiation interception, T_a and UTCI over an 8-week summer period at a daily time step. This entire section is actually the manuscript of a research paper submitted to a peer-reviewed international journal (Building and Environment) in November 2023 and which is still under review. This is why section 3.1 can be read independently.

Section 3.2 focuses on the same 2-month period as section 3.1 but presents the effects of a water restriction on tree physiology through the monitoring of stem diameter variation and leaf surface temperature (T_{leaf}). It also proposes a focus on three days of interest to assess the impact of the water restriction on the daily evolutions of the wall surface temperature, the complete radiation balance of the street and the spatial distribution of the climatic benefits. Finally, it evaluates the influence of the daily meteorological conditions on the variability of the climatic benefits.

3.1. Effect of an 8-week water restriction on radiation interception, tree transpiration and human thermal stress reduction

3.1.1. Introduction

The multiplication and intensification of extreme climatic events such as heatwaves accompanying climate change has been observed in all regions of the world (IPCC, 2023). In France, the average annual duration of heatwaves was 1.7 days.year^{-1} before 1989 whereas it reached 7.95 days.year^{-1} since 2000 (Météo-France, 2022). It should also obviously impact cities (Bastin et al., 2019) which are already experiencing an overheating phenomenon called Urban Heat Island (UHI). Already related to the city size (Oke, 1973) and quantified in various cities (Arnfield, 2003; Oke, 1978), the UHI is characterized by a temporal (Cantat, 2004) and a spatial variability (Bournez, 2018; Chen et al., 2022; Unger, 2006) and is influenced by multiple factors such as the nature of the materials or the urban geometry (Akbari et al., 1992; Bouyer, 2009; Sun et al., 2022). Thereby, canyon streets, which are a common urban configuration, appeared to be adapted to study urban overheating at street scale (Ali-Toudert and Mayer, 2007; Hang et al., 2022) and its impact on the pedestrians. Indeed, overheating and heatwaves expose the human body to a thermal stress which may cause sanitary issues (IPCC, 2023; Kuchcik, 2021). In France, around 15 000 deaths were attributed to the heatwave of summer 2003 and

the mortality risk appeared to be higher in cities where the UHI intensifies the overheating especially at night (Laaidi, 2012). Human thermal stress was approached by a variety of indicators aiming at taking the complete thermal balance of a human body into account. Among them, the Universal Thermal Climate Index (UTCI) (Bröde et al., 2010) is widely used in the literature for the assessment of outdoor thermal environment because it relies on a highly detailed human body model (Migliari et al., 2022).

Different promising strategies to mitigate the urban climate were studied in the literature (Bournez, 2018). They rely on urban materials (Akbari et al., 1992; Carlosena et al., 2023; Doulos et al., 2004; Salvati et al., 2022; Tabatabaei and Fayaz, 2023; Wardeh et al., 2022), urban geometry (Ali-Toudert and Mayer, 2006; Jamei et al., 2016) or vegetation such as green facades (Alsaad et al., 2022; Y. Zhang et al., 2022; Zuckerman and Lensky, 2023) and roofs (Frei, 2023; Wang et al., 2023), grass cover, urban parks (Bernard et al., 2022; Cheung et al., 2020; Liu et al., 2023; Yan et al., 2020) or street trees (Armson et al., 2012; Bowler et al., 2010; Jamei et al., 2016; Priya and Senthil, 2021; Rahman et al., 2020). The use of street trees has recently raised an increasing interest as they may counteract overheating at the pedestrian scale during the day by means of two main processes: cast shadow and transpiration. The cast shadow reduces the amount of solar radiation reaching the surrounding surfaces whereas the water transpired by the trees takes off energy of the surrounding atmosphere to evaporate.

The impact of individual trees on urban microclimate was highlighted through the quantification of the incident solar radiation they intercept (Deng et al., 2020; Heisler, 1986; Konarska et al., 2014; Kotzen, 2003; Shahidan et al., 2010), the temperature reduction of the surrounding surfaces (Armson et al., 2013, 2012; Gillner et al., 2015; Sharmin et al., 2023), the reduction of globe temperature (Armson et al., 2012) and mean radiant temperature (Armson et al., 2013) under their crowns, or the quantification of the energy dissipated through evaporation of the transpired water (Shashua-Bar et al., 2023; Zheng et al., 2021). A variety of studies on diurnal air temperature (Moreno et al., 2023; Souch and Souch, 1993; Vailshery et al., 2013) and UTCI reduction beneath the tree canopy compared to reference open areas can also be found in the literature (T. Chen et al., 2023; Coutts et al., 2016; T. Zhang et al., 2022). Some works relied on the use of reduced scale models which are more convenient to perform continual monitoring and allow to control more parameters such as building heights and surface materials (T. Chen et al., 2023; Hang and Chen, 2022). Mballo et al. (2021), for instance, estimated that cast shadows were responsible for 74 % of the cooling benefits of well-watered trees during a single sunny day inside a 1/5 scale north-south oriented canyon street whereas the remaining 26 % were attributed to the evaporation of the transpired water. For a large panel

of weather conditions and considering 120 studied days, Herpin et al. (2022) extended their work and calculated an average air temperature reduction of 2 °C and an average UTCI reduction of 5.3 °C under the studied well-watered trees compared to a non-vegetated zone of the canyon street.

However, the health and development of street trees rely on a sufficient access to water into the soil. Yet, the intensity, frequency and distribution of rainfalls are expected to be locally modified due to the ongoing climate change (IPCC, 2023) and the water resources of trees will not be guaranteed all along the growing season in the near future. (Schütt et al., 2022) monitored the soil water potential inside the tree pits of 17 street trees in 2018-2019 and revealed that street trees were already experiencing critical soil water potential during three to five months per year.

When exposed to a decreasing soil water potential, trees try to avoid cavitation and embolism by adjusting their stem water potential especially by closing their stomata or reducing their leaf area (Brendel and Cochard, 2011; Cochard and Granier, 1999; Lecoeur, 2007), two mechanisms that may alter their gas exchanges and light interception, and by the way, their photosynthetic activity and transpiration. The response time of these mechanisms may vary a lot (Brendel and Cochard, 2011). The stomatal closure can be noticed from one day to the next one (Zweifel et al., 2007) whereas morphological adjustments may take several weeks. Thus, the ability of street trees to maintain significant climatic benefits under such conditions needs to be studied as it is a major concern for urban planners who need to understand how nature-based solutions may help reduce human thermal stress in cities in a context of rarefying water resources. Yet, it appears that few works studying the climatic benefits of street trees carried out continuous monitoring (Gillner et al., 2015; Meili et al., 2021) enabling to assess the effect of dry periods, and none of them could so far control or monitor soil water availability.

Moreover, vegetation and especially street trees were included in numerical models resolving the urban water and energy balances at different scales based on experimental measurements. Such models are now widely used to carry out parametric studies assessing the impact of different urban greening scenarios on UHI, building energy consumption or human thermal stress. They generally compare varying tree planting densities (Aboelata, 2020; Aboelata and Sodoudi, 2020; Geletič et al., 2022; Ouyang et al., 2020; Teshnehdel et al., 2020; Wang et al., 2022) or tree morphological variables (height, crown projected area, leaf area index) (T. Chen et al., 2023; Ge et al., 2023; H. Liu et al., 2022; Meili et al., 2021) to provide urban planners with advices on the best strategies to design urban green areas. However, these modelling tools mostly consider well-watered vegetation whatever the input meteorological

conditions be. Most of the cited studies pointed out that further works should take into account water stress for a comprehensive estimation of the climatic benefits of street trees. To do so, detailed experimental data of the evolution of transpiration and related physiological processes as well as radiation interception and related morphological variables under water stress are still needed in order to improve the accuracy of the models.

Some studies assessed the seasonal changes of tree transpiration or related variables with a varying soil moisture (S. Chen et al., 2023). Others, highlighted significant reductions of transpiration ranging from 25 % (Caspari et al., 1993) to 92 % (Tan et al., 2020) when comparing well-watered and water-restricted trees of various species. Caspari et al. (1993), Gebauer et al. (2023) and Konarska et al. (2016) observed a significant decrease of stomatal conductance (i.e. stomatal closure) during dry periods. Dervishi et al. (2023) found lower morphological variables such as leaf area density for young potted water-restricted *Platanus x hispanica* and *Tilia cordata* compared to well-watered ones. However, the studies controlling or monitoring soil water availability were not meant to study climatic benefits or only assessed part of the variables related to the tree cooling potential. A preliminary work of Thierry et al. (2022) evaluated the effect of a 1-week water restriction on street trees climatic benefits but no impact on the tree foliage was reported as the water shortage was too short and moderate.

Thus, the objective of the present study is to understand and quantify the influence of a long water restriction period on the climatic benefits provided by street trees and the processes they rely on. It proposes an original assessment of the effect of the lack of water on both tree transpiration and shadows cast by the trees and analyses the evolution of their respective contributions to the climatic benefits over time. To achieve these goals, an original integrated approach of the soil-plant-atmosphere continuum is proposed including the continuous monitoring of the water availability in the soil, tree transpiration and radiation interception, and the surrounding microclimate inside a reduced scale canyon street vegetated with both water-restricted and well-watered trees during a 2-month summer period.

3.1.2. Materials and methods

3.1.2.1. Materials

3.1.2.1.1. General presentation of the street

The experiments were run in a 1/5 scale canyon street model located in Angers, France (47°28'47'' N, 0°36'33'' W). Angers is characterized by a Cfb temperate oceanic climate according to the Köppen-Geiger classification (Peel et al., 2007). The street (Figure 19) is oriented North-South and is bordered by two buildings made of 0.1 m thick white concrete walls insulated with 0.12 m thick expanded polystyrene on the inside. Wooden frames covered with steel panels were used to build the roofs and external walls of the buildings. The ground of the street is covered with a 0.04 m thick layer of asphalt. Some optical and thermal properties of the materials used to build the street can be found in appendix 7.1.1. Given that both buildings are 2 m high and that the street is 2 m wide, it forms an urban canyon which aspect ratio is 1 (height of the buildings divided by the width of the street). The street is divided into three zones: one treeless zone in the southern part of the street and two treed zones in the northern part and middle of the street. Both treed zones contain 5 ornamental apple trees (*Malus Coccinella*® 'Courtarou') aligned on the North-South central axis of the street. The trees were 4 years old at the time of the experiment, all issued from cutting and grown in the same nursery (André Briant Jeunes Plants). They were planted in the canyon street on January 19th 2022 and subjected to a winter structural pruning. Their upper and lateral axes were trimmed on June 23rd 2022 so they could fit in the dimensions of the reduced canyon street. For the purpose of this study, the three zones will be referred as:

- The well-watered zone or WW zone for the vegetated zone located in the northern part of the street as it was fully irrigated all year long;
- The water-restricted zone or WR zone for the vegetated zone located in the centre of the street as it was subjected to a water restriction during 8 weeks;
- The non-vegetated zone or NV zone for the southern part of the street which does not contain any tree.

Figure 19: Top view (left) and south view (right) pictures of the canyon street.

3.1.2.1.2. Soil compartment

Each tree was planted in an 80 L container placed below the street ground surface inside a pit dug along the central North-South axis of the canyon street (Figure 20). The containers were filled with 46.3 L of a topsoil-compost mixture in a 60/40 % volume ratio (from now on referred as "soil") placed on top of a layer of stones and a layer of concrete with a slight slope aiming at facilitating drainage, all layers being separated from each other by geotextile. The 46.3 L volume of top-soil-compost mixture corresponds to a 5.8 m^3 volume of top-soil-compost at full scale when applying a geometrical reduction factor of $(1/5)^3$ and to a 8.9 m^3 volume for the entire pit considering that tree pits are generally filled with a 65/35 % volume ratio of topsoil-compost mixture and rocks which is very consistent with the planting conditions in cities as trees are generally planted in 10 m^3 pits (CAUE 77, 2022). The 60/40 % volume ratio used for the topsoil-compost mixture was chosen on the basis of the common practices of urban greening and on studies showing that a 40 % volume ratio of compost could ensure both good agronomic quality of the soil and tree growth at the long-term scale (Cannavo et al., 2018; Vidal-Beaudet et al., 2012). The texture of the topsoil-compost mixture was measured in the laboratory using granulometry analysis after decarbonisation according to the French standard NF X31-107: the topsoil contains 6.6 % (mass ratio) of clay, 30.1 % of silt and 63.3 % of sand and its texture can be classified as loamy-sand regarding the French GEPPA classification and sandy loam regarding the United States Department of Agriculture classification (USDA Natural Resources Conservation Service, n.d.). The topsoil-compost mixture contains 8.9 % (mass ratio) of organic matter.

The containers were covered with lids, and the pits with asphalt sheets preventing rainfall infiltration and direct evaporation from the soil. The trees were drip-irrigated daily

between 20:00 and 22:00 UTC with fertilized water. The daily irrigation dose was chosen in order to maintain the soil moisture at field capacity and ensure well-watered conditions. The occasional drainage water was collected in a tank placed below every container and its volume was measured manually every working day (5 days/week).

The 3 central containers of each treed zone were equipped with 2 tensiometers and 2 capacitive probes each, all placed approximately at mid-depth of the topsoil-compost mixture, aiming at monitoring the water matric potential and the soil Volumetric Water Content (VWC) (Figure 20).

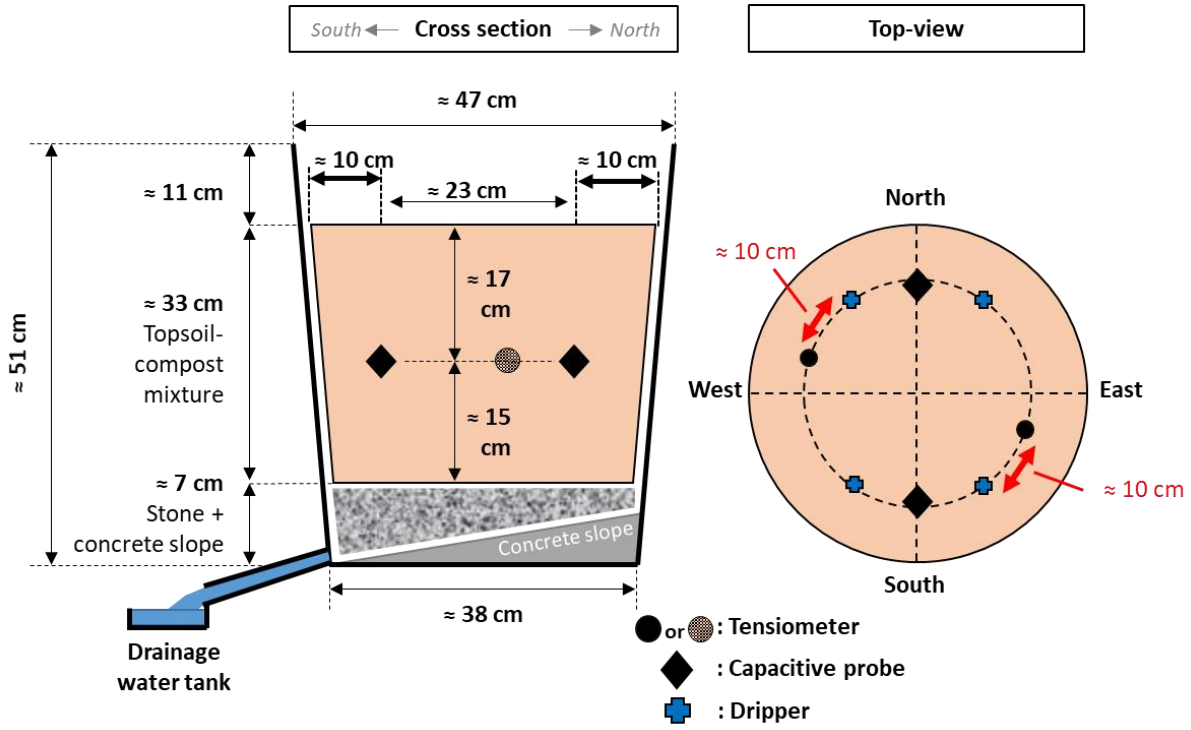

Figure 20: Sketch of one of the three central planting containers of the vegetated zones and location of the sensors.

The amount of water in the soil that a tree is able to collect is called the Total Available Water Storage (TAWS) and is defined by two soil VWC limits called field capacity and permanent wilting point. The field capacity is related to the texture of the soil and is generally associated to a water matric potential of approximately -0.033 MPa (Bouthier et al., 2022; Cassel and Nielsen, 1986). An experimental water retention curve, relating soil VWC and water matric potential, was established in the laboratory according to the French standard NF EN 13041 for the present topsoil-compost mixture and used to estimate the soil VWC associated to field capacity to 28 %. The permanent wilting point, depends on the soil texture but may also strongly rely on the considered plant. In the present experiment, the in-situ continuous monitoring of the soil VWC showed that when all water inputs and outputs were null except

the water debited by the trees, soil VWC could not decrease under 10 %. This lower limit was then assumed to correspond to the permanent wilting point (see Figure 24 presented and described later). The TAWS was then estimated to 18 % of the soil volume i.e. 8.3 L when considering the present soil volume of 46.3 L. Then, the TAWS is generally divided into a Readily AWS (R-AWS), where the plant is supposed to experience a comfortable access to water, and a Non-Readily AWS (NR-AWS) where pumping water may be more difficult for the plant which is likely to experience hydric stress. According to FAO et al. (2006), the threshold delimiting the R-AWS and the NR-AWS should be located approximately at half of the TAWS for apple trees which means at a soil VWC of approximately 19 % for the present experiment.

3.1.2.1.3. Meteorological sensors

Although the French meteorological institute (Météo-France) operates a weather station called “Angers-Beaucouzé” (station n°49020001) located approximately 400 m away from the studied site, from now on referred as “Météo-France meteorological station”, on-site reference measurements were carried out with two meteorological masts located outside the street. The first one was aligned with the central North-South axis of the street and located 6.5 m north from the street (Figure 19 and Figure 21). The second one was located approximately 8 m west from the street (Figure 19).

The central cross-section of each zone of the street was equipped with a set of meteorological sensors described in Figure 21 and mounted at different heights above ground level (a.g.l.) including 0.4 m a.g.l. which is particularly important for the evaluation of human thermal stress as it corresponds to 2 m a.g.l. at full-scale which is close to human height (Figure 21).

Air temperature and relative humidity were measured on the central axis of the street at 0.4 m a.g.l. and 1.5 m a.g.l. that is respectively under and inside the tree canopy. Both variables were also measured at the North mast at 2 m a.g.l. in order to carry out the calculation of the reference evapotranspiration presented hereinafter. The platinum and capacitive probes used for this measurement were placed in mechanically ventilated white painted cylindrical shelters. Both variables were used to compute the absolute humidity.

Globe temperature was measured at 0.4 m a.g.l. at the North mast as well as in each zone of the street on the central north-south axis using platinum probes mounted inside black painted copper spheres of 15 cm diameter.

The North mast was equipped with a net radiometer placed at 2.1 m a.g.l. Inside the street, both vegetated zones were equipped with 4-components net radiometers placed at 0.78 m a.g.l. and 2.1 m a.g.l. that is just under and above the tree crowns respectively, to measure incident downward short wavelength radiation and its transmission through the tree crown. In the NV zone, the downward short wavelength radiation was measured at 2.1 m a.g.l. with a pyranometer and the Photosynthetically Active Radiation (PAR) was measured at 0.65 m and 2 m a.g.l. with PAR radiometers. PAR measurements were used to calculate the downward short wavelength radiation at 0.65 m a.g.l. in the NV zone as detailed in section 3.1.2.2.5.

The wind speed and direction on the studied site were measured outside the street at 2 m a.g.l. on the West mast with a 2D sonic anemometer, and inside the street with a 3D sonic anemometer at 0.4 m a.g.l. between the NV and WR zones at approximately 4.1 m from the south end of the street.

The on-site reference evapotranspiration was calculated with the meteorological variables measured outside the street at the North mast and West mast whereas the Universal Thermal Climate Index (UTCI) was calculated with the measurements carried out inside the street in order to evaluate the human thermal stress at human height (0.4 m a.g.l. at reduced scale). The methods used for the calculation are described in section 3.1.2.2.

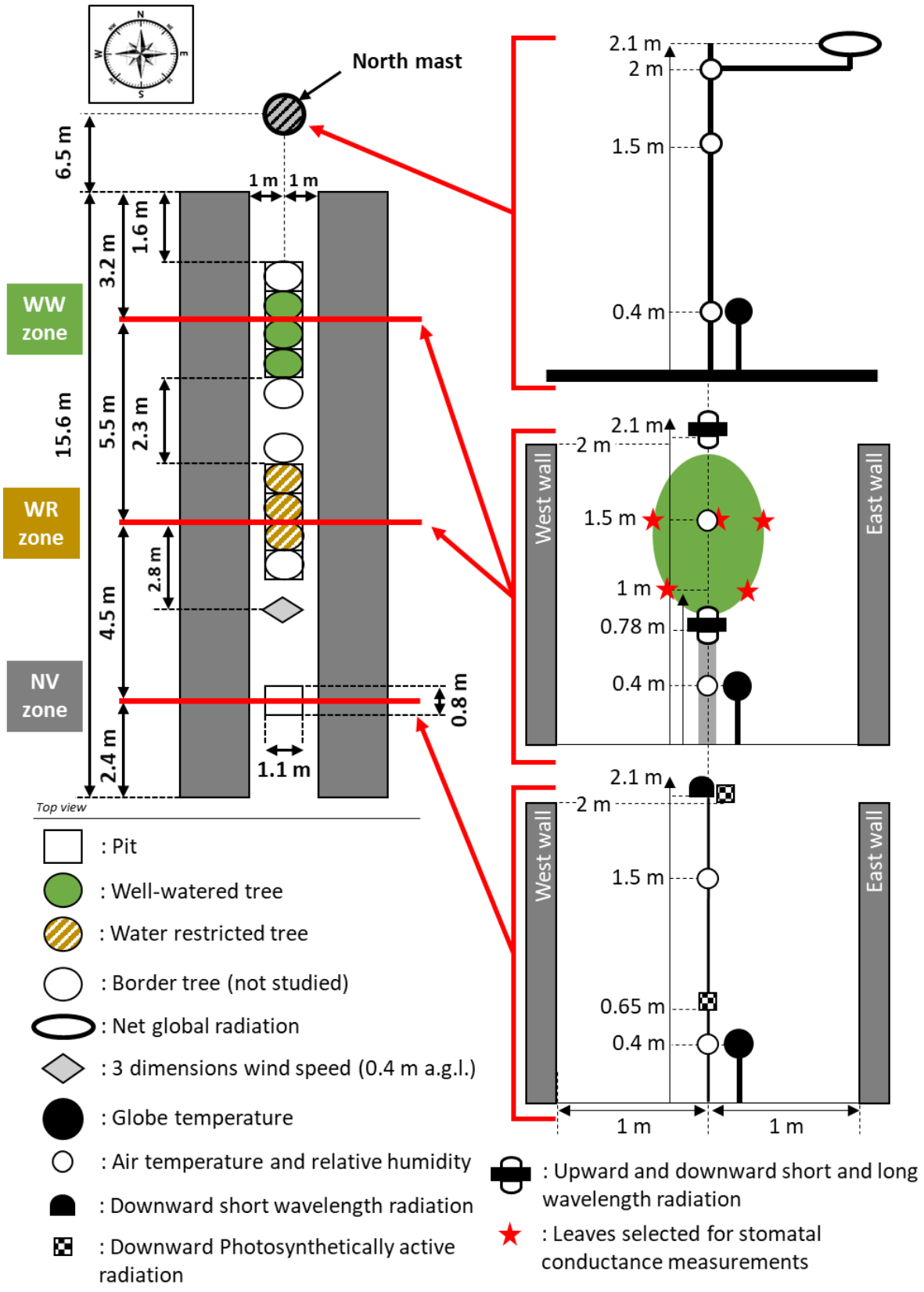

Figure 21: Sketch of the studied canyon street showing the respective positions of the well-watered zone (WW), the water restricted zone (WR) and the non-vegetated zone (NV) with the location of the sensors in the different zones.

Table 2: Characteristics of the sensors used for the experiment. Data-loggers were used to scan all sensors every 10 seconds and record average values every 10 minutes (n.c. = not communicated).

Measured variable	Sensor type	Measurement range	Accuracy	Reference, manufacturer
Volumetric water content (VWC)	Capacitive probe	0 to 100 %	± 2 % (± 0.02 cm^3/cm^3)	EC-5, Decagon
Water matric potential	Tensiometer	0 to -0.1 MPa	± 0.2 %	STCP 850, SDEC
Air temperature	Platinum	-40 to +60 °C	± 0.2 °C	HMT330 and HMP110, Vaisala
Air relative humidity	Capacitive	0 to 100 %	± 1.5 % for HR ≤ 90%	HMT330 and HMP110, Vaisala
Globe temperature	Platinum	-5 to +95 °C	± 0.15+0.002*T (°C)	PT100, RS Pro
Net radiation	Net radiometer	n.c.	± 10 % on daily sum	NR Lite, Kipp&Zonen
Short and long wavelength radiation	4 components Net radiometer	n.c.	± 10 % on daily sum	CNR1, CNR4, Kipp&Zonen
Short wavelength radiation	Pyranometer	n.c.	± 10 % on daily sum	CMP3, Kipp&Zonen
Photosynthetically active radiation	Radiometer	400 – 700 nm	± 1 %	LI-190SA, Li-Cor
Wind speed and direction	2D sonic anemometer	0 to 60 $m.s^{-1}$ 0 to 359°	± 2 % (at 12 $m.s^{-1}$) ± 3° (at 12 $m.s^{-1}$)	Mc Gill Windsonic
Wind speed and direction	3D sonic anemometer	0 to 30 $m.s^{-1}$ 0 to 359°	± 0.08 $m.s^{-1}$ ± 0.7° (at 1 $m.s^{-1}$)	CSAT-3D, Campbell Scientific

3.1.2.1.4. Leaf area and crown projected area of the trees

The leaf area of the 3 central trees of each vegetated zone was estimated on July 7th and August 27th 2022. For leaf-bearing axes, the length of all long axes (longer than 5 cm) was measured, the number of short axes was counted and the length and width of all leaves on a sample of 10 long and 10 short axes were measured. The area of each sampled leaf was calculated out of its length and width using an allometric relationship established on the basis of data acquired in previous experiments with the same experimental setup and the same trees (*Malus Coccinella*® 'Courtarou') giving one coefficient of leaf area per short axe and one per unit of foliated length for long axes. For each tree, the two coefficients were multiplied respectively by the number of short axes and the cumulative length of all long axes to compute the total leaf area.

The dimensions of the tree crowns were estimated for each zone by measuring the area of the horizontal rectangle encompassing the canopy of the 5 trees of each alignment. When divided by 5, this area was considered equal to the crown projected area on the ground per tree for each vegetated zone and was used to compute the Leaf Area Index (LAI) of each tree defined as the ratio of its total leaf area to its crown projected area. Linear interpolation and extrapolation were used to compute the crown projected area for each day of the studied period from July 8th and August 31st 2022 on the basis of the values measured on July 7th and August 27th. From July 1st to July 6th, the crown projected area was considered equal to the one measured on July 7th. Indeed, the trees were pruned on June 23rd and their dimensions were supposed to remain constant during the two following weeks, i.e. from June 23rd to July 7th 2022.

3.1.2.1.5. Stomatal conductance

Measurements of the stomatal conductance were carried out during 5 sunny, warm and rain-free days (July 5th, July 12th, July 19th, July 28th and August 9th 2022) approximately with a 1-hour time step on 5 mature leaves of the central tree of both vegetated zones with an AP4-UM-3 porometer (DeltaT Devices Ltd, Cambridge, UK). The 5 selected leaves were close to the edge of the tree crown in order to be exposed to the sun at least part of the day (Figure 21). As the WR trees experienced defoliation, some of the selected leaves fell during summer and new leaves had to be selected. A daily average stomatal conductance value was calculated for each one of the 5 selected leaves from 10:00 to 12:00 UTC and was used to compute a daily average stomatal conductance for the central tree of each vegetated zone.

3.1.2.2. Methods

3.1.2.2.1. Irrigation control

Until July 4th, 2022, all trees were drip-irrigated every day between 20:00 and 22:00 UTC with an amount of water sufficient to guaranty that soil VWC was at field capacity (approx. 28 %) every night and that drainage water was collected on the following day. The irrigation dose was adjusted according to the forecasted meteorological conditions. Different indicators were monitored to ensure that the irrigation dose was sufficient to bring soil moisture at field capacity:

- The amount of drainage water collected every day was expected to be strictly positive;
- The water matric potential measured with the tensiometers was expected to be close to field capacity (-0.033 MPa) after evening irrigation;
- The soil VWC, measured with the capacitive probes, was expected to be close to field capacity (28 %) after evening irrigation.

On July 5th, 2022, two different irrigation treatments were applied to the two vegetated zones:

- The WW (well-watered) zone, located in the northern part of the street, was kept fully irrigated as described hereinabove all summer long in order to maintain the soil at field capacity.
- The WR (water-restricted) zone, located in the centre of the street, was subjected to a water restriction lasting until September 1st. The last full irrigation occurred on July 4th, in the evening. Thus, the trees were still experiencing comfortable water supplies on July 5th, and July 6th was considered as the first day of the restriction period (also called day 1). Then, a small irrigation dose was poured every day from July 7th included. The dose was chosen in order to maintain the soil VWC in the NR-AWS. In total the water restriction lasted for 8 weeks.

3.1.2.2.2. Estimation of tree transpiration with a water balance

A daily water balance was carried out on the basis of all water inputs and outputs of the tree containers in order to evaluate daily tree transpiration (8), and adapted for well-watered (WW) trees and water-restricted (WR) trees.

$$P + I - \Delta S - ETR - D \pm R = 0 \quad \textbf{(8)}$$

P is the total rainfall, *I* is the irrigation poured into the soil, *ΔS* is the variation of water storage in the soil, *ETR* is the effective evapotranspiration, *D* is the drainage water, *R* is the runoff, all expressed in litre. *P* and *R* can be considered null as trees are planted in containers covered with lids.

Estimation of tree transpiration for well-watered (WW) trees

The measurement of the daily drainage water (*D*) could not be carried out during non-working days (week-ends and public holidays). This is why the water balance was simplified (9) for well-watered trees on a daily time period delimited by the estimated start time and end time of tree diurnal transpiration as proposed by Mballo et al. (2021) enabling to consider *I* and *D* null (Figure 22). Night-time transpiration is considered null in this case as it was found to be low compared to the diurnal transpiration on different tree species (Chen et al., 2011; Fisher et al., 2007).

$$ETR = -\Delta S_{daytime} = -\Delta\theta_{daytime}.V_{soil} \quad \textbf{(9)}$$

$\Delta\theta_{daytime}$ is the diurnal variation of the average soil VWC (points of %) calculated for each tree between the end time (approx. 19:30 UTC) and the start time (approx. 05:30 UTC) of diurnal transpiration using the two capacitive probes described in Figure 20, V_{soil} (46.3 L) is the volume of topsoil-compost mixture poured in each container.

Estimation of tree transpiration for water-restricted (WR) trees

During the water restriction period, as the soil of the WR trees dries, the water distribution might become very heterogeneous preventing the two capacitive probes, which are very local sensors, to accurately represent the overall water distribution and dynamics in the soil. Indeed, the daily soil VWC variation of some WR trees became null until the end of the growing season, whereas they were still irrigated with small doses of water, and thus transpiring. To face this issue, the daily water balance of the WR trees was run on a 24-hour time step (19:30 to 19:29 UTC next day) from July 6th until the end of the growing season. In

this way, *D* was set to zero (it was checked that the amount of daily drainage water of the WR trees was null on this period) and *I* was included in the water balance which led simplify equation (8) as follows:

$$ETR = I - \Delta S_{24h} = I - \Delta\theta_{24h}.V_{soil} \quad \textbf{(10)}$$

Figure 22 illustrates the daily water balance carried out in the present experiment and the hypotheses allowing the simplifications presented hereinabove.

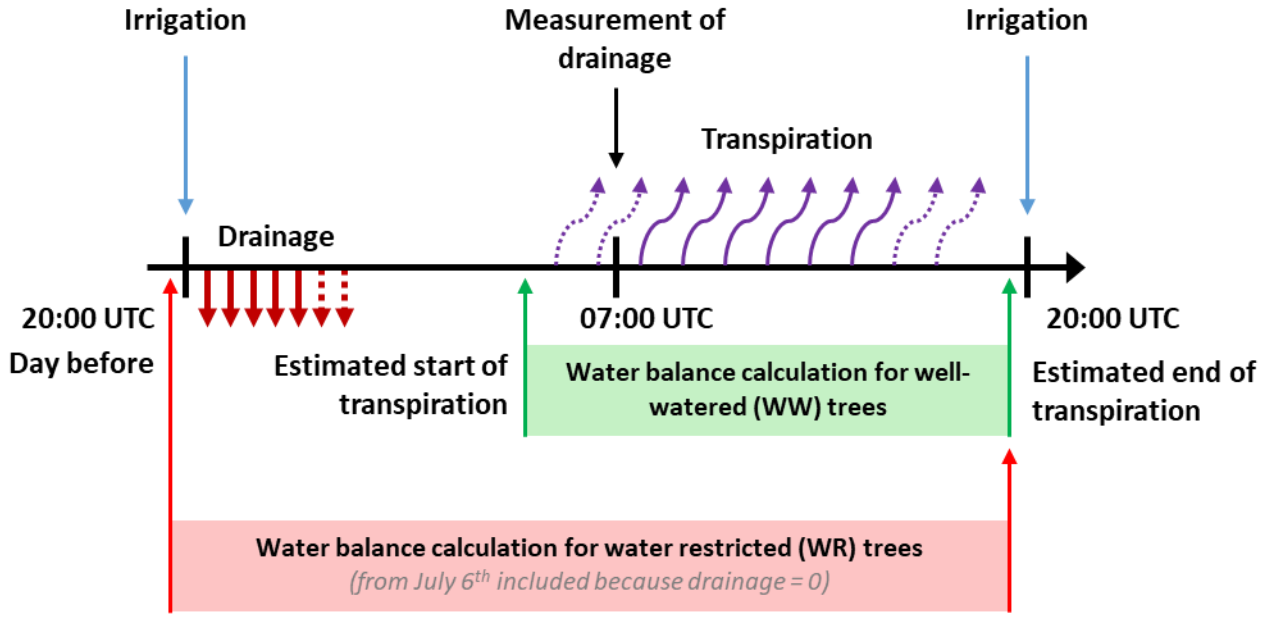

Figure 22: Daily water inputs and outputs taken into account for the calculation of the water balance and daily tree transpiration (adapted from Mballo et al. (2021)). *(For journal layout: 2-column fitting figure)*

The daily amount of water transpired by the trees was converted into a daily quantity of energy consumed by the evaporation of water with the use of the latent heat of vaporization of vapour at 20 °C (2.46 $MJ.kg^{-1}$) and transformed to a quantity of energy per surface unit ($MJ.m^{-2}.day^{-1}$) using the average projected area of the tree crowns interpolated for each day as detailed in section 3.1.2.1.4.

3.1.2.2.3. Reference evapotranspiration

The daily reference evapotranspiration ET_{ref} was calculated on-site at the north mast using the Penman-Monteith equation (FAO et al., 2006) already presented in section 2.1.1.2.4 in order to characterize the daily climatic conditions and to compare tree transpiration estimated with the water balance presented hereinabove to the climatic demand. Penman-Monteith equation corresponds to the evapotranspiration of a 1 m² reference surface of 0.12 m high well-watered grass crop fully exposed to sunlight radiation and with an albedo of 0.23. In the RSCS

experiment, the north mast was located over a lawn regularly trimmed but the height of the grass was not exactly 12 cm and the water availability for the grass was not controlled. Nonetheless, the term ET_{ref} will be used for the RSCS experiment even though the requirements of the Penman-Monteith equation were not exactly met.

3.1.2.2.4. Insolation ratio

The daily insolation ratio was characterized by computing the ratio of the daily integral of the incident global radiation on top of the studied canyon street R_{top_street}, measured at 2.1 m a.g.l. using the pyranometer located in the NV zone of the street, to the daily integral of the theoretical solar radiation received by the earth above the atmosphere R_{top_atm} (reported by FAO et al. (2006)) as proposed by Mballo et al. (2021) in equation (11).

$$Insolationratio = \frac{R_{top_{street}}}{R_{top_{atm}}} \quad \textbf{(11)}$$

The days were considered sunny when the insolation ratio exceeded 0.65 and cloudy when it was lower than 0.45 (Mballo et al., 2021).

3.1.2.2.5. Downward short wavelength radiation intercepted by the tree crowns

The downward short wavelength radiation was monitored at various locations inside and outside the canyon street enabling to estimate the amount of radiation intercepted by the tree crowns. In the NV zone, the Photosynthetically Active Radiation (PAR) measured at 0.65 m a.g.l. was used to compute the downward short wavelength radiation at this height. To do so, the measurements of downward short wavelength radiation and PAR carried out on top of the NV zone (respectively at 2.1 m and 2 m a.g.l.) were used to compute the proportion of PAR in the global incident radiation at every time step (10 minutes) as this ratio may vary with the hour, date and location (Britton and Dodd, 1976). Then, this ratio was applied to the PAR measured at 0.65 m a.g.l. at each time step in the NV zone as presented in equation (12).

$$R_{10min-0.65m-NV} = PAR_{10min-0.65m-NV} \times \frac{R_{10min-2.1m-NV}}{PAR_{10min-2m-NV}} \quad \textbf{(12)}$$

$R_{10min\text{-}0.65m-NV}$ *and* $R_{10min\text{-}2.1m-NV}$ are the downward short wavelength radiation calculated at 0.65 m a.g.l. and measured at 2.1 m a.g.l. in the NV zone at each time step, $PAR_{10min\text{-}0.65m-NV}$ and $PAR_{10min\text{-}2m-NV}$ are the PAR measured respectively at 0.65 m and 2 m a.g.l. in the NV zone at each time step.

Then, in order to compute the amount of radiation intercepted by the tree crowns, the difference of the daily integral of the short wavelength radiation calculated at 0.65 m a.g.l. in the NV zone and measured at 0.78 m a.g.l. in both vegetated zones was computed and compared to the daily total amount of radiation calculated in the NV zone through the calculation of a ratio presented in equations (13) and (14).

$$r_{inter.crownWW} = \frac{R_{0.65m-NV} - R_{0.78m-WW}}{R_{0.65m-NV}} \quad \textbf{(13)}$$

$$r_{inter.crownWR} = \frac{R_{0.65m-NV} - R_{0.78m-WR}}{R_{0.65m-NV}} \quad \textbf{(14)}$$

$R_{0.78m-WW}$, $R_{0.78m-WR}$ and $R_{0.65m-NV}$ are the daily integral of the downward short wavelength radiation in $MJ.m^{-2}.day^{-1}$ measured at 0.78 m a.g.l. in the WW zone, the WR zone and 0.65 m a.g.l. in the NV zone and $r_{inter.crownWW}$ and $r_{inter.crownWR}$ are the ratios of the daily integral of the short wavelength radiation intercepted by the crown of each vegetated zone (no unit).

3.1.2.2.6. Universal Thermal Climate Index (UTCI)

The Universal Thermal Climate Index (UTCI) was calculated at human height (0.4 m a.g.l at reduced scale) following the methodology developed by Bröde et al. (2012) on the basis of the measurement of air temperature, air relative humidity and wind speed all carried out at the same location and on the calculation of the mean radiant temperature (T_{mrt}) with equation (15) (Huang et al., 2014).

$$T_{mrt} = \sqrt[4]{\left(T_g + 273.15\right)^4 + \frac{1.06 \times 10^8 \times {V_a}^{0.58}}{\varepsilon \times D^{0.42}}\left(T_g - T_a\right)} - 273.15 \quad \textbf{(15)}$$

T_{mrt}, T_g and T_a are respectively the mean radiant temperature, the globe temperature and the air temperature in °C calculated and measured at the chosen location (Figure 21). ε and D are respectively the globe emissivity (0.95) and diameter (0.15 m), and V_a is the wind speed measured in $m.s^{-1}$ at 0.4 m a.g.l with the 3D sonic anemometer between the vegetated and non-vegetated zone for inside street T_{mrt} assessment.

3.1.3. Results

3.1.3.1. Meteorological conditions of the studied period

The two studied months were characterized by an alternation of warm, sunny and rain-free periods (especially the two first weeks of July and August) characterized by a high reference evapotranspiration and insolation ratio, and of cloudy and rainy periods (from July 19th to 22nd and from August 13th to 26th) which lowered both the reference evapotranspiration and the insolation ratio (Figure 23). The air temperature of the studied period was on average 2 °C higher than the reference average climatic conditions recorded at the Météo-France meteorological station (reference period: 1991-2020) whereas the total rainfall was twice lower.

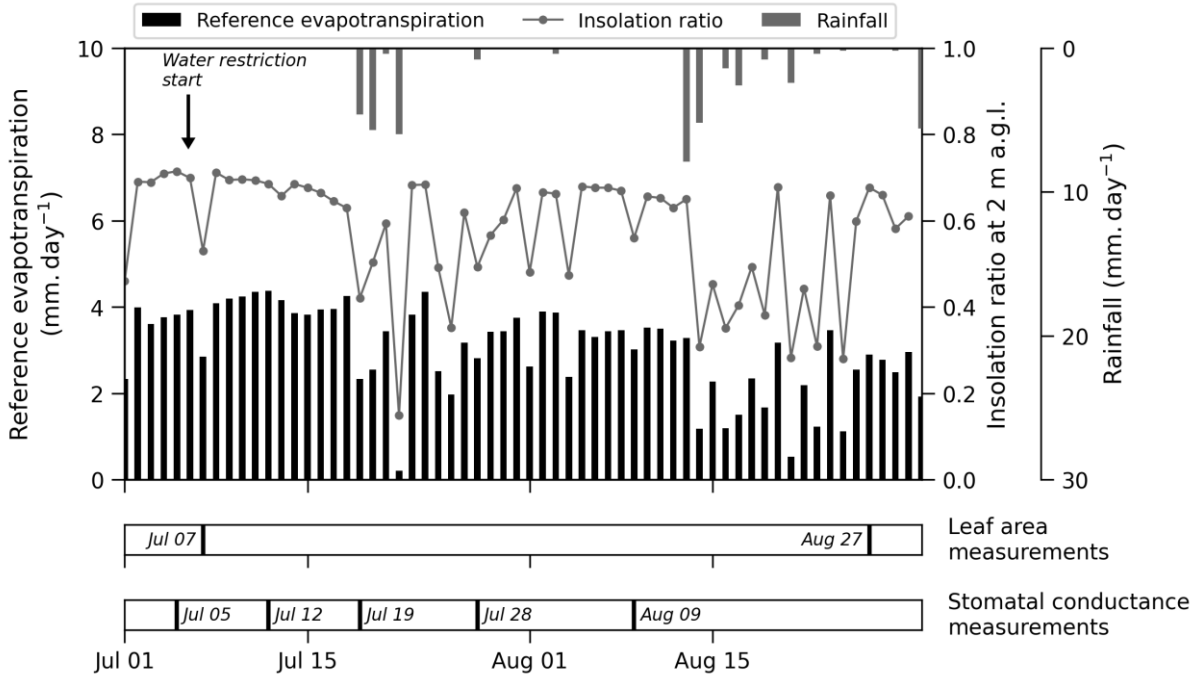

Figure 23: Evolution of the reference evapotranspiration calculated at the North mast, the insolation ratio calculated above the street and the rainfall measured at the Météo-France meteorological station during July and August 2022. The multiple days of interest are highlighted below the figure.

3.1.3.2. Soil volumetric water content

During the studied period, in the WW zone, the irrigation event was followed by a quick increase of the VWC which was close to the field capacity (approx. 28 %) every night (Figure 24). Then, the VWC quickly decreased during the night as part of the water was drained in depth in the container. Drainage water was collected every day which confirmed that the water supply was sufficient to cover the tree transpiration. During daytime, water was pumped by the

trees for their transpiration leading to a noticeable decrease of the VWC. The R-AWS was totally consumed most of the time at the end of the day before irrigation.

In the WR zone, the same behavior was observed before the beginning of the water restriction. Starting from July 6th, the soil VWC decreased and quickly approached the permanent wilting point (approx. 10 %). The small doses of water poured each day starting from July 7th enabled to maintain the VWC in the NR-AWS from July 6th and lower than 16 % at night after irrigation from July 14th with lower amplitudes of VWC variations compared to the WW zone. From August 15th, the irrigation dose poured to the WR trees was reduced as the reference evapotranspiration and insolation ratio were lower in order to prevent an increase of the soil VWC. Then, the soil VWC of the WR trees reached values even lower, close to the permanent wilting point, and the amplitude of the daily variations was also reduced.

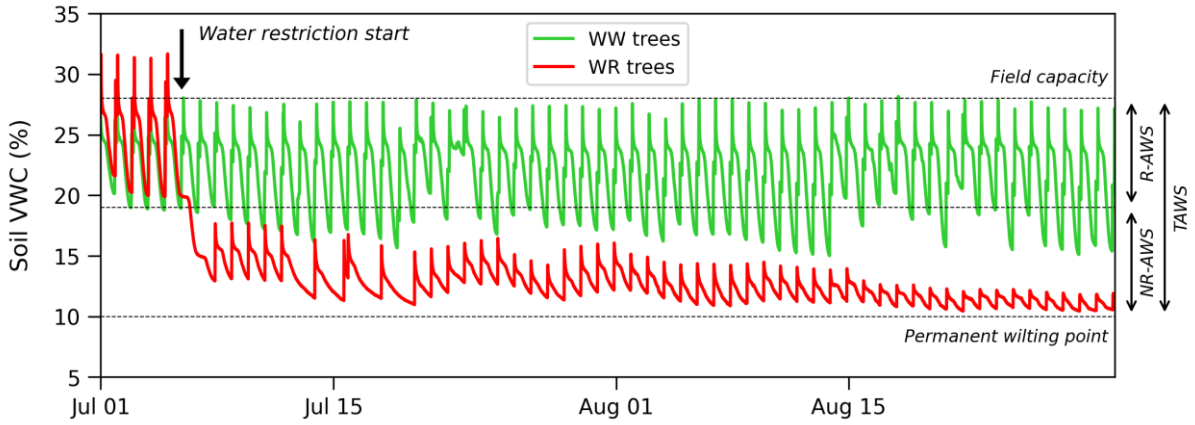

Figure 24: Evolution of the average soil volumetric water content (VWC) measured for 3 well-watered (WW) trees and 3 water-restricted (WR) trees during July and August 2022. Each tree was equipped with 2 soil water content sensors. Maximum standard deviation is 6.5 % for both WW trees and WR trees (n=6 capacitive probes for each zone). The ranges of soil VWC for the total available water storage (TAWS), the readily available water storage (R-AWS) and the non-readily available water storage (NR-AWS) are displayed.

3.1.3.3. Leaf area

The LAI reported in Table 3 were close to those measured by other full-scale studies. Shahidan et al. (2010) studied for instance *Mesua ferrea* L. and *Hura crepitans* L. with LAI ranging from 1.5 to 6.1. Therefore, the latent heat flux in the present study is comparable to the one expected at full-scale with trees having comparable LAI and under equal water availability and climatic conditions. During the studied period, the leaf area, crown projected area and LAI increased for the WW trees while these three variables decreased for the WR trees (Table 3).

Table 3: Average total leaf area, crown projected area and Leaf Area Index (LAI) per tree (± standard deviation) measured during summer 2022 in the well-watered zone (WW) and the water-restricted zone (WR).

Date	WW zone			WR zone		
	Leaf area ($m^2.tree^{-1}$)	Crown projected area (m^2)	LAI ($m^2.m^{-2}$)	Leaf area ($m^2.tree^{-1}$)	Crown projected area (m^2)	LAI ($m^2.m^{-2}$)
July 7th	2.6 (±0.2)	1.1	2.4 (±0.2)	2.5 (±0.2)	1.1	2.4 (±0.2)
August 27th	4.4 (±0.3)	1.3	3.3 (±0.2)	1.8 (±0.0)	1.0	1.7 (±0.0)

3.1.3.4. Tree transpiration

Before the water restriction started, both vegetated zones had the same behaviour (Figure 25a). The WR trees transpired on average 2.9 $L.tree^{-1}.day^{-1}$ and the WW trees 2.4 $L.tree^{-1}.day^{-1}$ which is slightly higher than the well-watered *Malus Coccinella*® 'Courtarou' of comparable LAI (2.5 $m^2.m^{-2}$) studied in 2020 by Mballo et al. (2021) in the same experimental facility during a sunny day (2.0 $L.tree^{-1}.day^{-1}$) with a 0.5 mm lower reference evapotranspiration. At full scale, Caspari et al. (1993) measured higher transpiration rates (from 3 to 4.8 $L.tree^{-1}.day^{-1}$) for two well-watered 5-year old Asian pear trees (*Pyrus serotine*) but with trees having a higher leaf area (6 $m^2.tree^{-1}$).

The beginning of the water restriction led to a quick and strong reduction of the transpiration of the WR trees. From July 6th to August 31st, the WR trees transpired on average 0.5 $L.tree^{-1}.day^{-1}$ which is 81 % less than the WW trees (3 $L.tree^{-1}.day^{-1}$ on average).

The daily average stomatal conductance of the central WW tree ranged from 5.7 to 12.1 $mm.s^{-1}$ and appeared to be influenced by the daily meteorological conditions (Figure 25b). On July 5th and 12th, the reference evapotranspiration and the cumulated incident radiation were high (respectively 3.7 and 4.3 $mm.day^{-1}$ and 28.3 and 27.0 $MJ.m^{-2}.day^{-1}$) which led to a high stomatal conductance for the WW tree exceeding 10 $mm.s^{-1}$. Conversely, the reference evapotranspiration and the incident radiation were low on July 28th and August 9th (respectively 2.8 and 2.9 $mm.day^{-1}$ and 18.0 and 21.7 $MJ.m^{-2}.day^{-1}$) which led to a lower stomatal conductance of 5.7 and 6.5 $mm.s^{-1}$ respectively. July 19th however was marked by a high stomatal conductance in spite of low reference evapotranspiration and incident radiation.

The stomatal conductance of the WR tree was already lower than the one of the WW tree on July 5th (5.7 $mm.s^{-1}$ compared to 12.1 $mm.s^{-1}$) but the difference was statistically significant according to the Welch's t-test only from July 12th when the stomatal conductance of the WR tree collapsed to 1.1 $mm.s^{-1}$ before remaining lower than 0.6 $mm.s^{-1}$ during the next

measurement days. Such values are consistent with those already reported in the literature. Konarska et al. (2016) measured midday stomatal conductance ranging from approximately 1.5 to 5 $mm.s^{-1}$ for 7 species of street trees but could not control their access to water. Bréda et al. (1993) measured approximately 8 $mm.s^{-1}$ for well-watered trees and 1 $mm.s^{-1}$ or less for water-stressed trees when studying *Quercus petraea* and *Quercus robur*.

The air absolute humidity was calculated in the centre of the tree canopy of each zone at 1.5 m a.g.l. and averaged around noon (from 11:00 to 13:00 UTC) when the trees are fully exposed to sunlight. The difference between the WW and WR zones was computed and expressed as a percentage of the absolute humidity calculated in the WW zone (Figure 25c). A negative difference means that the absolute humidity is lower in the WR zone than in the WW zone. The average difference of absolute humidity between both zones was -0.5 % before the water restriction start. Then, it noticeably decreased to -11.4 % on July 13 (day 8 of the water restriction). The difference between both zones was less important in August but an average difference of -4.7 % was calculated over the whole restriction period. which means that the concentration of water vapour was less important in the surrounding air of the WR trees compared to that of the WW trees.

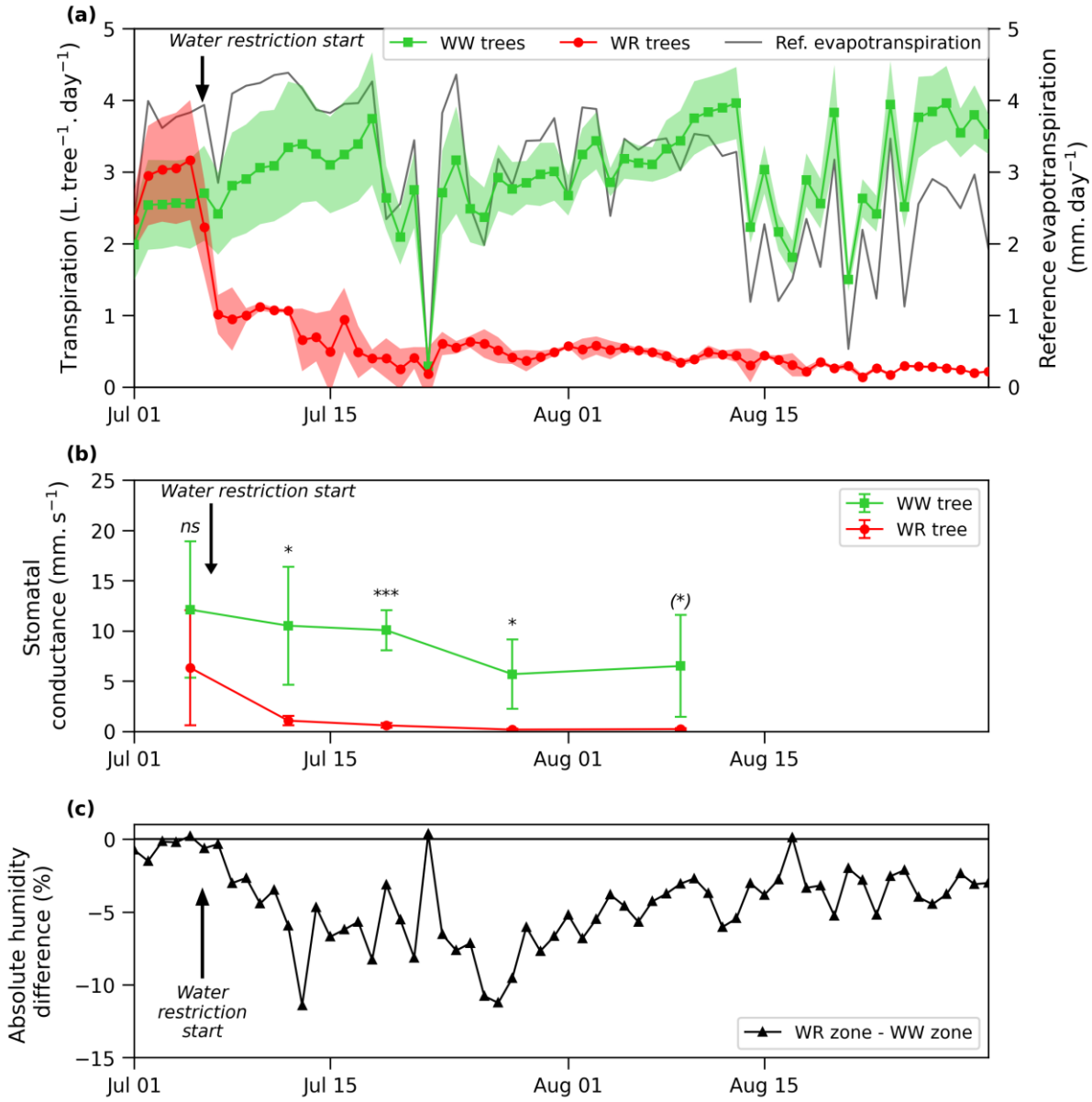

Figure 25: Evolution during July and August 2022 of: (a) the reference evapotranspiration calculated at the North mast and the average daily tree transpiration and the associated standard deviation (n=3) calculated for 3 well-watered (WW) trees and 3 water restricted (WR) trees. (b) The daily average stomatal conductance and the associated standard deviation measured on 5 leaves of the central tree of each zone from 10:00 to 12:00 UTC. Results of the daily Welch's t-test comparing the means of both vegetated zones are displayed (n=5 leaves): ns: $p > 0.1$, (*): $0.1 \geq p > 0.05$, *: $0.05 \geq p > 0.01$, ***: $1.0e\text{-}3 \geq p > 1.0e\text{-}4$. (c) The absolute humidity difference between WR and WW zones calculated at 1.5 m a.g.l. around noon (from 11:00 to 13:00 UTC) and expressed as a percentage of the absolute humidity measured in the WW zone.

3.1.3.5. Radiation interception

Until July 5th, before the start of the water restriction, the WW and WR trees intercepted a similar portion of downward short wavelength radiation (as defined in section 3.1.2.2.5), respectively 82 % and 83 % (Figure 26). Such results were found to be consistent with full scale results such as those from Shahidan et al. (2010) who found from 79 % to 93 % radiation interception with LAI ranging from 1.5 to 6.1 for *Mesua ferrea* L. and *Hura crepitans* L. Then, the radiation interception ratio of the WR trees slowly decreased and reached on average 76 % during August 2022, remaining over 69 % until the end of the studied period. At the same time, the ratio of radiation intercepted by the WW trees slowly increased and reached a plateau at 86 % on average of the incoming radiation in the end of July 2022, remaining lower than 90 % until the end of the studied period. During August 2022, the average difference recorded between both zones was 9.5 points of % and the maximum difference was 17 points of % (August 25th).

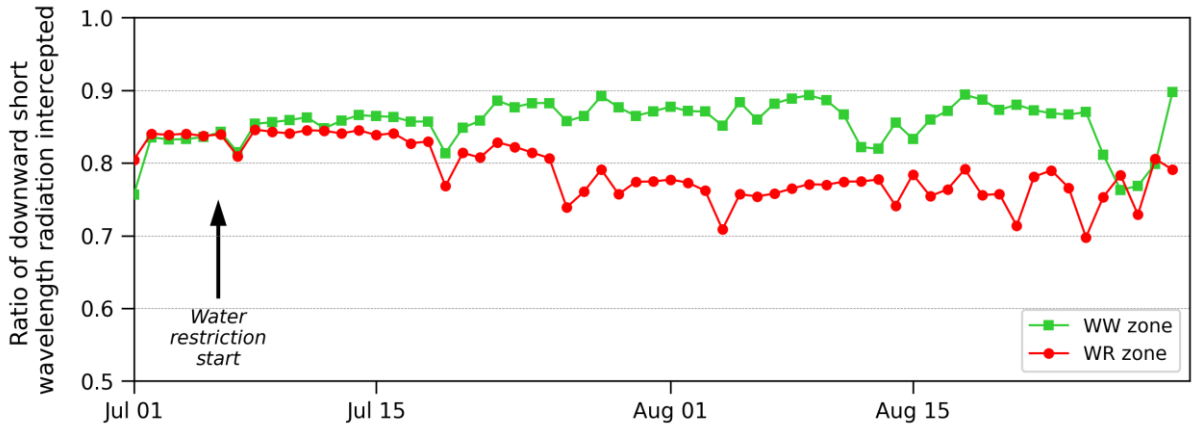

Figure 26: Evolution of the ratio of the daily integral downward short wavelength radiation intercepted by the tree crowns calculated in the centre of both vegetated zones at 0.78 m a.g.l. on the basis of the daily integral incident radiation calculated in the non-vegetated (NV) zone at 0.65 m a.g.l.

3.1.3.6. Energy balance approach

Following the methodology reported by Mballo et al. (2021), the sum of the daily amount of short wavelength radiation intercepted (section 3.1.2.2.5) and the daily amount of energy consumed by the evaporation of the transpired water (section 3.1.2.2.2) was considered as a daily amount of energy dissipated by the trees and graphed in Figure 27. The contribution of tree transpiration is also displayed and that of the radiation interception can be inferred as the difference between the total amount of energy dissipated and the contribution of transpiration.

The average total amount of energy dissipated by both vegetated zones were very close from July 1st to 5th (20.3 MJ.m^{-2}.day^{-1} with 5.7 MJ.m^{-2}.day^{-1} (29 %) attributed to transpiration for the WW zone compared to 21.6 MJ.m^{-2}.day^{-1} dissipated in total by the WR zone with 6.7 MJ.m^{-2}.day^{-1} (32 %) attributed to transpiration). Mballo et al. (2021) calculated a slightly lower contribution of tree transpiration during a sunny day of summer 2020 with well-watered apple trees (26 %) but with a lower transpiration rate as mentioned in section 3.1.3.4.

In the WW zone, the total amount of energy dissipated by the trees remained on average close to 17.3 MJ.m^{-2}.day^{-1} all along summer with a slight increase of the contribution of transpiration which reached 35 % on average during August 2022.

In the WR zone, the total amount of dissipated energy noticeably decreased from 21.6 MJ.m^{-2}.day^{-1} (average from July 1st to 5th) to 10.9 MJ.m^{-2}.day^{-1} (average during August 2022) and most of this reduction was attributed to the reduction of the WR trees transpiration (-6 MJ.m^{-2}.day^{-1}). In August 2022, the total amount of energy dissipated by the WR zone was 37 % lower than that of the WW trees and 8.1 % of this total amount came from the evaporation of transpired water.

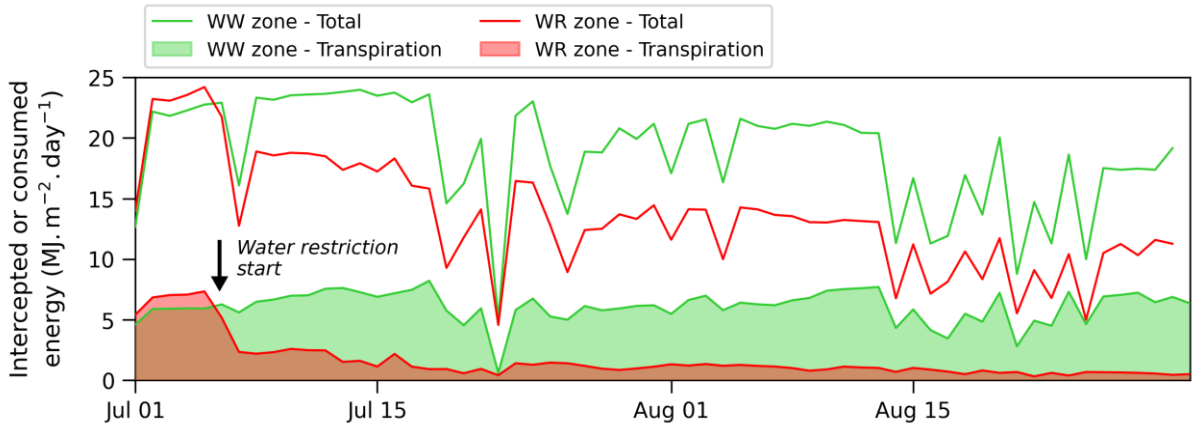

Figure 27: Evolution of the daily amount of energy consumed by the tree transpiration and of the daily total amount of energy dissipated (consumed by the evaporation of transpired water + intercepted by the tree crowns) by each vegetated zone during summer 2022. The daily amount of radiative energy intercepted by the tree crowns can be inferred as the difference between the total amount and the amount related to transpiration.

3.1.3.7. Climatic benefits of the trees

The air temperature and UTCI measured in the three zones at 0.4 m a.g.l. were averaged daily between 10:00 and 14:00 UTC during July and August 2022 (Figure 28) as the maximum climatic benefits provided by the well-watered trees were measured at solar noon by Mballo et al. (2021) in this canyon street. The differences between the WR zone and the WW zone (WR zone - WW zone) were also calculated and graphed in Figure 28c.

From July 1st to 5th (i.e. before the water restriction), the mean air temperature measured around noon was on average 2.7 °C lower in the WW zone and 1.8 °C lower in the WR zone compared to the NV zone. Thus, the WR zone was on average 0.9 °C warmer than the WW zone. Indeed, a non-constant pre-existing difference approaching 0.9 to 1 °C on average between the sensors was noticed and has to be considered when comparing both vegetated zones. Such results fit in the range of diurnal air temperature reductions found in the literature (from 0.7 °C (Souch and Souch, 1993) to more than 5 °C (Vailshery et al., 2013)) and are consistent with the maximum 2.7 °C reduction measured at midday by Mballo et al. (2021) for well-watered trees. In August 2022, the WR zone was on average 1.2 °C hotter than the WW one (these differences include the pre-existing difference mentioned earlier) and 1.3 °C hotter when focusing on the driest and sunniest days of August (11 days with no rainfall and an insolation ratio greater than 0.65). During these eleven days, the air temperature was on average 3.1 °C lower in the WW zone and 1.8 °C lower in the WR zone compared to the NV zone.

From July 1st to 5th , the UTCI was on average 6.3 °C lower in the WW zone and 5.7 °C lower in the WR zone compared to the NV zone which is consistent with the findings of other studies at full scale (Coutts et al., 2016) and with the 8 °C UTCI reduction measured at midday during a sunny day by Mballo et al. (2021) under well-watered trees in the present canyon street. The UTCI was on average 0.6 °C higher in the WR zone than in the WW one, which is probably caused by the pre-existing difference of air temperature mentioned hereinabove. During this period, the UTCI in the NV zone reached the high heat stress category almost every day unlike both vegetated zones which were maintained in the moderate heat stress category. During July and August 2022, the UTCI in the NV zone reached the very high heat stress category during 10 days whereas this category was reached only on July 18th in the WR zone and it was not reached in the WW zone. The UTCI difference between both vegetated zones increased along summer 2022. In August 2022, the UTCI was on average 1.6 °C higher in the WR zone compared to the WW one. This difference reaches 1.8 °C when focusing on the driest and sunniest days of August (11 days with no rainfall and an insolation ratio greater than 0.65). During these eleven days, the UTCI was on average 6.3 °C lower in the WW zone and 4.5 °C lower in the WR zone compared to the NV zone. At the end of August 2022, UTCI differences reaching up to 2.6 °C (July 30th) can be noticed between both vegetated zones.

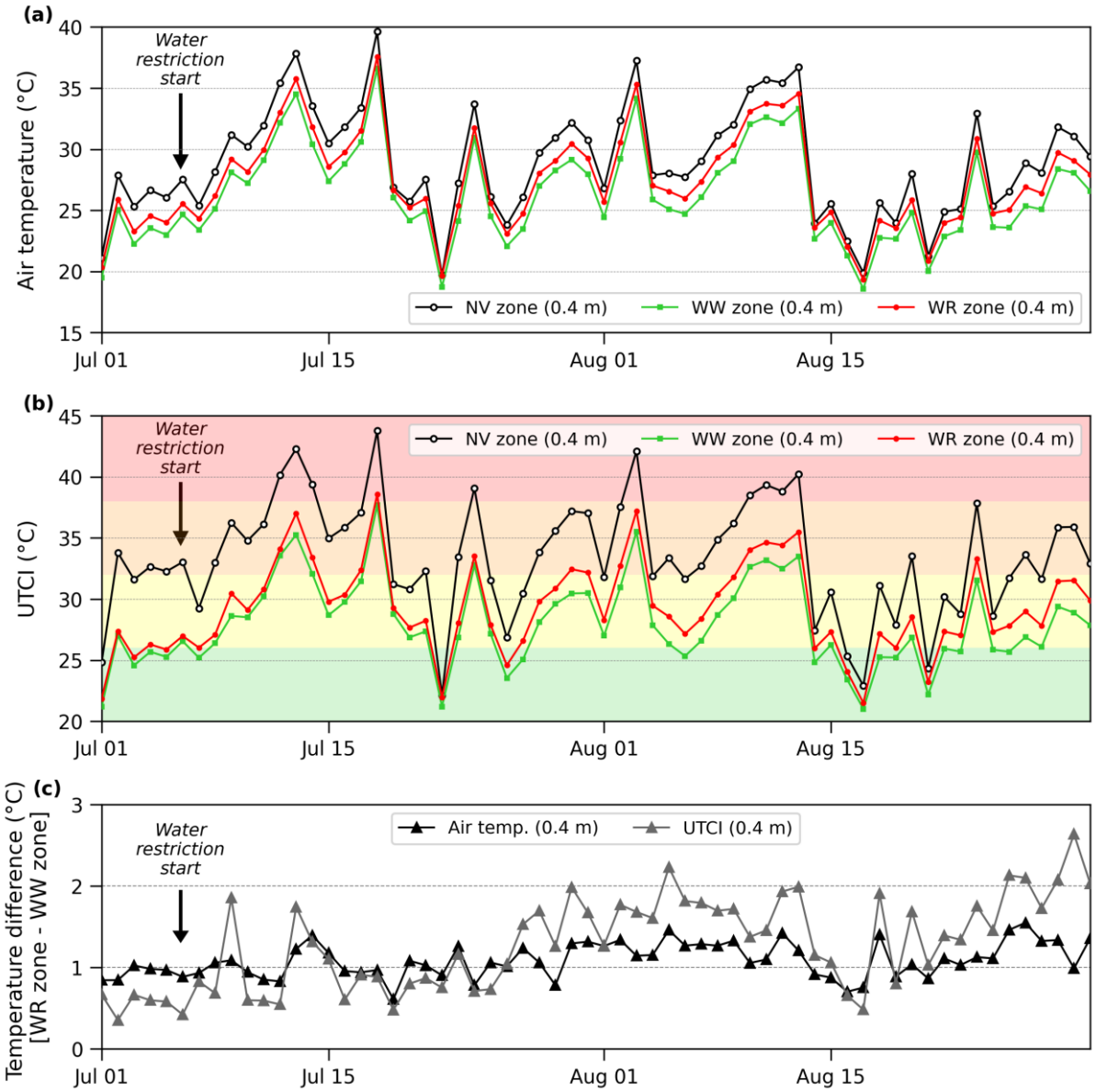

Figure 28: Evolution of: (a) the air temperature measured at 0.4 m a.g.l. in each zone of the street and averaged from 10:00 UTC to 14:00 UTC; (b) UTCI calculated at 0.4 m a.g.l. in each zone of the street and averaged from 10:00 UTC to 14:00 UTC regarding the different thermal stress categories: no thermal stress (9 to 26 °C UTCI, green), moderate heat stress (26 to 32 °C UTCI, yellow), high heat stress (32 to 38 °C UTCI, orange), very high heat stress (38 to 46 °C UTCI, red) and extreme heat stress (>46 °C UTCI, not shown); (c) the difference of air temperature and UTCI between both vegetated zones (WR zone - WW zone) calculated daily between 10:00 and 14:00 UTC at 0.4 m a.g.l. during summer 2022.

3.1.4. Discussion

The present study relies on a reduced scale experimental facility built in the frame of a wider research program aiming at studying the climatic benefits of street trees. So far, only data acquired in 2020 and 2021 relying on well-watered trees (Mballo et al., 2021; Demotes-Mainard et al., 2022; Herpin et al., 2022) or during a preliminary study (Thierry et al., 2022) with a very short water restriction (1 week) were partially released. Thus, the present contribution investigates, for the first time, the impact of a long water restriction (8 weeks) on street trees climatic benefits using new experimental data acquired over summer 2022. The use of a reduced scale facility enabled to perform continual monitoring and to guaranty the homogeneity of some parameters such as building heights and surface materials but the comparison of the results with full-scale studies is not trivial. However, Mballo et al. (2021) have already brought various answers to this aspect and the present results were found to be consistent with various full-scale studies, as shown in the results section.

Thereafter, we will discuss first how the spatial and temporal variability of the studied variables have to be taken into account to understand the phenomena at stake and then, how the present study highlighted the effect of a water restriction on the variables involved in the climatic benefits of street trees.

The climatic benefits provided by street trees are subject to a spatial variability induced by multiple factors such as the geometry of the surrounding environment, the surface materials or the trees attributes (Jamei et al., 2016). The present study relies on local sensors such as capacitive probes or radiometers which may fail to give an exhaustive representation of the phenomena at stake as they may be very sensitive to the positioning because of the heterogeneity of soil VWC or of the tree crowns architecture. Also, the two-month time series showed strong daily variation for many variables which is probably related to the daily meteorological conditions. The tree transpiration seemed to be highly driven by the daily reference evapotranspiration when considering WW trees whereas the transpiration of the WR trees appeared to be limited by the daily amount of water poured through the controlled irrigation. Then, as a cloudy weather comes with lower direct solar radiation, the daily insolation ratio highly influenced the amount of radiation intercepted by both vegetated zones as well as the total amount of energy they dissipate and induced daily variations of air temperature and UTCI reduction provided by the trees. This is consistent with the strong influence of the incident solar radiation on UTCI reduction highlighted by Herpin et al. (2022).

Nevertheless, the influence of the water restriction on the studied variables could be highlighted. The WW trees were not limited by water availability allowing an increase of their leaf area, crown projected area and LAI as well as their radiation interception ratio and transpiration (4 $L.tree^{-1}.day^{-1}$ during the very last days of August compared to 2.4 $L.tree^{-1}.day^{-1}$ in the beginning of July). However, even though on-site observations reported that the leaf area of the WW trees was still increasing in August 2022, their radiation interception did not exceed 90 %, meaning that they may have reached a maximal radiation interception capacity that cannot be exceeded even with a greater leaf area. (T. Chen et al., 2023) highlighted this threshold effect on various microclimatic variables through a numerical parametric study. Also, the lower insolation ratio observed around mid-August led to a slight decrease of the amount of radiation intercepted by the WW trees which induced an increase of the contribution of transpiration to the climatic benefits.

Conversely, the WR trees transpiration was strongly and quickly reduced: it was already half that of the WW trees on the second day of restriction and was on average 81 % lower than that of the WW trees during the entire water restriction period (Figure 25). Such results were very consistent with the quick partial closure of the WR trees stomata as well as the decreasing amount of water vapour measured into the atmosphere of the WR tree crowns (Figure 25). The crown projected area of the WR trees remained almost constant during the studied period suggesting that the branches stopped growing early in the summer meanwhile the leaf area and the LAI decreased, likely due to partial defoliation observed on-site (Table 3), which led to a decrease of their radiation interception ratio (Figure 26). Still, their remaining leaf area and stems appeared to be sufficient to intercept at least 69 % and on average 76 % of the radiation measured in the NV zone during August 2022. As a consequence, the total amount of energy dissipated by the WR trees noticeably decreased and most of this reduction was attributed to the reduction of the WR trees transpiration although transpiration was only responsible for one third of the total amount of energy dissipated for trees experiencing well-watered conditions (Figure 27).

Nevertheless, the WR zone kept providing noticeable climatic benefits until the end of the studied period in spite of the lack of water. Taking into account that air temperature and UTCI were slightly higher in the WR zone compared to the WW zone at the beginning of the studied period, the net difference of air temperature measured between both vegetated zones at 0.4 m a.g.l. increased by about 0.3 °C (Figure 28) which is almost negligible compared to the sensors accuracy (±0.2 °C, see Table 2). This could suggest that the air temperature reduction provided by the trees under their crown compared to the NV zone may be more related to the

interception of the incident radiation, which prevents the street surfaces from overheating, than to the evaporation of the transpired water. The effect of transpiration is noticeable at 1.5 m a.g.l. in the center of the tree crown (Figure 25c) but is probably gradually mixed with the surrounding atmosphere as we move away from the tree crown, especially during high wind situations.

UTCI is very sensitive to radiation and especially to direct short wavelength radiation and it appeared to be more impacted by the water restriction than air temperature. The net difference of UTCI increased by approximately 1 °C, which is noticeable, and highlights the effect of the decreasing radiation interception, but still low regarding the amplitude of the thermal stress categories defined for the UTCI interpretation (e.g. the moderate heat stress ranges from 26 to 32 °C UTCI). This suggests that preserving the shadows cast by the trees is essential to prevent human thermal stress increase during a water restriction.

However, the present measurements carried out under the tree crowns may have been too local to show the entire effect of the increase of the radiation transmitted by the WR trees on the temperature of the surrounding ground and building facades which may have modified both the buildings energy budget as well as human thermal stress in other parts of the street (Figure 27). Thus, it is important to assess the role of the crown of WR trees in the complete radiation balance of the street. To do so, the use of infrared imaging to assess the area of shaded street surfaces or the evaluation of the street surfaces temperature as well as the upward and downward short and long wavelength radiation with a thinner time step during both daytime and night-time could be interesting. Also, the effect of water restriction on UTCI being mainly mediated by radiation interception, the effect of water restriction on crown architecture should be further investigated to understand how it impacts axis and leaf growth as well as defoliation in relation with climatic benefits, especially as different tree species could have contrasted architectures and responses (M. Liu et al., 2022; Rahman et al., 2020).

3.1.5. Conclusion

The present study enabled to evaluate the influence of a long water restriction (8 weeks during summer season with soil VWC in the lower zone of NR-AWS) on the climatic benefits of street trees in a 1/5 scale canyon street. The impact on tree transpiration was quick and strong. A noticeable reduction of the LAI of the WR trees led to a slight decrease of their radiation interception which however remained high. Although the daily total amount of energy dissipated by the WR trees was noticeably reduced, the WR trees maintained efficient cooling benefits all along the water restriction period. No noticeable air temperature difference was measured under the tree crowns of both zones at 0.4 m a.g.l. (equivalent to human height at full scale) but the difference of UTCI calculated under the tree crowns at 0.4 m a.g.l. between the WR trees and the WW trees increased from 0.6 °C before the water-restriction to 1.6 °C in the end of the studied period. The differences of climatic benefits provided by both WW and WR trees remained low which is consistent with the low impact of the water restriction on the radiation interception of the WR trees, since radiation interception is responsible for the major part of the daily total amount of energy dissipated by the trees. The present work should be completed with the monitoring of complementary variables and with deeper analyses on a daily cycle to understand the role of the crown of WR trees in the complete radiation balance of the street. It should also be extended to other tree species in order to help stakeholders select the most adapted tree species regarding both the resistance to drought and the overheating mitigation in cities especially during heatwaves.

3.2. Physiology and spatio-temporal variability of the climatic benefits of well-watered and water-restricted trees during an 8-week summer period

The present section also focuses on the 8-week summer period presented in section 3.1. It takes advantage of the high density of sensors mounted in the reduced scale canyon street as well as of the thin time step of measurement (10 minutes). It focuses first on the effect of the water restriction presented in section 3.1 on tree physiology through the assessment of the evolution to stem diameter variation of the studied trees as well as their leaf temperature. Then, it presents a wider assessment of the influence of the WW and WR trees on the microclimate through the analysis of wall temperature, of a detailed radiation balance and of the microclimate at different locations inside the RSCS. Finally, it evaluates the influence of the daily meteorological conditions on the variability of the climatic benefits.

3.2.1. Materials

The studied canyon street was already widely presented in section 3.1. Figure 30 presents the location of the sensors in the same way as Figure 21 presented in section 3.1.2.1.3 with a top view of the street and a cross section of each zone of the street. The sensors which were not used and not presented in section 3.1 were added to Figure 30 and appear in red.

In addition to the previously introduced measurements, air temperature (T_a) and relative humidity (RH) were also measured at the north mast at 1 m a.g.l. and inside the street at 1 m a.g.l. on the central axis of the street as well as at 0.4 m a.g.l. close to the eastern wall of the street (approximately 15 cm from the wall). The platinum and capacitive probes used for this measurement were placed in mechanically ventilated white painted cylindrical shelters. Both variables were used to compute the absolute humidity (AH).

The globe temperature (T_g) was measured at 0.4 m a.g.l. at approximately 15 cm from the eastern wall in each zone of the street using platinum probes enclosed in black painted copper spheres of 15 cm diameter.

The outside surface temperature of the walls was measured in each zone on the facade of both buildings with fluxmeters mounted at 1 m a.g.l..

The surface temperature of the tree leaves was measured on 5 leaves of the central tree of each vegetated zone at 1.5 m a.g.l. Three leaves were located in the center of the tree crown,

one was located at the eastern edge of the crown and one at the western edge of the crown. Each selected leaf was equipped with a T-type thermocouple stuck on the down-facing side of the leaf with adhesive tape.

Trunk diameter variation was measured on the trunk of each studied tree (three central trees of each alignment) at approximately 0.7 m a.g.l. with microdendrometers (PépiPIAF, INRAE UMR PIAF, France (Adam et al., n.d.)). The installation of the microdendrometers as well as the monitoring of the trunk diameter variation were performed by researchers from the Institute of Research in Horticulture and Seeds (IRHS) in the frame of another PhD project (Canonne et al., 2023). The microdendrometers are made of a static body attached to the trunk which holds a needle able to move back and forth on an axis parallel to one radius of the trunk. The point of the needle is maintained in contact with the bark of the trunk with a spring and with glue applied between the point of the needle and the bark of the tree. Figure 29 shows an example of a microdendrometer mounted on the trunk of one studied tree.

Figure 29: Microdendrometer mounted on the trunk of a studied tree in 2022.

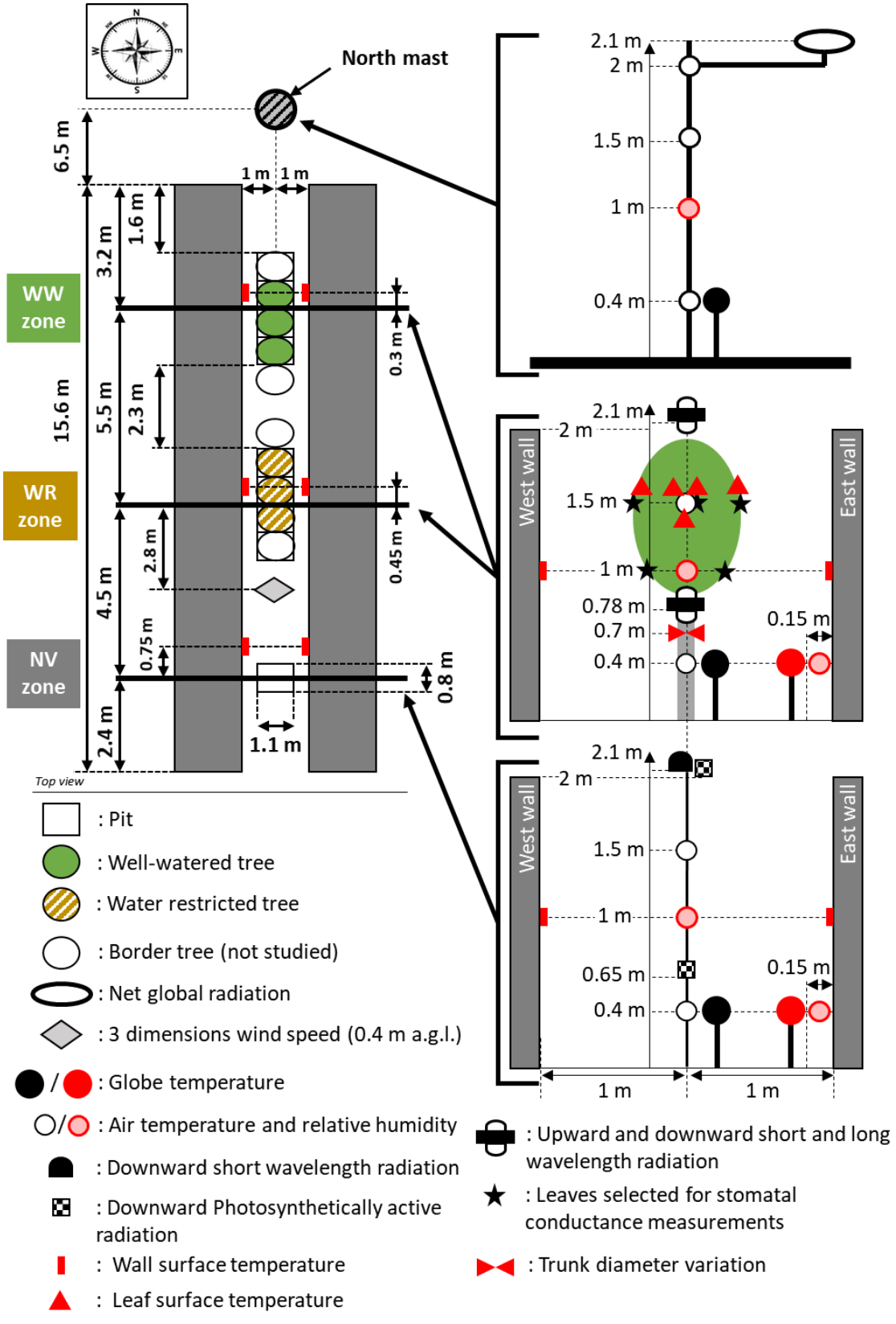

Figure 30: Sketch of the studied canyon street showing the respective positions of the well-watered zone (WW), the water-restricted zone (WR) and the non-vegetated zone (NV) with the location of the sensors in the different zones. The sensors not presented in section 3.1 and used in section 3.2 are in red.

Table 4: Characteristics of the sensors used for the experiment. Only the sensors not presented in section 3.1.2.1 are described. Data-loggers were used to scan all sensors every 10 seconds and record average values every 10 minutes (n.c. = not communicated).

Measured variable	Sensor type	Measurement range	Accuracy	Reference, manufacturer
Trunk diameter variation	Microdendrometer	± 7.5 mm	± 0.5 µm	PépiPIAF, INRAE UMR PIAF, Lycée Lafayette, France
Wall surface temperature	Fluxmeter	n.c.	n.c.	Thermal fluxmeter, Captec
Leaf surface temperature	Thermocouple T-type	-40 to +125 °C	± 0.5 °C	TC S.A.

3.2.2. Methods

3.2.2.1. Leaf temperature

An average leaf surface temperature was calculated for the central tree of each vegetated zone on the basis of the 5 selected leaves and compared to the air temperature measured at 1.5 m a.g.l. in the NV zone of the street which was therefore used as a reference.

3.2.2.2. Trunk diameter variation

The microdendrometers record for each time step the difference between the current position of their needle and the initial position of their needle at the beginning of the acquisition. For each tree, the signal of stem diameter variation was then divided into five indicators which were introduced in previous works found in the literature such as the one of Dietrich et al. (2018). In the present case, the five indicators were expressed in mm as described hereinafter and illustrated in Figure 31.

- DNV: The Daily Net Variation was calculated for each day (n) as the difference between the maximum diameter recorded on day (n) and the maximum diameter recorded on the previous day (n-1) as shown in equation (16). The DNV can then take positive or negative values.

$$DNV_n = Maximum\ diameter_n - Maximum\ diameter_{n-1} \quad (16)$$

- DAmp: The Daily Amplitude of diameter variation was calculated for each day (n) as the difference between the maximum diameter and the minimum diameter recorded on day (n) as shown in equation (17).

$$DAmp_n = Maximum\ diameter_n - Minimum\ diameter_n \quad (17)$$

- MDER: The Maximum Diameter Ever Recorded was calculated daily as the maximum value of trunk diameter ever recorded during the measurement campaign as detailed in equation (18).

$$\{MDER_n = Maximum\ diameter_n\ if\ Maximum\ diameter_n \geq MDER_{n-1}\} \quad (18)$$
$$\{MDER_n = MDER_{n-1}\ if\ Maximum\ diameter_n < MDER_{n-1}\}$$

- DG: The Daily net Growth was calculated for each day (n) as the difference between the MDER of day (n) and the MDER of the previous day (n-1) as shown in equation (19). DG can only take positive values and it assumes that biomass, once created, cannot be lost and that the eventual negative variation between day (n-1) and day (n) is caused by water induced stem shrinkage.

$$DG_n = MDER_n - MDER_{n-1} \quad (19)$$

- MDS: Maximum Daily Shrinkage was calculated daily as the difference between the MDER of day (n) and the minimum diameter recorded during day (n) as detailed in equation (20).

$$MDS_n = MDER_n - Minimum\ diameter_n \quad (20)$$

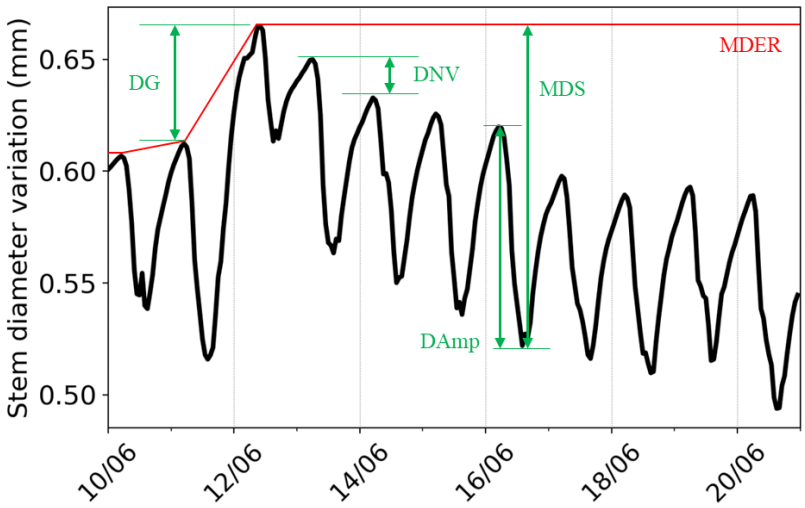

Figure 31: Theoretical representation of the five daily indicators calculated on the basis of the stem diameter variations: DNV: Daily Net Variation, DAmp: Daily amplitude, MDER: Maximum Diameter Ever Recorded, DG: Daily Growth, MDS: Maximum Daily Shrinkage, all expressed in mm.

3.2.2.3. Selection of 3 days of interest

The analyses presented in section 3.1 focused on the 2-month period lasting from July 1st to August 31st 2022. In the present section, some analyses also consider this 2-month period but others focus on 3 days of interest in order to take advantage of the 10-minute time step of the data set and to provide a better understanding of the physical processes on a diurnal cycle. The selected three days had close sunny, warm and rain-free meteorological conditions, more precisely, they were chosen because they had close ET_{ref}, insolation ratios, T_a, wind speed and direction (Figure 32) and no rainfall as described in Table 5. The three days of interest were also chosen in order to illustrate different stages of the water restriction: July 4th, 2 days before the start of the water restriction, July 23rd, day 18 of the water restriction, and August 20th, day 46 of the water restriction. From now on, these three days of interest will be referred as "typical sunny days".

Table 5: Meteorological data measured on site outside the canyon street and at the Météo-France meteorological station located approximately 400 m away from the studied site.

	Source	**July 4th 2022**	**July 23rd 2022**	**August 20th 2022**
Irrigation of WW zone	-	Well-watered	Well-watered	Well-watered
Irrigation of WR zone, Water restriction progress	-	Well-watered, 2 days before start	Water restricted, Day 18	Water restricted, Day 46
ET_{ref} ($mm.day^{-1}$)	Canyon street North mast 2 m a.g.l.	3.8	3.8	3.2
Insolation ratio	Canyon street North mast 2 m a.g.l.	0.71	0.68	0.68
Daily total rainfall ($mm.day^{-1}$)	Météo-France	0.0	0.0	0.0
Maximum T_a (°C)	Canyon street North mast 1.5 m a.g.l.	26.9	28.7	29.0
Average T_a (°C)	Canyon street North mast 1.5 m a.g.l.	19.0	21.3	21.2

	Source	July 4th 2022	July 23rd 2022	August 20th 2022
Minimum T_a (°C)	Canyon street North mast, 1.5 m a.g.l.	9.8	13.4	14.2
Average wind speed at 10 m a.g.l. (m.s^{-1})	Canyon street West mast, 10 m a.g.l.	1.3	0.8	1.1
Average wind direction at 10 m a.g.l.	Canyon street West mast, 10 m a.g.l.	N-W	W-N-W	W
Sunrise time (UTC)		04:11	04:29	05:05
Sunset time (UTC)		20:02	19:48	19:06

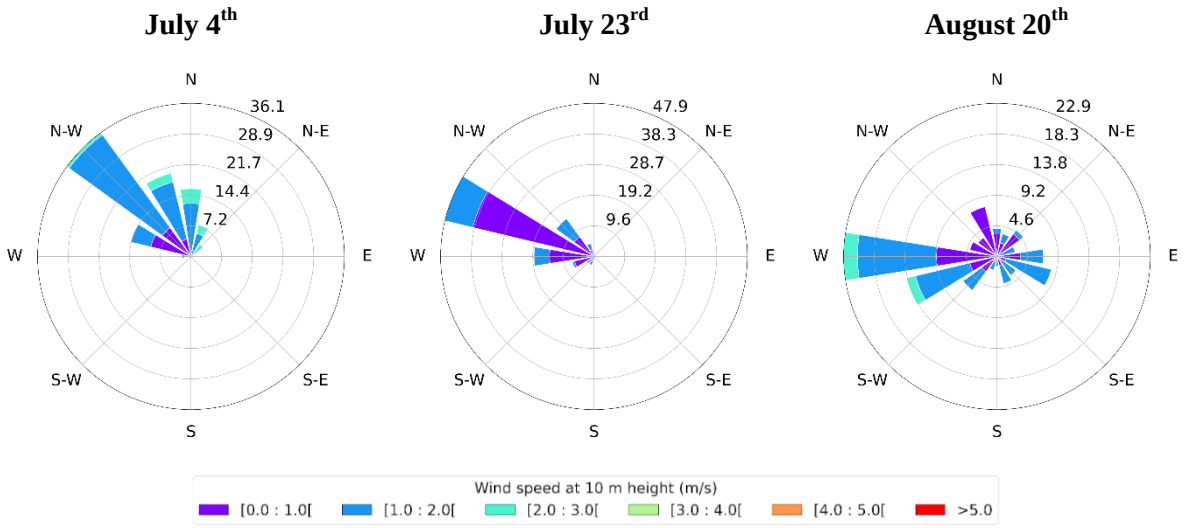

Figure 32: Windroses measured at the west mast of the canyon street at 10 m a.g.l. during the three typical sunny days.

3.2.2.4. Study of heatwaves

Two heatwaves were reported by Météo-France during July and August 2022 in the region of Angers (Figure 33). The first one was short but intense, it lasted 2 days from July 17th to July 18th and air temperature reached 40.7 °C on July 18th (Météo-France, 2022b). The second one lasted 4 days from August 10th to August 13th with air temperature exceeding 35 °C (Météo-France, 2022c). Both heatwaves were also characterized by very high VPD compared to the rest of summer. A daily average VPD of 3.7 kPa was calculated on July 18th and daily average

values ranging from 2.4 kPa to 2.6 kPa were recorded from August 10th to August 13th whereas the daily VPD was around 1.4 kPa on average all over July and August 2022.

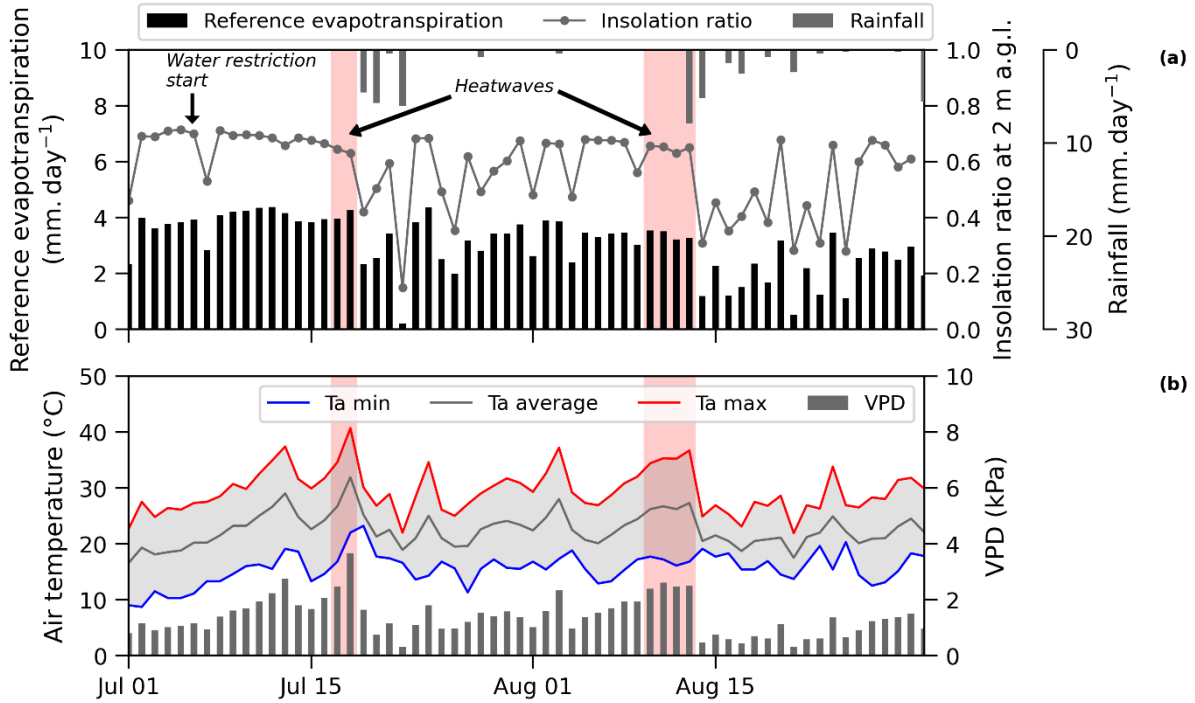

Figure 33: Evolution of (a) the reference evapotranspiration calculated at the North mast, the insolation ratio calculated above the street, the rainfall measured at the Météo-France meteorological station and (b) the average vapor pressure deficit (VPD) calculated at the north mast at 2 m a.g.l. and the daily minimum, mean and maximum air temperature measured by Météo-France during July and August 2022.

In order to analyze the effect of heatwaves and especially high temperatures on the different studied variables, each day of July and August 2022 was associated to one of the 4 following categories depending on its daily maximum air temperature recorded at the Météo-France weather station of Angers-Beaucouzé: $T_{a,\,MAX} < 30$ °C, $T_{a,\,MAX} \in [30$ °C ; 35 °C [, $T_{a,\,MAX} \in [35$ °C ; 40 °C [, $T_{a,\,MAX} \geq 40$ °C. These categories were then used to distinguish the different days on the scatter plots investigating the eventual dependence between the monitored variables.

3.2.2.5. Statistical analyses

Statistical analyses were performed using Python language version 3.9-64. The assumptions used by the different statistical tests were checked using the following packages: *pingouin* (for normality and sphericity), *SciPy* (for normality plot). The statistical tests were performed using the following packages: *SciPy* (Student's t-test). Linear regressions were performed to evaluate the eventual dependence between couples of variables using the

following packages: *sklearn* and *statsmodels*. Principal component analyses (PCA) were performed using the PCA method of the *sklearn* package.

3.2.3. Results

3.2.3.1. Tree physiology

3.2.3.1.1. Effect of maximum air temperature on Tree transpiration

Figure 25a presented in section 3.1.3.4 highlighted the strong reduction of the transpiration of the WR trees starting from the beginning of the water restriction (from July 7th to August 31st). It also suggested that the water restriction had an influence on the relation between tree transpiration and ET_{ref}. Figure 34 confirms that the transpiration of the WW trees was much more sensitive to the variation of ET_{ref} than the one of the WR trees which appeared to be limited by the lack of water. Indeed, the slope of the linear regression was much higher for the WW trees (0.42) than the one of the WR trees (0.14). The ET_{ref} variations therefore could not explain the variability of the transpiration of the WR trees. However, it also appeared that ET_{ref} was not the only variable driving the WW tree transpiration as the linear relation between both variables was not very strong (R^2 equals 0.41 for the WW trees).

The hottest days of the 2-month studied period were associated with high ET_{ref}, which was expected as ET_{ref}, among others, depends on air temperature. For a given ET_{ref}, the transpiration of the WW trees appeared to be generally slightly higher during the hottest days but this was mainly observed for days with ET_{ref} greater than 3.5 mm.day^{-1}. Indeed, for ET_{ref} around 3 mm.day^{-1}, the highest transpiration rates were observed for all the $T_{a, MAX}$ categories. Considering the WR trees, the hottest days did not appear to induce higher transpiration rates.

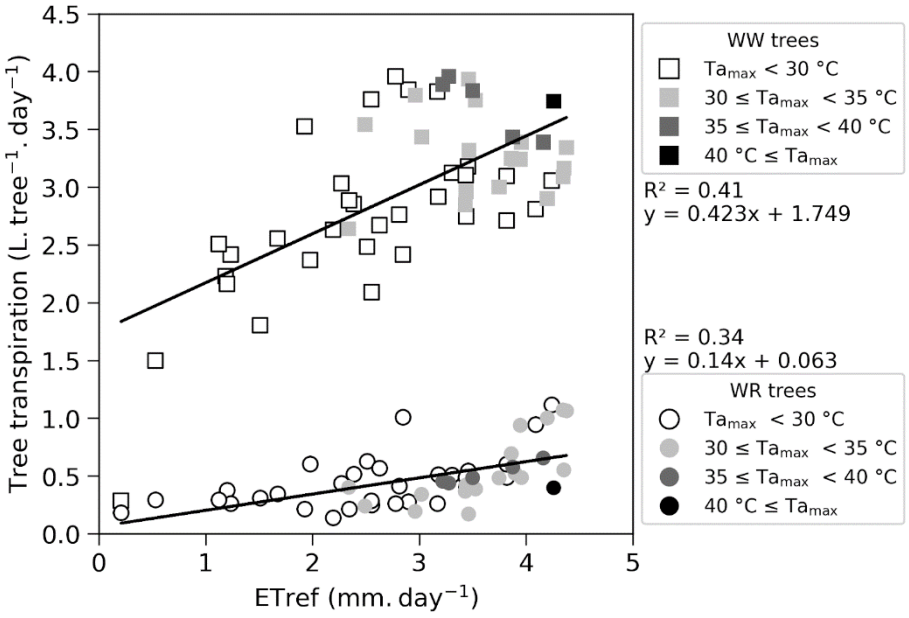

Figure 34: Average daily transpiration calculated in both vegetated zones as a function of the daily reference evapotranspiration measured at 2 m a.g.l. at the north mast from July 7th (2nd day of the water restriction) to August 31st.

3.2.3.1.2. Trunk diameter variations

The evolution of the trunk diameter was monitored over a large period from the end of April until mid-september 2022. Thanks to this long monitoring, it can easily be noticed that all trees were experiencing continuous radial growth from the start of the monitoring (end of April) until the beginning of July, although a small variability may exist for the growth rate between the different trees (Figure 35). From the beginning of the water restriction, the radial growth of the WR trees was stopped and the diameter of their trunk remained almost constant until mid-September. The stomatal closure highlighted in Figure 25 may therefore have strongly reduced the photosynthetic activity thus limiting the formation of new biomass. At the same time, it was highlighted in Table 3 that the crown projected area of the WR trees remained almost constant (slight decrease from 1.1 to 1.0 m².tree^{-1}) all over summer which suggested that the water restriction might also have stopped the elongation process of the WR trees' stems.

Around mid-July, a slight decrease of the stem diameter of the WR trees was noticed and could be linked to the very hot and an intense heatwave of July 17th and 18th (Figure 33). This heatwave which was characterized by a high evaporative demand (high ET_{ref}, VPD and insolation ratio), thereby appeared to lead to a partial drying of the tissues of the WR trees. This heatwave may have required an extremely high transpiration rate which could not be supplied by the low soil VWC and part of the water contained in the WR trees' tissues may have been used for transpiration although the stomatal conductance of the WR trees remained low all over

summer. The real tree transpiration may then be slightly higher than the one calculated with the proposed water balance applied to the soil compartment. Such hypotheses could however not be verified as they would need to measure tree transpiration with other methods for instance enabling to quantify the real amount of water vapor spread out of the leaves.

The water restriction also seemed to induce a slight general increase of Damp of the WR trees. Figure 36 illustrates the variability of DAmp measured for one WW tree and one WR tree before and after the water restriction start. DAmp was on average very close for the WW and the WR tree before the water restriction although a slightly higher variability was observed for the WW tree. The effect of the water restriction on DAmp is clearly noticeable for the WR trees as it led to an increase of both the average DAmp (from 240 to 375 µm) and its standard deviation (88 to 127 µm).

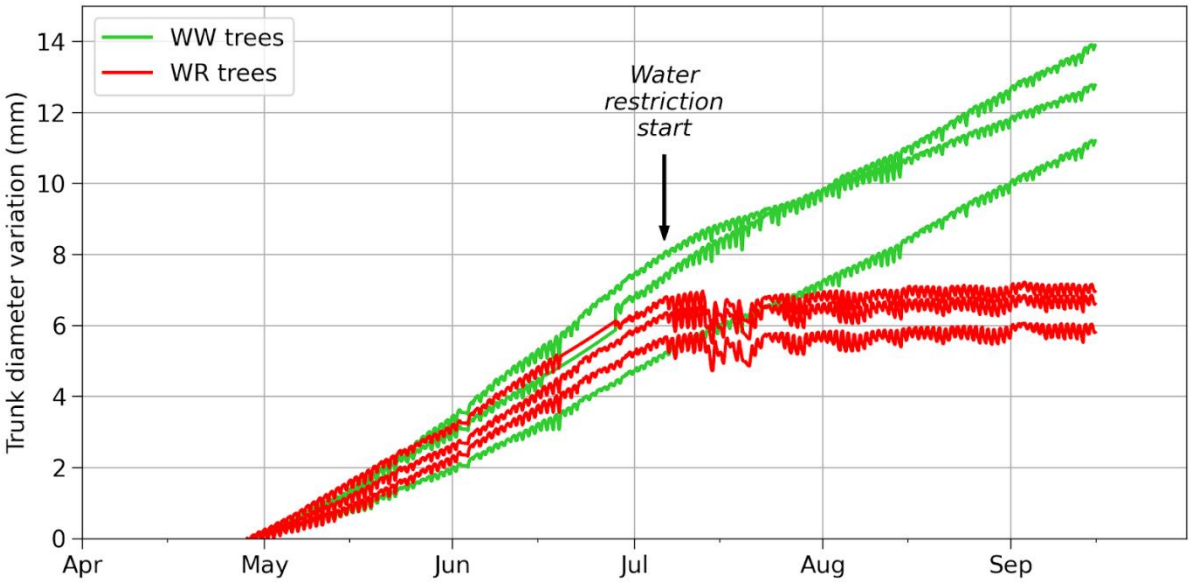

Figure 35: Net evolution of the trunk diameters of each studied tree over the year 2022 adapted from Canonne et al. (2023).

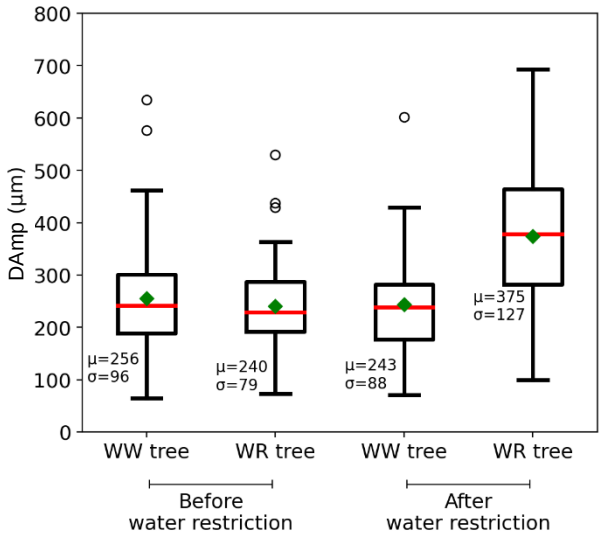

Figure 36: Boxplot of the daily amplitude of the trunk diameter variations recorded for one WW tree and one WR tree before the water restriction (from May 1st to July 6th) and after the water restriction (from July 7th to September 14th).

The sources of variability of DAmp were investigated in Figure 37 and Figure 38 which respectively present the evolution of DAmp as a function of the daily tree transpiration, the daily ET_{ref} and the daily $T_{a,\,MAX}$ during the water restriction period (from July 7th to August 31st). The DAmp pattern of the WW trees was close to the one of their transpiration ($R^2 = 0.55$), especially when transpiration was lower than 3 $L.tree^{-1}.day^{-1}$. When the WW trees transpiration exceeded 3 $L.tree^{-1}.day^{-1}$, a higher variability of DAmp, which appeared to be driven by the daily $T_{a,\,MAX}$, was reported. Similar observations were reported when comparing the evolution of DAmp and ET_{ref} for the WW trees (Figure 38). Then, extreme T_a appeared to have led to extreme DAmp (Figure 37) but not to remarkably high transpiration rate (Figure 34) for the WW trees. During the very warm days, higher DAmp may then indicate that part of the water contained in the WW trees' tissues could have been transpired in addition to the water retrieved from the soil. The real tree transpiration may then be slightly higher than the one calculated with the proposed water balance applied to the soil compartment as already explained earlier.

The WR trees showed a very contrasted behavior during the water restriction period. The variability of their DAmp was higher than the one of the WW trees as shown previously in Figure 36 even though their transpiration remained lower than 1.1 $L.tree^{-1}.day^{-1}$ during the entire water restriction period. Indeed, low daily transpiration rates were calculated for the WR trees even with high DAmp. ET_{ref} was not either useful to explain the variability of DAmp for the WR trees as the relation between both variables was very weak ($R^2 = 0.12$). Although DAmp is supposed to be related to the water fluxes inside the stems and thus to tree transpiration for

WW trees, it appears that it cannot be used as a reliable predictor of tree transpiration for WR trees.

Finally, no noticeable impact of daily $T_{a, MAX}$ could be reported for the WR trees as similar DAmp values could be recorded for days with very contrasted air temperatures. DAmp of approximately 575 µm were for instance recorded during multiple days belonging to all 4 $T_{a, MAX}$ categories.

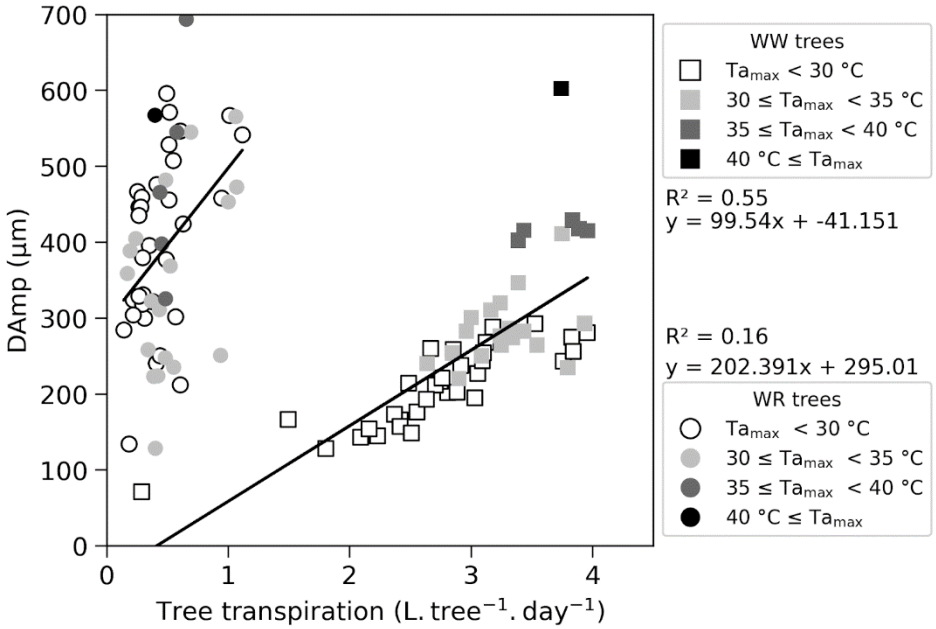

Figure 37: Daily amplitude of the trunk diameter variations (DAmp) of one WW tree and one WR tree as a function of their transpiration and the daily maximum air temperature ($T_{a, MAX}$) for one WW tree and one WR tree from July 7th to August 31st.

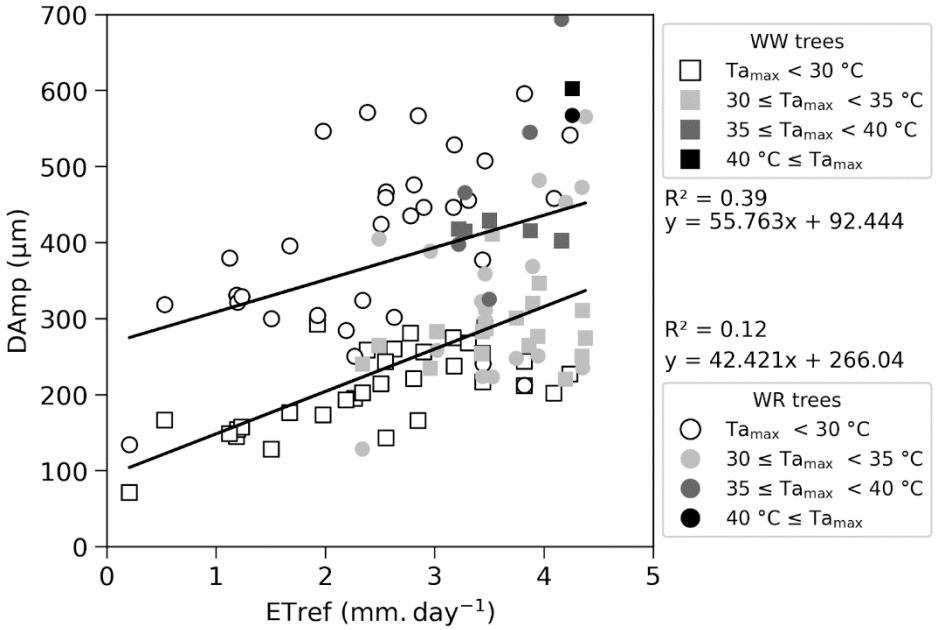

Figure 38 : Daily amplitude of the trunk diameter variations (DAmp) of one WW tree and one WR tree as a function of the reference evapotranspiration (ET_{ref}) and daily maximum air temperature ($T_{a, MAX}$) for one WW tree and one WR tree from July 7th to August 31st.

3.2.3.1.3. Leaf temperature

The average T_{leaf} was very close in both studied trees at night and appeared to be on average lower by 1.3 °C and 1 °C compared to T_a respectively in the WW and WR tree before 08:00 UTC and after 17:00 UTC on July 4th (Figure 39). During the day, when exposed to sunlight, a noticeable overheating of T_{leaf} was observed in both trees compared to T_a even before the water restriction. On July 4th, T_{leaf} was up to 5.7 °C higher and 4.9 °C higher respectively in the WW and the WR tree compared to T_a. However, the standard deviation drawn around T_{leaf} at each time step illustrates the very strong variability of T_{leaf} among the 5 selected leaves of each studied tree. This variability is only visible during the day and is almost null at night which highlights the strong effect of direct exposure to sunlight on the overheating of the leaves. On July 4th, the difference of T_{leaf} between both trees was up to 4 °C at 16:20 UTC and on average 0.4 °C from 08:00 UTC to 17:00 UTC, which was not significant according to a Student's t-test.

On July 23rd (i.e. 18th day of the water restriction), T_{leaf} was very close in both trees in the morning (average difference was 0.2 °C from 08:00 to 13:00 UTC). In the afternoon, T_{leaf} was on average higher by 3.6 °C in the WR tree compared to the WW tree. The difference reached 9.1 °C at 14:30 UTC. The average daytime difference (1.7 °C from 08:00 to 17:00 UTC) was however not considered significant according to a Student's t-test.

On August 20th (i.e. 46th day of the water restriction), T_{leaf} was on average higher during the whole daytime in the WR tree compared to the WW tree by up to 6.1 °C at 11:30 UTC and on average by 3.2 °C from 08:00 to 17:00 UTC. This average difference appeared to be statistically significant according to a Student's t-test considering the significance level of 5 %. A slight increase of leaf surface temperature was reported for the WR trees over summer (Figure 39). Such observation appears to be very consistent with the reduction stomatal conductance and tree transpiration previously highlighted, a lower transpiration inducing a lower amount of energy dissipated by the leaves through latent heat flux. Also, it should be considered that as the LAI of the WW trees kept increasing during the studied period (Table 3), the leaves equipped with the thermocouples in this zone may have been progressively less exposed to the sun throughout summer. At the same time, the decreasing LAI of the WR trees (Table 3) may have induced a progressively higher solar exposure of the leaves equipped with the thermocouples in the WR zone which may also have impacted the leaf surface temperature measurements presented in Figure 39.

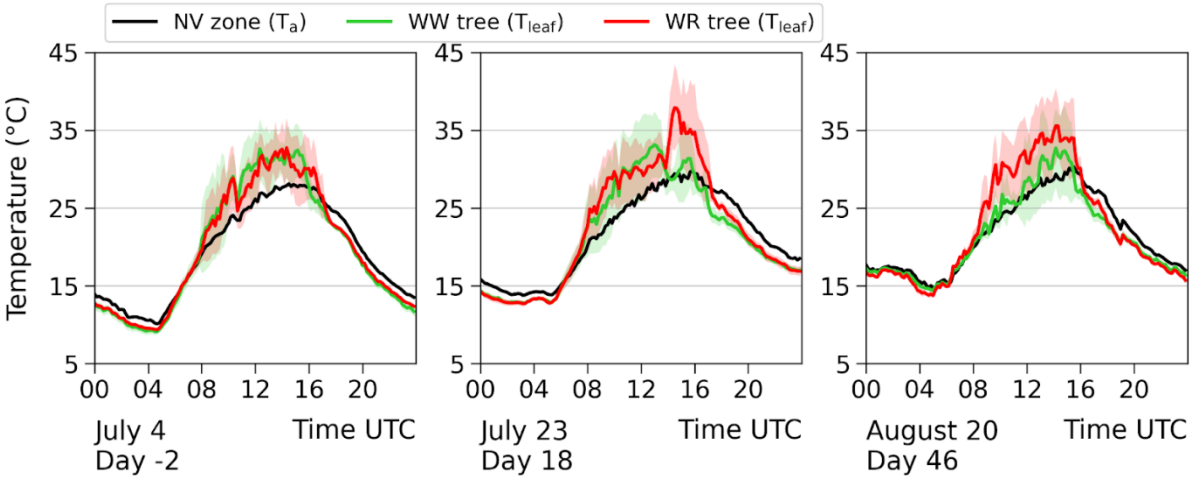

Figure 39: Evolution of the air temperature measured at 1.5 m a.g.l. in the NV zone and the average leaf temperature and the associated standard deviation (n=5 leaves) measured on the central tree of each vegetated zone over the three studied days.

3.2.3.2. Street microclimate

3.2.3.2.1. Wall surface temperature

Only the temperature of the eastern wall is presented because sensor dysfunction did not enable to exploit the measurements of the western wall temperature (Figure 40). On July 4th, the surface temperature of the eastern wall was very close in both vegetated zones all day long although slight temporarily differences can be observed in the afternoon (around 16:00 UTC).

The eastern wall is mainly exposed to the sun during the afternoon and due to the heterogeneity of the tree crowns, it is likely that the wall temperature sensors of the WW zone and WR zone may be unequally shaded at some moments of the day. Yet, the eastern wall was up to 6.9 °C lower in the WW zone and 8 °C lower in the WR zone compared to the NV zone at 16:30 UTC. The shadows cast by the trees in both zones thus play an important role in keeping the surface temperature lower than 30 °C while the surface temperature in the NV zone almost reached 35 °C during that day. Such results were found to be consistent with the wide range of surface temperature reduction reported in the shade of the trees (from 9 °C to 20 °C according to Armson et al. (2012), Armson and Ennos (2013) and Kotzen (2003)) which however strongly depends on the materials of the considered surfaces.

On July 23rd and August 20th, the eastern wall's surface temperature remained very close in both vegetated zones during the night and in the morning. However, an increasing difference can be observed between both vegetated zones in the afternoon. In the WR zone, the surface temperature reached 30 °C on July 23rd and August 20th and was respectively up to 3.9 °C and 4.7 °C higher compared with the WW zone. Thereby, the reduction of the total leaf area and LAI reported previously in Table 3 which decreased the amount of radiation intercepted by the WR trees (Figure 26) seemed to decrease their ability to cast shadows on the eastern wall of the street, leading to a noticeable overheating of this wall in the WR zone of the street. Yet, the increasing leaf area of the WW trees (Table 3) may also have increased the portion of the eastern wall shaded by their foliage which may have increased their effect on the eastern wall temperature throughout summer.

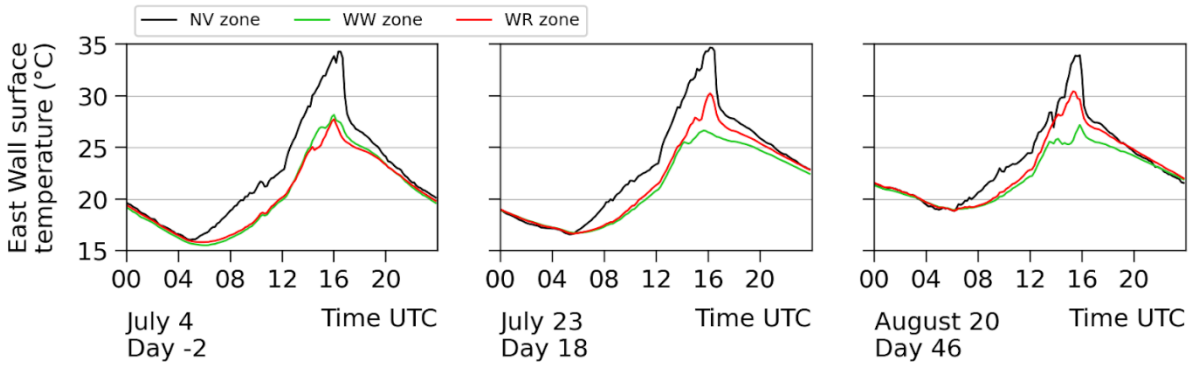

Figure 40: Evolution of the outdoor surface temperature of the eastern wall at 1 m a.g.l. in the three zones of the street during the three typical sunny days.

3.2.3.2.2. Radiation balance

Figure 41 presents the evolution of the SW and LW radiation fluxes inside the street at different positions during the three typical sunny days. Close meteorological conditions were reported during these three days as explained in section 3.2.2.3 which is why they were characterized by close amounts of ↓SW reaching the street (more than 800 $W.m^{-2}$ recorded around solar noon during the three days) although the maximum radiation flux is decreasing over time with the evolution of the position of the sun in the sky over the year (Figure 41a). The influence of the walls of the street is easily visible as the ↓SW measured at 0.65 m a.g.l. in the NV zone is marked by a very strong increase around 09:00 UTC and a very strong decrease around 15:00 UTC which correspond to the sensor being shaded by the walls or directly exposed to the sun. The amount of ↓SW measured under the tree crowns is very low especially around solar noon in both vegetated zones, which highlights the important amount of radiation intercepted by the trees. The heterogeneities of the foliage might lead to temporarily direct solar exposure of the sensors which may explain the temporarily strong increases of the radiation measured under the tree crowns. Table 6 highlights the ↓SW fluxes measured at different positions inside the street as well as the ratio of radiation intercepted by the tree crowns. The radiation interception provided by the WR trees progressively decreases. It remains however quite high (greater than 91 % on August 20th at 12:00 UTC while WW trees intercepted at the same time 95 % of ↓SW). This is obviously very consistent with the results presented hereinabove in section 3.1.3.5.

The amount of ↑SW radiation measured at 2 m a.g.l. is much higher than the one measured at 0.78 m a.g.l. in both vegetated zones (Figure 41b). At 2 m a.g.l., the down-facing pyranometer receives radiation reflected by the tree leaves and the white painted walls which are widely exposed to sunlight. At 0.78 m a.g.l., the down-facing pyranometer is only exposed to radiation reflected on the ground and the lower parts of the walls which are both mainly shaded by the tree crowns. There was no difference between the two vegetated zones for the ↑SW radiation fluxes at both 2 m and 0.78 m a.g.l. during the three studied days.

At 2 m a.g.l., the ↓LW are mainly caused by the LW radiation emitted by the atmosphere and the objects surrounding the studied canyon street. At 0.78 m a.g.l., the up-facing pyrgeometer received ↓LW mainly emitted by the tree foliage and to a lesser extent by the walls of the street. The resulting ↓LW radiation measured at 0.78 m a.g.l. is then higher than the one measured at 2 m a.g.l. (Figure 41c). The ↓LW radiation fluxes measured above and under the tree crowns were very similar in both vegetated zones during the three typical sunny days. No noticeable increase of the ↓LW measured at 0.78 m a.g.l. was noticed for the WR trees although

such an increase could have been expected as the leaf temperature slightly increased over the water restriction period as reported earlier in section 3.2.3.1.3 (Figure 39).

At 0.78 m a.g.l., the down-facing pyrgeometer receives ↑LW mainly emitted by the ground of the street and to a lesser extent by the lower part of the walls of the street. At 2 m a.g.l., the ↑LW are mainly caused by the LW radiation emitted by the tree foliage and the upper part of the walls of the street. The amount of ↑LW radiation measured at 0.78 m a.g.l. and 2 m a.g.l. were very close for both vegetated zones during the three typical sunny days. At 0.78 m a.g.l., the ↑LW radiation fluxes appeared to be slightly higher in the WR zone compared to the WW zone. The WR zone is located right next to the NV zone which, when exposed to the sun, is characterized by high surface temperatures. Thus, the warm surfaces of the NV zone might emit more LW radiation and part of it is likely to reach the down-facing pyrgeometer of the WR zone but not the one of the WW zone which is located further north. No noticeable increase of the ↑LW at both 0.78 m and 2 m a.g.l. in the WR zone was found over summer although such an increase could have been expected, especially at 2 m a.g.l. as the leaf temperature and the eastern wall temperature slightly increased over the water restriction period as reported earlier in section 3.2.3.1.3 (Figure 39) and 3.2.3.2.1 (Figure 40).

Thereby, the effect of the water restriction was mainly noticeable on the ↓SW fluxes and the effect on the other components of the radiation balance appeared to be either null or lower than the accuracy of the sensors (Table 2).

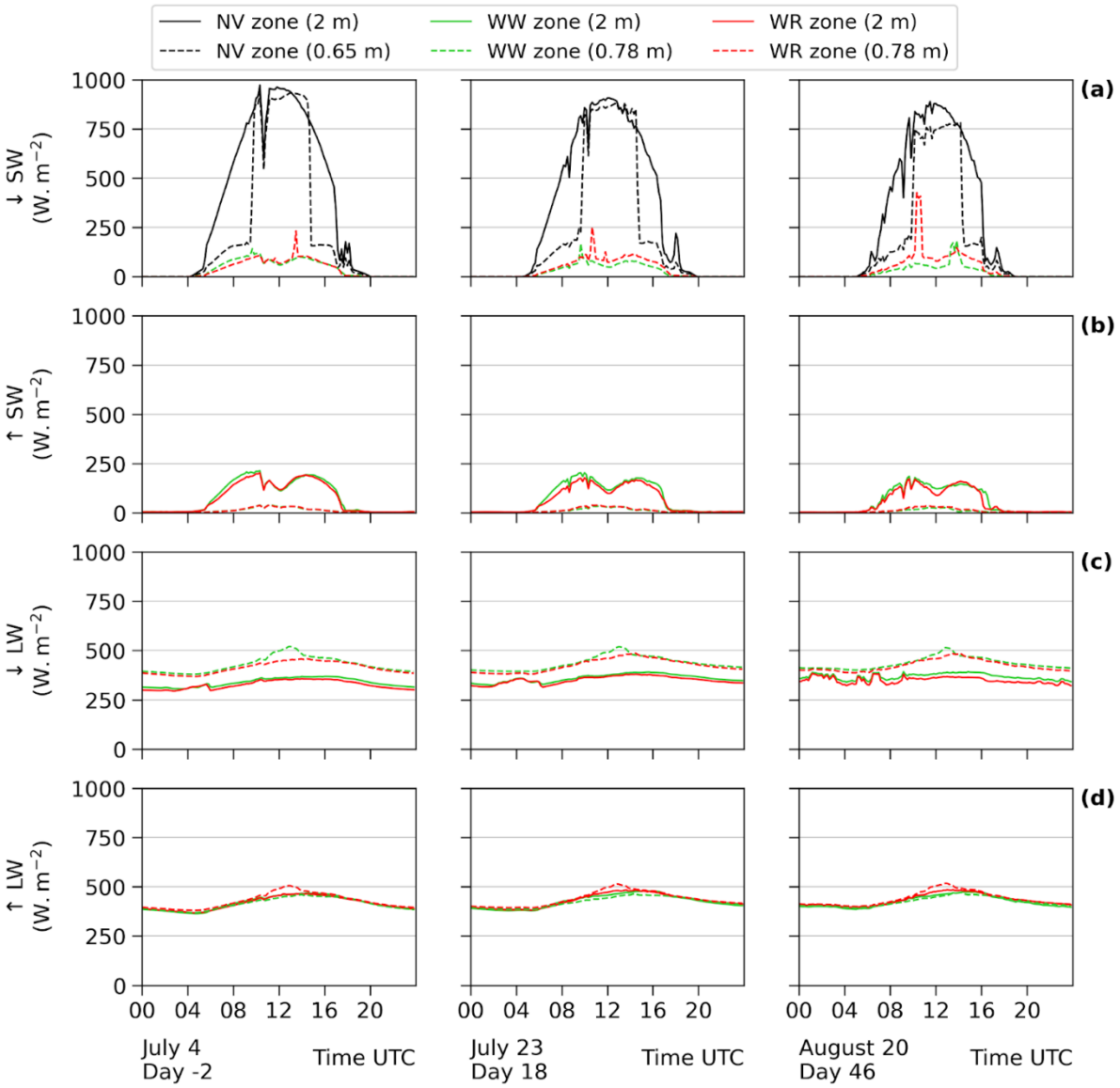

Figure 41: Downward (↓) and upward (↑) short (SW) and long (LW) wavelength radiation measured above (2.1 m a.g.l.) and under the tree crowns (0.78 m a.g.l. in the WW and WR zones and 0.65 m a.g.l. in the NV zone) in the different zones of the street (only ↓SW radiation for NV zone).

Table 6: Amount of ↓SW radiation measured at different positions in the street and % of ↓SW radiation intercepted by the tree crowns at 12:00 UTC for the three studied days.

Variable	Zone	July 4th	July 23rd	August 20th
↓SW radiation at 12:00 UTC ($W.m^{-2}$)	NV zone (2 m)	956	906	878
	WW zone (0.78 m)	59	48	41
	WR zone (0.78 m)	67	73	79
% of ↓SW radiation intercepted at 12:00 UTC	WW zone (0.78 m)	94	95	95
	WR zone (0.78 m)	93	92	91

3.2.3.2.3. Spatial distribution of air absolute humidity

Figure 42 displays the evolution of the air AH calculated at different positions inside the street during the 3 typical sunny days and summarizes the average AH differences calculated between both zones during a night-time period and a daytime period. For an easier visualization of the evolution of the air AH difference between both vegetated zones, the reader may also refer to Figure 91 presented in appendix 7.1.2.1.

Inside the tree crowns (i.e. at 1 m and 1.5 m a.g.l.), the AH difference calculated between both zones was very low on July 4th all day long. On July 23rd and August 20th, this difference remained very low at night (lower than 1 %) but the AH was noticeably higher in the WW zone during the day. Indeed, at 1.5 m a.g.l., the daytime average AH difference was null on July 4th, while the AH in the WR zone was on average 7 % lower on July 23rd and 6.2 % lower on August 20th than the one in the WW zone. Similar observations were made at 1 m a.g.l. (Table 7). During the water restriction period, the strong decrease of the transpiration of the WR trees highlighted in Figure 25 may then have reduced the amount of water vapor spread out into the atmosphere by these trees, thereby impacting AH.

The fact that the AH difference between both zones during the water restriction was only visible during daytime, could suggest that transpiration was probably mainly occurring during daytime. Although a few studies reported non-null night-time transpiration for multiple tree species (Fisher et al., 2007; Chen et al., 2011), the night-time transpiration of the trees studied in the RSCS could then be too low to be noticeable through AH measurement. As a reminder, the water balance used in the present experiment to estimate the transpiration of the WW trees was based on the hypothesis that their nocturnal transpiration was null. Thereby, the eventual error induced by this water balance should be limited.

Under the tree crowns (i.e. at 0.4 m a.g.l.) both on the central north-south axis of the street and close to the eastern wall, some preexisting differences were measured between both vegetated zones. They may have been partly induced by pre-existing offsets between sensors highlighted in appendix 7.1.3. The pre-existing difference was quite constant all day long for the sensors on the north-south central axis (Figure 42c) while it was mainly observed at night for the sensors close to the eastern wall (Figure 42d). The water restriction did not have any noticeable impact on the daily variation of air AH at both 0.4 m a.g.l. locations in the WR zone. Such result tends to suggest that the reduction of the WR transpiration is not noticeable at 0.4 m a.g.l. and by that means that the effect of tree transpiration on the microclimate is mainly visible close to the tree crowns.

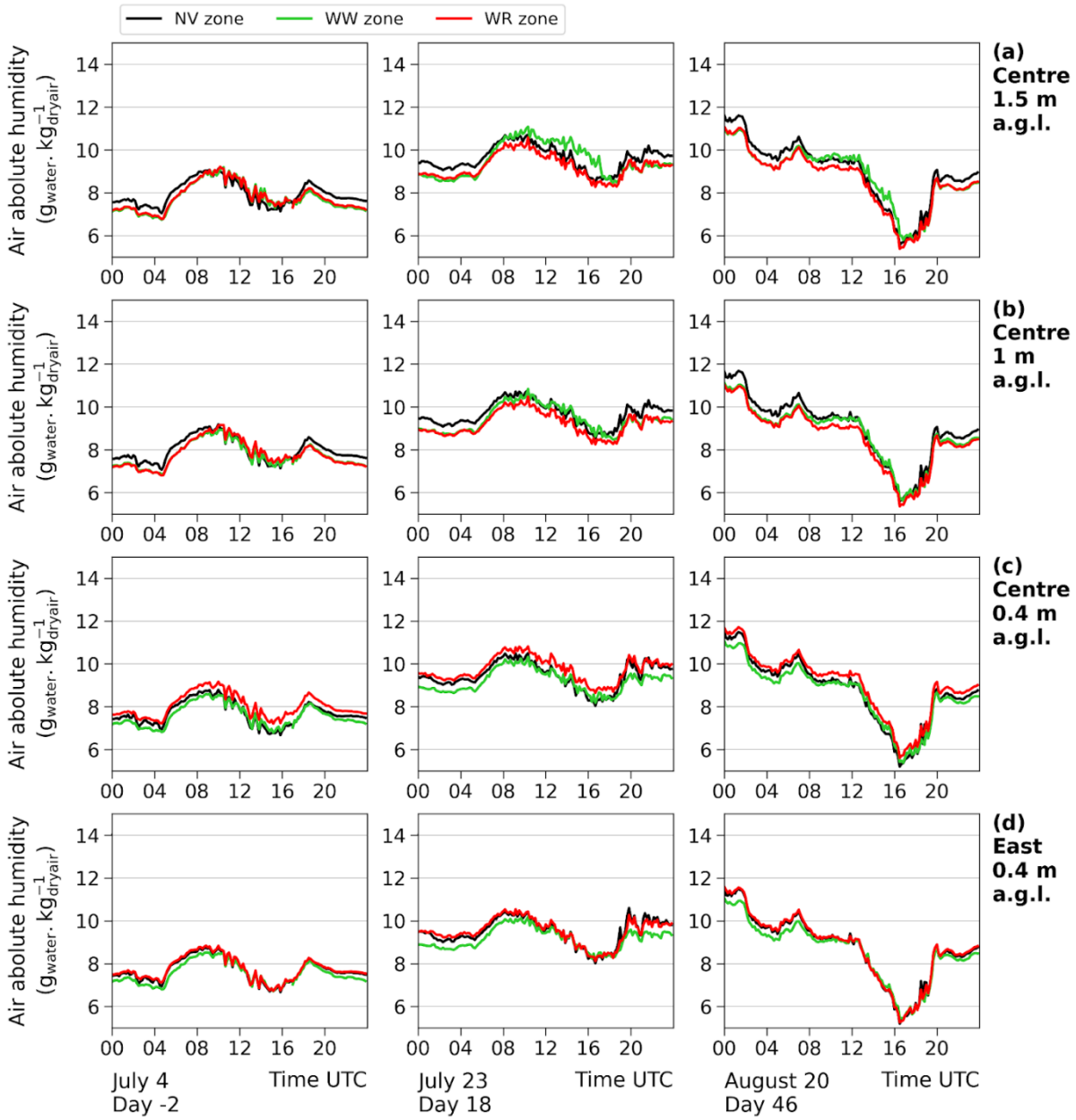

Figure 42: Evolution of the air absolute humidity measured at 4 different positions for the 3 typical sunny days.

Table 7: Average absolute humidity difference (WR zone - WW zone) in % during night-time (from 19:00 to 05:00 UTC) and daytime (from 07:00 to 17:00 UTC) during the three typical sunny days.

Location (m a.g.l.)	Time	July 4th	July 23rd	August 20th
1.5 center	Night	0.8	1	0.3
	Day	0	-7	-6.2
1 center	Night	-0.4	-0.5	-1
	Day	1.9	-4.1	-3.9
0.4 center	Night	6	7	5.8
	Day	6	5.3	4.6
0.4 east	Night	4.1	5.7	3.9
	Day	1.6	2.1	0.3

3.2.3.2.4. Spatial distribution of air temperature

Figure 43 displays the evolution of the T_a measured at different positions inside the street during the 3 typical sunny days and Table 8 summarizes the average Ta difference calculated between both zones during a night-time period and a daytime period. For an easier visualization of the evolution of the air Ta difference between both vegetated zones, the reader may also refer to Figure 92 presented in appendix 7.1.2.2.

Inside the tree crowns (i.e. at 1 m and 1.5 m a.g.l.), the T_a difference calculated between both zones was very low on July 4th all day long. On July 23rd and August 20th, this difference remained very low at night (lower than ±0.4 °C) but the T_a was noticeably increased in the WR zone during the day, in particular at 1.5 m a.g.l. where it reached 1.7 °C on July 23rd and 1.5 °C on August 20th.

Under the tree crowns (i.e. at 0.4 m a.g.l.) preexisting differences were measured between both vegetated zones on both the central north-south axis of the street and close to the eastern wall. They may have been partly induced by pre-existing offsets between sensors highlighted in appendix 7.1.3. The pre-existing difference is quite constant all over the day for the sensors on the north-south central axis (Figure 43c) while it is much higher during daytime than during night-time for the sensors close to the eastern wall (Figure 43d). The water restriction did not have any noticeable impact on the daily variation of T_a at both 0.4 m a.g.l. locations in the WR zone as the evolution of the average difference remained low regarding the measurement accuracy of the T_a sensors (±0.2 °C).

Such results were consistent with those reported in the previous section regarding AH. During the water restriction period, the strong decrease of the transpiration of the WR trees highlighted in Figure 25 reduced the amount of energy dissipated by the evaporation of

transpired water which led to an increase of T_a in the WR zone. However, this effect was only noticed inside the tree crowns (1 m a.g.l. and 1.5 m a.g.l.) which suggests that the effect of tree transpiration on the microclimate is mainly noticeable close to the tree crowns but not at the equivalent human height (0.4 m a.g.l.).

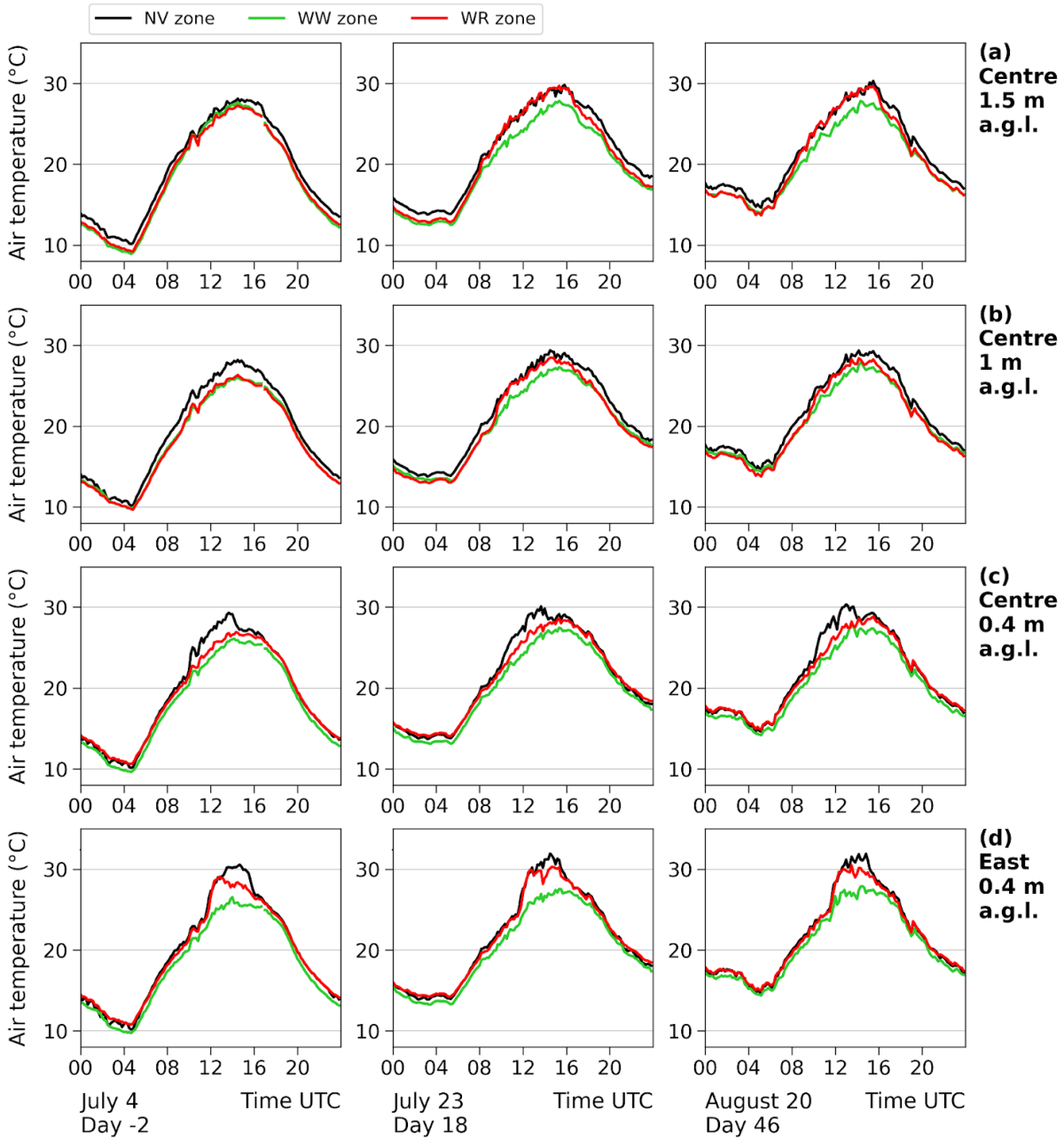

Figure 43: Evolution of the air temperature measured at 4 different positions for the 3 typical sunny days.

Table 8: Air temperature difference (WR zone - WW zone) in °C during night-time (from 19:00 to 05:00 UTC) and daytime (from 07:00 to 17:00 UTC) during the three typical sunny days.

Location (m a.g.l.)	Time	July 4th	July 23rd	August 20th
1.5 center	Night	0.3	0.4	0
	Day	-0.1	1.7	1.5
1 center	Night	-0.1	-0.3	-0.3
	Day	0.1	1	0.6
0.4 center	Night	0.9	0.9	0.9
	Day	0.9	1.1	1.1
0.4 east	Night	0.9	0.8	0.7
	Day	1.7	1.9	1.5

3.2.3.2.5. Spatial distribution of mean radiant temperature

Figure 44 displays the evolution of the T_{mrt} calculated at different positions inside the street during the 3 typical sunny days and Table 9 summarizes the average T_{mrt} difference calculated between both zones during a night-time period and a daytime period. For an easier visualization of the evolution of the T_{mrt} difference between both vegetated zones, the reader may also refer to Figure 93 presented in appendix 7.1.2.3.

This indicator is very sensitive to direct solar radiation as it depends on T_g. Indeed, the T_{mrt} measured in the NV zone on the central axis of the street quickly increased above 50 °C starting from 10:00 UTC while the globe thermometer was leaving the shadow of the eastern wall and was getting exposed directly to the sun. Conversely, a quick decrease was observed starting from 14:00 UTC as the shadow of the western wall reached the globe (Figure 44a). Similar observations were reported close to the eastern wall except that the highest T_{mrt} values were recorded later in the afternoon according to the direct exposure to sunlight of this location (Figure 44b). In both vegetated zones, the T_{mrt} remained most of the day below 40 °C which is much lower than the one measured in the NV zone. Thereby, the effect of the tree crowns is clearly visible at the equivalent human height (0.4 m a.g.l.) both on the central axis of the street and close to the eastern wall which highlights the spatial extent of the shadow cast by the trees.

On July 4th, T_{mrt} was similar in both vegetated zones all day long except on a few short time periods due to the spatial heterogeneity of the crowns, as mentioned previously. During the water restriction period, the mean radiant temperature tended to increase in the WR zone while that of the WW zone remained at comparable level as before the water restriction. The highest T_{mrt} differences between both zones were observed approximately from 10:00 to 14:00 UTC and from 12:00 to 16:00 UTC respectively on the central axis of the street and close to

the eastern wall, which corresponds to periods with direct solar exposure of the sensors. Thereby, the reduction of the total leaf area and LAI reported previously in Table 3 which decreased the amount of radiation intercepted by the WR trees (Figure 26 and Figure 41) seemed to partly decrease their ability to cast shadows at the equivalent human height (0.4 m a.g.l.) leading to a noticeable increase of T_{mrt} as T_{mrt} highly depends on T_g which is highly impacted by SW.

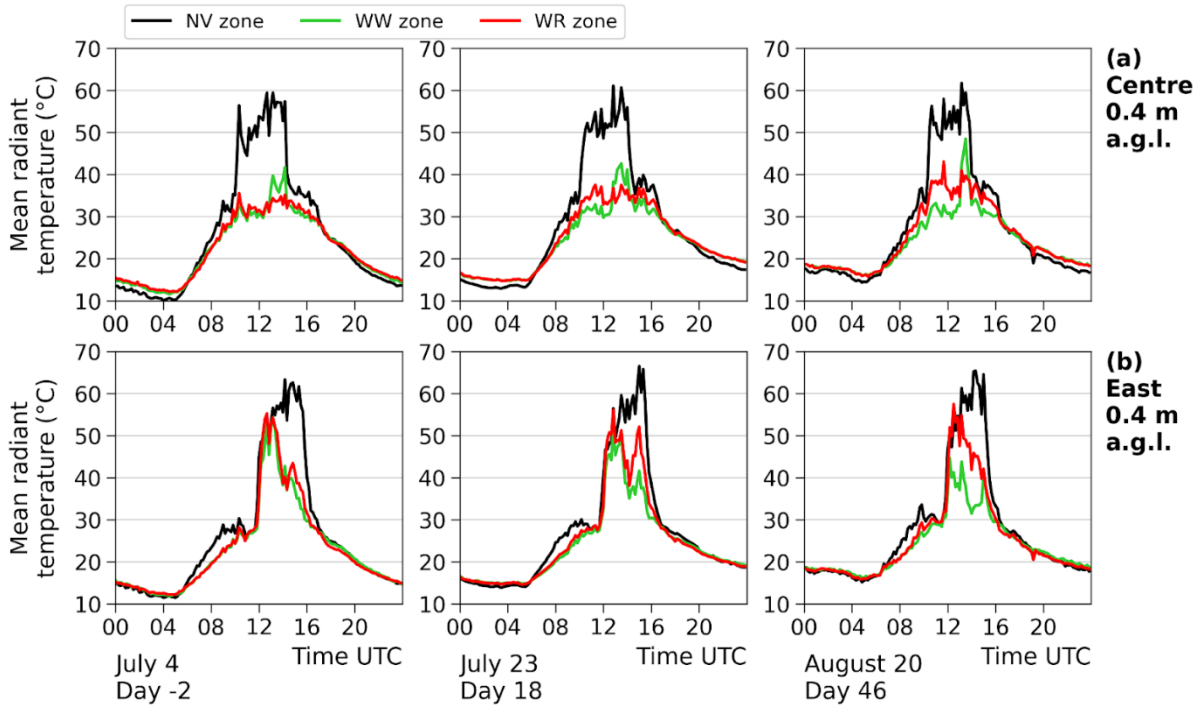

Figure 44: Evolution of the mean radiant temperature calculated at 2 different positions for the 3 typical sunny days.

Table 9: Mean radiant temperature difference (WR zone - WW zone) in °C during night-time (from 19:00 to 05:00 UTC) and daytime (from 07:00 to 17:00 UTC) during the three typical sunny days.

Location (m a.g.l.)	Time	July 4th	July 23rd	August 20th
0.4 center	Night	0.4	0.1	-0.1
	Day	0	1.1	2.5
0.4 east	Night	-0.2	-0.2	-0.5
	Day	1.2	2.4	3.9

3.2.3.2.6. Spatial distribution of UTCI

Figure 45 displays the evolution of the UTCI calculated at different positions inside the street during the 3 typical sunny days and Table 10 summarizes the average UTCI difference calculated between both zones during a night-time period and a daytime period. For an easier visualization of the evolution of the UTCI difference between both vegetated zones, the reader may also refer to Figure 94 presented in appendix 7.1.2.4.

T_{mrt} is involved in the calculation of UTCI which means that UTCI is also highly influenced by T_g and therefore direct solar radiation. Thereby, strong temporary UTCI increase and decrease could be noticed during daytime and were attributed to temporary direct exposure of the globe thermometers to sunlight caused by the heterogeneity of the foliage in both vegetated zones. The evolution of the UTCI at a given location is also quite similar to the evolution of the mean radiant temperature at the same location. During the day, the UTCI calculated in the central axis of the street in the NV zone exceeded 32 °C and reached the high heat stress category from the moment the globe thermometer was directly exposed to sunlight (approximately from 10:00 to 14:00 UTC). In this zone, UTCI was higher than 32 °C during 3.5 hours on average on July 4th, July 23rd and August 20th. The influence of the shadows cast by both buildings is clearly noticeable in the morning and afternoon. Around noon, both vegetated zones play an important role in UTCI reduction at human's height, the UTCI remaining almost always below 32 °C (i.e. in the moderate heat stress zone) during the three typical sunny days except during 10 minutes in the WW zone on August 20th.

On July 4th, the UTCI calculated at human height already appeared to be higher in the WR zone all day long compared to the WW zone (Table 10). This was attributed to the pre-existing difference of T_a already mentioned earlier and highlighted in appendix 7.1.3.

The UTCI calculated in the WR zone remained close at night to the one calculated in the WW zone all over the water restriction period. However, a progressive increase of the UTCI difference between both zones was observed during daytime, especially during the period of direct solar exposure. During daytime, UTCI was then on average 0.6 °C higher, 1.1 °C higher and 1.4 °C higher under the WR trees on the central axis of the street compared to the WW zone respectively on July 4th, July 23rd and August 20th (Table 10). Still, the WR trees kept providing efficient human thermal stress reduction at 0.4 m a.g.l. on the central axis of the street where UTCI remained in the moderate heat stress zone (Figure 45).

The UTCI increase under the WR trees observed along summer recalls the T_{mrt} increase reported in the previous section (Figure 44) under the WR trees on the same period. Moreover,

it was highlighted with Figure 43 that the effect of water restriction was not noticeable at 0.4 m a.g.l. or lower than the sensors accuracy meaning that the reduction of the WR trees transpiration was not noticeable at this height. Such observations thereby tend to suggest that the UTCI increase under the WR trees was mainly caused by the reduction of radiation interception while the reduction of transpiration did not appear to impact human thermal stress at 0.4 m a.g.l.

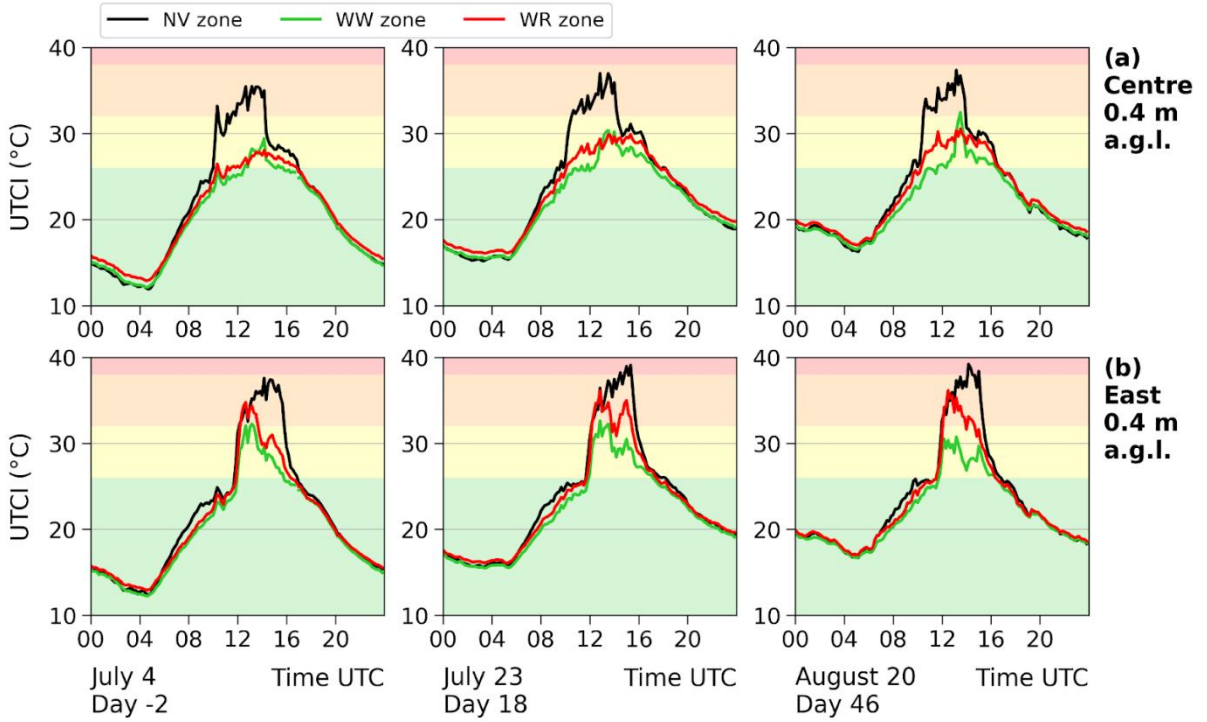

Figure 45: Evolution of the UTCI calculated at 2 different positions for the 3 studied days regarding the different thermal stress categories: no thermal stress (9 to 26 °C UTCI, green), moderate heat stress (26 to 32 °C UTCI, yellow), high heat stress (32 to 38 °C UTCI, orange), very high heat stress (38 to 46 °C UTCI, red) and extreme heat stress (>46 °C UTCI, not shown).

Table 10: UTCI difference (WR zone - WW zone) in °C during night-time (from 19:00 to 05:00 UTC) and daytime (from 07:00 to 17:00 UTC) during the three typical sunny days.

Location (m a.g.l.)	Time	July 4th	July 23rd	August 20th
0.4 center	Night	0.7	0.6	0.5
	Day	0.6	1.1	1.4
0.4 east	Night	0.5	0.5	0.3
	Day	1.3	1.8	1.9

3.2.3.3. Variability of the climatic benefits over time

In order to investigate the daily variability of the climatic benefits, the UTCI differences calculated between each vegetated zone and the NV zone at 0.4 m a.g.l. in the center of the street were averaged daily from 10:00 to 14:00. Then a PCA analysis was run in order to evaluate the relationship that may exist between such UTCI differences and the daily reference meteorological variables measured at the Météo-France meteorological station (Figure 46). The UTCI difference appeared to be highly linked to the daily integral of the downward global radiation in both vegetated zones but no strong relation was highlighted with the other meteorological variables.

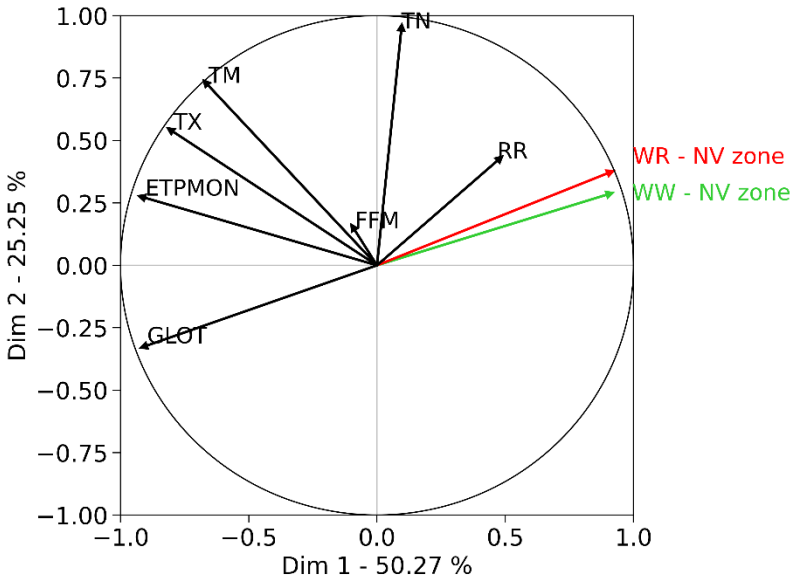

Figure 46: Correlation circle of the daily UTCI reduction calculated in each vegetated zone at 0.4 m a.g.l. in the center of the street from 10:00 to 14:00 UTC compared to the NV zone (green and red arrows) and the daily meteorological variables measured at the Météo-France meteorological station (black arrows) from July 1st to August 31st. RR = rainfall, TN, TM and TX = minimum, mean and maximum air temperature, VPD = vapor pressure deficit, ETPMON = reference evapotranspiration (Penman-Monteith method), GLOT = integral of incoming global radiation, FFM = mean wind speed.

To illustrate this strong relation, both variables were graphed in the form of a scatter plot in Figure 47. Over the studied period, very contrasted human thermal stress reductions were measured in both zones as the UTCI differences ranged from approximately 0 to -8 °C. A strong linear relationship was noticed between the UTCI difference and GLOT in both zones (R^2 = 0.71 in the WW zone and R^2 = 0.88 in the WR zone) meaning that GLOT explained an important part of the variability of the UTCI difference. The highest UTCI reductions (the most negative differences) were then measured during the sunniest days of the studied period.

Such results were very consistent with the previous findings of Herpin et al. (2022) who also reported a strong correlation between GLOT and UTCI reduction in the present RSCS at

0.4 m a.g.l. under well-watered trees ($R^2 = 0.75$). The strong influence of radiation interception on the human thermal stress reduction provided by the trees is therefore highlighted and recalls the results of section 3.1.3.6 highlighting a stronger contribution of radiation interception than transpiration to the climatic benefits. They also recall the results presented in sections 3.2.3.2.3 to 3.2.3.2.6 which suggest that at human height, human thermal stress seems to be much more sensitive to radiation interception than tree transpiration. Moreover, the present results extend those of Herpin et al. (2022) highlighting that a strong correlation still exists between GLOT and UTCI reduction provided by WR trees meaning that radiation interception was still important and efficient in the WR zone.

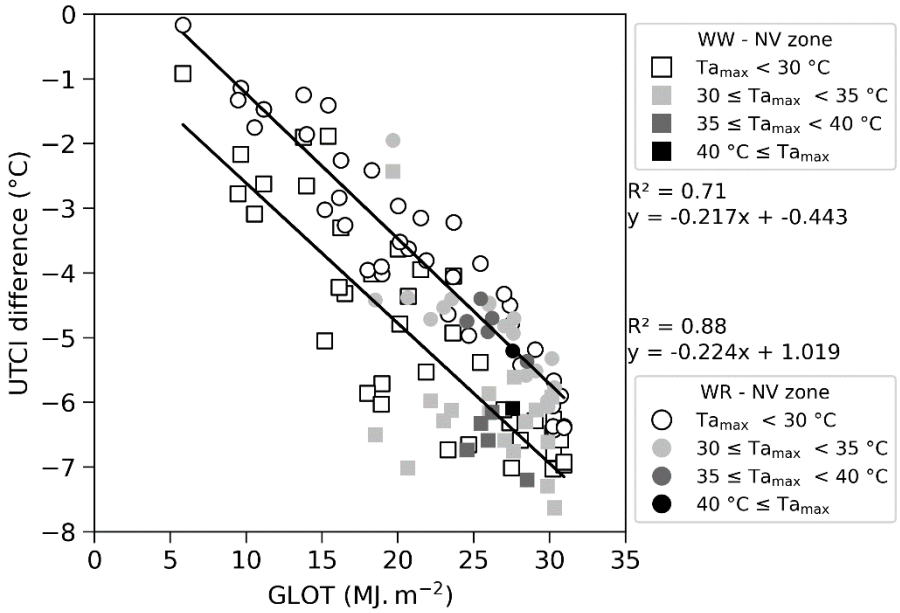

Figure 47: Average daily UTCI difference calculated in both vegetated zones at 0.4 m a.g.l. in the center of the street from 10:00 to 14:00 UTC compared to the NV zone as a function of the daily reference evapotranspiration measured at 2 m a.g.l. at the north mast from July 7th (2nd day of the water restriction) to August 31st.

Finally, it appears the daily UTCI reduction under the tree crowns was not related to the daily maximum air temperature (Figure 46) and that both the WW and WR trees provided strong UTCI reduction under the tree crowns even during the heatwaves (Figure 47). Considering the strong dependence of UTCI reduction on radiation interception highlighted hereinabove, such results suggest that the tree foliage and the resulting radiation interception were probably unaffected by the heatwaves in both vegetated zones.

Chapter

4. Quantification of the summer climatic benefits provided by mature street trees from 9 different species in 5 sites in Paris

The “Trees and Climate” (T&C) study was initiated in 2018 by the green spaces department of the city of Paris in order to provide keys to answer the two following questions:

- Are mature street trees able to provide efficient cooling benefits when exposed to severe climatic events such as heatwaves and droughts?
- What important criteria should be considered when selecting trees to plant in cities regarding both the resistance to extreme climatic events and the climatic benefits they provide?

The T&C study was launched through a public contract involving the green spaces department of the city of Paris and a group of private firms responsible for the design, the setting up and the maintenance of the experimental facility as well as the analysis of the acquired data (Hydrasol and Ecosustain for the selection of the studied sites and species, sensors installation and data collection of all sensors except soil water potential sensors; Urbasense for soil water potential sensors installation and data collection; Geosat for the LiDAR scanning campaign and the calculation of the morphological variables). Although first analyses were provided by the group of private enterprises, the entire data set could not be analyzed in the frame of this public contract. The present PhD project was therefore meant to deepen the analysis of the complete data set of the T&C study. The T&C study relies on the long-term monitoring of various variables along the soil-tree-atmosphere continuum of 36 mature street trees from 9 different

tree species growing in 5 Parisian streets with a short time step (1 hour) from 2019 to 2022. This experimental facility was designed to fulfil the following objectives:

- Quantify the cooling potential of mature Parisian street trees in real urban conditions.
- Assess the resistance to heatwaves and droughts of Parisian street trees.
- Investigate the potential physiological, hydric and energetic behavior differences between species.
- Investigate the potential differences between trees of the same species located in different sites.
- Identify the factors (characteristics of the trees and species) that may influence the climatic benefits provided by street trees.

The present chapter will first describe the experimental facility and the methods used to exploit the acquired variables and will then present the results of the T&C study.

4.1. Materials and methods

4.1.1. Materials

4.1.1.1. Selection of the tree species

The green spaces department of the city of Paris manages approximately 500,000 trees located in the public spaces among which approximately 100,000 are alignment trees located in streets (APUR, 2023a; Ville de Paris, 2024b). In order to facilitate their management, the green spaces department of the city of Paris created in 2001 a database referencing all the trees located in the public space and managed by the municipality services. In this database, information about the tree species, the plantation date, the trunk circumference, the total height and the phytosanitary status can be found for each tree. A yearly quick diagnosis is carried out for each tree to spot potential dead woods and diseases. Then, a more detailed inspection is carried out for each tree at least once every 5 years and the database is updated accordingly. The trunk circumference is measured at 1.3 m a.g.l. by means of a tape measure, the height of the tree is visually estimated and the eventual tree damages are assessed on the basis of multiple criteria. The sanitary status of the trees is evaluated in order to detect potential sick trees which are then very likely to be cut down.

To select the tree species to be studied, an analysis of this database was first run in 2018 in order to assess the tree species present in Paris regarding their representativeness in the Parisian tree population and their ability to thrive in the Parisian urban environment. The latter was assessed through the calculation of the average for each tree species of:

- The average growth rate over 30 years;
- The general and physiological status;
- The annual cutting down rate.

Tree species having a high growth rate, a good general and physiological status and a low cutting down rate were then considered to be able to adapt to the Parisian environment and were pre-selected for the T&C study. This pre-selection was discussed in 2019 with experts from the scientific community as well as representatives of the green spaces department of various municipalities in order to focus on tree species expected to show a good resistance to extreme climatic events and provide interesting climatic benefits. Nine tree species (Figure 48), representing 45.1 % (Table 11) of all the alignment trees present in Paris in 2022, were then finally selected. The representativeness of the 9 species in the Parisian patrimony is quite heterogeneous as it ranges from 0.1 % to 29.6 % of all the alignment trees in Paris respectively for *Zelkova serrata* and *Platanus x hispanica*.

Celtis australis ***Gleditsia triacanthos*** ***Platanus x hispanica***



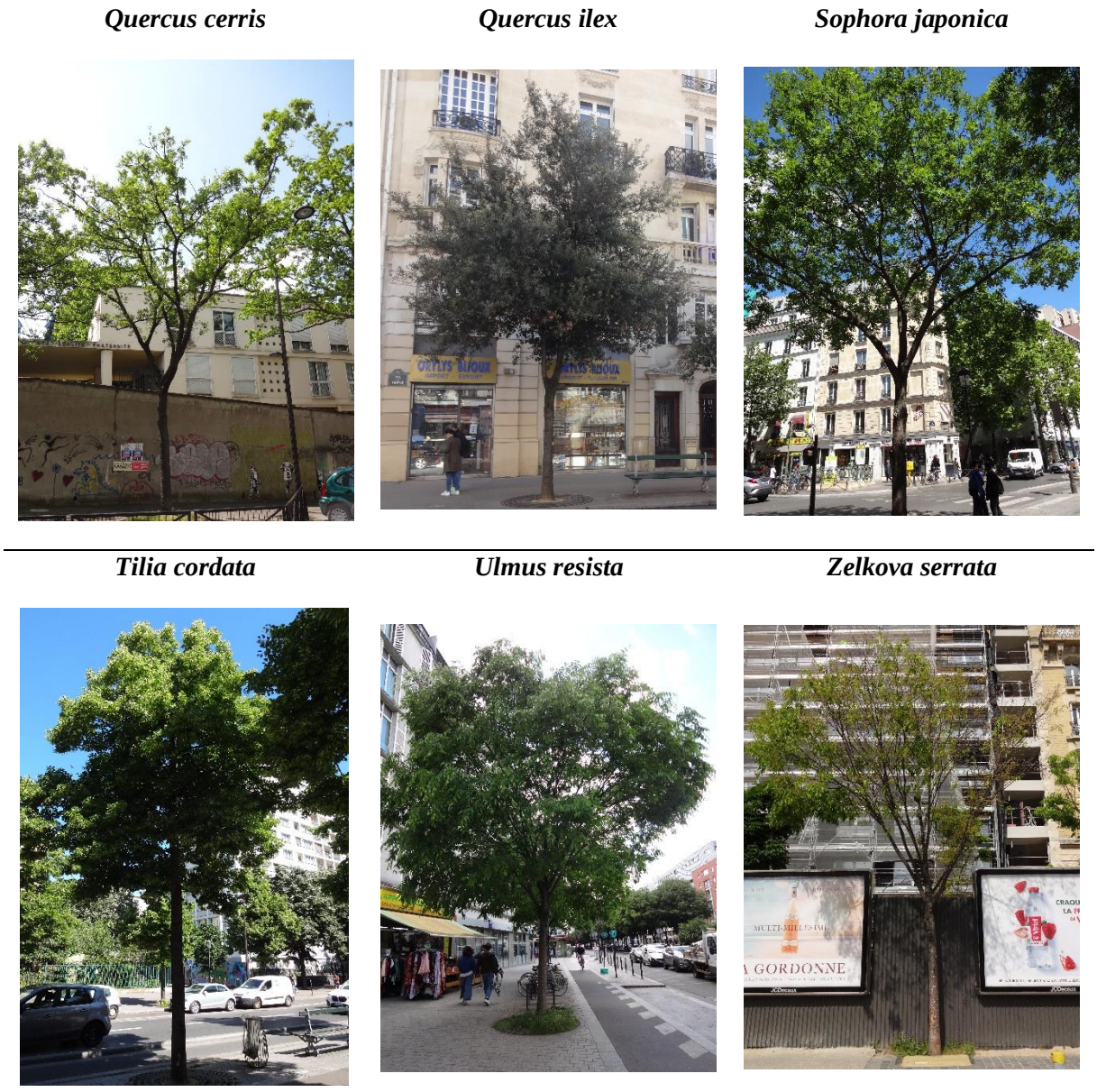

Figure 48: Picture of one studied tree for each of the 9 tree species selected in the Trees and Climate study.

Then, Table 12 summarizes a few characteristics of the studied tree species which have been collected in the literature as well as from internal sources by the green spaces department of the City of Paris in the form of a "Tree species guide". In this guide, a grade concerning the potential for local climate regulation has been attributed to each tree species based on its main morphological characteristics and on its estimated transpiration rate. Each tree species was also ranked regarding its theoretical resistance to both heat and drought on the basis of literature and experts feedbacks (Ville de Paris, 2023).

Table 11: Location of the studied tree species in the studied sites and representativeness in Paris.

Tree species	Nbr. of trees present in alignment in Paris in 2022	% of all the alignment trees in Paris in 2022	Nbr. of new trees planted in alignment from 2020 to 2022	Studied sites
Celtis australis	2978	2.8 %	142	Flandre Temple
Gleditsia triacanthos	586	0.6 %	107	Ordener
Platanus* x *hispanica	31378	29.6 %	1024	Flandre Temple Victor
Quercus cerris	162	0.2 %	37	Nohain
Quercus ilex	396	0.4 %	14	Temple
Sophora japonica	8566	8.1 %	207	Flandre
Tilia cordata	2262	2.1 %	118	Flandre
Ulmus resista	1332	1.3 %	131	Flandre
Zelkova serrata	137	0.1 %	70	Victor
Total	47 797	45.1 %	1850	-

Table 12: Main characteristics of the studied tree species based on the "Tree species guide" of the City of Paris (Ville de Paris, 2023).

Tree species	Deciduous / Evergreen	Mean height (in m)	Crown shape	Leaf size	Leaf density	Grade on local climate regulation for Paris (out of 10)	Drought resistance	Heat resistance
Celtis australis	Deciduous	18	ovoidal	Average	Average	5	Very resistant	Very resistant
Gleditsia triacanthos	Deciduous	25	spread out	Small	Low	3	Very resistant	Very resistant
Platanus* x *hispanica	Deciduous	35	ovoidal	Large	Average	10	Very resistant	Very resistant
Quercus cerris	Deciduous	25	ovoidal	Average	Average	7	Very resistant	Very resistant
Quercus ilex	Evergreen	20	ovoidal	Small	Strong	4	Very resistant	Very resistant
Sophora japonica	Deciduous	25	ovoidal	Small	Average	4	Very resistant	Very resistant
Tilia cordata	Deciduous	25	ovoidal	Average	Strong	10	Not resistant	Resistant
Ulmus resista	Deciduous	14	conical	Average	Average	5	Not resistant	Not resistant
Zelkova serrata	Deciduous	20	spread out	Average	Average	5	Resistant	Resistant

4.1.1.2. Selection of the studied sites

Multiple sites were considered in the frame of the T&C study, firstly because it was not possible to find trees of all 9 selected species on the same site, and secondly because one objective of the T&C study was to investigate the eventual differences between trees of the same species located in different sites. The studied sites were meant to gather at least 3 alignment trees of one of the 9 selected tree species with a good phytosanitary status, planted in individual tree pits on sidewalks or central walkways and not subject to forecasted building works or roadworks during the duration of the T&C study. As a consequence, 5 sites enabling to study 12 groups of 3 trees (1 group = 3 trees of the same species located on a same site), i.e. 36 trees in total, were then selected (Table 13, Figure 49). Two sites (NOHAIN and ORDENER) only contained 3 trees of one species whereas the three other ones enabled to compare multiple species on a same site (2 species for VICTOR, 3 species for TEMPLE and 5 species for FLANDRE). Only two species were studied on multiple sites: *Celtis australis* in FLANDRE and TEMPLE, and *Platanus x hispanica* in FLANDRE, TEMPLE and VICTOR.

Table 13: Main characteristics of the 5 sites of the Trees & Climate study.

Street	N°	Abbreviation	Tree species studied
Avenue de Flandre **Avenue Corentin Cariou**	n° 38 to 175 n° 7 to 22	FLANDRE	*Celtis australis* *Platanus* x *hispanica* *Sophora japonica* *Tilia cordata* *Ulmus resista*
Rue Franc-Nohain	n°5 to 13	NOHAIN	*Quercus cerris*
Rue Ordener	n° 5 to 9	ORDENER	*Gleditsia triacanthos*
Rue du Temple **Rue de Bretagne**	n° 158 to 205 n° 7 to 40	TEMPLE	*Celtis australis* *Platanus* x *hispanica* *Quercis ilex*
Boulevard Victor	n°5 to 45	VICTOR	*Platanus* x *hispanica* *Zelkova serrata*

The studied sites were quite heterogeneous in terms of orientation, aspect ratio and sky view factor. Their ground was generally made of asphalt with varying tints of dark and the façades of the surrounding buildings painted with varied colors.

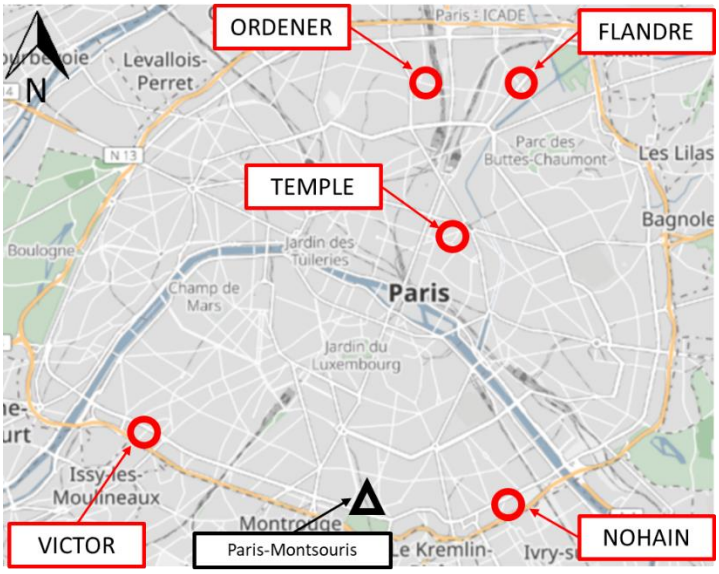

Figure 49: Location of the studied trees on the 5 selected sites in Paris and of the Météo-France meteorological station Paris-Montsouris

FLANDRE is a very long avenue (approximately 1.5 km long) NE-SW oriented and bordered by buildings on both sides (Figure 50). The width of the avenue varies from approximately 40 m to 50 m. Close to the studied trees, the height of the surrounding buildings can vary from approximately 11 m to 50 m which means that FLANDRE forms an urban canyon with a varying aspect ratio. It is composed of successive monospecific alignments of trees and therefore enables studying 5 tree species. Each studied tree was therefore surrounded by other non-studied trees of the same species and the different studied trees may be located quite far from each other, indeed, the distance between the southernmost studied tree and the northernmost one reaches 1.3 km. From south to north, *Tilia cordata*, *Sophora japonica*, *Celtis australis*, *Ulmus resista* and *Platanus x hispanica* were studied. The studied *Tilia cordata*, *Sophora japonica* and *Celtis australis* were located on a central pathway vegetated with two rows of trees and bordered by a roadway on both sides. They were located randomly in either one row or the other of the central pathway. The studied *Ulmus resista* and *Platanus x hispanica* were located either on the north-west or south-east sidewalks as there was no more central pathway in the northern part of the avenue. The distance between the studied trees and the surrounding buildings and between the studied trees and the other surrounding trees is therefore highly variable. Three lamp posts aiming at collecting reference meteorological data were also studied. The selected lamp posts were scattered along the avenue. CANDFlandre1 and CANDFlandre2, respectively located in the southern part and in the middle part of the avenue, were located on the eastern sidewalk. CANDFlandre3, located in the northern part of the

avenue, was located on the western sidewalk. All studied lamp posts and trees of FLANDRE were therefore not located on the same longitudinal axis of the street.

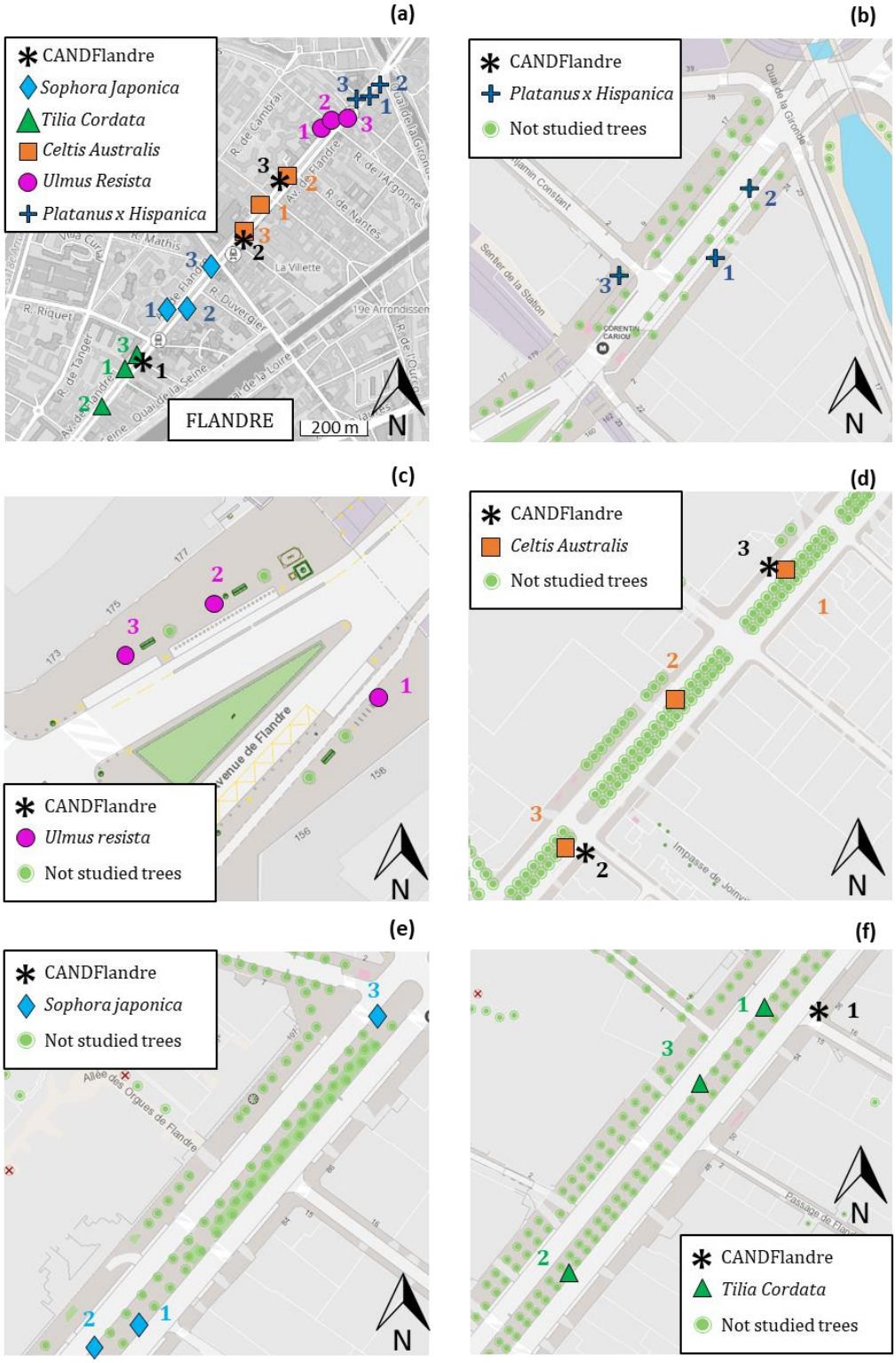

Figure 50: Location of the studied trees on FLANDRE. (a) global view, (b) *Platanus x hispanica*, (c) *Ulmus resista*, (d) *Celtis australis*, (e) *Sophora japonica*, (f) *Tilia cordata*.

NOHAIN is a small NNW-SSE oriented street (Figure 51). Only the northern part of the street is bordered by buildings on both sides whereas the southern part is bordered by a small urban park and a mineral open area which forms part of the playground of a school. This street is composed of a central roadway bordered by two sidewalks where *Quercus cerris* are planted, among which three trees were studied. The maximum distance between two studied trees is approximately 50 m. The reference lamp post of this site (CANDNohain) was located north of the studied street at the junction with a perpendicular street.

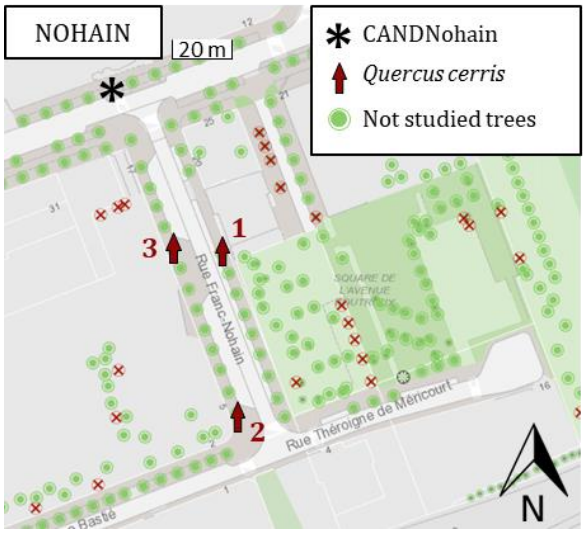

Figure 51: Location of the studied trees on NOHAIN.

ORDENER is a small square (Place Louis Baillot) bordered on its northern side by rue Ordener, a WNW-ESE oriented street and on its southern side by buildings (Figure 52). This square is treed with multiple *Gleditsia triacanthos* among which three trees were studied. Two of them were located right alongside rue Ordener while the third one was located in the southern part of the square close to the buildings. The reference lamp post of this site (CANDOrdener) was located approximately 70 m east from the closest studied square at the junction between rue Ordener and a perpendicular street.

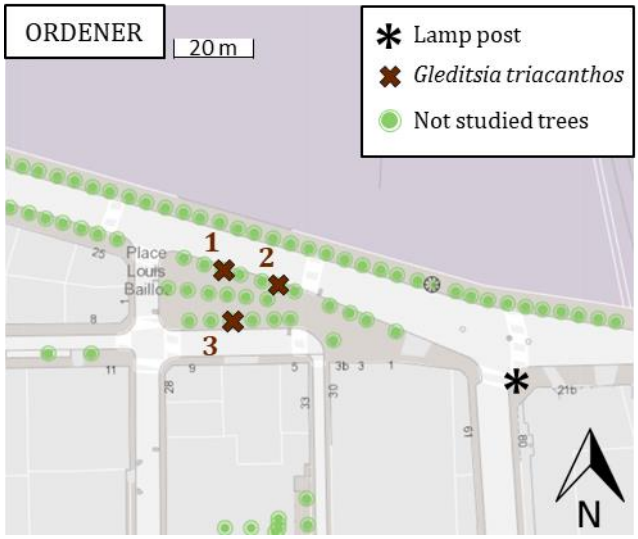

Figure 52: Location of the studied trees on ORDENER.

TEMPLE is composed of two perpendicular narrow streets bordered by buildings on both sides forming canyon streets very representative of European city centers (Figure 53). Rue du Temple is NE-SW oriented and is on average 30 m wide and bordered by buildings on both sides. Rue de Bretagne is NW-SE oriented, is on average 20 m wide and bordered by buildings on both sides. Both streets are composed of a central roadway bordered by sidewalks on both sides. The northernmost part of rue du Temple is treed with alignments of *Platanus x hispanica* on both sidewalks among which three trees were studied and its southernmost part is only treed with several *Quercus ilex* on the eastern sidewalk among which three trees were studied. The easternmost part of rue de Bretagne is treed with alignments of *Celtis australis* located on both sidewalks among which three trees were studied. The reference lamp post of this site (CANDTemple) was located on the north-west sidewalk of rue du Temple very close to the studied *Platanus x hispanica*. It was therefore approximately 150 m away from the three studied *Quercus ilex*. No reference lamp post was equipped in rue de Bretagne which is perpendicular to rue du Temple and has a contrasted orientation. CANDTemple is therefore located at approximately 550 m (walking distance) from the closest *Celtis australis*.

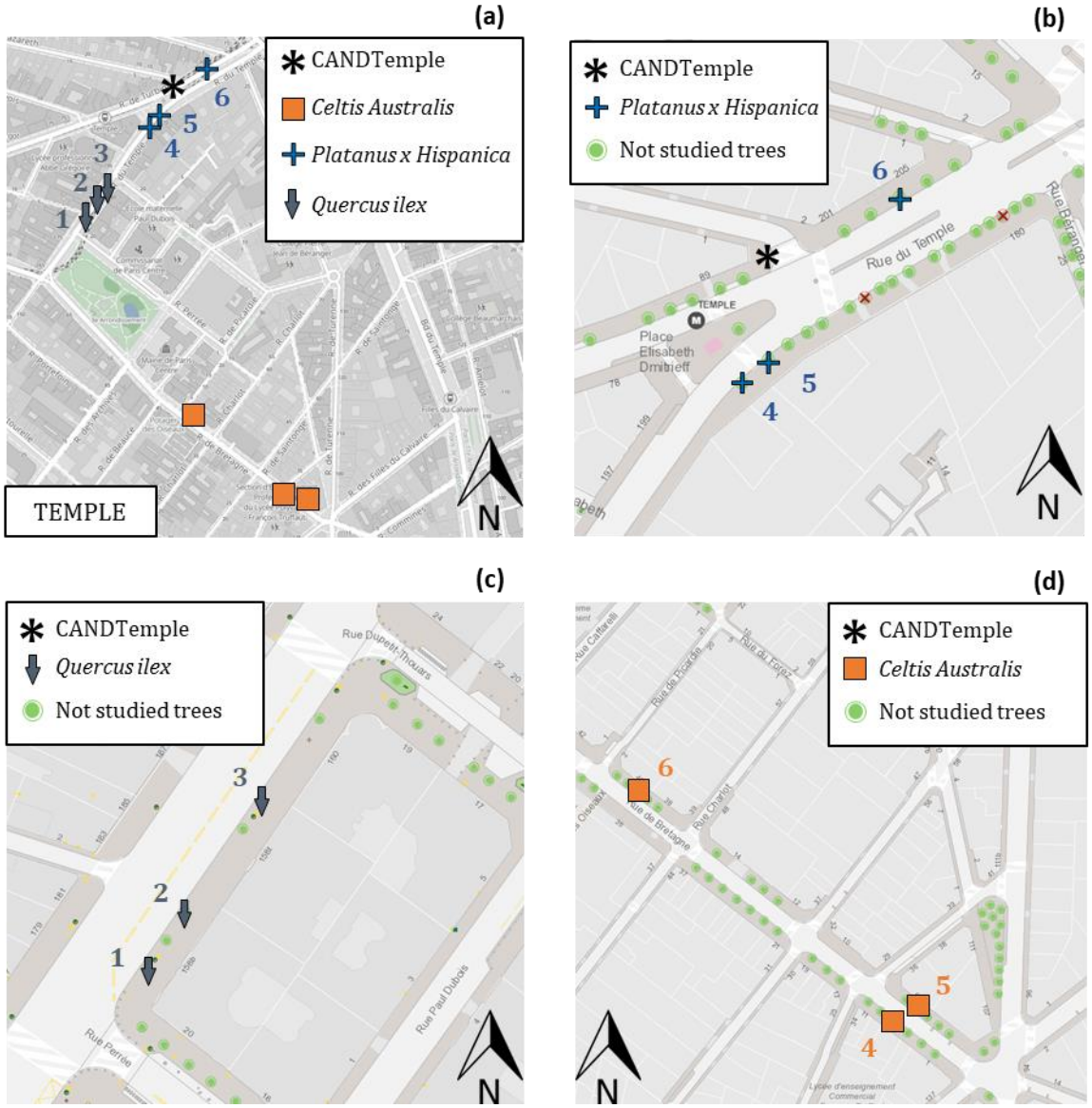

Figure 53: Location of the studied trees on TEMPLE.

VICTOR is a long NW-SE oriented boulevard composed of a wide central roadway (approximately 50 m wide) bordered by sidewalks on both sides, a few scattered small buildings on its southern side and buildings on its northern side. The northern sidewalk is treed with two rows of trees. The westernmost side of the boulevard is treed with *Platanus x hispanica* among which three trees were studied and the easternmost part is treed with *Zelkova serrata* among which three trees were studied. The reference lamp post of this site (CANDVictor) was located on the southern sidewalk of the avenue in a wide open area

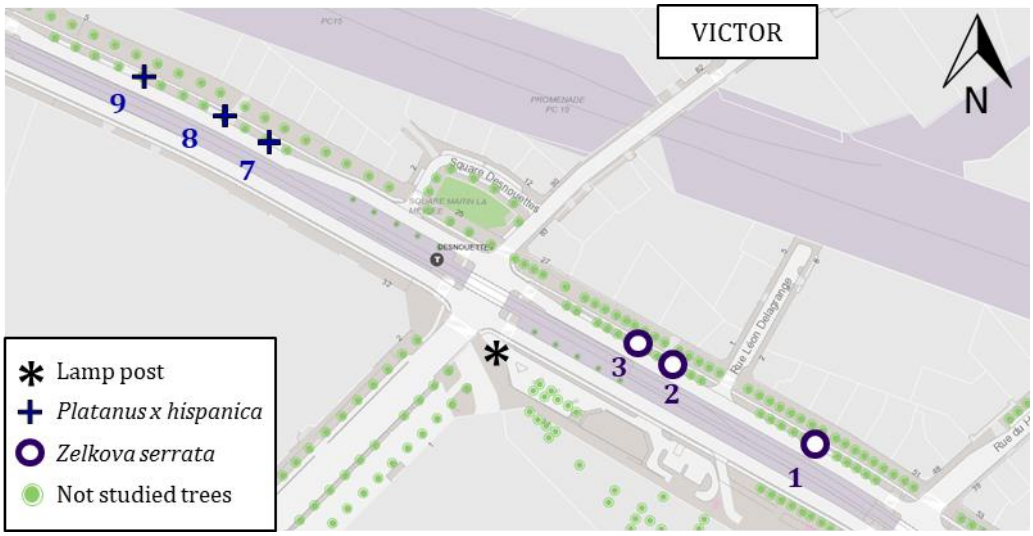

Figure 54: Location of the studied trees on VICTOR.

4.1.1.3. Characteristics of the studied trees

The multiple characteristics of the 36 studied trees cited in the present section are reported in Table 24 in appendix 7.2. The studied trees will be referred with the names indicated in Table 24 (e.g. celtis_1, celtis_2 and celtis_3 for the three *Celtis australis* of FLANDRE).

The studied trees were meant to have a good phytosanitary status. According to the information reported in the tree database of the green spaces department of the city of Paris, most of them had a good phytosanitary status while one *Sophora japonica* (FLANDRE), the three *Ulmus resista* (FLANDRE), two *Quercus cerris* (NOHAIN) and one *Platanus x hispanica* (VICTOR) had a moderately deteriorated phytosanitary status.

The trees were also selected on the basis of their circumference at breast height (measured at 1.3 m a.g.l. at the beginning of the study in May 2019) in order to ensure, if possible, a homogeneous distribution of the trunk circumferences within the 3 trees of each group. The date of plantation was found for 20 of the 36 studied trees in the tree database of the green spaces department of the city of Paris and remained unknown for 16 studied trees. The trunk circumference appeared to be slightly related to the time elapsed since planting but it cannot be used as a good predictor of the tree age (Figure 55). For instance, two *Gleditsia triacanthos* with equal trunk circumference were planted with a 7-year interval. Considering the 36 studied trees, the circumference ranged from 0.53 m to 1.15 m and Figure 55 shows that the circumferences of trees of the same species on a same site were generally close (see *Ulmus resista* on FLANDRE, *Gleditsia triacanthos* on ORDENER and *Celtis australis* and *Quercus ilex* on TEMPLE). The date of plantation could be used to estimate tree age knowing that in

Paris the trees are generally planted at 8 to 10 years old (APUR, 2023b) but this information could not be confirmed and was therefore not considered as reliable for all the studied trees.

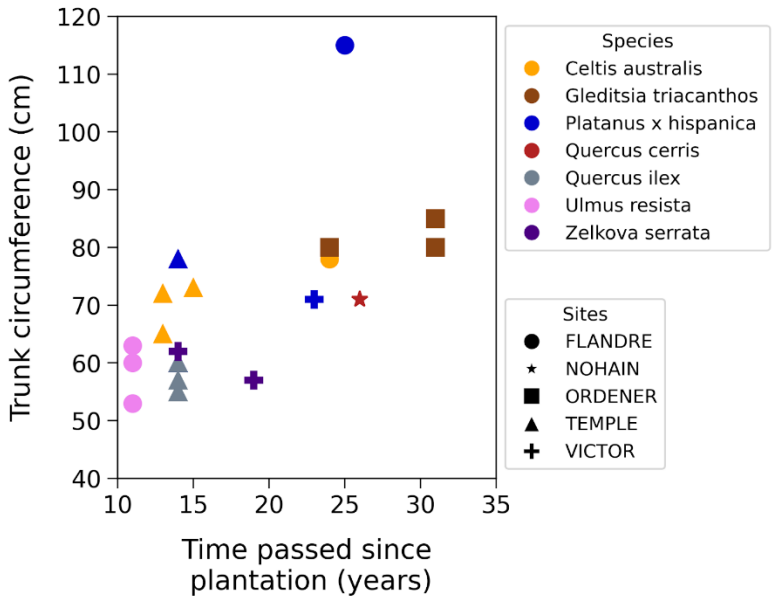

Figure 55: Distribution of the trunk circumference of the studied trees (n=20) measured in 2019 as a function of the time elapsed between the tree planting and the start of the Trees & Climate study (2019).

All studied trees were planted in individual tree pits with unknown exact dimensions but which are very likely to comply with the Parisian standards: 3 m long, 3 m wide and 1.5 m deep. The bottom of the pits is generally composed of drainage materials and is unsealed from the surrounding urban soil in order to prevent water accumulation and allow root exploration. The sides of the pits may be made of tough materials preventing the tree roots from expanding close to eventual nearby infrastructures such as water, gas or electricity networks. The top of the pits is generally covered with asphalt but a 1.8 m diameter circular or 1.5 m edge square open surface centered on the trunk of the tree generally remains unsealed and is sometimes protected from stamping by a metal grid.

In Paris, newly planted trees are manually irrigated during three years following their plantation in order to help them adapt to their new growing conditions. Then, they have to rely on the water contained in the soil of their pits which mainly comes from rainfall. However, the amount of rainwater entering the tree pits is very likely to vary according to the amount of water running off to the open surface of the tree pits. The underground compartment remained unfortunately unexplored and eventual underground sources of water (e.g. eventual leaks from water networks or nearby low depth underground water) could not be spotted. Some trees may also have benefited from other over ground water sources, for instance coming from the cleaning of the streets carried out by the municipality services.

The trees were supposed to remain untrimmed during the duration of the T&C study. However, evidences of branch removal were spotted for sophora_1 (FLANDRE, one branch removed), qcerris_1 (NOHAIN, trimming of the lower branches of the crown), qcerris_3 (NOHAIN, one branch removed) and zelkova_3 (VICTOR, trimming of the lower branches of the crown). The exact date of the aforementioned trimming however remained unknown.

4.1.1.4. Continuous monitoring

4.1.1.4.1. Meteorological sensors

The assessment of the climatic benefits provided by the studied trees relied on the measurement of 4 meteorological variables. Wind speed was measured with a cup anemometer. Globe temperature (T_g) was measured with a platinum probe enclosed inside a 15 cm diameter black painted copper sphere. Air temperature (T_a) and relative humidity (RH) were measured using a TFA Dostmann® temperature and humidity transmitter mounted inside a naturally ventilated screen made of white painted overlapping cups. Both T_a and RH were used to compute the absolute humidity (AH). The technical characteristics of these sensors are reported in Table 14.

It has already been reported in the literature that the different existing designs of screens used for T_a and RH measurements can have contrasted efficiencies, some of them inducing errors of the measured variables especially when exposed to direct sunlight (Lacombe et al., 2011; Bernard et al., 2019). Given the importance of the T_a and RH measurements in the present study, the TFA Dostmann® screens were therefore compared to a reference Davis® screen (model 7714) widely used in the literature and reputed for its high accuracy. The TFA Dostmann® screens appeared to overheat when exposed to direct sunlight and to induce important errors for T_a and RH measurements. A correction of T_a and RH measured inside the TFA Dostmann® screens was then proposed on the basis of the T_g measurements which were always performed close to the T_a and RH sensors (equations (21) and (22)). This comparison is presented in detail in appendix 7.2.8.

$$T_a^{corrected} = T_a^{T\&C} - 0.108 * T_g^{T\&C} + 1.593 \quad (21)$$

$$RH^{corrected} = RH^{T\&C} - 0.315 * T_g^{T\&C} - 4.633 \quad (22)$$

The sensors were mounted inside the crown of each studied tree on two branches high enough to avoid any deterioration during the entire duration of the study. The first branch was equipped with the TFA Dostmann® thermo-hygrometer and the second one with the globe

thermometer and the cup anemometer. As a consequence, the sensors were mounted at different positions inside the tree crowns and especially at different heights a.g.l. In this way, the sensors of the small trees were closer to the ground than those of the tall trees. The height of the sensors was reported for each tree in Table 24 and it ranged from 3.5 m to 8.2 m a.g.l.

One lamp post was also equipped with the same aforementioned meteorological sensors mounted at approximately 6.5 m a.g.l. in order to record reference measurements outside the tree crowns. In FLANDRE, 3 lamp posts were equipped with the meteorological sensors due to the long length of the avenue de Flandre.

In FLANDRE, the studied trees were equipped with the aforementioned sensors from mid-May 2019 to mid-October 2022. In the four other sites, T_a and RH measurements were performed, from mid-May 2019 and T_g, wind speed measurements from mid-July 2020 and all sensors were unmounted in mid-October 2021.

The thermo-hygrometer and the globe thermometer were scanned every hour during one minute (5 scans) and an average value was stored at an hourly time step by a data-logger. The cup anemometer was scanned multiple times every hour and an hourly maximal and average value was stored by a data-logger.

Figure 56: Pictures of the meteorological sensors mounted on two branches of one of the studied trees (left) and on one reference lamp post (right).

4.1.1.4.2. Soil sensors

Each tree was equipped with 3 Watermark® sensors aiming at measuring the soil water potential (Ψ_{soil}) at approximately 0.25, 0.5 and 0.75 m depth. Two trees (platanus_1 and platanus_9) could not be equipped as the soil of their pits was too dense and it was not possible to insert the sensors. The Watermark® sensors are able to measure Ψ_{soil} ranging from 0 to -0.25 MPa. When the real Ψ_{soil} is lower than -0.25 MPa, the value stored equals -0.25 MPa. The Watermark® sensors were scanned three times a day at 06:00, 14:00 and 20:00 UTC and a daily average value was stored for each sensor. The daily median of the values recorded by the three sensors was finally calculated for each tree and considered in the following analyses. Ψ_{soil} was monitored in all studied sites from January 2020 to December 2021 and also during year 2022 for a few trees.

4.1.1.4.3. Branch diameter variation

The evolution of the diameter of one branch of each studied tree was monitored with a microdendrometer (Figure 57) (Adam et al., n.d.). The microdendrometer was mounted on the branch carrying the aforementioned thermo-hygrometer. The branches were selected on the basis of their initial diameter in order, if possible, to get a homogeneous distribution of the initial diameters of the studied branches. Due to technical limitations of the used microdendrometer, branches with diameter exceeding 15 cm could not be studied. The circumference of the equipped branches was measured with a tape measure when installing the microdendrometer. The initial diameter of each branch was calculated considering a circular branch section for each branch. The diameter of the studied branches ranged from 50 mm to 91 mm (Figure 58). The average branch diameter was 69 mm with a standard deviation of 10 mm. The axis order of the studied branches could vary from 2 to 4 depending on the studied tree.

The microdendrometer was scanned every hour and an hourly value was stored by data-loggers. In FLANDRE, the branch diameter variations were monitored on the studied branches from mid-May 2019 to mid-October 2022. In the four other sites, the monitoring started in mid-May 2019 and ended in mid-May 2022.

Figure 57: Picture of one microdendrometer mounted on a studied branch.

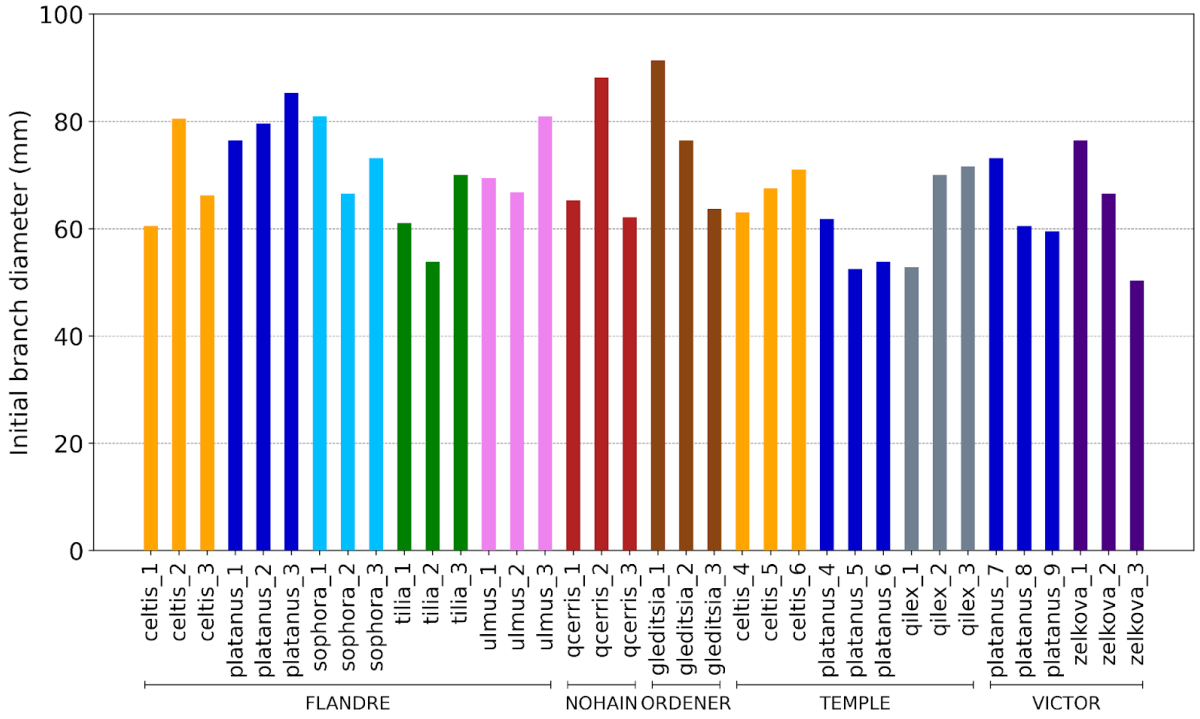

Figure 58: Initial diameter of the branch equipped with the microdendrometer calculated for each tree on the basis of the branch circumference measured when installing the microdendrometer.

4.1.1.4.4. Summary of the continuous monitoring experimental facility

The technical characteristics of the different sensors used for the continuous monitoring of the meteorological variables, Ψ_{soil} and the branch diameter variation are presented in Table 14. An overview of the experimental facility of the T&C study is proposed in Figure 59 which

illustrates a hypothetical configuration. Indeed, the T&C study is characterized by a very high heterogeneity of the studied configurations as all parameters (dimensions of the trees, their location inside each site, the composition of the surrounding environment…) may vary between sites as well as within each site.

In the present work, the records will be presented in UTC time in order to be comparable with those exposed in the previous chapter 3 of this manuscript. In metropolitan France, local time is UTC+2 from March to October (UTC+1 during the rest of the year) and during this period, the sun reaches its zenith around 11:50 UTC.

The aforementioned sensors were not installed exactly at the same time, which makes it impossible to run complete analyses of all the studied variables during the entire January 2019-December 2022 period. The recorded data underwent a validation process highlighting that part of the records could not be exploited as temporarily sensor malfunctions led to unreliable data. In this way, figures Figure 99 to Figure 102 (see appendix 7.2.2) respectively propose an overview of the available and exploitable data for the following variables: Ψ_{soil}, branch diameter variation, T_a and UTCI. The UTCI calculation (see section 4.1.3.1) relies on the measurement of T_a, RH, T_g (through the T_{mrt}) and wind speed which means that UTCI calculation can only be performed when all these four variables are available. Screening of data was undertaken over the four years of the T&C study but revealed that it never happened that all hourly variables were available to calculate the UTCI for all the 36 studied trees at the same time.

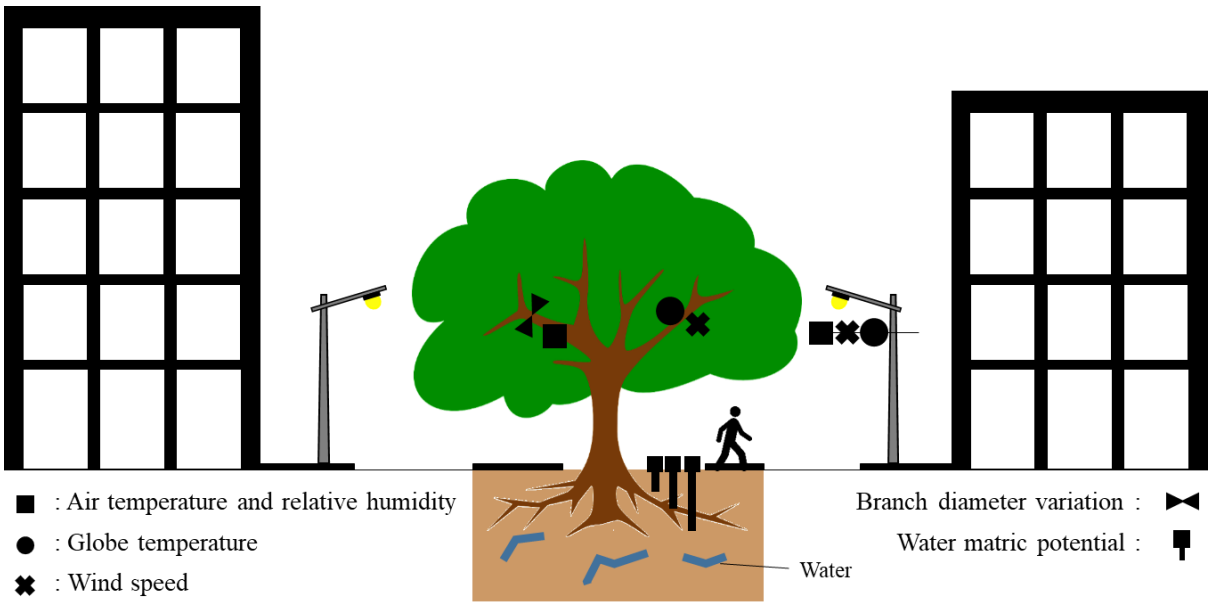

Figure 59: Scheme of the experimental facility of the "Trees & Climate" study. The respective location of the trees, buildings and sensors may vary in between the different studied sites.

Table 14: Characteristics of the sensors used in the "Trees & Climate" study.

Measured variable	Sensor type	Measurement range	Accuracy	Reference, manufacturer
Air temperature	Thermo-hygrometer	-40 to +60 °C	± 0.2 °C	TFA Dostmann, Germany
Air relative humidity	Thermo-hygrometer	0 to 99 %	± 1.5 %	TFA Dostmann, Germany
Globe temperature	Platinum probe enclosed inside a 15 cm diameter black painted copper sphere	-10 to +100 °C	± 0.25 °C	TP875, DeltaOhm
Wind speed	Cup anemometer	5 to 200 $km.h^{-1}$	± 1 $km.h^{-1}$	Vortex_OEM, Littoclime, France
Branch diameter variation	Microdendrometer (Linear Variable Differential Transformer)	± 7.5 mm	± 0.5 µm	PépiPIAF, INRAE UMR PIAF, Lycée Lafayette, France
Soil water potential		0 to -0.25 MPa	± 10 %	Campbell Scientific, USA

4.1.1.5. Morphological measurements

The 36 studied trees were scanned with a terrestrial LiDAR in order to get a numerical point cloud of each tree enabling to measure some of their morphological characteristics. For each tree, 4 scans were performed around the tree with an approximately 90° angle increment (depending on the eventual obstacles and the space available in the surrounding area of the tree). The measurement campaign was carried out on August 23rd, 24th and 25th 2022 for the 36 studied trees. At this time, only the trees located in FLANDRE were still equipped with the monitoring sensors. The scans were performed with a FARO Focus 3D X130 mounted on a tripod at approximately 1.5 m a.g.l. with a ¼ resolution (i.e. 1 point of measurement every 6 mm for an object located 10 m away from the scanner) and a 2x quality. The "Clear sky" and "clear contour" filters were disabled and the color was not used.

Figure 60: Picture of the FARO Focus 3D X130 mounted on a tripod scanning one of the studied trees.

4.1.1.6. Reference meteorological measurements

The French meteorological institute (Météo-France) operates a weather station called "Paris-Montsouris" (station n°75114001) located in the Montsouris park right at the south frontier of Paris (Figure 49). This station is located approximately 4 km east / south-east from VICTOR, 2.8 km west from NOHAIN, 5 km south from TEMPLE, 7.6 km south from ORDENER and 8 km south from FLANDRE. This weather station is located in an urban park and is therefore not totally subject to the urban overheating but is not either representative of a truly natural rural area. Dahech et al. (2020) characterized the meteorological measurements performed by this weather station compared to two other stations located approximately 15 km south of Paris and highlighted that the Paris-Montsouris station was partly shaded in the afternoon by the surrounding trees and that the surrounding rugosity lowered the wind speed compared to an open rural area. Nevertheless, the Paris-Montsouris station is used in the present study as a source of reference measurements for the climatic variables as it is the closest and the most densely equipped weather station of Paris. From now on, this weather station will be referred on as "Paris-Montsouris".

4.1.2. General meteorological conditions of the 4 studied years

The meteorological conditions over the 4 years of study (2019-2022) were compared to the average climatic conditions over the 1991-2020 period recorded at Paris-Montsouris. Only the year 2021 was characterized by an average air temperature close to the reference climatic conditions reported by Météo-France from 1991 to 2020 (Table 15). The three other years were on average warmer by 0.6 °C, 1.2 °C and 1.2 °C respectively for years 2019, 2020 and 2022. The total amounts of rainfall recorded in 2019 and 2020 were slightly higher than the 1991-2020 average one. However, the year 2021 was noticeably wetter (15 % more rainfall) and 2022 was noticeably dryer (14 % less rainfall) than the average reference. The total insolation duration and ET_{ref} were higher than the average reference values every year. Year 2022 was the sunniest year and the one with the highest evaporative demand, followed by 2020, 2019 and 2021.

Table 15: Main climatic variables measured at Paris-Montsouris meteorological station annually from 2019 to 2022 and on average from 1991 to 2020 (Météo-France, 2024).

Year	Average daily minimum air temperature (°C)	Average air temperature (°C)	Average daily maximum air temperature (°C)	Total rainfall (mm)	Total insolation duration (h)	ET_{ref} (mm)
Average 1991-2020	9.2	12.8	16.5	634	1717	891
2019	9.8	13.4	17.5	667	2015	1070
2020	10.3	14	18.3	644	2080	1142
2021	9.1	12.5	16.6	727	1886	988
2022	10.3	14	18.3	543	2185	1127

Météo-France, in association with the French ministry of health, carefully monitors T_a every summer in order to forecast eventual heatwaves and raise awareness among the population. In France, a heatwave is defined at a regional scale and corresponds to a succession of at least 3 days with a daily average of the daily minimal and maximal T_a exceeding a given alert threshold. This threshold was defined regionally on the basis of epidemiological studies and is associated with a higher risk of heat-related mortality (Santé Publique France, 2022).

The alert threshold is not necessarily exceeded during each forecasted heatwave as the meteorological conditions are sometimes less extreme than expected. Multiple heatwaves were forecasted by Météo-France in the region of Paris during the duration of the T&C study (from 2019 to 2022). They are reported in Table 16 and the corresponding number of days with T_a exceeding the alert threshold is indicated.

Table 16: List of the heatwaves reported by the French meteorological institute (Météo-France) in the region of Paris from 2019 to 2022 (Santé Publique France, 2022, 2020, 2019).

	Forecasted heatwave			Real observations	
Year	**Start date**	**End date**	**Number of days**	**Nbr. of days with T_a exceeding the regional alert threshold**	**Maximal T_a recorded at Paris-Montsouris (°C)**
2019	June 23rd	June 30th	8	4	36.5
	July 21st	July 27th	7	6	42.6
	August 26th	August 27th	2	0	33.4
2020	June 24th	June 25th	2	0	35.2
	July 30th	July 31th	2	0	39.3
	August 5th	August 13th	9	7	39.1
	Sept. 13th	Sept. 15th	3	0	34.3
2021	June 15th	June 16th	2	0	33.3
2022	June 15th	June 20th	6	0	36.7
	July 11th	July 21th	11	6	40.5
	August 1st	August 14th	14	0	35.9

4.1.3. Methods

4.1.3.1. Universal Thermal Climate Index (UTCI)

The Universal Thermal Climate Index (UTCI) was calculated inside the tree crowns as well as at the reference lamp posts of each site following the methodology developed by Bröde et al. (2012) on the basis of the measurement of T_a, RH and wind speed all carried out at the same location and on the calculation of the mean radiant temperature (T_{mrt}) with equation (15) (Huang et al., 2014).

4.1.3.2. Calculation of morphological variables

For each tree, 4 scans were performed around the tree with an approximately 90° angle increment. Four point clouds were then obtained and were mixed together to form a unique point cloud using the softwares FARO Scene 5.4 and Polyworks. The points associated with

the tree were extracted from the rest of the point cloud which may have included the surrounding trees, buildings and other street furniture. A few issues may have been encountered during this step, especially for trees forming part of a dense canopy. Such trees may have some of their branches overlapping branches of the surrounding trees making it hard to distinguish which tree the overlapping branches belong to. In this case, a virtual arbitrary border between both trees was used to separate the points between the two trees. The point clouds of the 36 studied trees are presented in appendix 7.2.4.

The point cloud of each tree was then subdivided into:

- voxels: The entire 3D coordinate system was subdivided into 10 cm edge virtual cubes called voxels and all voxels containing at least one point of the point cloud were considered;
- Convex polygons: The point cloud was divided into 10 cm wide horizontal layers and the convex polygon encompassing each layer was computed;
- Concave polygons: The point cloud was divided into 10 cm wide horizontal layers and the concave polygon encompassing each layer was computed.

These voxels and polygons were then used to compute 7 morphological parameters listed and described in Table 17. These calculations however have to face some limitations. Especially, as the scans were realized with a terrestrial LiDAR, it is very likely that the uppermost part of the tree crowns may sometimes not have been scanned accurately as the uppermost foliage may have been screened by lower branches and leaves. The uncertainty associated with this issue cannot be quantified but some parameters such as the total tree height and the crown volume are likely to be slightly underestimated.

Table 17: Description of the morphological parameters calculated for the 36 studied trees on the basis of the point clouds acquired with LiDAR measurements.

Morphological parameter	Abbreviation	Unit	Description
Total tree height	Htot	m	Distance between the uppermost and lowermost points of the point cloud.
Crown projected area	Sproj	m^2	Area of the concave polygon encompassing all points of the point cloud when projected on the ground. The eventual holes found in the crown were not excluded from the computation.
Crown volume (convex polygon method)	Vpoly	m^3	Sum of the area of all the convex polygons multiplied by the width of the horizontal layers (10 cm). The crown volume calculated here takes into account the leaves, the branches and all the empty spaces encompassed in the entire foliage.
Crown volume (voxel method)	Vvox	m^3	Sum of all the voxels multiplied by the volume of one voxel (volume of a 10 cm edge cube). The size of the voxel was chosen in order to optimize the accuracy while keeping a low computation time. The crown volume calculated here takes into account the leaves as well as the branches.
Crown density	Density	no unit	Ratio of the crown volume calculated with the voxel method to the crown volume calculated with the convex polygon method. This ratio should not be confused with the leaf area index or density often mentioned in the literature. This ratio is more representative of the proportion of leaves and branches among the total volume of the crown.
Crown base height	Hbase	m	Height of the lowermost leaf of the crown.
Crown's maximal extension height	Hsurf_max	m	Height of the largest convex polygon calculated hereinabove.

4.1.3.3. Analysis of branch diameter variations

The microdendrometers aim at monitoring the temporal evolution of the branch diameter, which is linked to the tree growth and to internal water use of the tree. The microdendrometers record for each time step the difference between the current position of their needle and the initial position of their needle at the beginning of the acquisition. The first value of branch diameter variation was set to zero at the beginning of each year in order to be able to compare, for each tree, the amplitude of branch diameter variation of the four years of study. A few gaps of data lasting multiple days were spotted for some of the studied trees. In this case, the first value of branch diameter variation recorded after the period of lacking data was set to zero and the real dynamic of the branch diameter variation during the period of lacking data remained unknown. Consequently, the total annual branch diameter variation could not be assessed for the concerned trees.

The T&C study focused on trees of different ages and different species. Moreover, the branches equipped with the microdendrometers had different initial diameters, different axis orders and different sun exposures. A strong variability is therefore likely to exist among the branch diameter variations recorded for the 36 studied trees. In order to investigate this variability, two *Celtis australis* of FLANDRE (celtis_1 and celtis_3) were equipped with 4 microdendrometers each from March to November 2023 in order to compare the diameter variations of branches bearing leaves with contrasted solar exposure and also branches with different hierarchical insertion in the crown structure. The details of this monitoring campaign, presented in appendix 7.2.9, highlighted that the variability of the amplitudes of branch diameter variations that may exist in between the branches of a single tree may be higher than the variability between two branches of different trees. Yet, the growth dynamics appeared to be similar for different branches of a same tree. The comparison of the branch diameter variations recorded for the 36 trees of the T&C study is therefore not trivial and the two following strategies were then adopted to cope with this variability:

- The branch diameter variations were first normalized in order to compare the branches of the 36 studied trees on a common basis at a yearly scale. The branch diameter variations as well as the initial circumference of the branch measured when installing the microdendrometers were respectively converted into a branch section variation and an initial branch section considering a circular shape section. An initial branch section was then calculated at the beginning of each year considering the initial branch section and the total branch section variation of the previous year. Finally, the branch section variation of each

branch was expressed as a percentage of its initial section at the beginning of each year. Branch section was preferred to branch diameter for normalization as it integrates the complete formation of new tissues all around the branch circumference.

- For each tree, the signal of branch section variation was then divided into multiple indicators which were introduced in previous works found in the literature such as the one of Dietrich et al. (2018) and already presented in the previous chapter (see section 3.2.2.2). But, in order to prevent the analyses from being impacted by the important variability between branches of a same tree highlighted in appendix 7.2.9, only maximum diameter ever recorded (MDER) and the daily growth (DG) were used in the present analyses. The effects of warm and dry periods on the studied trees were assessed through the quantification of the growth trend and especially the number of days with no growth (DG = 0) was quantified for each tree during the periods of interest which will be described in section 4.1.3.5.

4.1.3.4. Calculation of the average climatic benefits

The difference between the meteorological variables measured inside the tree crowns and the ones measured at the reference lamp posts was calculated for T_a, AH, T_{mrt} and UTCI at each time step. For each one of these four variables, the following subtraction was calculated: $variable_{tree\ crown}$ - $variable_{lamp\ post}$, and called "Δvariable". Considering for instance T_a, this means that a negative ΔT_a reflects a lower T_a inside the tree crown compared to its reference lamp post. For all sites except FLANDRE, each tree was then compared to the reference lamp post located on the same site (respectively called CANDNohain, CANDOrdener CANDTemple and CANDVictor). For FLANDRE, which contains 3 studied lamp posts, all the studied trees were compared to CANDFlandre2 as CANDFlandre1 had a similar signal for all 4 meteorological variables and CANDFlandre3 was located in an area mainly shaded in the afternoon and was therefore not really representative of the maximum overheating phenomenon existing in the avenue de Flandre. Moreover, CANDFlandre2 was located approximately at equal distance (approximately 650 m) from both the northernmost and the southernmost studied trees.

Average daily differences focusing on different periods during the day were calculated in order to easily assess the long-term evolution of the difference between trees and lamp posts:

- The average difference from 00:00 to 23:59 UTC (entire day);
- The average difference from 02:00 to 04:00 UTC (night-time);

- The average difference from 11:00 to 13:00 UTC (solar noon);
- The average difference from 15:00 to 17:00 UTC (afternoon);
- The maximum difference of the day which does not occur at the same time every day.

These differences were calculated every day during an extended summer period (from May 1st to September 30th) when trees are likely to bear their entire foliage and when heatwaves and droughts are expected to occur. Then, these daily differences were averaged for each tree in order to calculate the average climatic benefits provided by each tree. However, in order to compare all trees on a common basis, these overall differences have to be computed on a same list of days for all the studied trees as meteorological conditions can vary a lot from one day to the next one. Yet, as highlighted previously, it was not possible to find any single day with data available for all the 36 studied trees at the same time. To cope with this issue, a list of days with common data availability for all the trees of the same site was established for each site in order to compare at least all the trees of the same site on a common basis. This however implies that the overall average differences aforementioned were calculated considering different lists of days for the different sites. The days considered for each analysis conducted hereinafter will be presented in the results section right before the associated results for more clarity.

4.1.3.5. Effect of dry and warm periods

In order to study the effects of warm and dry conditions on the growth of the studied street trees and the climatic benefits they provide, different periods of interest were searched for. However, the definition of such periods is not easy as heatwaves and dry events are likely to occur simultaneously which makes it difficult to assess the effect of high temperatures and low water availability independently. Indeed, it was not possible to find a period enabling to study the effect of heatwaves while ensuring a high water availability for the studied trees. As a consequence, a focus was made on the assessment of the effects of decreasing water availability on both the branch section variations of the trees and the climatic benefits they provide. To do so, the branch section variations and soil water content were first compared during both a dry and a wet summer. Then, the evolution of branch section variation and of the climatic benefits provided by the trees were assessed a 40-day period without rainfall.

4.1.3.5.1. Comparison of a dry and a wet summer

Years 2020 and 2021 were characterized by contrasted climatic conditions, 2020 being warm and dry while 2021 was cooler and wetter as previously presented in Table 15. Given

that soil water potential data were available for all the studied trees in 2020 and 2021, the relationship between soil water potential and branch growth was investigated by comparing both years. Two periods centered on July were defined for each year considering the availability of soil water potential data: June 29th, 2020 to August 11th, 2020 and July 9th, 2021 to August 11th, 2021. The following indicators were calculated over both periods for each studied tree in order to approach the sensitivity of the trees to the water availability:

- The percentage of days with branch growth interrupted (DG = 0) during the dry period;
- The percentage of days with Ψ_{soil} lower or equal to -0.25 MPa (lower limit of the Watermark® probes measurement range).

The latter was preferred to the average Ψ_{soil} over the studied period as the real Ψ_{soil} values remained unknown as soon as Ψ_{soil} was lower than the lower limit of the measurement range of Watermark® probes (-0.25 MPa) which happened very often in summer.

4.1.3.5.2. Focus on a dry period

As the water content of the tree pits was not controlled and soil water potential was not monitored deep enough to fully represent the water availability for the trees, the dry period presented here was selected on the basis of the daily rainfall data and the inventory of the heatwaves carried out by Météo-France from 2019 to 2022, as mentioned previously (see appendix 7.2.3). During the selection process, years 2020 and 2021 were preferred in order to take into account trees from the 5 studied sites as all trees were fully monitored during these two years.

The evolutions of branch growth, ΔT_a and ΔUTCI were assessed over a period starting on July 1st, 2020 and lasting until August 10th, 2020 chosen for its important number of successive days without any rainfall (Figure 61). Before this period, the month of June was characterized by a total rainfall of 47 mm which was close to the average monthly total rainfall recorded by Météo-France from 1991 to 2020 (51.3 mm) (Météo-France, 2024). June 2020 was characterized by a strong rainfall event on June 3rd (28.8 mm) and smaller but regular rainfall events until July 1st (2 mm). It was therefore hypothesized that the studied trees were not yet subject to a strong water stress on July 1st. Except for one rainfall event reported on July 25th (6.3 mm), the trees were subjected to 40 days without any rain between July 1st and August 10th. This period was followed by multiple rainfall events on August 11th (2 mm), 12th (14.8 mm), 13th (6.1 mm) and later on in August 2020. Three heatwaves were reported a few

days before (June 24th to 25th), during (July 30th to August 1st) and right at the end (August 5th to August 13th) of the studied dry period.

The impact of the dry period on the branch diameter variation was assessed through the calculation of the three following indicators for each studied tree in order to approach their sensitivity to the lack of water and their resilience after the end of the dry event:

- The number of days between the start of the dry period (July 1st 2020) and the interruption of branch growth (DG = 0);
- The percentage of days with branch growth interrupted (DG = 0) during the dry period (from July 1st to August 10th 2020);
- The number of days between the end of the dry period (August 10th) and the restart of branch growth calculated until September 30th.

The impact of the dry period on the climatic benefits provided by the studied trees was assessed by the calculation of ΔT_a and ΔUTCI during three groups of 2 sunny (more than 10 hours of insolation as measured by Météo-France at Paris-Montsouris) and rain-free days with close meteorological conditions. The three groups of 2 days were scattered at the beginning, at the middle and at the end of the studied period (Table 18) close to the three heatwaves of June and July 2020 mentioned hereinabove.

Table 18: Meteorological variables measured by Météo-France at Paris-Montsouris during three groups of two days scattered before, in the middle and at the end of the studied dry period (July 1st to August 10th, 2020). GLOT: Daily integral of the incoming global radiation measured at Paris-Montsouris.

	Before dry period		**Middle of dry period**		**End of dry period**	
	June 23rd	June 24th	July 29th	July 30th	August 5th	August 6th
Rainfall ($mm.day^{-1}$)	0	0	0	0	0	0
Insolation duration (hours)	15	14.8	13.8	14.3	14	13.6
GLOT ($MJ.m^{-2}.day^{-1}$)	30.5	30.5	27.8	27.8	26.9	25.9
Average wind speed ($m.s^{-1}$)	2.5	2.9	1.9	2.1	2.2	1.6
Minimal T_a	15.3	17.9	14.4	15	13.8	17.1
Average T_a	23.8	26.7	20.6	25	23.7	27
Maximal T_a (°C)	30.3	33.4	27.1	33.2	31.4	35.1
ET_{ref} ($mm.day^{-1}$)	7.1	8.4	5.9	7.2	6.8	7.1

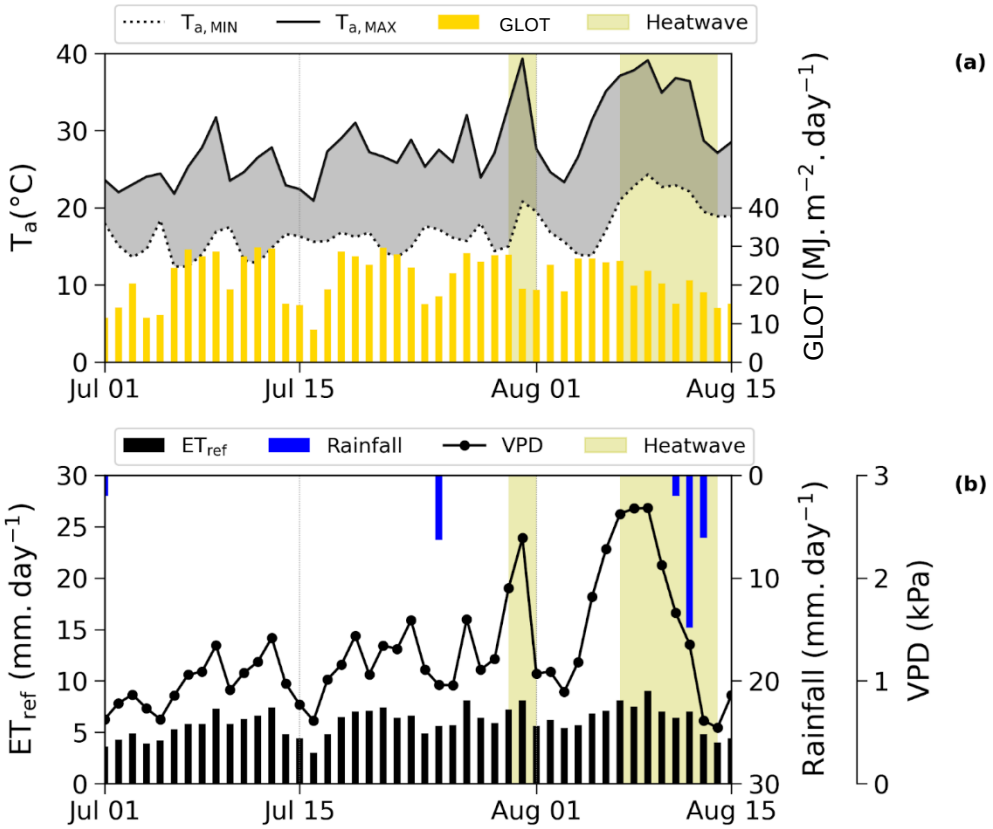

Figure 61: Evolution of (a) the daily integral of downward global radiation (GLOT), the daily minimum and maximum air temperature ($T_{a, MIN}$ and $T_{a, MAX}$) and (b) the daily reference evapotranspiration (ET_{ref}), the daily rainfall and the daily average VPD measured by Météo-France at Paris-Montsouris from July 1st to August 15th 2020.

4.1.3.6. Statistical analyses

Statistical analyses were performed using Python language version 3.9-64. Linear regressions were performed to evaluate the eventual dependence between couples of variables using the following packages: *sklearn* and *statsmodels*. Principal component analyses (PCA) were performed using the PCA method of the *sklearn* package.

4.2. Results

4.2.1. Morphological diversity of the studied trees

The numerical point clouds obtained through the terrestrial LiDAR scanning campaign for the three studied *Celtis australis* of FLANDRE are presented as an example in Figure 62. The point clouds of the 36 studied trees can be found in appendix 7.2.4 and the results for the different calculated morphological parameters can be found in Table 25 in appendix 7.2.5.

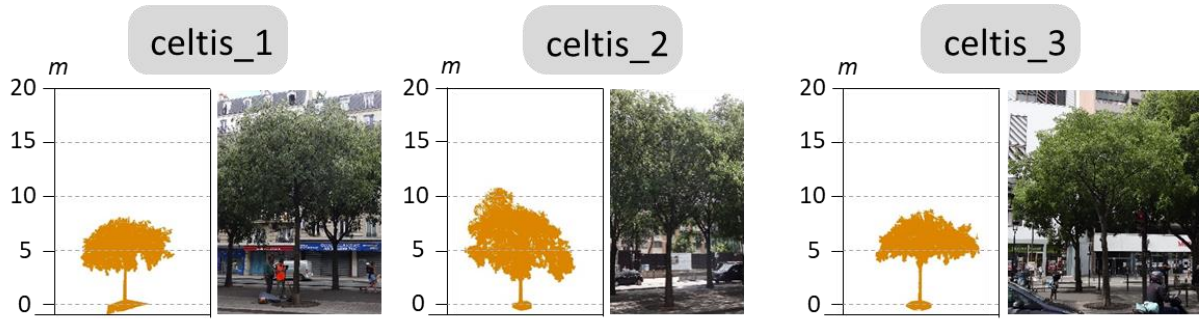

Figure 62: Numerical point clouds obtained for the 3 *Celtis australis* of FLANDRE with the terrestrial LiDAR scanning campaign performed in August 2022.

The different morphological parameters calculated for all trees on the basis of their numerical point clouds are gathered in Figure 63 which shows the strong morphological variability of the studied trees. Contrasted results were reported between different species and sometimes within each group of three trees of the same species and located on the same site. The morphological parameters appeared to be slightly homogeneous for the *Celtis australis* studied in FLANDRE and TEMPLE and the nine *Platanux x hispanica* studied in FLANDRE, TEMPLE and VICTOR.

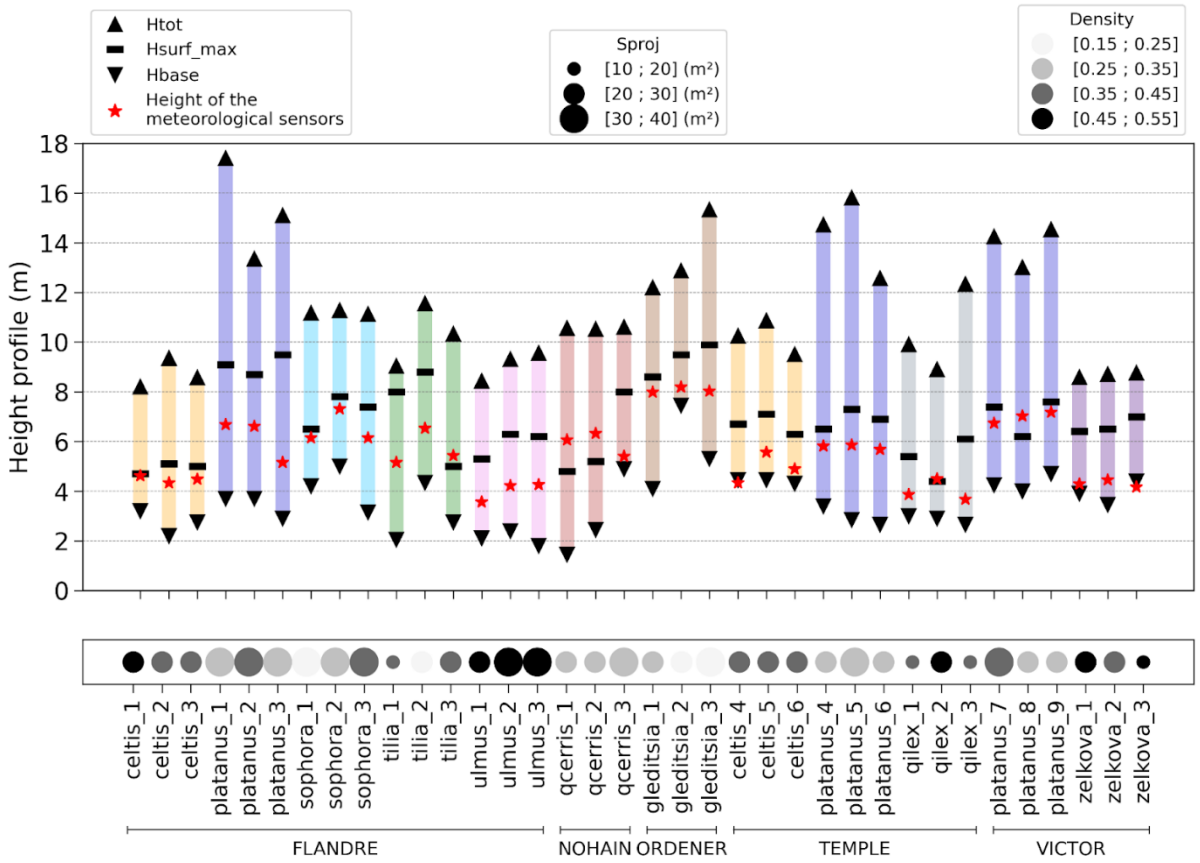

Figure 63: Total height of the trees (Htot), height of the base of the crown (Hbase), height of the larger convex polygon of the crown (Hsurf_max), height of the meteorological sensors mounted inside the tree crowns, crown projected area (Sproj) and crown density for the 36 studied trees measured on numerical point clouds acquired through terrestrial LiDAR scanning in August 2022.

A PCA run with the calculated morphological variables highlighted the low relationship existing between them (Figure 64). The first principal component was mainly correlated with Htot, Sproj and Vpoly while the second one was mainly correlated with Hbase, Vvox and density. Only Sproj appeared to be highly related to Vpoly which is consistent as the trees with the highest total volume are very likely to induce a wide crown projected area.

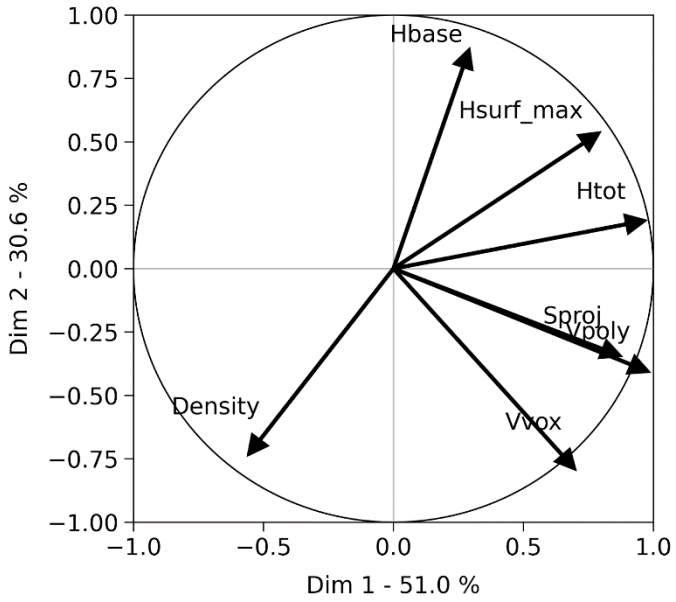

Figure 64: Correlation circle obtained through a principal components analysis performed on the 36 studied trees for 7 morphological variables: Hbase, Hsurf_max, Htot, Sproj, Vpoly, Vvox, Density.

The distribution of the 36 studied trees among the two first principal components is presented in Figure 65. The remoteness of the different trees along the horizontal axis indicates contrasted values for the morphological characteristics correlated with the first principal component (Htot, Sproj and Vpoly) while remoteness of the different trees along the vertical axis indicates contrasted values for the morphological characteristics correlated with the second principal component (Hbase, Vvox and density).

A few trends can be summarized, having a look at both the distribution of the studied trees along the two first principal components (Figure 65) and the absolute values of the morphological parameters presented in Figure 63. The total height of the trees ranged from 8.2 to 17.4 m. The *Gleditsia triacanthos* and the *Platanus x hispanica*, on the three sites where they were studied, appeared to be the tallest trees while the three *Celtis australis* of FLANDRE, the three *Ulmus resista* and the three *Zelkova serrata* were among the smallest ones as none of them exceeded 9.5 m. *Platanus x hispanica* also had on average the tallest crowns as their high Htot was also accompanied by a generally low Hbase meaning that their foliage started low and ended high.

The crown projected area (Sproj) of the studied trees ranged from 17 m² to 38 m² while their density ranged from 0.19 to 0.55. *Ulmus resista* trees appeared to have on average the highest crown densities and they were also characterized by large crown projected areas. *Sophora Japonica* trees also had large crown projected areas but very contrasted crown

densities. Both *Gleditsia triacanthos* and *Quercus cerris* were characterized by low crown projected areas and low crown densities.

The height of the meteorological sensors was quite heterogeneous as it ranged from 3.5 m to 8.2 m and it appeared to be highly influenced by the dimensions of the tree crown as the sensors were generally located close to the base of the tree crown.

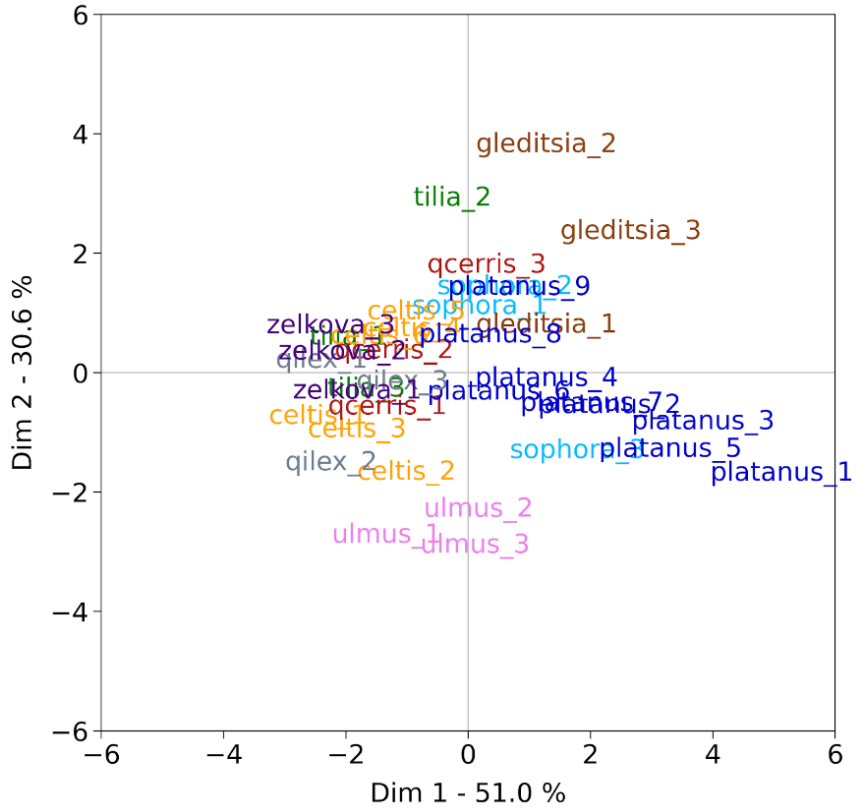

Figure 65: Distribution of the 36 studied trees regarding the two first principal components resulting from a principal components analysis performed for 7 morphological variables: Hbase, Hsurf_max, Htot, Sproj, Vpoly, Vvox, Density.

4.2.2. Microclimate of the 5 sites

The general microclimate of the different sites was compared by analyzing the meteorological variables measured at the different reference lamp posts as well as reference measurements carried out at Paris-Montsouris focusing on a period when all lamp posts had available data at the same time (May 1st, 2021 to September 30th, 2021). At night, T_a was on average higher in all sites compared to Paris-Montsouris by approximately 0.5 °C from 20:00 to 04:00 UTC except on TEMPLE where the average difference reached 1.1 °C (Figure 66). During the day, contrasted T_a dynamics were reported in the different sites. TEMPLE appeared to be the warmest site during the day with an average T_a difference with Paris-Montsouris of 0.8 °C from 08:00 to 16:00 UTC while NOHAIN was cooler than Paris-Montsouris by 1.2 °C on average from 08:00 to 16:00 UTC making it the coolest site. VICTOR and ORDENER were respectively cooler by 0.1 and 0.6 °C on average from 08:00 to 16:00 UTC. The three reference lamp posts located on FLANDRE showed contrasted behaviors and strong variations during the day. On one hand, CANDFlandre3 remained warmer than Paris-Montsouris in the morning by on average 0.4 °C from 08:00 to 12:00 UTC. On the other hand, CANDFlandre1 and CANDFlandre2 which were cooler than Paris-Montsouris approached the T_a of Paris-Montsouris in the afternoon and were then on average 0.7 °C warmer than CANDFlandre3 around 16:00 UTC. The dynamics of the overheating phenomenon observed at each lamp post are very consistent with the respective positions of the lamp posts in their site. This is particularly noticeable in FLANDRE as CANDFlandre1 and CANDFlandre2 were located on the eastern sidewalk of the street and then exposed to sunlight in the afternoon, while CANDFlandre3 was located on the western sidewalk and exposed to the sun in the morning (see Figure 50).

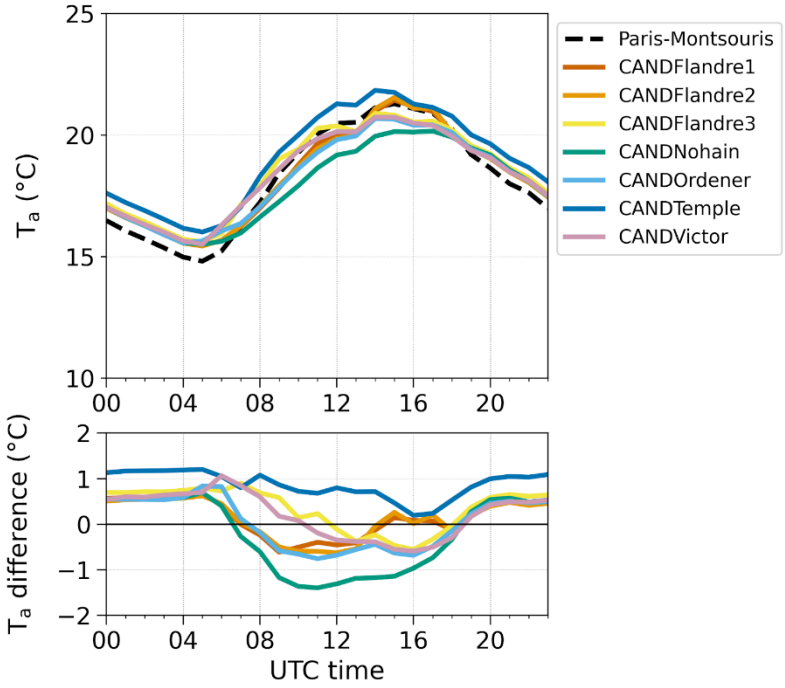

Figure 66: Average daily evolution of the air temperature (T_a) measured at each lamp post as well as at Paris-Montsouris and of the air temperature difference between each lamp post and the Paris-Montsouris meteorological station from May 1st, 2021 to September 30th 2021. The hourly standard deviation of T_a was not drawn for more clarity but it remained lower than 4.5 °C for all lamp posts as well as for Paris-Montsouris.

VPD was on average lower in all studied sites compared to Paris-Montsouris all over the day except during night-time in TEMPLE and NOHAIN (Figure 67). During daytime, VPD reached much higher values in TEMPLE (on average 0.15 kPa higher VPD around noon) compared to all other sites and CANDFlandre1 and CANDFlandre2 were also characterized by an increasing VPD in the afternoon (around 16:00 UTC) reaching the average VPD recorded in TEMPLE at this time of the day.

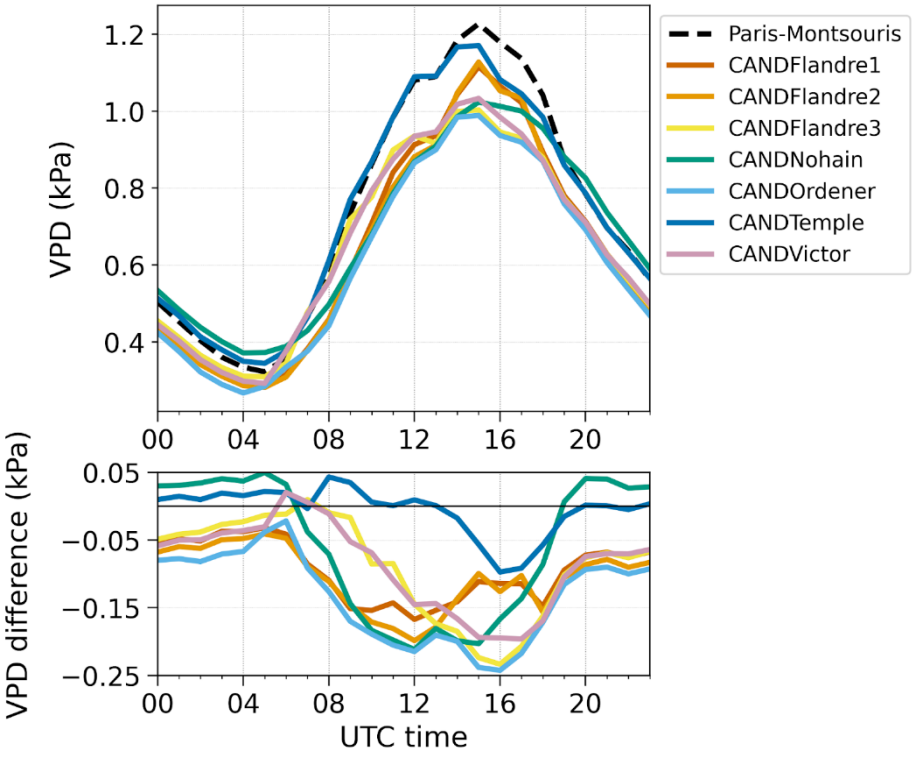

Figure 67: Average daily evolution of the vapor pressure deficit (VPD) measured on each lamp post as well as at Paris-Montsouris and of the VPD difference between each lamp post and Paris-Montsouris from May 1st, 2021 to September 30th, 2021.

At night, CANDTemple and CANDFlandre3 measured slightly higher radiation fluxes compared to the other sites as their T_{mrt} was on average 17.6 °C from 20:00 to 04:00 UTC while T_{mrt} remained lower than 17 °C at all other lamp posts (Figure 68). During the day (i.e. from 08:00 to 16:00 UTC), T_{mrt} reached on average 28.5 °C in ORDENER, 30.4 °C in NOHAIN, 32.2 °C at CANDFlandre1, 31.9 °C at CANDFlandre2, 30.7 °C at CANDFlandre3, 33.3 °C in TEMPLE and 35.3 °C in VICTOR. T_{mrt} is very sensitive to SW as it relies on globe temperature and its evolution over the day is likely to illustrate the periods of direct insolation of the reference lamp posts. The different solar exposure of the three lamp posts of FLANDRE is therefore easily noticeable, CANDFlandre3 being exposed to the sun in the morning while CANDFlandre1 and CANDFlandre2 were exposed to the sun in the afternoon. The lamp posts of NOHAIN and ORDENER also appear to be mainly exposed to the sun in the afternoon while the solar exposure of lamp posts of TEMPLE and VICTOR appears to be more homogeneous throughout daytime.

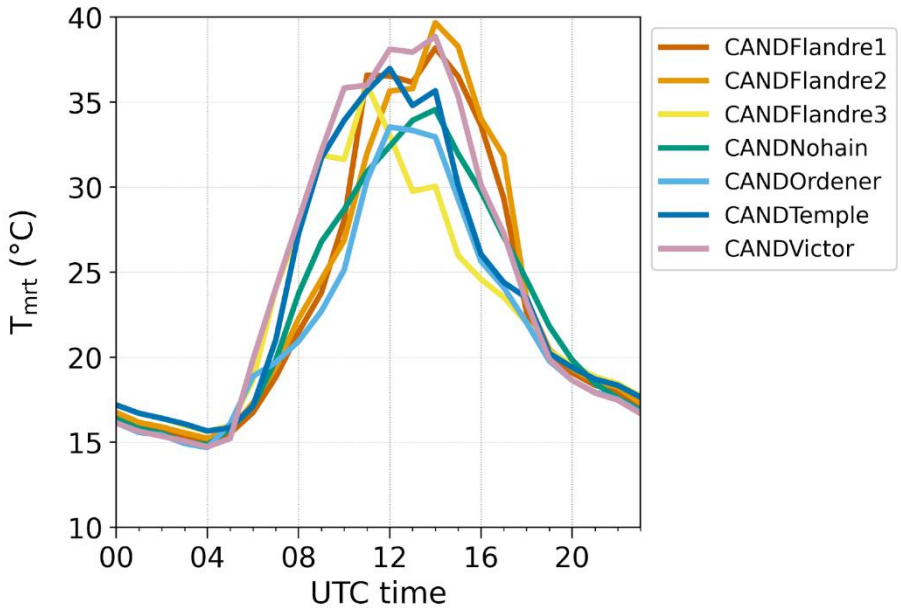

Figure 68: Average daily evolution of the mean radiant temperature (T_{mrt}) calculated at each lamp post from May 1st, 2021 to September 30th, 2021. T_{mrt} was not calculated at Paris-Montsouris. Standard deviation is not represented for more clarity but can reach 13.9 °C.

Regarding UTCI, the daily evolutions presented in Figure 69 showed similar trends to those reported previously for T_{mrt}, which is consistent with the dependence of UTCI on T_{mrt}. However, unlike what was observed for T_{mrt}, the UTCI is on average higher in TEMPLE during the day which is likely to be caused by the higher T_a measured in this site. In the late afternoon, CANDFlandre1 and CANDFlandre2 both measure the highest UTCI values which is probably induced by their high solar exposure at this time of the day highlighted in Figure 68 considering T_{mrt}. Although the UTCI appears to remain in the no thermal stress category in each site all day long except temporarily in TEMPLE and close to CANDFlandre1, it is important to recall that Figure 69 presents average daily evolutions on a 5-month period of time with a wide range of meteorological conditions. Therefore, the UTCI calculated on each site during warm and sunny days is obviously higher than the one presented in Figure 69. The standard deviation which can reach up to 6.4 °C has the same order of magnitude as the amplitude of the moderate heat stress category defined for the UTCI analysis which ranges from 26 °C to 32 °C. Thereby, the moderate heat stress and even the high heat stress category are likely to be reached frequently.

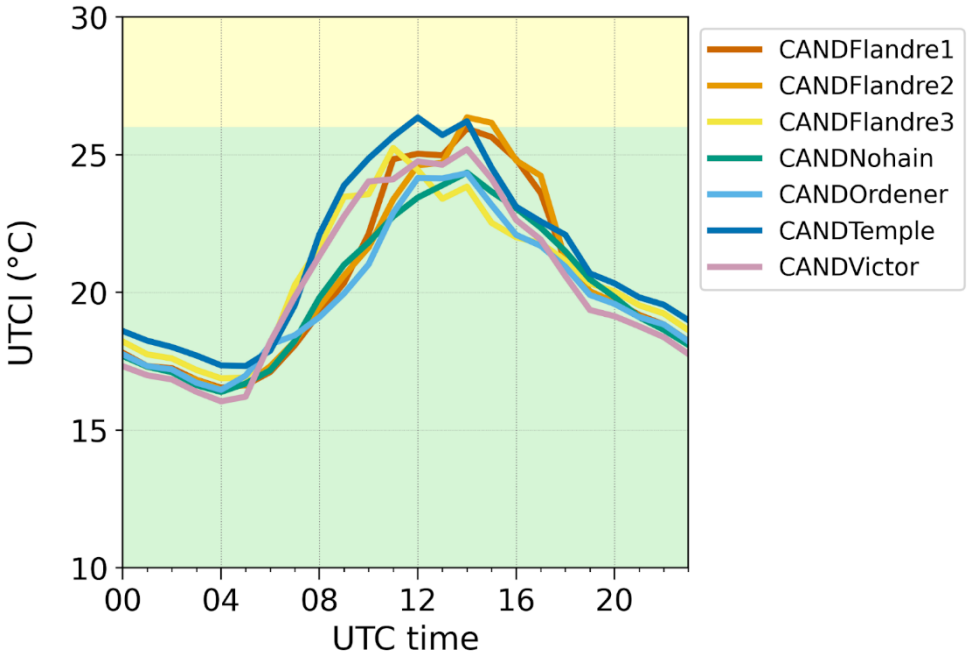

Figure 69: Average daily evolution of the UTCI calculated on each lamp post from May 1st, 2021 to September 30th, 2021 regarding the different thermal stress categories: no thermal stress (9 to 26 °C UTCI, green), moderate heat stress (26 to 32 °C UTCI, yellow), high heat stress (32 to 38 °C UTCI, not shown), very high heat stress (38 to 46 °C UTCI, not shown) and extreme heat stress (>46 °C UTCI, not shown). Standard deviation is not represented for more clarity but can reach 6.4 °C.

The different studied trees then are likely to be exposed to slightly different evaporative demand depending on the site they are located in. Especially, the trees located in TEMPLE, FLANDRE and VICTOR are likely to experience a higher average evaporative demand compared to the trees located on the other sites due to the high Ta and VPD of TEMPLE and the high T_{mrt} in FLANDRE and VICTOR.

4.2.3. Overview of the branch diameter variation

The branches of the 36 studied trees grew approximately from mid-April until the end of August (start of growth not visible in 2019 as the monitoring began in mid-May) but very contrasted amplitudes of total growth were reported. The evolution of the branch section variation of the trees located in FLANDRE are presented in Figure 70 as an example while those of the trees located in the other sites are presented in appendix 7.2.6.

First, a strong variability was noticed among the groups of three trees of the same species located on the same site. In FLANDRE, two *Sophora japonica* experienced a very low total growth in 2019 (lower than 2 % of the initial branch section) while the third one grew by more

than 10 %. Similar observations were reported for other groups of trees such as the three *Ulmus resista* of FLANDRE in 2021.

A strong variability was also reported in between trees of different species. In 2020 and 2021, it can then be noticed that the *Ulmus resista* generally grew more than all other studied trees in FLANDRE while the three *Tilia cordata* appeared to grow much less as their annual total growth remains under 5 % of their initial branch section.

A given tree may also have experienced a variable total growth from one year to the next one. The growth of the *Ulmus resista* barely reached 6 % in 2019 while almost all of them grew by more than 10 % in 2020 and 2021. Similar observations can be reported for the other species.

Also, very contrasted growth dynamics were observed along the growing season for the different trees. Indeed, multiple trees experienced branch shrinkage during their growing season, which takes the form of a reduction of their branch section. In 2019, the branch shrinkage of one *Sophora japonica* (sopora_1) is for instance easily noticeable as the branch section of this tree was even lower than its initial value at the beginning of the monitoring period during most of the growing season. It can also easily be noticed that while some trees may experience branch shrinkage, other trees of the same species may still be growing without interruption all along the growing season. This phenomenon was observed for instance in 2022 when the branch of one *Platanus x hispanica* and one *Ulmus resista* grew continuously while most of the other studied branches were shrinking.

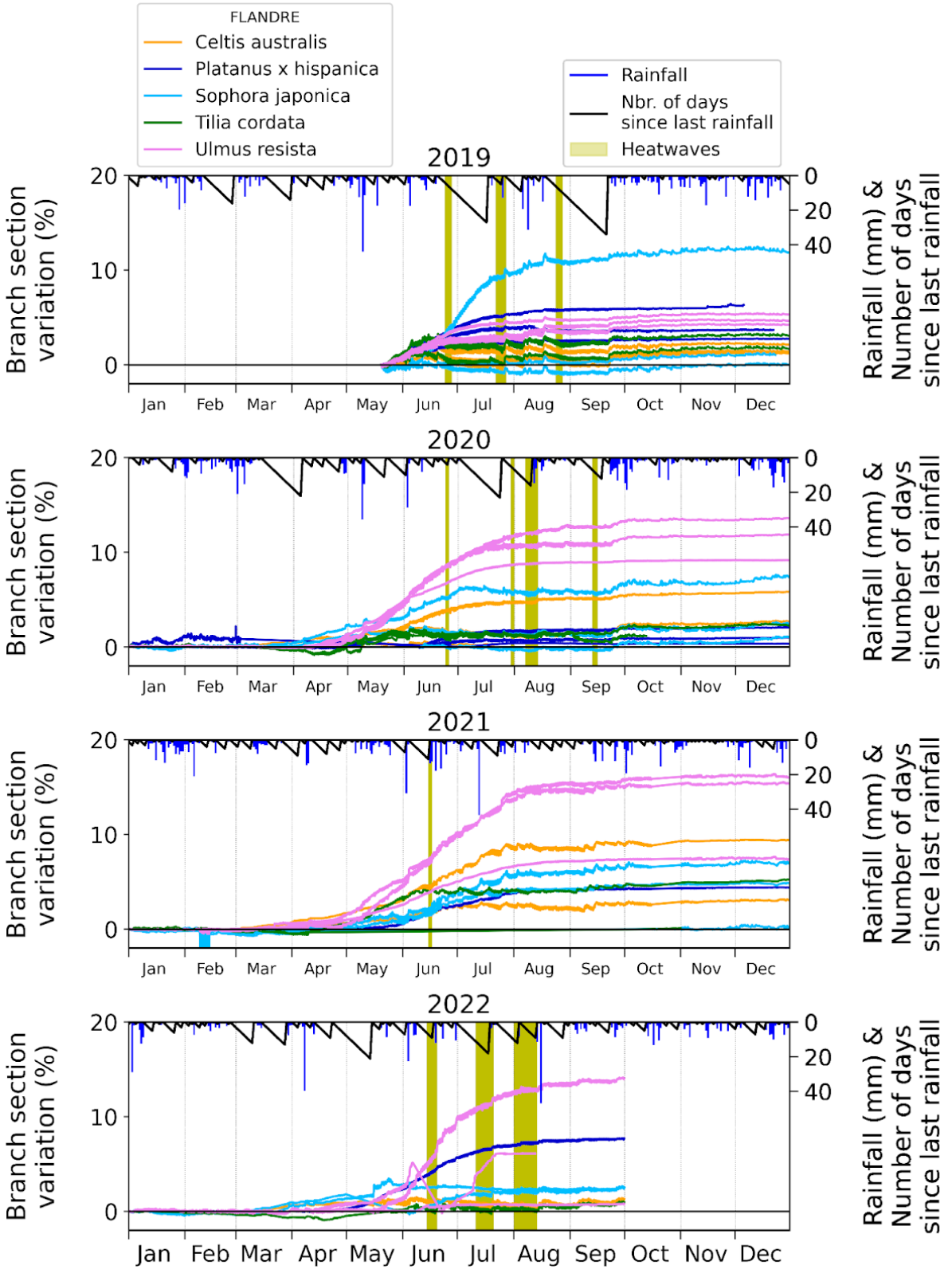

Figure 70: Evolution of the branch section variation on the basis of the initial branch section calculated at the beginning of each year for the trees located in FLANDRE and of the daily rainfall and the daily elapsed number of days since the last rain event from 2019 to 2022. The heatwaves identified by Météo-France are highlighted with yellow areas.

4.2.4. Climatic benefits of the trees

4.2.4.1. General assessment of the variability of the climatic benefits

In the present section, the average daily evolution of AH, T_a, T_{mrt} and UTCI measured and calculated inside the tree crowns and at the reference lamp posts as well as the average daily difference calculated between trees and lamp posts are analyzed for all the studied trees on each studied site (Figure 72, Figure 73, Figure 74, Figure 75 and Figure 76). As explained previously, these average daily evolutions were calculated over multiple days considering a common list of days for each site which induces that the list of studied days may vary a lot between the studied sites. In order to minimize the sources of variability, especially those coming from the ever-changing meteorological conditions, only dry and sunny days (no rainfall and insolation duration greater than 10 hours according measurements carried out by Météo-France at Paris-Montsouris) from May 1st to September 30th were considered for the analysis. Platanus_3, sophora_1 and sophora_2 on FLANDRE and celtis_4 on TEMPLE could not be considered due to their poor data availability. The location of the measurement days considered for the analysis is presented in Figure 71. Two days were finally considered for FLANDRE, 13 days for NOHAIN, 42 days for ORDENER and 6 for TEMPLE and 3 for VICTOR.

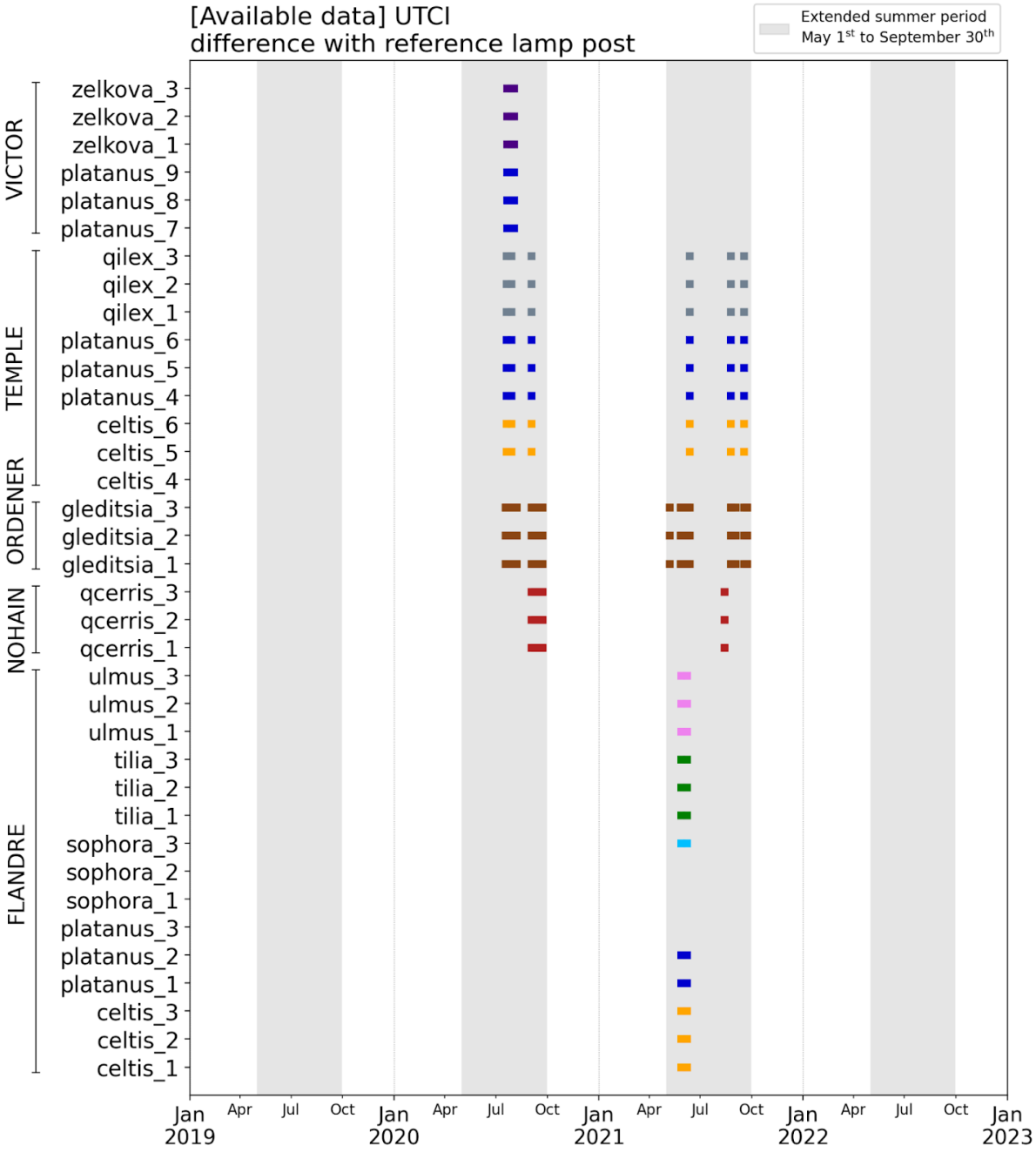

Figure 71: Location of the days with UTCI data available for all the studied trees from 2019 to 2022 when considering for each site only the days with data available for all the trees of this given site.

AH measured inside the tree crowns remained generally very close to the one measured at the reference lamp posts during night-time in all sites. However, different evolutions were observed during daytime. In FLANDRE and TEMPLE, the AH difference was alternatively lower and higher inside the tree crowns compared to the reference lamp posts depending on the considered trees. In NOHAIN, ORDENER and VICTOR, AH increased during daytime and

was generally 5 % and up to 10 % higher inside the tree crowns compared to the reference lamp posts which could be attributed to the transpiration of the trees.

T_a was also very close at night inside the tree crowns and at the reference lamp posts. During daytime, the difference was sometimes positive meaning that T_a measured inside the tree crowns was higher than at the reference lamp posts. This phenomenon was observed in all sites: in the morning for the *Platanus x hispanica* in FLANDRE, around noon in NOHAIN, ORDENER and VICTOR, and in the afternoon for the *Platanus x hispanica* of TEMPLE. It also appeared the T_a was lower inside the tree crowns compared to the reference lamp posts at different times of the days depending on the considered sites. T_a was lower by on average 2 °C around 16:00 in FLANDRE and 2 °C in the morning, mainly around 08:00 UTC in TEMPLE. Lower T_a reductions were reported on the three other sites and especially for the *Gleditsia triacanthos* of ORDENER which experienced a generally higher Ta than their reference lamp post.

The effect of trees on T_{mrt} was easily noticeable in all the studied sites. T_{mrt} was slightly higher at night inside the tree crowns compared to the reference lamp posts especially in FLANDRE, NOHAIN and ORDENER. A very strong increase of T_{mrt} can be noticed at each lamp post in the morning followed by a very strong decrease in the late afternoon. The exact times of such increases and decreases vary with the considered lamp post and reflect the respective exposure to sunlight of the different lamp posts. CANDFlandre2 and CANDOrdener then appeared to be mainly exposed to sunlight in the afternoon while CANDTemple was mainly insolated before noon and NOHAIN and VICTOR were homogeneously exposed to sunlight over daytime. Noticeable and very strong negative T_{mrt} differences were noticed for all the studied trees, highlighting the strong radiation interception provided by the tree crowns. T_{mrt} is sensitive to both LW and SW and as SW has a much higher energy content, it is therefore more likely to influence T_{mrt}. The maximum T_{mrt} reduction exceeded on average 20 °C for almost all trees in FLANDRE and TEMPLE, it approached 20 °C in VICTOR and was generally between 10 °C and 15 °C in NOHAIN and ORDENER. Strong and quick T_{mrt} variations were noticed from one time step to the next for most of the trees which obviously induced strong variations of the T_{mrt} difference with the lamp posts. Such variations are very likely to be caused by the heterogeneities of the tree crowns which induce temporarily direct solar exposure of the globe thermometers mounted inside the tree crowns. In this way, the respective positions of the trees and lamp posts may also lead to T_{mrt} being higher inside the tree crowns even when the lamp posts are not yet directly insolated. It can sometimes lead to a positive T_{mrt} difference exceeding +5 °C (see for instance the *Platanus x hispanica* of FLANDRE).

The daily evolution of UTCI is highly influenced by the daily evolution of T_a and T_{mrt}, which are both involved in its calculation. Just like T_{mrt}, UTCI was slightly higher at night inside the tree crowns compared to the reference lamp posts, especially in FLANDRE, NOHAIN and ORDENER, and was characterized to a lesser extent by strong increases and decreases induced by the direct insolation of the globe thermometers. Noticeable negative differences were reported for all the studied trees reaching almost 10 °C in FLANDRE and TEMPLE and on average 5 °C in the three other sites. A strong variability of the UTCI difference was noticed during the day and appears to be very similar to the one reported hereinabove concerning T_{mrt}.

Wind speed, which is not presented here, was strongly reduced inside the tree crowns. Due to the relatively high trigger point of the cup anemometers (5 $km.h^{-1}$), the low wind speeds could not be accurately reported and were often considered null in the data set. To comply with the UTCI calculation method, null wind speeds were considered equal to 0.5 $m.s^{-1}$ at all times. Otherwise, too many time steps would have been lost.

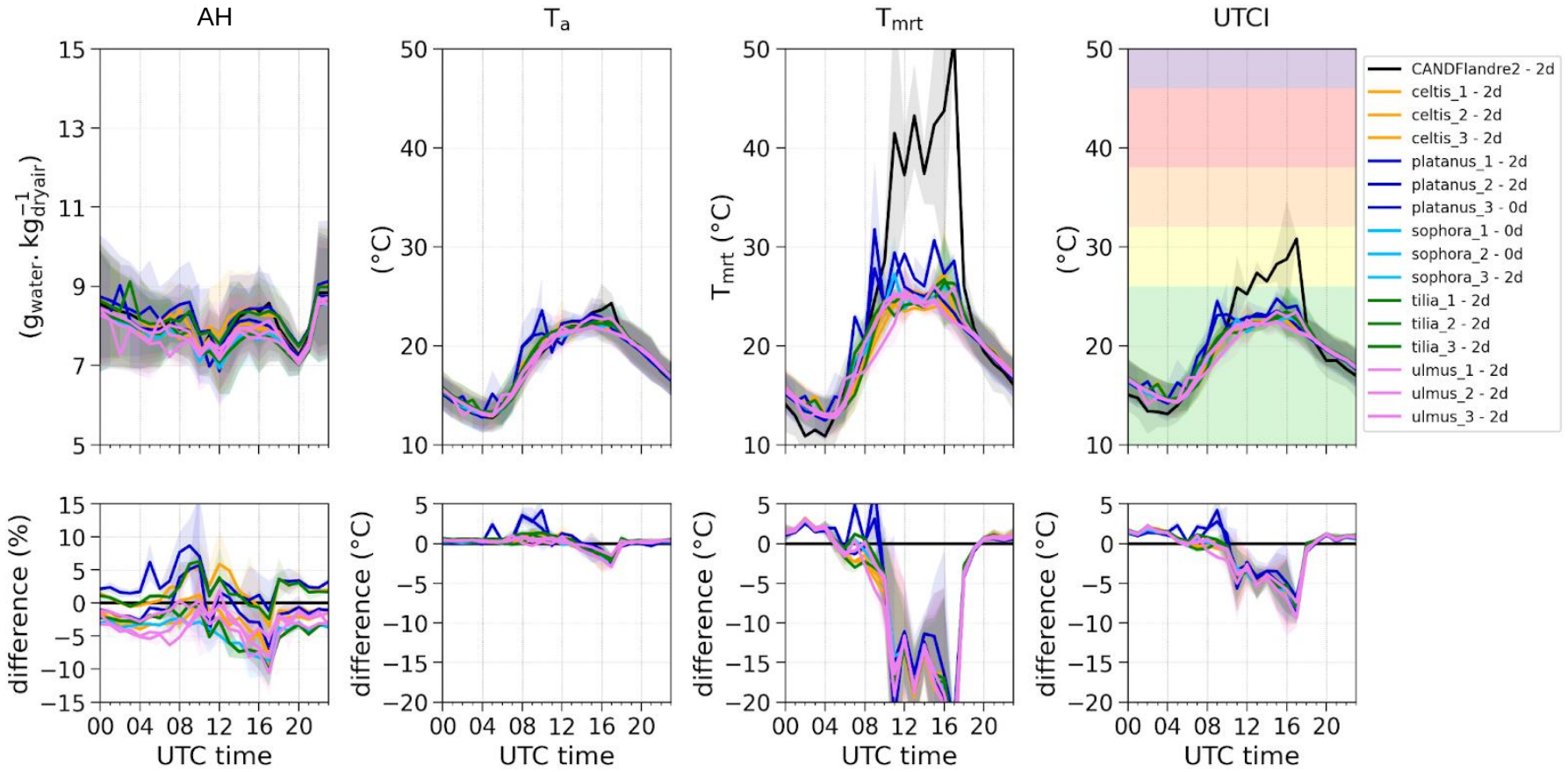

Figure 72: Average daily evolution of the absolute humidity (AH), air temperature (T_a), mean radiant temperature (T_{mrt}) and UTCI measured in the crown of each studied tree of FLANDRE and at the reference lamp post CANDFlandre2 as well as the difference [tree - lamp post] for the four variables. The number of days considered for each tree is reported in the caption next to the labels of the trees. The light colored halo drawn behind each average line represents the standard deviation. The number of studied days is equal for all trees within each site except for the trees withdrawn from the analysis because of too poor data availability (0 days).

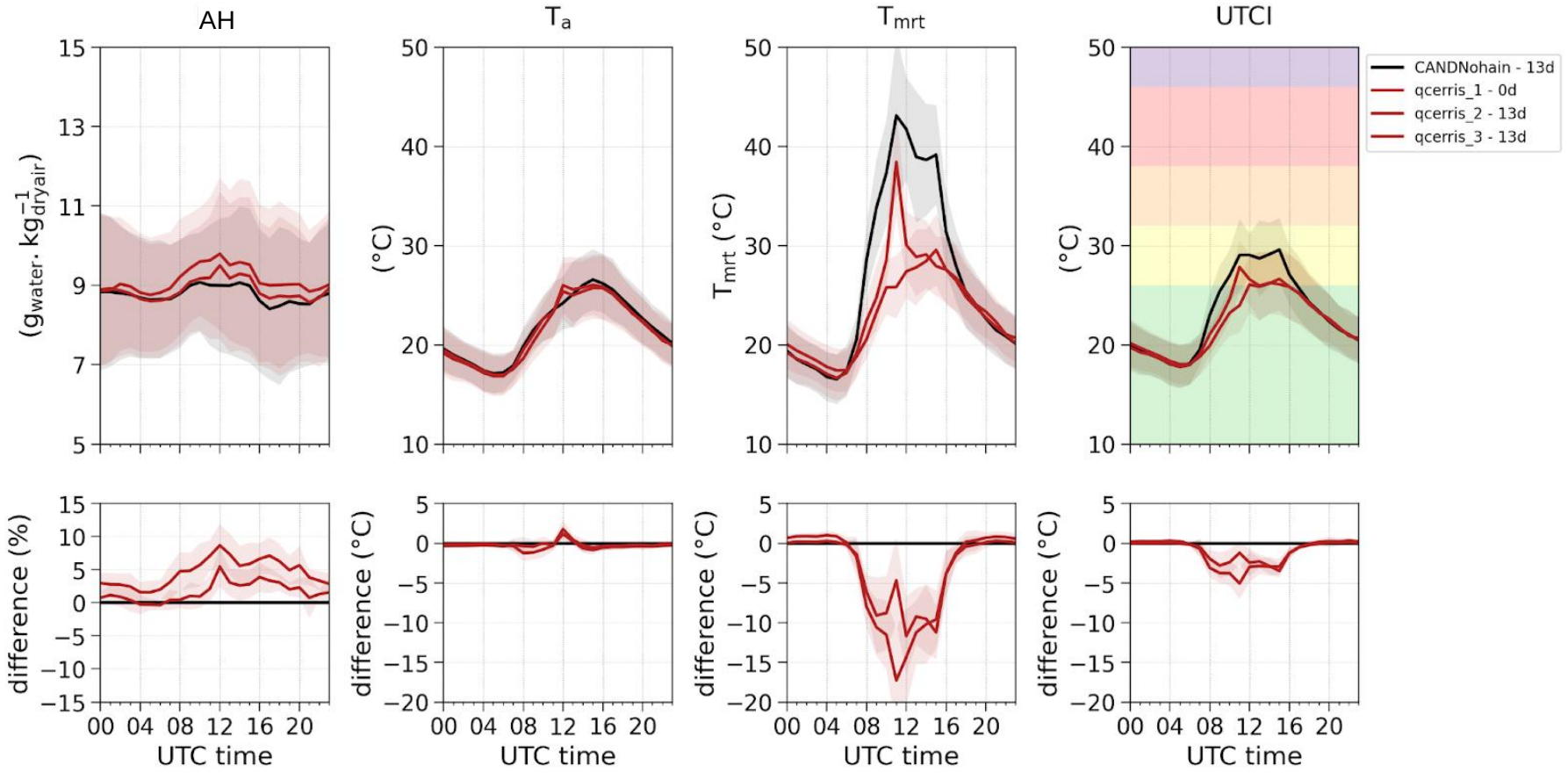

Figure 73: Average daily evolution of the absolute humidity (AH), air temperature (T_a), mean radiant temperature (T_{mrt}) and UTCI measured in the crown of each studied tree of NOHAIN and at the reference lamp post CANDNohain as well as the difference [tree - lamp post] for the four variables. The number of days considered for each tree is reported in the caption next to the labels of the trees. The light colored halo drawn behind each average line represents the standard deviation. The number of studied days is equal for all trees within each site except for the trees withdrawn from the analysis because of too poor data availability (0 days).

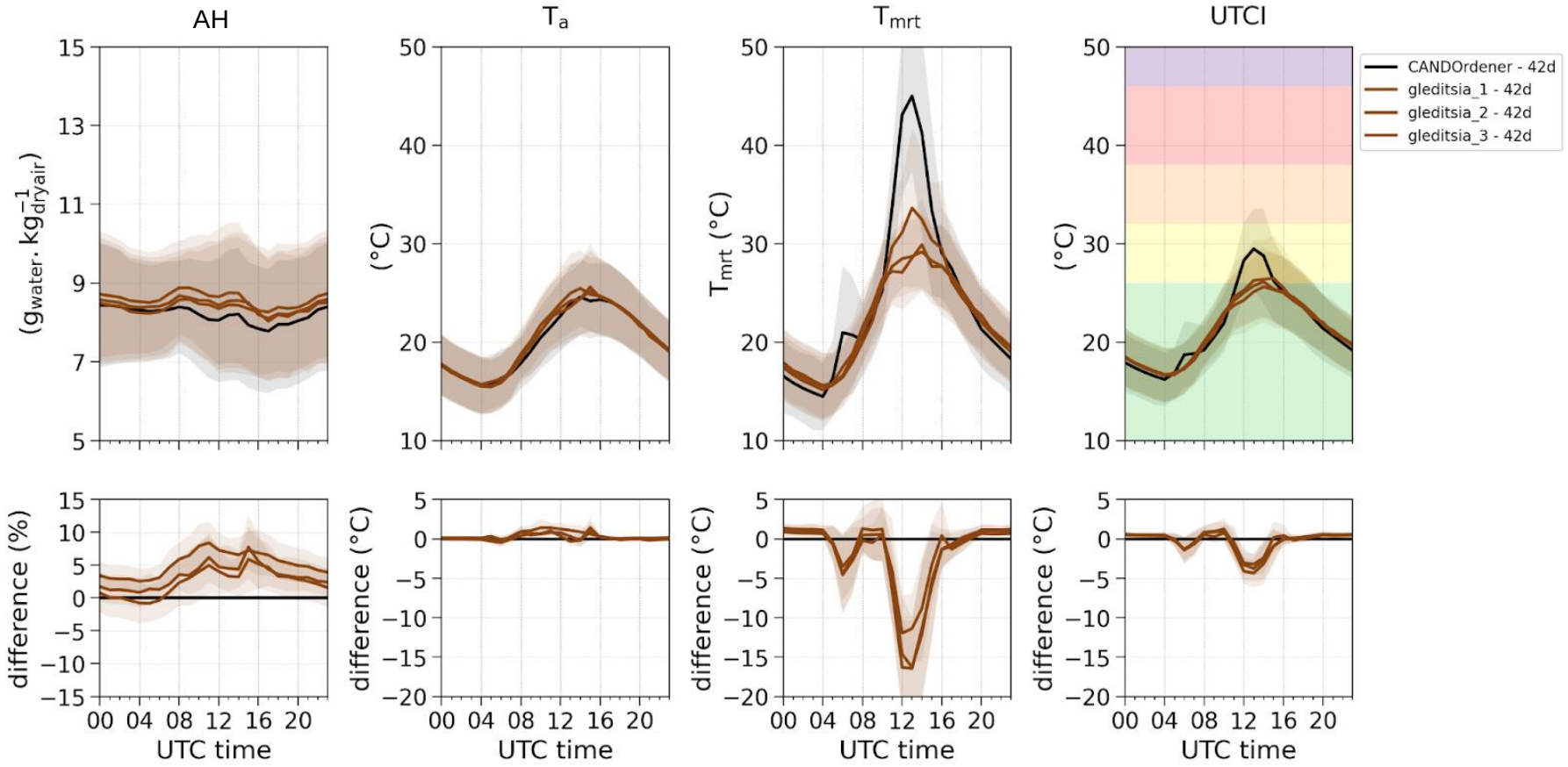

Figure 74: Average daily evolution of the absolute humidity (AH), air temperature (T_a), mean radiant temperature (T_{mrt}) and UTCI measured in the crown of each studied tree of ORDENER and at the reference lamp post CANDOrdener as well as the difference [tree - lamp post] for the four variables. The number of days considered for each tree is reported in the caption next to the labels of the trees. The light colored halo drawn behind each average line represents the standard deviation. The number of studied days is equal for all trees within each site except for the trees withdrawn from the analysis because of too poor data availability (0 days).

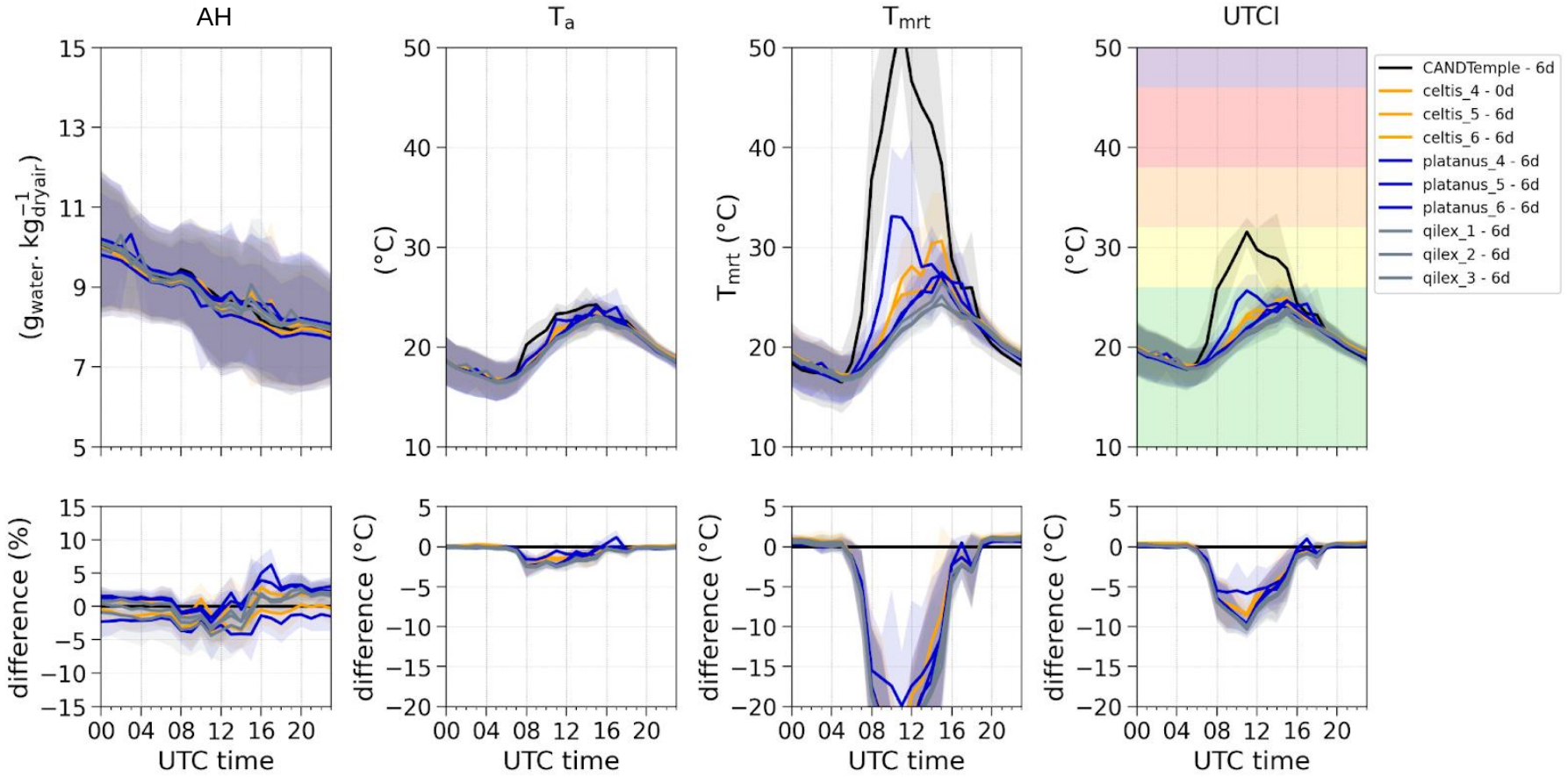

Figure 75: Average daily evolution of the absolute humidity (AH), air temperature (T_a), mean radiant temperature (T_{mrt}) and UTCI measured in the crown of each studied tree of VICTOR and at the reference lamp post CANDTemple as well as the difference [tree - lamp post] for the four variables. The number of days considered for each tree is reported in the caption next to the labels of the trees. The light colored halo drawn behind each average line represents the standard deviation. The number of studied days is equal for all trees within each site except for the trees withdrawn from the analysis because of too poor data availability (0 days).

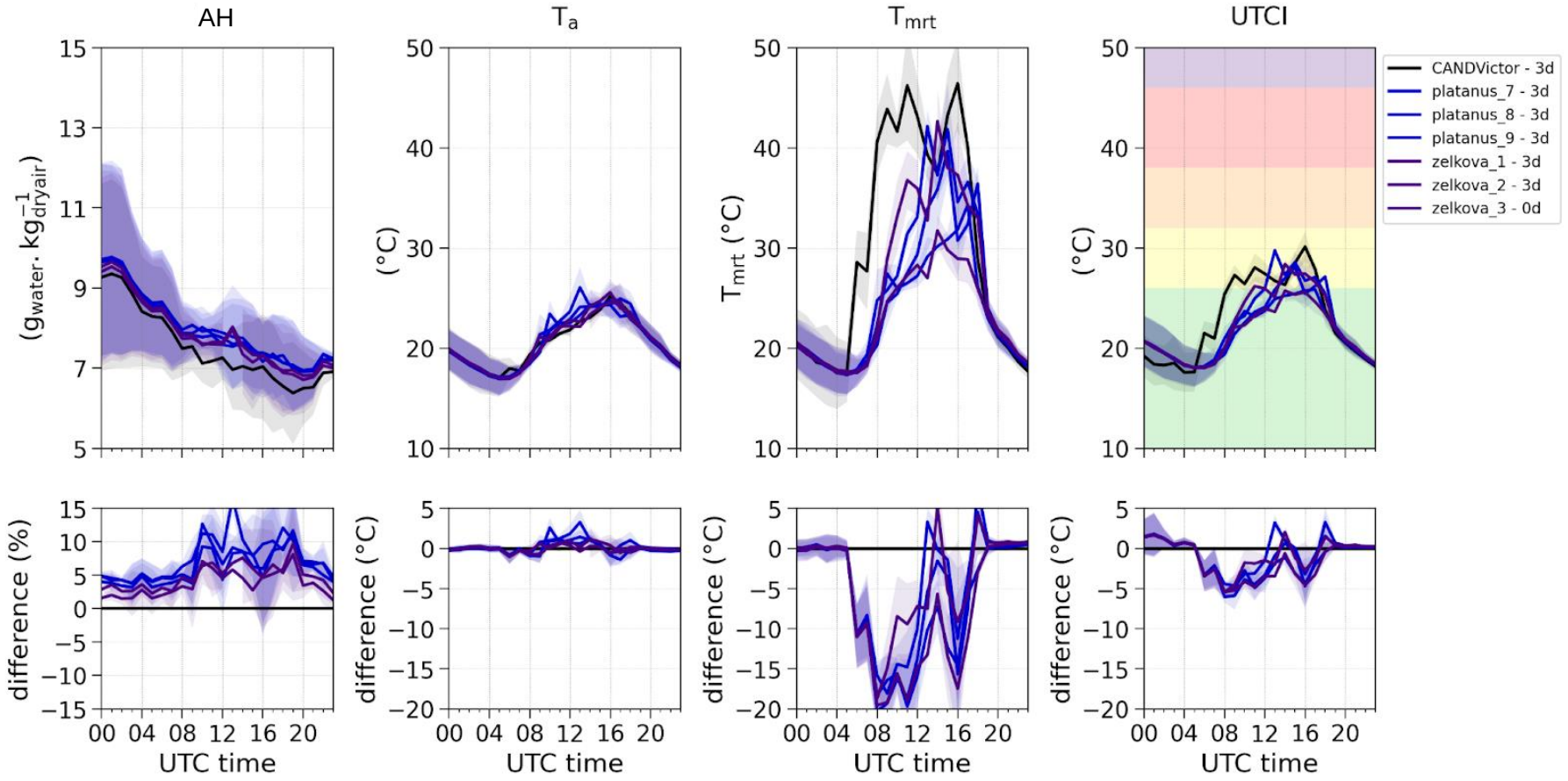

Figure 76: Average daily evolution of the absolute humidity (AH), air temperature (T_a), mean radiant temperature (T_{mrt}) and UTCI measured in the crown of each studied tree of VICTOR and at the reference lamp post CANDVictor as well as the difference [tree - lamp post] for the four variables. The number of days considered for each tree is reported in the caption next to the labels of the trees. The light colored halo drawn behind each average line represents the standard deviation. The number of studied days is equal for all trees within each site except for the trees withdrawn from the analysis because of too poor data availability (0 days).

The influence of the trees on the studied variables appears to be highly variable over a single day as well as depending on the considered site. In order to provide a simple comparison of the effects of the different studied trees, the differences calculated for each variable between the measurements carried out inside the tree crowns and at the lamp posts were averaged over a few periods of interest scattered over the day as explained in section 4.1.3.4. Figure 77 and Figure 78 present these average differences for the 36 studied trees respectively for T_a and UTCI.

When averaged over the entire day, the T_a difference is very low and can even be slightly positive. Only the trees located in TEMPLE provided noticeable negative ΔT_a over the entire day (ranging from -0.4 °C for celtis_5 to -0.9 °C for qilex_2) meaning that their influence on T_a was quite homogeneous over daytime. The three *Quercus ilex* provided on average the most important T_a reductions (from 0.8 to 0.9 °C Ta reduction). Regarding UTCI, the difference was negative for all trees when averaged over the entire days with contrasts between the studied sites as this difference was on average -0.3 °C for the three *Gleditsia triacanthos* of ORDENER while it ranged from -1.9 °C to -2.8 °C UTCI for the trees of TEMPLE, the three *Quercus ilex* providing the most important UTCI reduction compared to the reference lamp post.

At night (from 02:00 to 04:00 UTC), ΔT_a ranged from -0.3 °C to 0.3 °C for all sites except FLANDRE where it could reach 0.6 °C for two *Tilia cordata*. The ΔUTCI ranged from -0.3 °C to 0.5 °C in NOHAIN, ORDENER and TEMPLE but it reached on average 0.8 °C for all the trees located in VICTOR and 1.4 °C for the trees of FLANDRE.

During the day, it can easily be noticed that the evolution of both ΔT_a and ΔUTCI depends on the considered site as explained previously. Indeed, the trees of FLANDRE for instance were characterized by more important T_a and UTCI reductions around 16:00 than around noon while an opposite observation can be made for the trees of TEMPLE.

Around noon (from 11:00 to 13:00 UTC), only the trees located in TEMPLE had a negative ΔT_a meaning that at that moment, T_a was higher inside the tree crowns compared to the reference lamp posts for all other trees. In TEMPLE, T_a differences ranged from -0.9 °C to -2.2 °C and the three *Quercus ilex* provided at least a 2 °C Ta reduction. At this time, the UTCI differences were quite homogeneous for all the trees located in FLANDRE and reached on average -3.9 °C UTCI. More heterogeneous UTCI differences were observed on the other sites, especially in NOHAIN, ORDENER and VICTOR where they ranged from -1.1 °C to -4 °C UTCI with important contrasts among trees of the same species. The strongest UTCI reductions around noon were observed in TEMPLE with at least 5.5 °C and up to 8.5 °C UTCI reduction.

UTCI was reduced by at least 8.1 °C inside the tree crowns of the three *Quercus ilex* around noon.

In the afternoon (from 15:00 to 17:00 UTC), ΔT_a ranged from -0.8 °C to 0.5 °C in all sites except FLANDRE where they ranged from -1 to -2.1 °C, celtis_2, ulmus_2 and ulmus_3 providing the most important T_a reductions. At this time, the most important UTCI reductions were also observed in FLANDRE as UTCI differences ranged from -5.1 °C to -7.3 °C. In all other sites, the UTCI differences ranged from -3.7 °C to +0.1°C with differences close to zero for the three *Gleditsia triacanthos*.

The 36 studied trees were also compared through the respective average of their daily maximum ΔT_a and ΔUTCI. It is however important to remember that the maximum T_a (or UTCI) reduction can occur at a different time every day for a given tree. The resulting average is therefore likely to be different from the maximum differences that can be read in figures Figure 72 to Figure 76 which were built by averaging for each hour of the day the ΔT_a and ΔUTCI differences at this very moment.

Very similar trends were observed for both T_a and UTCI. The trees located in FLANDRE and TEMPLE provided the greatest T_a and UTCI reductions compared to their reference lamp posts. The reductions ranged from 1.9 °C to 3.2 °C for T_a and from 7.8 to 10.7 °C considering the trees of these two sites. In VICTOR, the studied *Platanus x hispanica* and *Zelkova serrata* provided T_a and UTCI reduction ranging respectively from 1.6 °C to 1.8 °C and 5.4 °C to 6.8 °C. The reductions provided by the *Quercus cerris* of NOHAIN and the *Gleditsia tricanthos* of ORDENER were generally lower as they ranged from 0.6 to 1.8 °C for T_a and 4.2 to 5.5 °C for UTCI.

This overview of the T_a and UTCI reduction provided by the 36 studied trees suggests that there is a strong influence of the considered site. Indeed, trees of the same species located on different sites can provide very contrasted results. The site appears to impact both the daily evolution of the T_a and UTCI reductions and the average maximum reductions. Indeed, the *Platanus x hispanica* of VICTOR were on average less efficient than those of TEMPLE and FLANDRE to reduce both T_a and UTCI. Regarding the *Celtis australis* of FLANDRE and TEMPLE, all of them provided close average maximum reduction of T_a from 2.7 °C to 3 °C. Yet, the influence of the site is likely to be induced by the different locations of the trees and lamp posts in the studied sites.

A noticeable variability may exist among the three trees of a same species and also for a given tree among the different studied days as pointed out by the standard deviation displayed

in figures Figure 77 and Figure 78. Both sources of variability will be explored in the following sections.

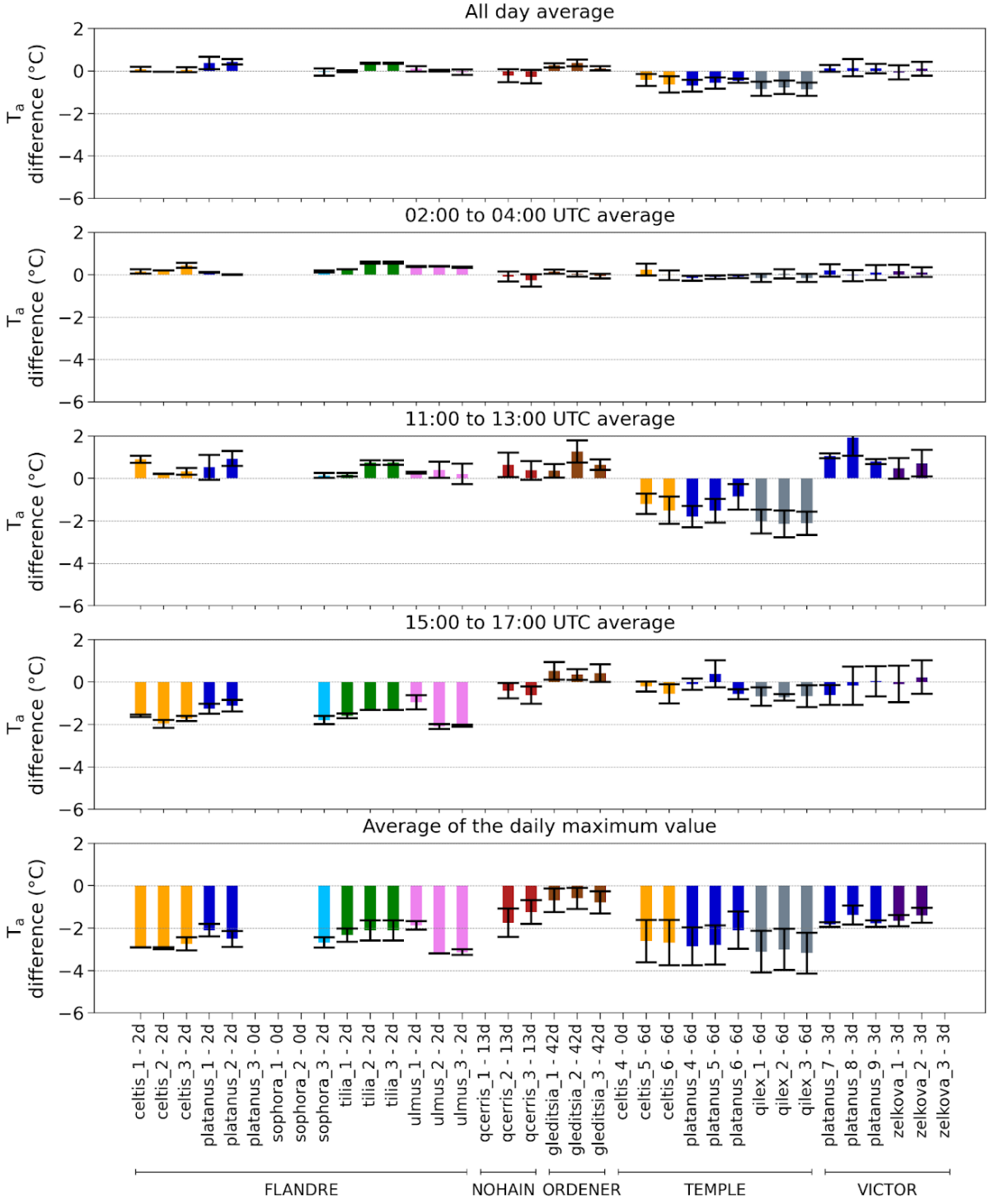

Figure 77: Average T_a difference [tree - lamp post] calculated for each tree compared to its reference lamp post for different periods of the day. The number of days considered for each tree is reported next to the labels of the trees. The number is equal for all trees within each site except for the trees withdrawn from the analysis (0 days).

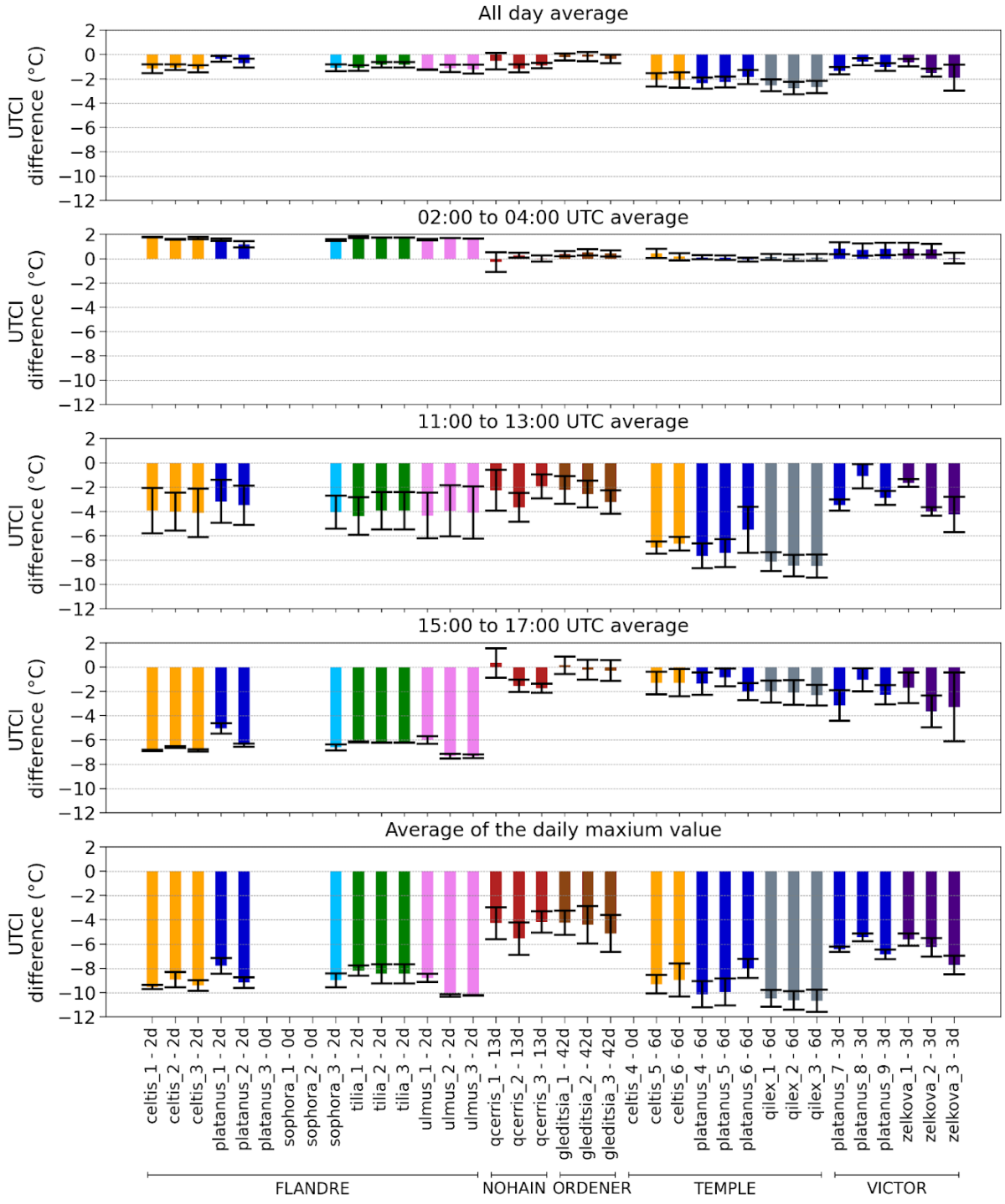

Figure 78: Average UTCI difference [tree - lamp post] calculated for each tree compared to its reference lamp post for different periods of the day. The number of days considered for each tree is reported next to the labels of the trees. The number is equal for all trees within each site except for the trees withdrawn from the analysis (0 days).

4.2.4.2. Influence of the meteorological conditions

It was shown in the last section that the climatic benefits provided by street trees may be subject to a noticeable daily variability. At the same time, the influence of solar exposure was highlighted especially on the ΔT_{mrt} and ΔUTCI measured between the tree crowns and the reference lamp posts. The present section therefore uses PCA to investigate the influence of the meteorological conditions on the climatic benefits provided by the trees. This analysis focused independently on each one of the 36 studied trees and on a wide panel of days located from May 1st to September 30th of each studied year (2019 to 2022). Unlike what was presented in the previous section, the selected days were not supposed to be common for all the trees located on the same site, which means that this analysis was run on a different list of days for each tree. For each tree, the daily maximum T_a and UTCI differences between each tree and its reference lamp post were calculated and compared to the meteorological variables measured by Météo-France at Paris-Montsouris at a daily time step. Figure 79 presents for each tree the location of the days that were used for the PCA.

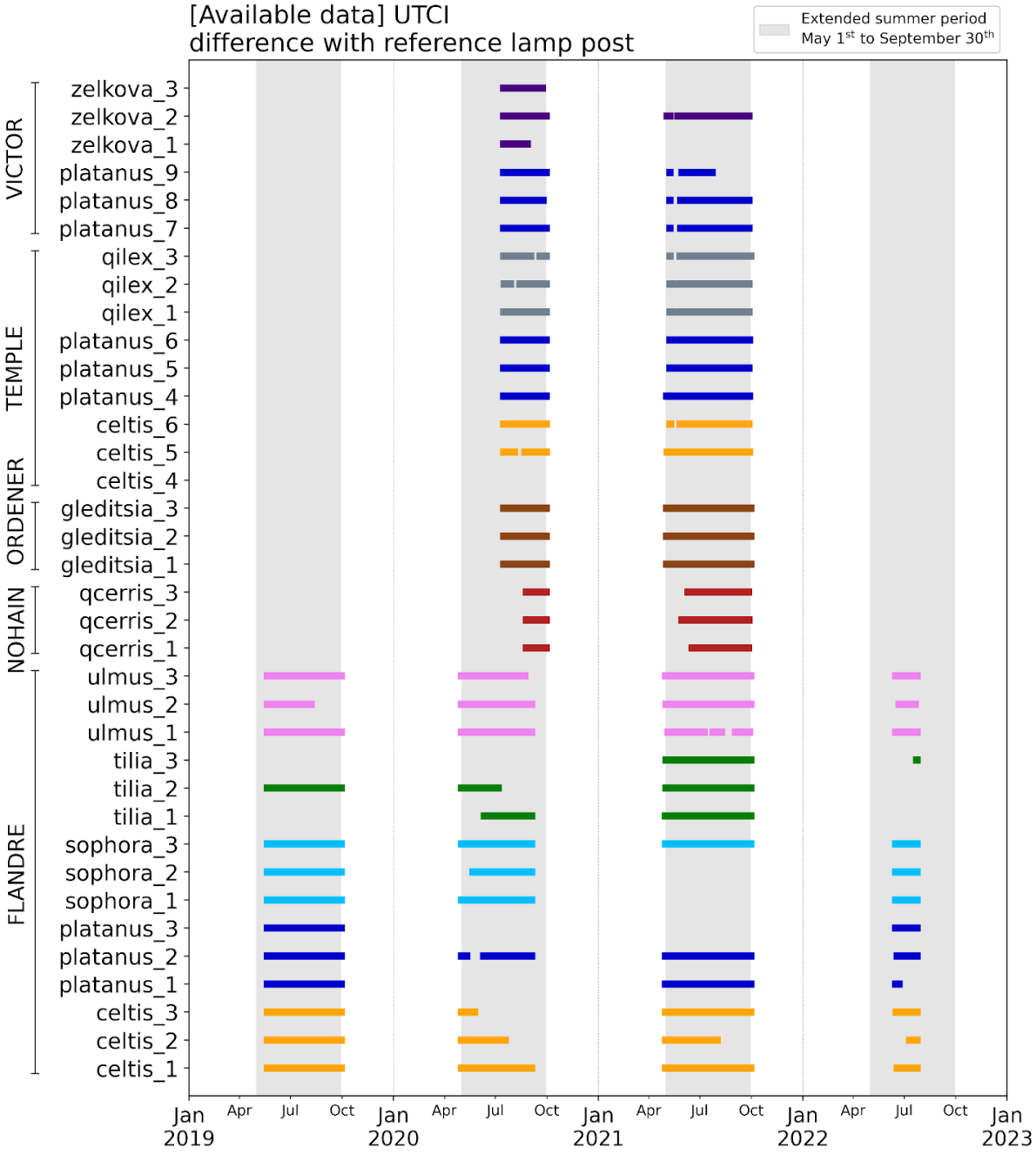

Figure 79: For each tree, location of the days with UTCI data available from May 1st to September 30th from 2019 to 2022.

The correlation circles obtained for celtis_1 (FLANDRE) and qcerris_2 (NOHAIN) are presented as an example in Figure 80, especially to highlight the contrasted results that were obtained for different studied trees. On the one hand, a relation is likely to exist between both the ΔT_a and ΔUTCI and the daily insolation for celtis_1 (Figure 80a). On the other hand, insolation seems to be less suitable to explain the variability of ΔUTCI when focusing on qcerris_2 and it does not seem to explain the variability of ΔT_a at all (Figure 80b).

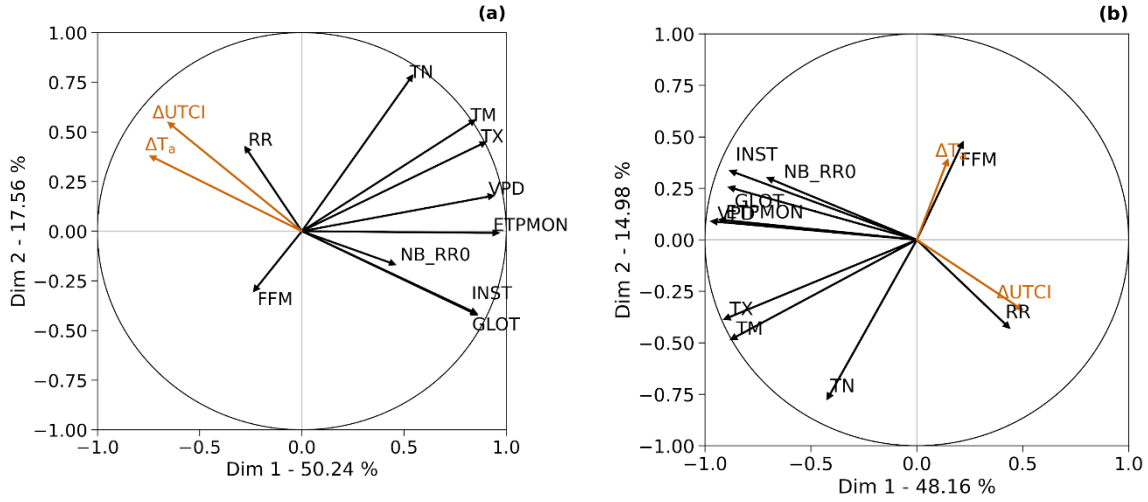

Figure 80: Correlation circle of the climatic benefits provided by (a) celtis_1 during 429 days and (b) qcerris_2 during 118 days located from May 1st to September 30th from 2019 to 2022. ΔT_a and ΔUTCI (orange arrows) are respectively the daily maximum air temperature and UTCI difference [tree - lamp post]. All other variables (black arrows) were measured at Paris-Montsouris at a daily time step: RR = rainfall, NB_RR0 = number of elapsed days since the last rainfall event, TN, TM and TX = minimum, mean and maximum air temperature, VPD = vapor pressure deficit, ETPMON = reference evapotranspiration (Penman-Monteith method), INST = insolation duration, GLOT = integral of incoming global radiation, FFM = mean wind speed.

The contrasted influences of insolation for celtis_1 and qcerris_2 are illustrated in Figure 81 which presents their respective ΔUTCI as a function of GLOT. Celtis_1 and qcerris_2 were characterized by contrasted ΔUTCI as it could reach -14 °C for celtis_1 whereas it remains higher than -10 °C for qcerris_2 but ΔUTCI appeared to decrease with the increasing GLOT in both cases (Figure 81). Although GLOT only explains half of the variability of ΔUTCI for celtis_1 (R^2 = 0.47), it did not seem to be a good predictor at all for qcerris_2 (R^2 = 0.17).

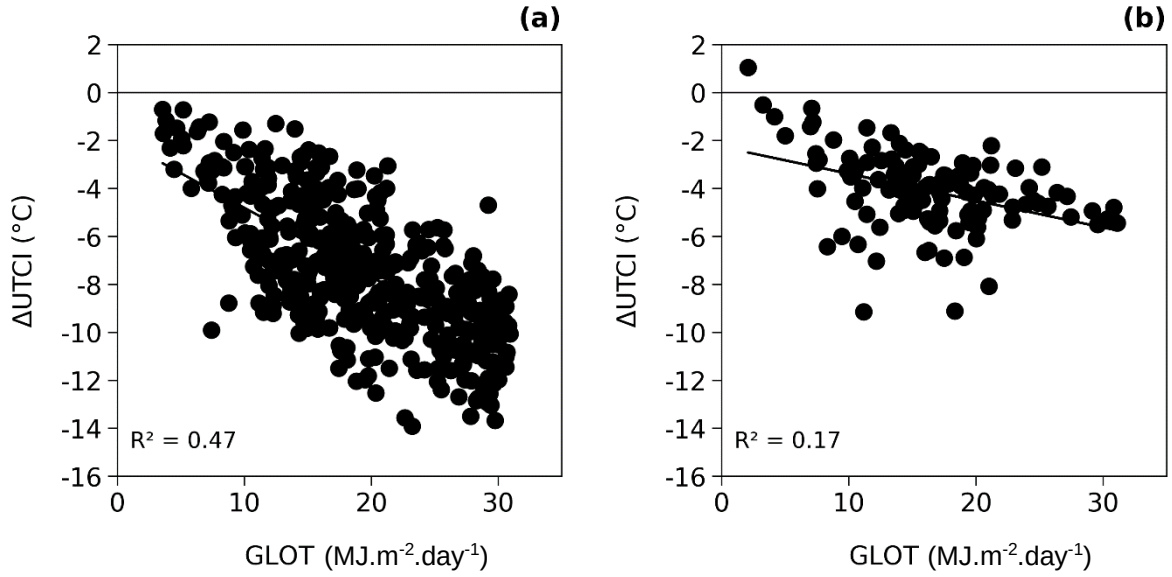

Figure 81: Daily UTCI difference (ΔUTCI) [tree - lamp post] as a function of the daily integral of the incident global radiation (GLOT) for (a) celtis_1 (FLANDRE) during 429 days and (b) qcerris_2 (NOHAIN) during 118 days located from May 1st to September 30th from 2019 to 2022.

In order to summarize the PCA results for the 36 studied trees, the correlation coefficients calculated between ΔT_a and GLOT as well as between ΔUTCI and GLOT are displayed for each tree in Figure 82. ΔUTCI appears to be more related to GLOT than T_a for almost all trees except the trees located in VICTOR. Also, the correlation coefficient between ΔUTCI and GLOT is quite homogeneous (it ranges from -0.61 to -0.76) in FLANDRE and TEMPLE and closer to -1 than in the three other sites. When considering NOHAIN, ORDENER and VICTOR, the correlation coefficient between ΔUTCI and GLO is higher than -0.56 for all the trees and even higher than -0.4 for most of the trees located in those three sites. This important contrast recalls the results of average ΔT_a and ΔUTCI presented in the previous section.

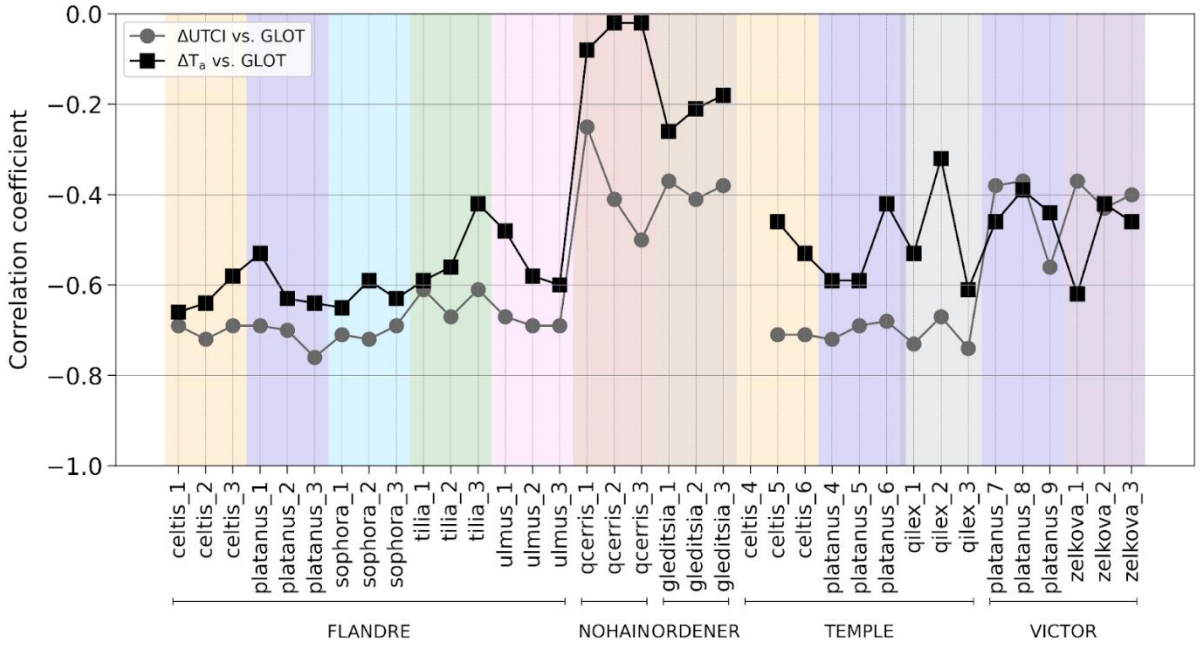

Figure 82: For each tree, correlation coefficient between the daily air temperature difference (ΔT_a, tree - lamp post) and daily UTCI difference (ΔUTCI, tree - lamp post) with the daily integral of the incident global radiation (GLOT) for days located from May 1st to September 30th from 2019 to 2022.

4.2.4.3. Influence of tree morphology

It was highlighted in the previous sections that although the influence of radiation interception on T_a is low, UTCI is strongly reduced inside the tree crowns, especially during the sunny days. Yet, radiation interception is likely to be influenced by the morphological characteristics of the considered trees. In order to investigate the eventual existing relationships, the present section focuses on the influence of the morphological parameters of the trees, presented previously in section 4.2.1 and on T_{mrt} which is the most suitable variable available to report the radiation fluxes due to its strong dependence on globe temperature.

The average daily evolution of T_{mrt} measured inside the tree crowns and at the reference lamp posts was therefore calculated during 18 sunny (more than 10 hours of insolation measured at Paris-Montsouris) and rain-free days of August and September 2022 (i.e. close to the LiDAR scanning campaign which took place at the end of August 2022). The morphological parameters calculated on the basis of the LiDAR scans were then considered to be representative of the foliage of the trees during these two months. However, only the trees located in FLANDRE were included in this analysis considering that T_{mrt} was not measured in all the other sites during summer 2022. Only 11 trees out of the 15 ones studied in FLANDRE were included in the analysis due to lacking data on the considered period.

During daytime, all the trees located in FLANDRE provided a strong T_{mrt} reduction from approximately 10:00 to 18:00 UTC (Figure 83). ΔT_{mrt} could then exceed 20 °C but was not constant during daytime. Inside the tree crowns, strong T_{mrt} variations could sometimes be noticed and were attributed to the heterogeneities of the tree crowns which may lead to temporarily exposure of the globe thermometers to direct sunlight.

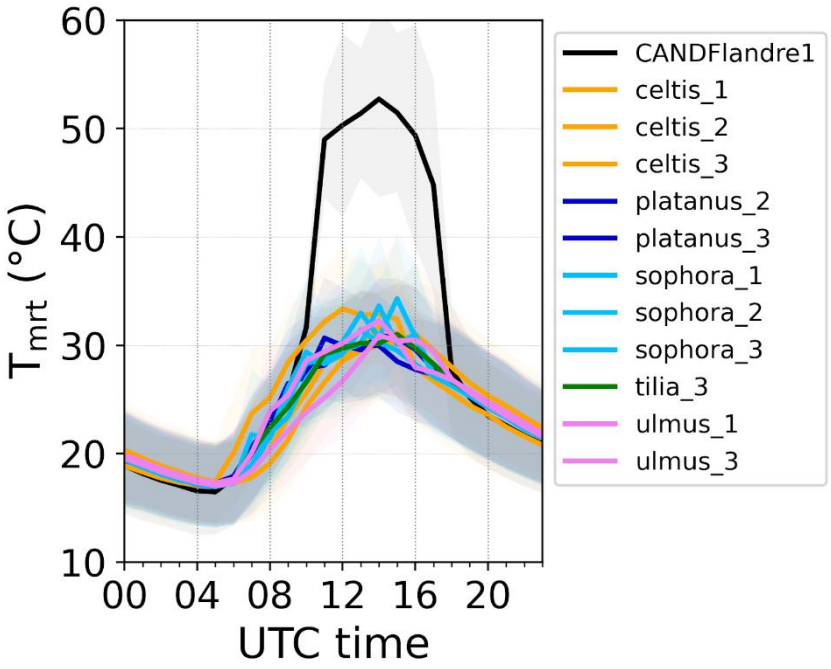

Figure 83: Average daily evolution of the mean radiant temperature (T_{mrt}) calculated in the crown of the studied trees of FLANDRE and at their reference lamp post during 18 sunny (more than 10 hours of insolation) and rain-free days of August and September 2022. The light colored halo drawn behind each average line represented the standard deviation.

T_{mrt} was then averaged around noon in order to be sure that all trees were equally insolated and an average value was calculated over the 18 studied days for each tree of FLANDRE. This average value was compared to the different morphological parameters of the trees through the calculation of a correlation matrix. The correlation coefficients between ΔT_{mrt} and the morphological parameters ranged from -0.2 to +0.22 (Figure 84). They were then very close to 0 meaning that none of the studied morphological parameters was correlated with ΔT_{mrt}.

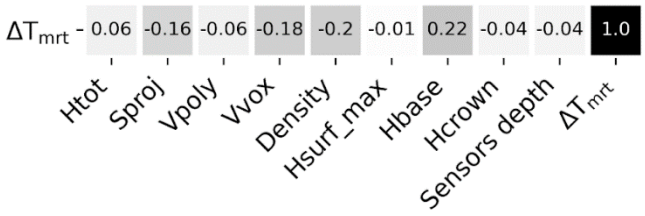

Figure 84: Sample of the correlation matrix established for the trees of FLANDRE including the mean radiant temperature difference (ΔT_{mrt}, tree - lamp post) calculated around noon during 18 sunny (more than 10 hours of insolation) and rain free days of August and September 2022 and the morphological parameters of the studied trees calculated in August 2022 on the basis of LiDAR scans.

As an example, ΔT_{mrt} was graphed as a function of the crown density in Figure 85 as this variable was expected to influence the radiation interception. According to the very low correlation coefficient presented hereinabove between both variables, very contrasted ΔT_{mrt} were measured for trees having close crown density. This parameter, just like the other ones calculated on the basis of the LiDAR scans, therefore cannot explain the variability of ΔT_{mrt} observed among the studied trees.

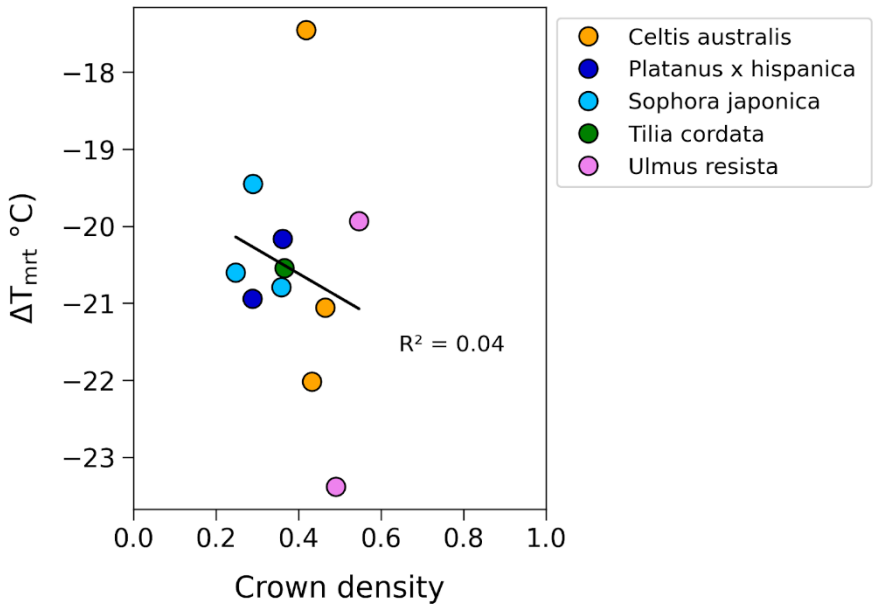

Figure 85: Mean radiant temperature difference (ΔT_{mrt}, tree - lamp post) calculated during 18 sunny (more than 10 hours of insolation) and rain free days of August and September 2022 as a function of the crown density calculated in August 2022 on the basis of LiDAR scans.

4.2.5. Comparison of a dry and a wet summer

The global dynamics of Ψ_{soil} and branch growth over summer 2020 and 2021 are presented for all trees in Figure 86 following the method presented previously in section 4.1.3.5.1. An example of the evolution of Ψ_{soil} over the entire study for celtis_1 can also be found in appendix 7.2.7.

The water potential was generally lower in summer 2020 for most of the trees as this summer was dryer and warmer compared to summer 2021 which is very consistent with the respective climatic conditions of both years. Summer 2021 was indeed much wetter with a high amount of rainfall and a lower ET_{ref} which means that, compared to summer 2020, the tree pits might have received higher amounts of water coming from rainfall while the trees probably uptook less water from the soil as they were exposed to a low evaporative demand (Figure 86).

A strong variability of Ψ_{soil} was observed among the different trees even when considering trees of a same species located on a same site, especially during summer 2020. In 2020, the three *Ulmus resista* were for instance exposed to a Ψ_{soil} lower than -0.25 MPa respectively 0 %, 79 % and 100 % of the time although they were located on the same site (FLANDRE). During summer 2021, most of the trees never experienced a Ψ_{soil} lower than -0.25 MPa.

A very strong variability of growth dynamic was observed for the different trees, even in between trees of the same species. In 2020, the three *Ulmus resista* showed very low interruption of their growth in spite of the very contrasted water availability. The growth of the *Platanus x hispanica* appeared to be slightly related to the water availability as the trees experiencing low water availability were also characterized by a more interrupted growth. Other tree species such as *Quercus cerris, Gleditsia triacanthos* or *Sophora japonica* were all characterized by high rates of growth interruption although some trees of these species experienced a high water availability.

During summer 2021, similar behaviors were observed even though most of the trees were subjected to a Ψ_{soil} higher than -0.25 MPa during the major part of studied period. Especially, the *Ulmus resista* and *Platanus x hispanica* experienced very low interruption of their growth unlike *Sophora japonica*, *Tilia cordata* or *Quercus cerris*.

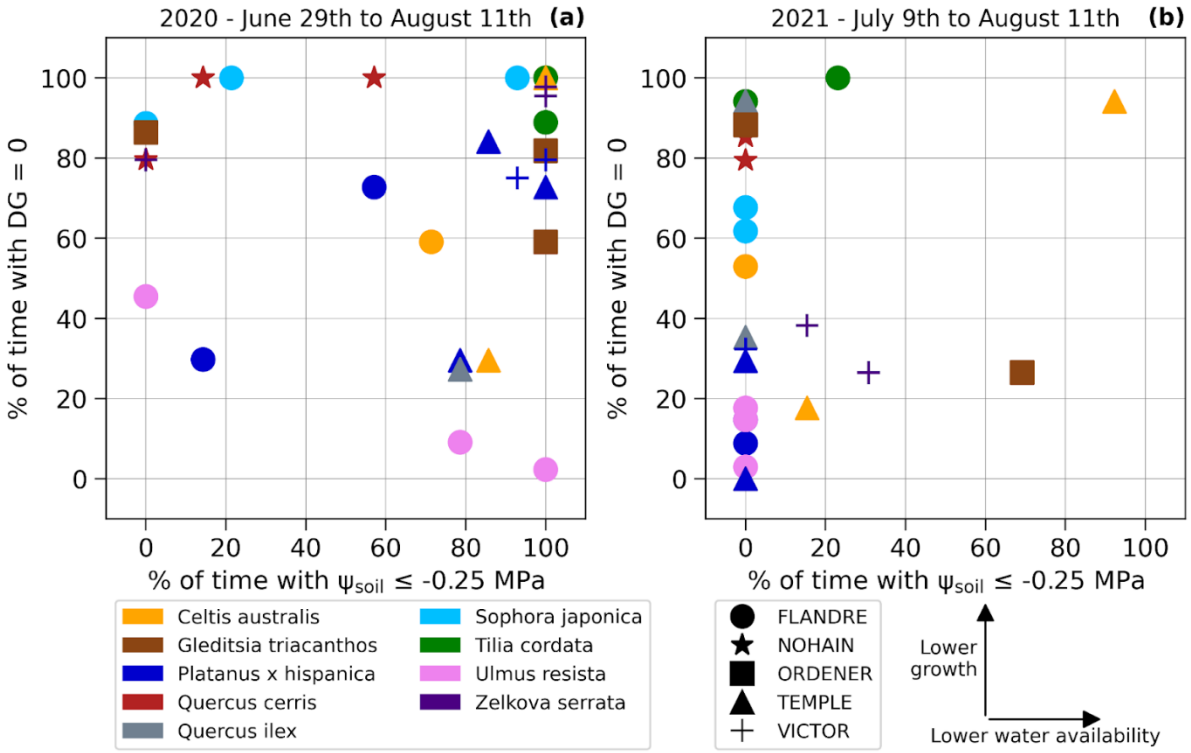

Figure 86: Percentage of time without growth of the studied branches as a function of the percentage of time with soil water potential Ψ_{soil} lower than the measurement range of the probes (-0.25 MPa) for the 36 studied trees during summer 2020 ((a) from June 29th to August 11th) and 2021 ((b) from July 9th to August 11th).

4.2.6. Focus on a dry period

The different indicators calculated for the studied dry period mentioned in section 4.1.3.5.2 (July 1st 2020 to August 10th 2020) are presented in Figure 87. Growth was already stopped for most of the trees on July 1st and remained interrupted during most of the dry period. A few trees among which the *Platanus x hispanica* and *Ulmus resista* of FLANDRE kept growing longer after the start of the dry period: 14 days for platanus_3, 16 days for platanus_1 and from 20 to 35 days for the three *Ulmus resista*. Branch growth remained interrupted during most of the dry period for multiple trees especially for *Sophora Japonica* and *Tilia cordata*, both species being characterized by homogeneous results for their three studied trees. At the end of the dry period, the growth of most of the trees started again quickly as rainfall events were occurring. However, the growth of a few trees, among which the *Sophora japonica* and *Tilia cordata* (except tilia_3) remained interrupted almost until the end of September 2020.

The average ΔT_a and ΔUTCI were characterized by a noticeable standard deviation, especially for the trees located in FLANDRE, although they were calculated considering only groups of two days with close meteorological conditions. For each tree, ΔT_a and ΔUTCI remained quite close at the different stages of the dry period. The eventual differences observed between the different stages of the dry period were close or comparable to the aforementioned daily variability illustrated by the standard deviation of each average.

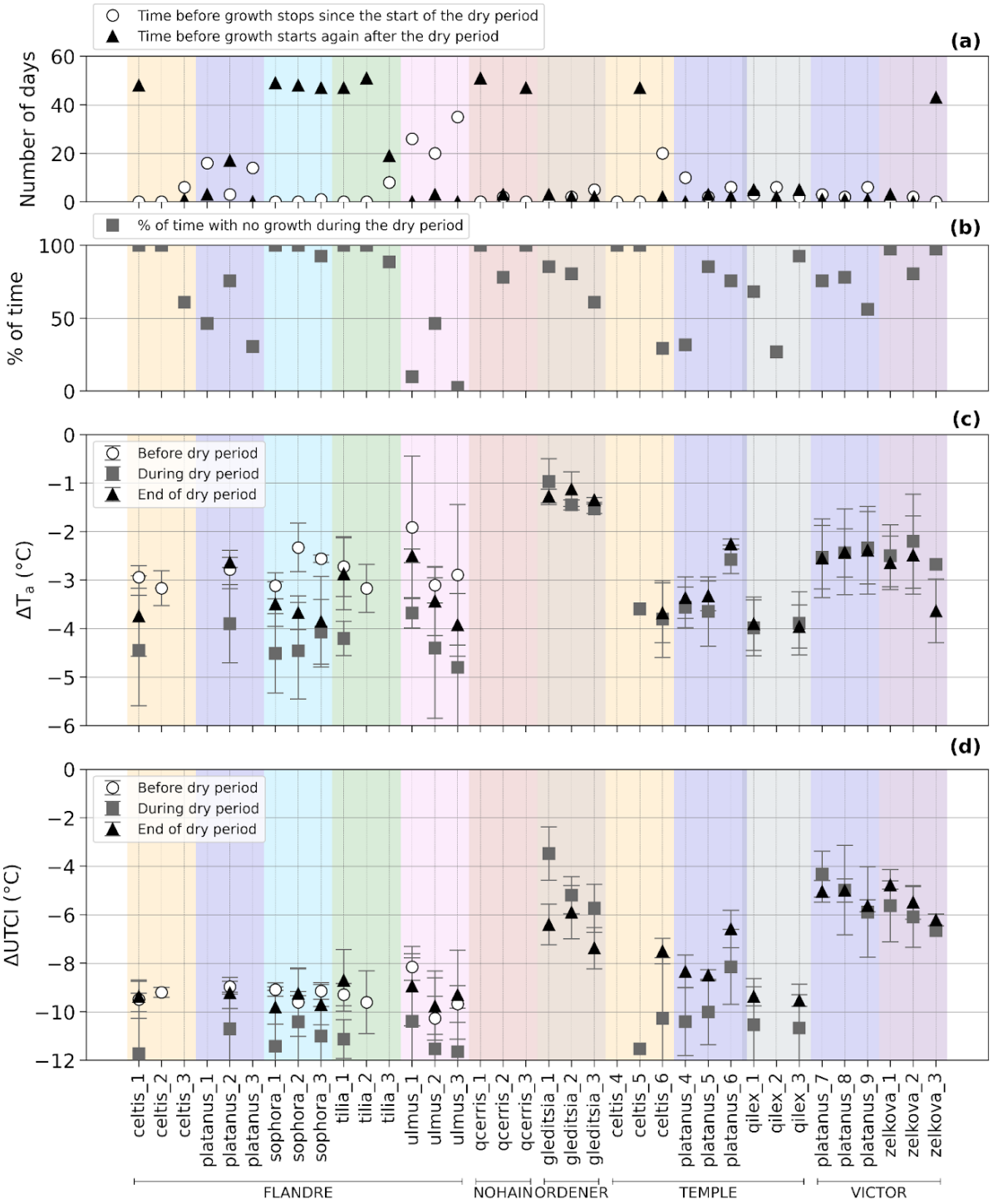

Figure 87: For each tree, (a) number of elapsed days between July 1st 2020 and the interruption of growth and number of elapsed days between August 10th 2020 and the growth restart, (b) percentage of days with growth interrupted between July 1st and August 10th 2020, (c) average maximal air temperature difference (ΔT_a, tree - lamp post) and (d) average maximal UTCI difference (ΔUTCI, tree - lamp post) with their respective standard deviation calculated before (June 24th to 25th), during (July 30th to August 1st) and right at the end (August 5th to August 6th) of the studied dry period.

To go deeper into the analysis, the relationship between ΔT_a and ΔUTCI was investigated focusing on the sunny (more than 10 hours of insolation) and rain-free days of the

dry period. The evolution of ΔT_a and $\Delta UTCI$ as a function of the progress of the dry period is then presented as an example for celtis_1 in Figure 88. Noticeable ΔT_a and $\Delta UTCI$ were measured for celtis_1 and both were characterized by a strong variability all over the studied dry period. Although the T_a and UTCI reductions appeared to be lower when daily integral of incident radiation measured at Paris-Montsouris (GLOT) was lower than 25 $MJ.m^{-2}$, the influence of the daily insolation is not clear when GLOT exceeds 25 $MJ.m^{-2}$. Also, strong ΔT_a and $\Delta UTCI$ were reported even at the end of the dry period. Finally, there is no simple linear relation that could relate ΔT_a or $\Delta UTCI$ and the progress of the dry period.

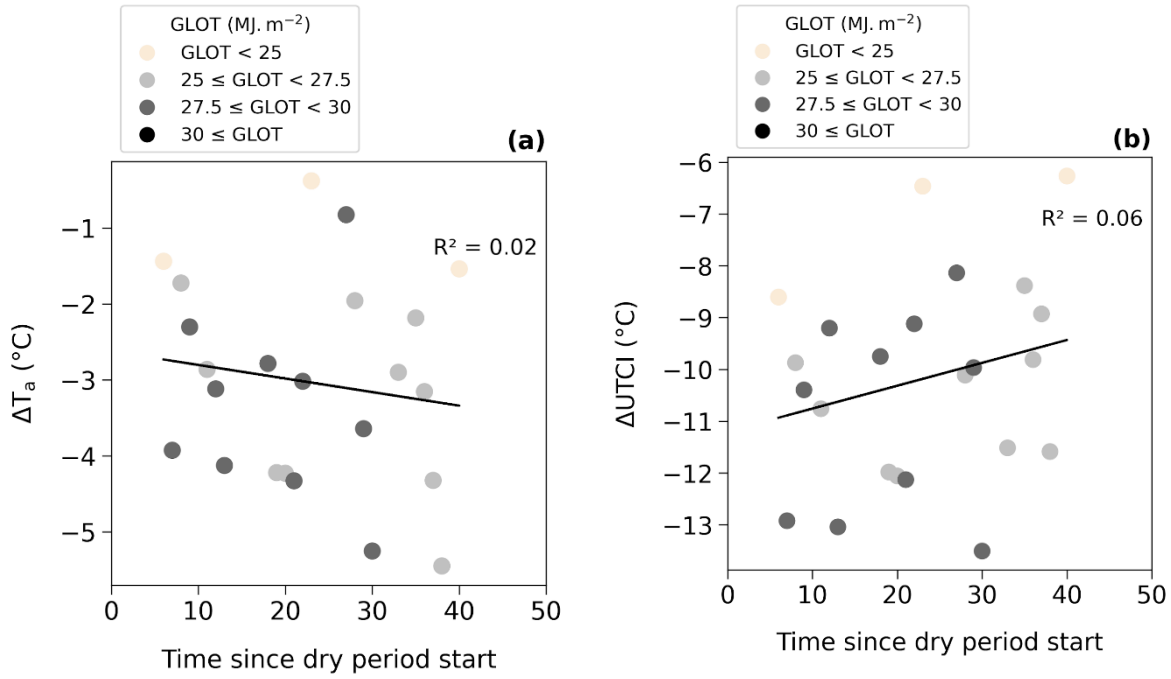

Figure 88: (a) air temperature difference (ΔT_a, tree - lamp post) and (b) UTCI difference ($\Delta UTCI$, tree - lamp post) as function of time elapsed since the beginning of the studied dry period (July 1st 2020) for celtis_1 and the daily integral of incident radiation measured at Paris-Montsouris (GLOT) during sunny (more than 10 hours of insolation) and rain-free days of the studied dry period (July 1st to August 10th, 2020).

Similar results were obtained for the rest of the studied trees as shown in Figure 89. Correlation coefficients mainly ranging between -0.50 and +0.25 were calculated for all studied trees between ΔT_a or $\Delta UTCI$ and the progress of the dry period. The dry period therefore did not appear to have a noticeable effect on the climatic benefits provided by the studied trees.

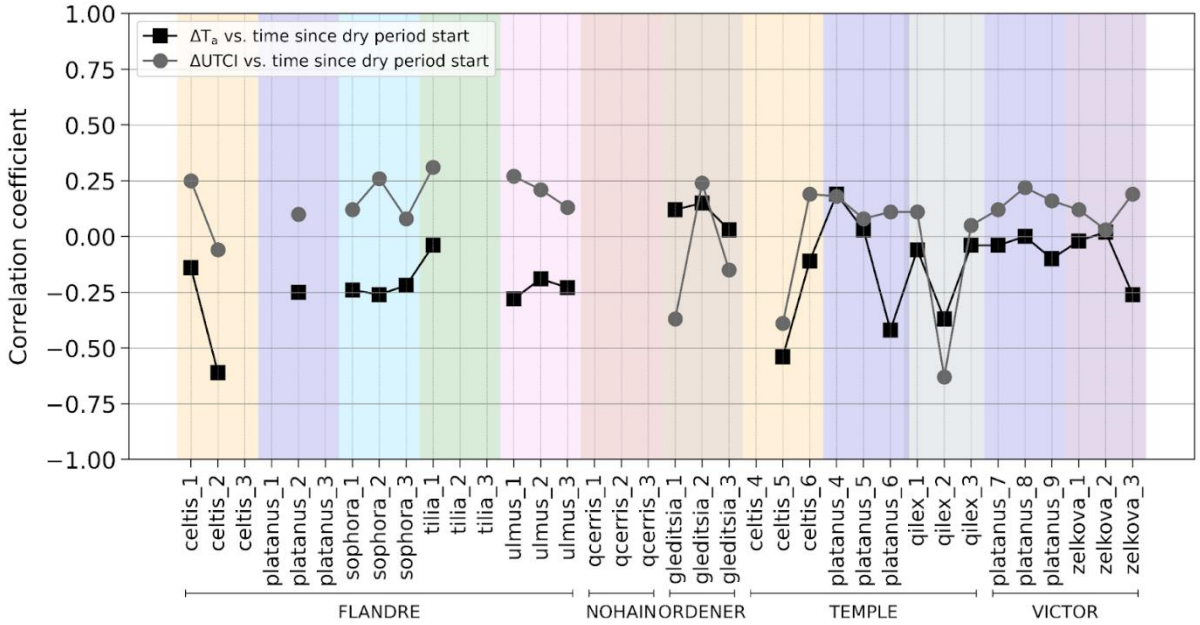

Figure 89: For each tree, correlation coefficient between the daily air temperature difference (ΔT_a, tree - lamp post) and daily UTCI difference (ΔUTCI, tree - lamp post) with the progress of the studied dry period for days sunny (more than 10 hours of insolation) and rain-free days from July 1st to August 10th 2020.

Chapter

5. General discussion and complementarity of the two experimental approaches

In order to study the climatic benefits provided by street trees and especially the factors influencing them, the analysis of the complete soil-tree-atmosphere continuum appears to be necessary as illustrated in Figure 90 (already presented and explained in section 2.3). Many studies proposed some evaluations of the climatic benefits provided by urban trees but the complete understanding of these benefits is not easy regarding the high number of variables involved, the high heterogeneity of the urban configurations and the important diversity of tree morphologies and physiological responses. Thereby, a diversity of methodologies can be found in the literature which all have some advantages and drawbacks. The present project proposes to combine two different approaches in order to provide a wide overview of the climatic benefits provided by street trees and the factors influencing them.

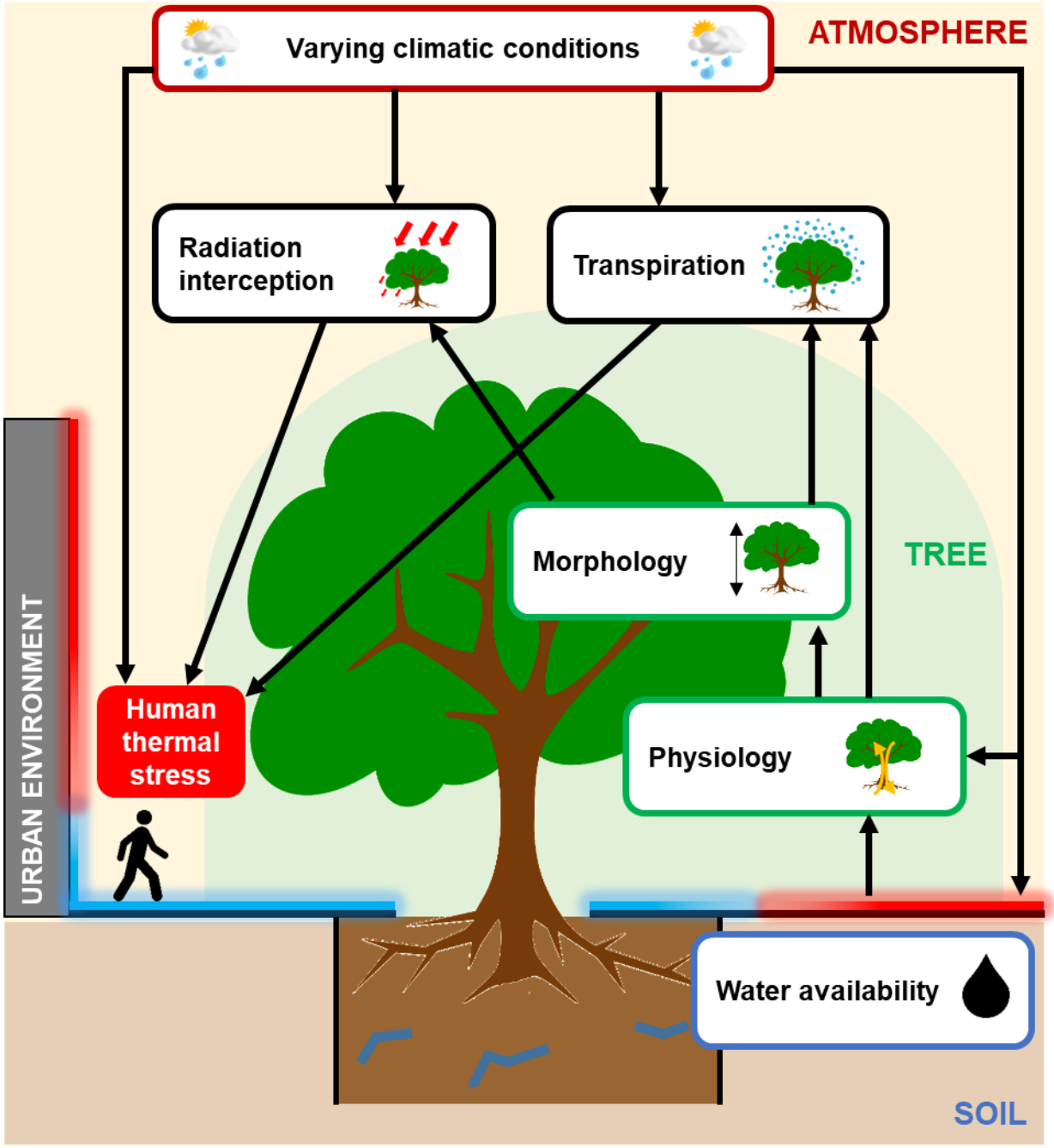

Figure 90: General drawing of the processes involved in the climatic benefits provided by trees in the urban environment.

On the one hand, a 1/5 scale canyon street, partially planted with young potted drip-irrigated ornamental apple trees (*Malus Coccinella*® 'Courtarou') located in Angers, France, was monitored to quantify the effect of street trees experiencing different water supplies on the microclimate. This first experimental facility also called "Reduced Scale Canyon Street" (RSCS) was presented and studied in chapter 3.

On the other hand, an in-situ monitoring of the microclimate inside and outside the canopy of 36 mature street trees from 9 different tree species located in 5 sites in Paris, France, was performed to compare the summer climatic benefits provided by different tree species. This second experimental facility also called "Trees & Climate study" (T&C) was presented and studied in chapter 4.

Although both experimental facilities are based on the monitoring of variables along the soil-tree-atmosphere continuum, they bring different insights as they come with different characteristics summarized in Table 19. RSCS is a ⅕ scale north-south oriented canyon street while T&C is based on real scale in-situ measurements in 5 sites in Paris with contrasted configurations (aspect ratio, orientation, etc.). While both facilities enable to assess human thermal stress through the calculation of the UTCI, the RSCS comes with a higher density of meteorological sensors with more variables monitored and multiple positions studied. Especially, RSCS makes it possible to calculate the amount of radiation intercepted by the crowns of the trees which was not possible in T&C. Seven morphological variables were calculated for the trees studied in T&C but the LAI could not be calculated unlike for the trees of the RSCS. RSCS also enabled to monitor more physiological variables and especially to estimate tree transpiration through a water balance while tree transpiration could not be assessed in T&C. One of the main advantages of the RSCS was also to compare at the same time trees experiencing contrasted water availability. To do so, the potted trees were drip-irrigated and soil VWC was monitored. Conversely, the T&C trees experienced real water availability, they were not irrigated but Ψ_{soil} was monitored. Finally, the different variables were monitored with a short time step in both facilities but RSCS focused only on one tree species during a 2-month campaign while trees from 9 species were monitored during 4 years in T&C.

Table 19: Comparison of the characteristics of the two experimental facilities.

Characteristics	**Reduced Scale Canyon street (RSCS)**	**Trees & Climate study (T&C)**
Scale	1:5	Real scale
Site typology	North-south oriented canyon street Aspect ratio = 1	5 sites Varying orientations Varying aspect ratios
Studied trees	2 alignements of 5 trees	36 individual trees
Mineral reference	non-vegetated zone of the street	1 lamp post per site
Non-urban reference	North mast outside the street	Paris-Montsouris Météo-France meteorological station

Characteristics	Reduced Scale Canyon street (RSCS)	Trees & Climate study (T&C)
Meteorological measurements	In each alignment of trees + in the non-vegetated zone: Ta *(4 positions)* AH *(4 positions)* T_{mrt} *(2 positions)* UTCI *(2 positions)* ↓SW, ↑SW *(under + above crown)* ↓LW, ↑LW *(under + above crown)* Wall temperature *(1 position)*	Inside each tree crown + at each reference lamp post: Ta AH T_{mrt} UTCI *(All at 1 position)*
Morphological measurements	Total leaf area Crown projected area LAI	Branch diameter variation
Water availability	Controlled (drip-irrigation) Monitored (Soil VWC)	Uncontrolled (natural conditions) Partially monitored (Ψ_{soil})
Tree species	*Malus Coccinella*® 'Courtarou'	*Celtis australis* *Gleditsia triacanthos* *Platanus x hispanica* *Quercus cerris* *Quercus ilex* *Sophora japonica* *Tilia cordata* *Ulmus resista* *Zelkova serrata*
Time step	10 minutes	1 hour
Monitoring duration	2 months	4 years

In the present chapter, the results obtained with both approaches are cross-analyzed in order to check the ability of the RSCS to reproduce the climatic benefits provided by street trees in a real urban environment and also to provide explanations to some of the processes involved. The complementarity of both approaches is then highlighted and an integrated assessment of the climatic benefits provided by street trees and their different sources of variability is proposed in the frame of the 3 objectives stated in section 2.3.2.

5.1. Exploring the variability of the climatic benefits

Both studies, through the continuous monitoring of different variables along the soil-tree-atmosphere continuum enabled to underline the high variability that characterizes the climatic benefits provided by street trees and investigate its different sources. This section will focus on the first objective stated in section 2.3.2 and detailed hereunder in Table 20.

Table 20: Respective contributions of the two experimental facilities to the first objective of the project.

Scientific questions and objectives	Reduced scale canyon street (RSCS)	Trees & Climate (T&C)
[1.] Exploring the variability of the climatic benefits		
Spatial distribution	X	
Temporal variability	X	X
Varying climatic conditions	X	X
Respective contributions of transpiration and cast shadows	X	
Morphological characteristics		X

5.1.1. Order of magnitude of the benefits

In T&C, the average maximum T_a reductions measured in the crowns of the studied trees ranged from 0.5 °C to 3 °C (Figure 77). In the RSCS, Ta measured inside the WW zone was lower by 0.5 °C at 1.5 m a.g.l., 1.8 °C at 1 m a.g.l., 3.3 °C at 0.4 m a.g.l. in the center of the street and 3.1 °C at 0.4 m a.g.l. close to the eastern wall compared to the NV zone from 11:00 to 13:00 UTC on July 4th (Figure 43). Therefore, both studies provided comparable Ta reductions when comparing the air inside the tree crowns and a non-vegetated area. Also, the results found in the crowns of the T&C trees were then consistent with those at the equivalent human height inside the RSCS. The T_a reductions reported hereinabove were consistent with those found in the literature which range from 0.7 °C (Souch and Souch, 1993) to more than 5 °C (Vailshery et al., 2013) and were also consistent with the maximum 2.7 °C reduction measured at midday by Mballo et al. (2021) for well-watered trees in the present RSCS at 0.4 m a.g.l. in the center of the street during a sunny day.

In T&C, the average maximum T_{mrt} reductions measured in the crowns of the studied trees ranged from 14 °C to 26 °C (Figure 72 to Figure 76). In the RSCS, T_{mrt} measured inside

the WW zone was lower by 20.4 °C at 0.4 m a.g.l. in the center of the street from 11:00 to 13:00 UTC and by 14.2 °C at 0.4 m a.g.l. close to the eastern wall from 13:00 to 15:00 UTC compared to the NV zone around noon on July 4th (Figure 44). Therefore, the results found in the crowns of the T&C trees were then consistent with those at the equivalent human height inside the RSCS. The T_{mrt} reductions reported hereinabove were consistent with the average 25 °C T_{mrt} reduction reported by Rahman and Ennos (2016) in their review.

In T&C, the average maximum UTCI reductions measured in the crowns of the studied trees ranged from 4 °C to 11 °C (Figure 78). In the RSCS, UTCI measured in the WW zone was lower by 7.4 °C at 0.4 m a.g.l. in the center of the street from 11:00 to 13:00 UTC and by 6.2 °C at 0.4 m a.g.l. close to the eastern wall from 13:00 to 15:00 UTC compared to the NV zone around noon on July 4th (Figure 45). Therefore, the results found in the crowns of the T&C trees were then consistent from those at the equivalent human height inside the RSCS. The UTCI reductions reported hereinabove were consistent with the findings of other studies at full scale of Coutts et al. (2016) and of Mballo et al. (2021) who measured up to 8 °C UTCI reduction at midday under well-watered trees compared to a non-vegetated zone of the street.

Both facilities then appeared to provide comparable results, consistent with those found in the literature, although they have to face multiple limits.

First, the RSCS is a reduced scale model and the comparison with full-scale experiments is not trivial. Some aspects have already been discussed in detail by Mballo et al. (2021). Compared to a full-scale canyon street, the radiation and conduction fluxes are not impacted by the scale reduction as long as the geometrical aspect ratio is conserved and the building materials have equal properties and dimensions (thickness, thermal conductivity, emissivity, etc.). Regarding the sensible heat flux which is related to the convective heat transfer, the temperature gradient between the surfaces and air as well as the wind flow appeared to be well reproduced but the natural convection regime was found to be difficult to reproduce as the vertical thermal effects on the flow field are reduced by the reduction factor of the street height in the scale model. In this way, it was concluded that the present experimental device was better suited for experiments carried out under forced or mixed convection regimes. More details about the calculation of the non-dimensional numbers such as Reynolds number and Richardson number can be found in the study of Mballo et al. (2021). They also highlighted a slight vertical air temperature gradient in the NV zone. Indeed, T_a was found to be approximately 1 °C higher at 0.4 m a.g.l. compared to 1 m a.g.l. during a sunny but not during a cloudy day in the NV zone. Conversely, they reported no vertical T_a gradient in the center of the vegetated zones located in the northern part of the street during both a sunny and a cloudy

day. Thereby, T_a measured at 0.4 m a.g.l. in the NV zone is likely to overestimate the real T_a that would be measured at human height at real scale, because it is in the thermal boundary layer developing on the ground in the reduced-scale model. The T_a reduction provided by the WW and WR trees at 0.4 m a.g.l. is then likely to be slightly overestimated but remains comparable to the T_a reductions reported in the literature as well as in the T&C study.

Then, the T&C T_a and RH measurements were carried out inside naturally ventilated screens which turned out to record biased values especially when directly exposed to sunlight as highlighted in appendix 7.2.8. To cope with this issue, T_a and RH measured at the reference lamp posts and inside the tree crowns were corrected on the basis of T_g measured at the same location. This correction was however not perfect as T_g could not explain the entire variability of the error induced by the screen. A slight error is then still very likely to exist when considering T_a and RH measurements. Also, the cup anemometers used in T&C were characterized by a low sensitivity to low wind speeds as their trigger point was at 5 $km.h^{-1}$ (approximately 1.4 $m.s^{-1}$) meaning that null values were recorded as soon as real wind speed was lower than 5 $km.h^{-1}$. Wind speed was therefore very likely to be underestimated in conditions of low wind days especially inside the tree crowns where the presence of the foliage and branches slows down the air flow. A lower wind speed may result in a slightly higher UTCI inside the tree crowns which could slightly underestimate the UTCI reduction provided by the trees. However, this underestimation is likely to be very low, especially during hot days as the effect of wind speed on UTCI is decreased as pointed out by Bröde et al. (2012), since the gradient between skin temperature and air temperature is reduced in warm conditions. Also, a minimum value of wind speed of 0.5 $m.s^{-1}$ was considered in order to comply with the UTCI calculation method which again limits the impact of the wind speed underestimation.

Also, the T&C study was based on the monitoring of meteorological variables inside the crowns of the studied trees. The sensors were then mounted at different heights ranging from 3.6 m a.g.l. to 8.2 m a.g.l. Such measurements may therefore not be exactly representative of the meteorological conditions at human height both because the influence of the crown may be different when comparing inside and under-crown measurements and also because vertical gradients have already been spotted in urban environment. Also, the height of the sensors relatively to the base of the crown (their position on the vertical axis) may be of high importance as it directly influences the amount of radiation received by the sensors, especially the globe thermometers. Indeed, the globe thermometers are very likely to receive high amounts of SW radiation reflected on the ground or LW radiation emitted by the ground and the surrounding low height surfaces if placed right at the bottom of the crown, close to its lowest leaves.

Conversely, the globe thermometers are very likely to be more protected from radiation if placed for instance 1 m higher than the bottom of the crown. Yet, in the present study, the height difference between the location of the sensors and the bottom of the tree crown varies from 0 to more than 3 m.

Finally, the trees studied in T&C were located in very heterogeneous configurations. First, the different studied sites had heterogeneous forms, FLANDRE and TEMPLE were typical urban canyons while ORDENER was a small square and VICTOR and NOHAIN were semi-open streets. All sites had different orientations and the trees and lamp posts were at different locations inside the street even when considering trees from a same given site. Therefore, the trees were exposed to contrasted solar exposure. Some trees were quite isolated like the *Quercus cerris* of NOHAIN while others formed part of a dense and continuous canopy just like the *Celtis australis* and *Sophora japonica* of FLANDRE which were part of a double alignment of trees. The establishment of the numerical point clouds of the trees on the basis of the LiDAR scans had to face this issue as it was sometimes hard to attribute some branches to the studied tree or to its neighbors. It is therefore not easy to know whether the measured climatic benefits may be also influenced by the other surrounding trees.

5.1.2. Spatial distribution

The effect of the trees on the microclimate is likely to be noticeable at different locations in the street. They are first expected to have a direct effect on human thermal stress for a pedestrian standing under their crown but the shadow they project also reduces the temperature of the street surfaces far from their trunk, depending on the position of the sun in the sky, the position of the trees in the street and the dimensions of the trees as suggested by Bouyer (2009) (Figure 12). The assessment of their global effect on the street microclimate therefore requires a high density of sensors.

In T&C, the measurements were carried out at only one location for each tree (inside the tree crown) which prevents from assessing the total spatial extent of the influence of the trees. Conversely, the RSCS was characterized by a higher density of sensors enabling to assess the effect of the climatic benefits provided by WW trees at different locations, although the sensors remained pointwise, and in limited number.

In the RSCS, the shadow cast by the trees could be highlighted at human height through the T_{mrt} measurement both under the tree crowns and close to the eastern wall (Figure 44). The trees could cast shadows on the buildings up to at least 1 m a.g.l. (height of the surface

temperature sensors) as highlighted by the eastern wall surface temperature which was up to 6.9 °C lower in the WW zone and 8 °C lower in the WR zone compared to the NV zone at 16:30 UTC on July 4th (before the water restriction). Such results were consistent with those already reported in the literature. Indeed, according to the review of Rahman et al. (2020), the trees of the RSCS which LAI ranged from 1.7 (WR trees in the end of the studied period) to 3.3 $m^2.m^{-2}$ (WW trees in the end of the studied period) should therefore provide from 6 °C to 9 °C surface temperature reduction.

Also, the reduction of the transpiration of the WR trees studied in the RSCS appeared to have only a noticeable impact inside their crown and not at the equivalent human height. Indeed, the strong reduction of the WR tree transpiration only led to noticeable AH and T_a differences between both vegetated zones at 1 m a.g.l. and 1.5 m a.g.l. (i.e. inside the trees crowns) while no difference appeared at 0.4 m a.g.l. (Figure 42 and Figure 43). In other words, such observations tend to suggest that the thermal effect of the evaporation of the transpired water is probably very localized close to the tree crowns. Conversely, the effect of radiation interception appeared to be noticeable on a wider area inside the street highlighting the greater spatial extent of cast shadow. This could be further be confirmed and quantified by using thermal infrared thermography, as a perspective to this study.

5.1.3. Temporal variability and varying climatic conditions

It could be highlighted that the effect of the trees was not constant over the day as already reported by Coutts et al. (2016) and the microclimate differences between a tree and its surrounding environment are almost exclusively observed during daytime.

First, the effect of tree transpiration appeared to be mainly visible during daytime. In the RSCS, it could be observed on July 4th (before the water restriction) at 1 m a.g.l. and 1.5 m a.g.l. (inside the tree crowns) that AH was generally lower at night but slightly higher during the day in both vegetated zones compared to the NV zone (Figure 42). This confirms that water vapor was mainly released during daytime. Yet, the eventual variations of the transpiration rate occurring over daytime could not be evaluated as the water balance was run on a daily basis.

In T&C, a noticeable increase of AH inside the tree crowns was observed during daytime for the trees of NOHAIN, ORDENER and VICTOR which also suggests that the release of water vapor through transpiration occurred during daytime (Figure 73, Figure 74 and Figure 76). In FLANDRE and TEMPLE, ΔAH appeared to be highly variable over the day and

especially to be often lower inside the crowns compared to the reference lamp posts. Therefore, in the case of T&C, AH did not appear to provide sufficient information on the release of transpired water and could not explain the daily variability of the measured climatic benefits.

During night-time, radiation interception was obviously null in the absence of solar radiation. As a consequence, T_{mrt}, which strongly depends on LW and SW fluxes, was obviously not reduced at night in both the RSCS (Figure 44) and T&C (Figure 72 to Figure 76). However, T_{mrt} appeared to be slightly higher at night (from 0.3 °C to 1 °C higher from 02:00 to 04:00 UTC) inside the tree crowns of the T&C trees compared to their reference lamp post (in FLANDRE, NOHAIN and ORDENER) and also under the crowns of both the WW and the WR trees of the RSCS at 0.4 m a.g.l. in particular on the central axis of the street (approximately 1.5 °C higher from 02:00 to 04:00 UTC) compared to the NV zone. Such observations illustrate the fact that, due to the presence of branches and leaves, the tree crowns reduce the SVF of the surfaces they cover. Thereby, compared to the same surfaces located in an open area, the surfaces located under the tree crowns remain hotter as their LW exchanges with the night sky are lower. Thus, they emit higher LW radiation to the sensors located inside the tree crowns which increases T_g and as a consequence T_{mrt} at these locations. Such observations were very consistent with other works found in the literature which already highlighted this radiative trapping phenomenon at night for the LW exchanges (Coutts et al., 2016). In the RSCS, this phenomenon was mainly observed on the central axis of the street as the SVF at this location is lower than the one close to the facades.

During daytime, a strong interception of solar radiation was highlighted through both the ↓SW and Tmrt measurements. In the RSCS, a reduction of the ↓SW was measured under the tree crowns compared to the NV zone as soon as the sun rises (Figure 41). This reduction increased with the increasing insolation until reaching its maximum value around noon (approximately 95 % of the ↓SW intercepted by the tree crowns at this time). Strong temporary increases of the ↓SW measured under the tree crowns could be observed which were very likely to be caused by the heterogeneities of the foliage which may lead to temporary direct exposure of the sensors to sunlight. Similar observations were reported for T_{mrt} in both the RSCS (Figure 44) and T&C (Figure 72 to Figure 76).

Also, it appeared that the main T_{mrt} reductions were not measured at the same time depending on the location inside the street. Indeed, in the RSCS the maximum T_{mrt} reductions compared to the NV zone were observed around 12:00 UTC at the center of the street and around 14:00 UTC close to the eastern wall (Figure 44). Also, the maximum surface temperature reduction of the eastern wall at 1 m a.g.l. was measured around 16:00 UTC right

when it was mainly exposed to sunlight (Figure 40). Although the surface temperature of the western wall could not be analyzed here, the effect of cast shadow on the western wall's temperature is expected to occur during the morning when this wall is mainly exposed to sunlight. In T&C, the maximum T_{mrt} reductions were also observed at different times during the day which may partly depend on the street orientation and on the respective locations of the trees and lamp posts in the studied sites, with respect to the street central axis (Figure 72 to Figure 76). Thereby, during some periods of the day, some trees may be in a sunny area while their reference lamp post may be in a shaded area which greatly impacts the measured variables.

To sum up, radiation interception is subject to strong daily temporal variability which depends on the positions of the sun in the sky, the location of the measurements inside the trees and of the trees inside the studied site.

Daily T_a and UTCI evolutions seemed to be consistent with the observations reported hereinabove. Due to the absence of radiation interception and to the null or very low transpiration at night, no T_a and UTCI reduction was reported at night. However, UTCI could be slightly higher inside or under the tree crowns, for instance in T&C for the trees located in FLANDRE and VICTOR which is likely to be induced by the night-time higher T_{mrt} measured under some tree crowns highlighted earlier. During daytime, it could be noticed in both the RSCS and T&C that the temporal variability of the radiation interception mentioned hereinabove also led to a strong temporal variability of the UTCI, due to its strong dependence on T_{mrt}, and to a lesser extent of the T_a reduction.

Finally, a strong variability was observed from one day to the next as suggested in T&C by the high standard deviations characterizing the average daily evolutions of ΔT_a, ΔTmrt and ΔUTCI even when computed with a low number of days (e.g. only 2 days were considered for the trees of FLANDRE in Figure 72). A PCA performed in both the RSCS and T&C to cross-analyze the daily climatic benefits with the meteorological conditions showed that ΔUTCI was highly influenced by the daily insolation (GLOT), the higher the GLOT, the higher the UTCI reduction (Figure 46 and Figure 80). The strong influence of radiation interception on the climatic benefits, especially in terms of human thermal stress reduction is then again underlined. Such results were very consistent with the previous findings of Herpin et al. (2022) who also reported a strong correlation between GLOT and UTCI reduction in the present RSCS at 0.4 m a.g.l. under well-watered trees ($R^2 = 0.75$).

5.1.4. Respective contributions of transpiration and cast shadows

On the one hand, section 5.1.3 highlighted that the variability of ΔUTCI over a single day or from one day to the next appeared to be highly influenced by the variability of radiation interception and section 5.1.2 highlighted the spatial extent of radiation interception.

On the other hand, noticeable increases of AH inside the tree crowns compared to non-vegetated areas were reported during daytime in the RSCS (at 1 m a.g.l. and 1.5 m a.g.l., see Figure 42) as well as in T&C for the trees of NOHAIN, ORDENER and VICTOR (Figure 73, Figure 74 and Figure 76). Such AH increase could possibly highlight the release of water transpired by the trees into the atmosphere. In the RSCS, this AH increase inside the tree crowns was consistent with a T_a reduction at this same location (Figure 43). In T&C, however, this AH increase was associated with very low T_a reduction and even positive ΔT_a during most of daytime for the concerned trees. Also, in FLANDRE and TEMPLE, ΔAH appeared to be highly variable over the day and especially to be often negative (meaning that AH was lower inside the crowns compared to the reference lamp posts) while the trees of these two sites provided the greatest T_a reductions. In T&C, AH did not appear to provide sufficient information on the release of transpired water, maybe ΔAH was low compared to the sensors accuracy and also compared to the eventual errors remaining after the correction of T_a and RH detailed in section 4.1.1.4.1. In addition, it was highlighted in section 5.1.2 hereinabove on the basis of the RSCS that the spatial extent of the effect of tree transpiration appeared to be low.

Such results thereby suggest that radiation interception should have a stronger impact on the climatic benefits than tree transpiration. To enlighten this aspect, the RSCS was used to estimate and compare the daily amount of energy dissipated by both tree transpiration and radiation interception. Such comparison could not be run in T&C as tree transpiration and radiation interception could not be estimated with this experimental facility. Then, the energy balance presented in figure Figure 27 suggests that, from an energetic point of view, daily radiation interception contributed to approximately 70 % of the total amount of energy dissipated by WW trees while WW tree transpiration was responsible for the remaining 30 % which confirms the stronger influence of radiation interception on the climatic benefits.

Yet, it should obviously be kept in mind that the radiation measurements were very local. Indeed, the ↓SW measured under the tree crowns may be very sensitive to the positioning of the radiometers because the heterogeneity of the tree crowns may create unequally shaded areas as explained previously in section 5.1.3. It is then difficult to extrapolate the measured

intercepted radiation to the entire crown projected area. In order to get a more accurate estimation of the total radiation interception and of its integrated effect on the street energy balance, a more precise description of the tree geometry, through 3D numerical reconstruction for instance, would be necessary and the solar angle should be taken into account as it influences the area of shaded street surfaces. Infrared images of the surrounding surfaces could also be shot to get more global surface temperature measurement on the studied zone.

5.1.5. Influence of tree species and morphological characteristics

Although only one tree species was studied in the RSCS, WW and WR trees were characterized by different morphological parameters in the end of the studied 2-month summer period (see discussion about the effect of the water restriction in the following sections). Especially, the LAI of the WW trees was 3.3 $m^2.m^{-2}$ on August 27th 2022 while the one of the WR trees was 1.7 $m^2.m^{-2}$. In parallel, the WW trees intercepted approximately 95 % of the ↓SW around noon on August 20th while the WR trees intercepted approximately 91 %. Such results suggest that a lower LAI is associated with a lower radiation interception as already pointed out in the literature by Shahidan et al. (2010) and Armson et al. (2013). Yet, although the LAI of the WW trees was almost twice the one of the WR trees, the difference of radiation interception remained low which suggests that the WR trees had enough leaves to intercept an important amount of radiation. However, LAI could only be measured twice during the studied period which did not enable to study its relationship with radiation interception in detail with a wide range of LAI.

The influence of tree species and morphological characteristics on the climatic benefits could be deeper analyzed with T&C which compared 9 tree species at the same time and quantified some of their morphological characteristics.

First, according to the information found in the literature and summarized in Table 12, the 9 studied tree species should provide contrasted climatic benefits. *Platanus x hispanica* and *Tilia cordata* were expected to provide the most important cooling benefits. Conversely, *Gleditsia triacanthos, Sophora japonica* and *Quercus ilex* were characterized by the lowest grades concerning the potential for local climate regulation attributed in the "Tree species guide" of Ville de Paris (2023) on the basis of their main morphological characteristics and theoretical transpiration rate. In T&C, *Gleditsia triacanthos* was indeed characterized by lower T_a and UTCI reductions compared to the other trees. However, *Platanus x hispanica*, *Tilia*

cordata and also *Sophora japonica* and *Quercus ilex* all appeared to provide very important T_a and UTCI reductions which does not totally agree with the information of the "Tree species guide" of Ville de Paris (2023). Yet, in this in-situ monitoring study, the real transpiration rates of the studied trees as well as their morphological characteristics may have been different from the theoretical ones considered in the literature due to the sometimes water limiting conditions and the limitations of the urban environment.

Indeed, compared to the general morphological characteristics that are considered in the literature, the total heights of the studied trees were on average half the average height found in the literature for each species (see Figure 63 and Table 12). Yet, according to the information found in the tree database managed by the green spaces department of the city of Paris, the studied trees were almost all considered as "young trees" and the oldest one was planted approximately 30 years ago. It is then very likely that they have not reached their maximum volume and height yet.

The crown densities calculated in the present study also vary from those found in the literature for the 9 studied species. According to the information collected in the "Tree species guide" of Ville de Paris (2023), both *Tilia cordata* and *Quercus ilex* are known for their high density of leaves. In the present study, the trees of both species had average density while the *Ulmus resista* were the densest trees. However, *Gleditsia triacanthos* which are considered as low leaf density species in the literature, were indeed characterized by very low density in the present study. In cities, trees are managed in order to comply with the different constraints of the urban environment. Especially, they are trimmed in order to avoid contact with the surrounding urban objects such as buildings. Therefore, their shape is very likely to be highly influenced by the urban limitations and then to differ from the usual morphological characteristics of the different species which have been reported for trees experiencing optimal growing conditions.

Finally, it should be kept in mind that although the T&C study enabled to perform a continuous monitoring over a long period, it was not possible to compare all the 36 studied trees at the same time due to the important amount of data that was lacking as explained previously. As a compromise, each site was studied independently on its own list of days which means that the comparisons between the different sites have to be considered carefully due to the strong variability of the meteorological conditions, and their impact on the climatic benefits provided by the trees highlighted previously. Also, a few trees were sometimes removed from the analyses due to a too poor data availability which makes it difficult to draw strong trends regarding eventual tree species effect or site effect. To cope with this issue, and considering the

high influence of radiation interception on the climatic benefits, the relationship between the morphological characteristics of the trees and T_{mrt} reduction was investigated focusing on a common list of days close to the LiDAR scanning campaign in August 2022 (see section 4.2.4.3). However, the morphological variables calculated in the present study were not able to explain the variability of ΔT_{mrt} around noon across the different studied trees. More precisely, crown density did not appear to be a suitable explanatory variable unlike what was expected. However, it is important to recall that the crown density calculated in the present study cannot be compared to LAI especially as the total leaf area was not estimated. Crown density was calculated on the basis of Vvox considering voxels are 10 cm side cubes. It may therefore not represent well enough the foliage and may lead to an overestimation of the leaf density as the voxels were taken into account in the calculation of Vvox as soon as they contained one point of the point cloud. Moreover, crown density as well as the location of the studied sensors may both be heterogeneous. Then, the studied meteorological variables and especially T_g which is very local may not be representative of the entire cast shadow. The impact of the heterogeneity of the crowns on the T_{mrt} and UTCI measurements has already been discussed earlier. It is also possible that the range of crown densities of the T&C trees was too small to lead to noticeable contrasts of cast shadows. Indeed, it is likely that the shadow cast by the trees with the lowest densities was already sufficient to provide noticeable T_{mrt} reduction.

The other crown dimensions such as Htot, Sproj or Vpoly were not expected to have a strong influence on the studied sensors which were very local and mounted inside the tree crowns but they are very likely to influence the spatial extent of the shadows cast by the trees. Thereby, such crown dimensions could be considered when it comes to selecting trees with interesting cast shadows although the spatial extent of radiation interception could not be assessed in T&C.

5.2. Impact of heatwaves and droughts on tree physiology and morphology

Some physiological and morphological variables were measured in both studies in order to assess the effect of severe climatic events such as heatwaves and droughts on trees. The present section will discuss the main observations in the frame of the second objective stated in section 2.3.2 and detailed hereinunder in Table 21.

Table 21: Respective contributions of the two experimental facilities to the second objective of the project.

Scientific questions and objectives	Reduced scale canyon street (RSCS)	Trees & Climate (T&C)
[2.] Impact of heatwaves and droughts on tree physiology and morphology		
Effect on stomatal conductance	X	
Effect on transpiration	X	
Effect on leaf temperature	X	
Effect on stem diameter variations	X	X
Effect on leaf area density	X	

5.2.1. Effect on stomatal conductance, transpiration and leaf surface temperature

Stomatal conductance, tree transpiration and leaf surface temperature could only be assessed in the RSCS. The water restriction implemented in the RSCS quickly and strongly reduced the water availability for the studied trees. Although the pots of the trees were designed to model real-life urban tree pits at a ⅕ scale ratio, the TAWS of the studied soil was low (8.3 L) compared to the average transpiration of WW and WR trees at the beginning of summer 2022 (respectively 2.4 and 2.9 $L.tree^{-1}.Day^{-1}$ on average before the water restriction start) (Figure 24). Thereby, the TWAS of the studied soil only provided enough water for around 3 days of normal transpiration. As a consequence, the soil VWC of the WR trees approached the permanent wilting point only two days after the start of the water restriction.

The stomatal conductance of the WR trees strongly decreased between July 5th and July 12th (Figure 25) which was consistent with other measurements described in the literature as

detailed in section 3.1.3.4. This decrease appeared to be very quick although more frequent stomatal conductance measurements would have been needed to assess more precisely this dynamic. Yet, the trees appeared to have limited their water loss probably to limit the drying of their tissues.

As a consequence, the WR trees transpiration was strongly and quickly reduced as soon as the water restriction started, it was already half that of the WW trees on the second day of restriction and was on average 81 % lower than that of the WW trees during the entire water restriction period (Figure 25). Again, the transpiration measurements were found to be consistent with other works as detailed in section 3.1.3.4 although the calculation of tree transpiration in the RSCS relies on capacitive probes which are very local and that cannot be representative of the whole soil volume available for the trees. While the WW trees transpiration appeared to be partly related to ET_{ref}, low daily transpiration rates were calculated for the WR trees even with high ET_{ref} which means that the WR trees transpiration was not related to ET_{ref} (Figure 34) and was mainly limited by the low soil VWC all over summer.

A lower transpiration induces a lower amount of energy dissipated by the leaves through latent heat flux which is why T_{leaf} is in this case expected to increase. Although the variability of T_{leaf} appeared to be very high for a single tree, a slight increase of Tl_{eaf} was reported for the WR trees over summer (Figure 39) and T_{leaf} was on average 3.2 °C higher (statistically significant) on August 20th for the WR trees compared to the WW trees.

Regarding the influence of very high temperatures, heatwaves, which were characterized by high T_a, ET_{ref} and insolation, were associated with a high daily transpiration for the WW trees. However, equally high transpiration rates were also reported for the WW trees during cooler days with lower ET_{ref} (Figure 34). The response of stomatal conductance to the high T_a recorded during heatwaves could however not be assessed as the stomatal conductance measurements were not frequent enough.

5.2.2. Effect on stem diameter variation

Stem diameter variations were monitored in both the RSCS and T&C respectively on the trunk and on one branch of each studied tree. Yet, only the RSCS enabled to compare at the same time WW and WR trees. During the water restriction implemented in the RSCS, the radial growth of the WR trees was quickly stopped as soon as water was lacking and the low soil VWC did not enable the growth to start again all along summer (Figure 35). Such radial growth stop was consistent with the previous observations of Améglio and Archer (1996). The

reduction of stomatal conductance highlighted in the previous section is then likely to have reduced and maybe stopped the photosynthetic activity of the WR trees preventing them to create new tissues and to sustain radial growth. At the same time, DAmp, which appeared to be slightly related to tree transpiration for the WW trees, was noticeably increased for the WR trees (in agreement with the observations of Améglio and Archer (1996) in spite of the reduction of their transpiration. Indeed, high DAmp were calculated for the WR trees even with low daily transpiration. Then, although the stem diameter variations are caused by the water fluxes inside the tree stem, DAmp, which could be expected to illustrate tree transpiration for WW trees, does not appear to be possible indicator of tree transpiration for trees experiencing a water restriction.

However, it is important to remember that the transpiration considered in the RSCS was computed through a water balance applied only to the soil compartment. It was explained in chapter 2 that tissues of trees experiencing water shortage may partly dry in case of high transpiration needs. The water contained in the tissues of trees may thus be transpired through the stomata of the leaves. In the present study, noticeable stem shrinkage was reported for the WR trees, especially around mid-July when an intense heatwave with T_a exceeding 40 °C reached the region of Angers (Figure 37). The extremely high T_a and VPD associated to this heatwave may have required an extremely high transpiration rate which could not be supplied by the low soil VWC and part of the water contained in the tissues of the WR trees may have been used for transpiration although the stomatal conductance of the WR trees remained low all over summer. Considering the WW trees, extreme T_a also appeared to have led to extreme DAmp but not to remarkably high transpiration rate (Figure 37). During the very warm days, higher DAmp may then indicate that part of the water contained in the WW trees' tissues could have been transpired in addition to the water retrieved from the soil. The real tree transpiration may then be slightly higher than the one calculated with the proposed water balance applied to the soil compartment. However, this unquantified amount of transpired water is likely to be low as it did not prevent the leaves of the WR trees from overheating as explained in the previous section. Such hypotheses could not be verified as they would need to measure tree transpiration with other methods for instance enabling to quantify the real amount of water vapor spread out from the leaves. Also, the very low number of days with extreme T_a did not enable to draw strong trends regarding the influence of T_a on DAmp.

In T&C, contrasted branch growths were reported for the 36 trees. However, in the case of T&C, the trees were exposed to natural uncontrolled water availability. The comparison of summer 2020 and 2021 proposed in section 4.2.5 first highlighted that very contasted Ψ_{soil} could

be measured in the tree pits even if trees were exposed to the same rainfall events, especially during the dry summer of 2020. Yet, many factors may explain such disparities. First, the reference rainfall data used in the present study were measured at Paris-Montsouris and they may not be representative of the real rainfall events that occurred in each of the 5 sites, especially as Paris-Montsouris is located from 2.8 to 8 km from the studied sites. Also, the real amount of rainfall entering the pits remained unknown as well as the eventual presence of other sources of water for some of the studied trees. Moreover, the studied trees may uptake different amounts of water for their respective transpiration. Finally, the lowest depth for Ψ_{soil} measurement was approximately 0.75 m which may be very low compared to the root depth expected for mature urban trees. Therefore, they cannot be perfectly representative of the availability of water for the trees.

Yet, very contrasted branch growth could be observed even when the trees were exposed to high Ψ_{soil} during summer 2021 (Figure 86). In particular, a low branch growth interruption was reported for *Platanus x hispanica, Ulmus resista* and *Zelkova serrata* and an important branch growth interruption for the *Tilia cordata, Quercus cerris* and *Sophora japonica*.

Regarding the dry period of summer 2020, it appeared that the branch growth of multiple trees was already stopped at the beginning of the studied period (Figure 87). Thereby, these trees may have been more sensitive to the climatic conditions of spring 2020 which was drier than an usual one (95.6 mm total rainfall in April and May 2020 against 114.8 mm on average during these two months from 1991 to 2020). Therefore, all the studied trees were not experiencing comfortable water conditions on July 1st unlike what was hypothesized when selecting the studied period.

When comparing the effects of the dry period, it appears that all trees experienced branch growth interruption during the studied period. However, contrasted general behaviors appeared for the different groups of trees.

Sophora japonica and *Tilia cordata* although they were exposed to different Ψ_{soil} (Figure 86) were all already experiencing branch growth interruption on July 1st, their growth remained interrupted during most of the period and also a long time after the end of the period (almost until the end of September). This suggests that they were very sensitive to the lack of water as their growth can be impacted even at high Ψ_{soil}.

Gleditsia triacanthos, Platanus x hispanica of both TEMPLE and VICTOR, *Qercus ilex* and *Zelkova serrata* experienced a quick branch growth interruption at the beginning which lasted for most of the dry period but their branch growth started again quickly after the end of

the period with the rainfall events of August 2020. Although they appeared to be sensitive to the lack of water, they appeared to be more resilient that *Sophora japonica* and *Tilia cordata*.

Platanus x hispanica of FLANDRE and *Ulmus resista* kept growing on average longer than the rest of the trees after the start of the dry event. Their growth was less interrupted and it started again very quickly at the end of the dry period. The three *Ulmus resista* experienced contrasted water availability during July 2020 which may indicate that they could keep growing even at low Ψ_{soil} (Figure 86). The *Platanus x hispanica* of FLANDRE experienced generally higher water availability than the other *Platanus x hispanica* of TEMPLE and VICTOR (Figure 86). It is then likely that their growth be impacted when Ψ_{soil} decreases close to -0.25 MPa, the lower limit of the measurement range of the Watermak® probes.

More contrasted behaviors were observed for the rest of the trees (*Celtis australis* of both FLANDRE and TEMPLE, and *Quercus cerris*).

According to the information found in the literature and summarized in Table 12, all studied tree species were initially considered resistant or very resistant to drought except *Tilia cordata* and *Ulmus resista* which were considered not resistant. Although the term "resistance" should obviously be considered carefully as its definition is not trivial, the present results tend to confirm that *Tilia cordata* appears to be more sensitive to the lack of water. However, unlike what was stated in Table 12 the studied *Sophora japonica* appeared to be more impacted than the other species while the three *Ulmus resista* of the present study appeared to be able to keep growing during a long dry event while the other species generally stopped growing which does not confirm the data from the literature. Yet, in the absence of a comparison of the trees studied in T&C with other trees of the same species experiencing controlled comfortable water availability, it is not easy to draw strong conclusions about an eventual species effect regarding the branch growth dynamic under dry conditions.

In the frame of the results obtained with the RSCS and detailed hereinabove, it could be hypothesized that the periods of branch growth interruption and branch shrinkage observed for the T&C trees were associated with stomatal closure and tree transpiration reduction. Although DAmp appeared to increase during periods of branch growth interruption and stem shrinkage, especially during heatwaves, just like for the WR trees of RSCS, this variable could not be used as an indicator of tree transpiration. Indeed, it did not appear to be related to tree transpiration for trees experiencing a water restriction, as explained previously with the results of the RSCS hereinabove. Thereby, the whole tree transpiration of the studied trees should be estimated including the quantification of the respective contributions of the water uptaken in the soil and

the water contained in the tissues in order to understand how the behavior of the different tree species during the dry period.

5.2.3. Effect on tree foliage

During the water restriction run in the RSCS, the crown projected area of the WR trees remained almost constant (very slight decrease) all along summer while the total leaf area and the LAI were strongly reduced (Table 3). Thus, the water restriction, by inducing a reduction of stomatal conductance, may have reduced the photosynthetic activity and at the same time the elongation process of the stems which is consistent which the radial growth interruption highlighted in the previous section. Also, the strong reduction of the total leaf area induces that the formation of new leaves was probably stopped while the trees experienced leaf loss. Leaf wilting and leaf loss were indeed visually noticed during the measurement campaign but could not be quantified. Leaf loss, in addition to stomatal closure, may also have contributed to limit the WR trees transpiration but its impact is likely to have occurred later during July according to on-site observations while stomatal closure occurred soon after the beginning of the water restriction. The eventual impact of heatwaves on leaf loss could not be distinguished from the impact of the water restriction as only two measurement campaign of the total leaf area were performed. Thereby, more frequent measurements of the total leaf area would have been required to assess more precisely the dynamic of the elongation process interruption and of the leaf loss.

In T&C, it is likely that the studied trees experienced similar effects to those described hereinabove. Their photosynthetic activity may have been reduced or stopped when they were experiencing branch growth interruption. Thereby, their elongation process and their leaf formation may have been reduced just like their radial growth and they may also have experienced leaf wilting and leaf loss. However, only one measurement campaign of the morphological variables was performed which did not enable to assess the evolution of such variables during dry periods, to understand whether some tree species may respond quicker or stronger than others and also whether mature trees may behave differently from the young trees of the RSCS.

5.3. Impact of heatwaves and droughts on the climatic benefits

Different meteorological variables were measured in both studies in order to assess the effect of severe climatic events such as heatwaves and droughts on the climatic benefits provided by the trees. The present section will discuss the main observations in the frame of the third objective stated in section 2.3.2 and detailed hereinunder in Table 22.

Table 22: Respective contributions of the two experimental facilities to the third objective of the project.

Scientific questions and objectives	Reduced scale canyon street (RSCS)	Trees & Climate (T&C)
[3.] Impact of heatwaves and droughts on the climatic benefits		
Effect on absolute humidity	X	
Effect on radiation interception	X	
Effect on surface temperature	X	
Effect on radiation balance	X	
Effect on air temperature	X	X
Effect on UTCI	X	X

5.3.1. Effect on absolute humidity

In the RSCS, a reduction of AH was noticed during daytime in the WR zone compared to the WW zone during the water restriction. This reduction was consistent with the reduction of the transpiration of the WR trees highlighted previously which induces that less water vapor was spread out into the surrounding atmosphere of the WR trees. This AH reduction was however only noticeable inside the crowns of the WR trees (i.e. at 1 and 1.5 m a.g.l.) which suggested that the effect of tree transpiration on the street microclimate should be very localized close to the crowns of the trees as already discussed earlier.

5.3.2. Effect on radiation interception, surfaces temperature and radiation balance

A noticeable decrease of the amount of radiation intercepted by the WR was reported in Figure 26 (from 83 % of the daily integral of ↓SW to 76 % on average during August 2022) and was very consistent with the decrease of the LAI highlighted in Table 3. Its impact may however have been low especially as the WR trees kept intercepting on average 91 % of ↓SW on August 20th and 76 % of the daily integral of the ↓SW on average during August 2022, which is still important. Thereby, although the WR trees experienced an interruption of leaf formation as well as leaf loss, their remaining leaf area was still sufficient to provide important radiation interception. Signs of leaf wilting were also observed on-site and might have influenced the radiation interception but such phenomena could not be quantified nor monitored.

Still in the RSCS, the amount of ↓SW radiation measured under the crowns of the WR trees increased due to the reduced amount of radiation intercepted by their crowns (Figure 41). The different street surfaces of the WR zone then received a higher amount of solar radiation which was likely to increase their surface temperature. Such hypotheses were verified for the eastern wall of the street but not for other surfaces of the street such as the western wall due to sensor dysfunction. However, the increase of ↓SW transmitted by the WR trees did not lead to an increase of the amount of ↑SW radiation reflected on the street surfaces which could have been expected. The LW radiation fluxes were not influenced by the water restriction either. No noticeable increase of the ↓LW measured at 0.78 m a.g.l. (under the tree crowns) was noticed for the WR trees which could have been caused by slight overheating of the WR trees' foliage highlighted previously (Table 3). No noticeable increase of the ↑LW at 0.78 m in the WR zone was found, as could have been expected by an eventual overheating of the ground in this zone as ↓SW radiation intercepted by the tree crowns progressively decreased during summer. Also, no noticeable increase of the ↑LW at 2 m in the WR zone was found which could have been caused by the slight overheating of the tree foliage and of the street's facades as highlighted for the eastern building.

Finally, the PCA presented in section 3.2.3.3 to cross-analyze the daily climatic benefits with the meteorological conditions showed that ΔUTCI was highly influenced by the daily insolation (GLOT) in both the WW and the WR zone (Figure 46 and Figure 47). Such results were consistent with the noticeable but low impact of the water restriction on radiation interception highlighted in the RSCS. Radiation interception still explains the major part of the

UTCI reduction even for WR trees as R^2 of the relationship between GLOT and ΔUTCI was 0.71 in the WW zone and 0.88 in the WR zone. Such results confirmed the previous findings of Herpin et al. (2022) who also reported a strong correlation between GLOT and UTCI reduction in the present RSCS at 0.4 m a.g.l. under well-watered trees ($R^2 = 0.75$).

The evolutions of radiation interception and of LAI could not be assessed in T&C. Nonetheless, it can be hypothesized that the growth interruption highlighted earlier during dry periods could lead to leaf loss and in the end to a decrease of radiation interception. Yet, the results of the RSCS show that the effect of a small defoliation on radiation interception tends to be limited and that only a strong leaf loss could affect strongly the radiation interception. It remains however unclear how different levels of hydric stress could affect the intensity and the temporal response of leaf loss.

5.3.3. Effect on air temperature and UTCI

In the RSCS, the water restriction had no noticeable impact on the air temperature measured under the tree crowns at 0.4 m a.g.l. although the WR trees strongly reduced their transpiration and gradually intercepted less short wavelength radiation, impacting the east wall surface temperature at 1 m a.g.l. as well as air temperature and absolute humidity at 1.5 m a.g.l.

An increased T_{mrt} difference was observed during daytime between both vegetated zones at 0.4 m a.g.l. both at the central axis of the street and close to the eastern wall. T_{mrt} was then progressively higher in the WR zone compared to the WW zone (Figure 44). On August 20th (day 46 of the water restriction), T_{mrt} was higher by 2.5 °C on average during daytime in the center of WR zone compared to the WW one while the difference between both zones was null before the water restriction (Table 9). T_{mrt} being only influenced by the SW and LW fluxes, this T_{mrt} increase was very likely caused by the decreasing amount of ↓SW radiation intercepted by the WR trees which led to an increasing exposure of the globe thermometers to direct sunlight. Considering the UTCI at 0.4 m a.g.l., very similar trends to the ones observed for T_{mrt} were reported both at the central axis of the street and close to the eastern wall. The UTCI calculation relies on 4 variables: T_a, RH, T_{mrt} and wind speed. Considering that UTCI is calculated with the same input wind speed data in both vegetated zones and that Ta and RH were not impacted by the water restriction at 0.4 m a.g.l., it can be inferred that UTCI increase under the WR trees (from 0.6 °C before to 1.6 °C in the end of the water restriction when averaged from 10:00 to 14:00 (Figure 28)) was driven by the T_{mrt} increase. Therefore, it means

that the reduction of the amount of radiation intercepted by the tree crowns was the main driver of the human thermal stress increase reported at 0.4 m a.g.l.

Still, the WR trees kept providing efficient human thermal stress reduction at 0.4 m a.g.l. Indeed, although their transpiration was strongly and quickly reduced, this effect was only noticeable inside the tree crowns. Moreover, the WR trees kept providing efficient cast shadows which, from an energetic point of view, form the major part of the energy dissipation provided by the trees (Figure 27).

Considering T&C, the climatic benefits provided by the different studied trees did not seem to be impacted by the studied dry event. The comparison of the benefits at the different stages of the dry event is not easy due to the changing climatic conditions and the daily variability of ΔT_a and ΔUTCI appeared to be greater than the eventual alteration of ΔT_a and ΔUTCI. The impact of the dry event on tree transpiration could not be studied especially as transpiration was not measured but it could be hypothesized that transpiration should be reduced when trees are experiencing branch growth interruption. However, considering the great contribution of radiation interception which was widely highlighted hereinabove, it is very likely that the dry event did not have any significant effect on the radiation interception provided by the trees which is why the trees kept providing important climatic benefits.

Finally, the effect of heatwaves on the climatic benefits provided by the trees was harder to study, especially because the definition of such periods is not easy. Indeed, heatwaves and dry events are likely to occur simultaneously which makes it difficult to assess the effect of high temperatures and low water availability independently. Thereby, it was not possible to find a period enabling to study the effect of heatwaves while ensuring a high water availability in T&C. In the RSCS, the hottest days came with high transpiration rates for the WW trees but similar high transpiration rates were also reported during cooler days with lower ET_{ref} (Figure 34). However, the hottest days were associated to unusually high DAmp for the WW trees (Figure 37) which may suggest that part the water contained in their tissues was used to sustain transpiration. In this case, the real amount of water transpired by the trees might have been slightly higher than the one calculated by the proposed water balance which only focuses on the soil compartment. The hottest days did not seem to have any impact on both the transpiration rate and DAmp for the WR trees. Moreover, it appeared that the UTCI reduction under the tree crowns was not related to the daily maximum T_a (Figure 47) and that both the WW and WR trees provided strong UTCI reduction under the tree crowns even during the heatwaves. Considering the strong dependence of UTCI reduction on radiation interception highlighted earlier, such results suggest that the tree foliage and the resulting radiation interception were

probably unaffected by the heatwaves in both vegetated zones. To go deeper into the analysis, further works should consider a higher number of days with contrasted T_a in order to be able to draw strong trends regarding the influence of T_a on the different uppermentioned variables. Also, more frequent assessment of the stomatal conductance and of the leaf area could be useful in order to analyze the short-term effects of heatwaves on tree physiology and morphology.

Chapter

6. Conclusion

With the multiplication and intensification of heatwaves induced by climate change, there is an urgent need to prevent human thermal stress from increasing especially in cities which are already characterized by an overheating phenomenon. Street trees provide interesting cooling benefits through the shadows they cast and are therefore widely promoted for the overheating and human thermal stress mitigation especially in cities. However, trees rely on a sufficient access to water to grow and the multiplication of droughts is likely to reduce the water availability for street trees which already need to cope with hard urban conditions. Then their ability to keep mitigating urban overheating under severe conditions such as heatwaves and droughts is at stake and remains widely unexplored. Yet, such benefits are subject to different sources of variability which have already been partly studied in the literature but the complete understanding of these benefits is not easy regarding the high number of variables involved, the high heterogeneity of the urban configurations and the important diversity of tree morphologies and physiological responses.

The present works proposed a wide assessment of the climatic benefits provided by street trees under varying climatic conditions through an original methodology relying on two complementary experimental facilities: a 1/5 scale canyon street, partially planted with young potted drip-irrigated ornamental apple trees (*Malus Coccinella*® 'Courtarou') located in Angers, France and the in-situ monitoring of the microclimate inside and outside the canopy of 36 mature street trees from 9 different tree species located in 5 sites in Paris (Trees & Climate study). Both experimental facilities were based on the detailed monitoring of the influence of trees on the urban microclimate with measurements along the soil-tree-atmosphere continuum.

6.1. Main results

The Trees & Climate study enabled to study trees experiencing real urban conditions but it highlighted the complexity of urban in-situ monitoring mainly caused by the high heterogeneity of the studied configurations and the high number of uncontrolled parameters. The reduced scale canyon street, although it only focused on one tree species, could provide a detailed assessment of the effect of a water restriction on the climatic benefits of street trees which can be used to provide a better understanding of the observations provided by the Trees & Climate study. In the end, the main conclusions of this work can be summarized as follows:

- The climatic benefits provided by street trees are characterized by an important temporal variability over the day as much as between consecutive days. The benefits are observed during daytime and may depend on the location of the trees inside the street. Also, the daily insolation is responsible for an important part of their variability, the greatest benefits being generally measured during the sunniest days. A PCA performed in both experimental facilities to cross-analyze the daily climatic benefits with the meteorological conditions showed that the daily UTCI reduction was highly influenced by the daily integral of the global incident radiation (R^2 of the linear relationships was 0.71 for the well-watered trees and 0.88 for the water-restricted trees in the reduced scale canyon street).

- The climatic benefits provided by street trees are characterized by an important spatial variability. While the effect of transpiration appears to be very localized and noticeable mainly close to the tree crowns, therefore at tree crown height, the shadows cast by the tree crowns have important effects on human thermal stress at human height as well as regarding the buildings surface temperature at different locations in the street depending on the position of the sun in the sky.

- In spite of their contrasted characteristics, both experimental facilities enabled to measure comparable climatic benefits. On one hand, T_a reductions ranging from 0.5 to 3 °C and UTCI reductions ranging from 4 to 11 °C were measured inside the tree crowns of the T&C trees compared to the outside canopy reference measurements (reference lamp posts). On the other hand, T_a was 1.8 °C lower inside the tree crowns (1 m a.g.l.) of the well-watered trees of the

reduced scale canyon street compared to the non-vegetated zone at the same location on average from 11:00 to 13:00 UTC during a sunny day. At the exact same time, T_a was lower by 3.3 °C and UTCI was lower by 7.4 °C under the crowns of the well-watered trees at the equivalent human height (0.4 m a.g.l.).

- Radiation interception appeared to be responsible for the greatest part (approximately 70 %) of the climatic benefits from an energetic point of view, the remaining 30 % being attributed to tree transpiration. The effect of radiation interception also appeared to be greater than the one of tree transpiration regarding the human thermal stress reduction.

- Due to their important dependence on radiation interception, the climatic benefits of street trees are very likely to be influenced by their morphological characteristics. Such an influence was not reported in the Trees & Climate study, probably because the meteorological measurements were too local and carried out inside the tree crowns and also because a complete radiation balance could not be performed in the Trees & Climate study. Nevertheless, a decrease of LAI appeared to lead to a decrease of radiation interception for the trees studied in the reduced scale canyon street (see hereinafter).

- The lack of water led to quick interruption of tree growth and a strong and quick decrease of tree transpiration for the potted *Malus Coccinella*® 'Courtarou' studied in the reduced scale canyon street. Transpiration of the water-restricted trees was already half the one of the well-watered trees on the second day of restriction and was on average 81 % lower than the one of the well-watered trees during the entire water restriction period. A decrease of the total leaf area and LAI of the water-restricted trees was reported (respectively from 2.5 to 1.8 $m^2.tree^{-1}$ and from 2.4 to 1.7 $m^2.m^{-2}$) which led to a decrease of their radiation interception (from 83 % of the daily integral of ↓SW before the water restriction to 76 % during the second month of the water restriction). However, their remaining foliage kept intercepting the major part of the incoming solar radiation even after 8 weeks of water restriction. A slight decrease of their UTCI reduction was measured but they kept providing efficient climatic benefits regarding both air temperature and human thermal stress.

- Although the impact of heatwaves could only be slightly approached, it did not appear to have a noticeable influence on tree transpiration nor on their radiation interception. As a consequence, street trees kept providing efficient climatic benefits even during very hot days.

- Contrasted growth dynamics were observed during a dry period for the different studied trees of the Trees & Climate study. On the one hand, *Sophora japonica* and *Tilia cordata* appeared to be very sensitive to the lack of water as their growth was strongly impacted even at high soil water potential. On the other hand, *Platanus x hispanica* and *Ulmus resista* appeared to be able to keep growing longer during the studied dry event. However, the low number of studied trees, the contrasted and uncontrolled soil water potential and the variability existing among the different trees of a given species caused by the high heterogeneity of the studied configurations, made it difficult to highlight an eventual species effect.

- In the Trees & Climate study, all the studied trees appeared to keep providing important climatic benefits even during a 40-day dry summer period. Although the transpiration rate of the trees could not be monitored, they were very likely to provide strong radiation interception all over the studied period which resulted in strong air temperature and human thermal stress reductions.

6.2. Perspectives

Although the short-term impact of the lack of water on the climatic benefits provided by street trees appeared to be low, noticeable impacts on tree physiology were reported. Different trees are likely to behave differently as suggested by the Trees & Climate study, but more detailed comparisons should be carried out using more controlled conditions and enabling to estimate precisely radiation interception and tree transpiration. In this way, the reduced scale canyon street studied in the present project or a similar approach could be used to compare different tree species. Also, the water restriction studied in the reduced scale canyon street started in July while the foliage of the trees was already well developed. However, water restriction occurring earlier in the growing season of the trees could have more important impact on their morphology which should be studied given the multiplication of early droughts induced by climate change in some regions.

Also, the medium-term effect of the lack of water on tree development could not be assessed in the frame of the present study. Yet, the succession of droughts may first lead to important morphological adjustments and also endanger the tree health. The trees resistance to drought must then also be assessed over longer periods of time in order to understand how long the different tree species are able to live under severe climatic conditions in the urban environment. Indeed, when urban trees have to be cut down, they are likely to be replaced by younger trees having a lower morphological development and thus providing lower climatic benefits. Thereby, it appears important to ensure that the trees planted in cities can live for a long time in order to provide a good continuity of services.

6.3. Take-home messages for stakeholders

Stakeholders and urban planners are at the moment looking for advices regarding the selection of tree species adapted to the future climates and providing interesting ecosystem services among which overheating mitigation. The present work may provide them with a few suggestions.

First, the noticeable benefits provided by the different tree species assessed in the Trees & Climate study showed that a variety of tree species may be selected. Yet, maximizing radiation interception appears to be very important regarding human thermal stress reduction. Therefore, trees should be selected, among others, on their ability to cast shadows. To do so,

morphological considerations such as the leaf density, the crown volume and crown projected area could be used. Also, the location of the trees inside the different urban sites should be studied carefully in order to maximize their radiation interception potential.

Then, trees require a sufficient access to water to keep developing their branches and foliage and by that means increasing their radiation interception potential. Thereby, attention should be paid to the soil compartment and tree pits should be wide and deep enough to maximize the amount of rainwater they receive as well as the volume of soil the tree roots can prospect. Also, ensuring a good development of the tree roots is likely to enable them to develop a wide crown, thereby maximizing their radiation interception.

Finally, the long-term resistance of trees to severe climatic conditions in urban environment being at stake, it appears crucial to collect data on the development and death of urban trees. The tree database managed by the green spaces department of the City of Paris is a good example and such a tool should be developed and generalized in order to better understand the life expectancy of the different tree species in urban environment, the different causes of death and try to relate tree death to the severe climatic events.

References

Aboelata, A., 2020. Vegetation in different street orientations of aspect ratio (H/W 1:1) to mitigate UHI and reduce buildings' energy in arid climate. Build. Environ. 172. https://doi.org/10.1016/j.buildenv.2020.106712

Aboelata, A., Sodoudi, S., 2020. Evaluating the effect of trees on UHI mitigation and reduction of energy usage in different built up areas in Cairo. Build. Environ. 168. https://doi.org/10.1016/j.buildenv.2019.106490

Adam, B., Ameglio, T., Coste, D., n.d. Système PépiPIAF.

AFP, 2022. A Paris, des feuilles mortes se ramassent (déjà) à la pelle.

Agence Parisienne du Climat, Météo-France, 2022. Changement climatique et adaptation sur la métropole du Grand Paris. Agence Parisienne du Climat.

Aida, M., 1982. Urban albedo as a function of the urban structure — A model experiment. Bound.-Layer Meteorol. 23, 405–413. https://doi.org/10.1007/BF00116269

Akbari, H., Davis, S., Dorsano, S., Huang, J., Winnett, S., 1992. Cooling our communities : A guide book on tree planting and light-coloured surfacing. United States Environmental Protection Agency EPA, Berkeley (CA) Usa.

Alderfasi, A.A., Nielsen, D.C., 2001. Use of crop water stress index for monitoring water status and scheduling irrigation in wheat. Agric. Water Manag. 47, 69–75. https://doi.org/10.1016/S0378-3774(00)00096-2

Ali-Toudert, F., Mayer, H., 2007. Thermal comfort in an east–west oriented street canyon in Freiburg (Germany) under hot summer conditions. Theor. Appl. Climatol. 87, 223–237.

Ali-Toudert, F., Mayer, H., 2006. Numerical study on the effects of aspect ratio and orientation of an urban street canyon on outdoor thermal comfort in hot and dry climate. Build. Environ. 41, 94–108. https://doi.org/10.1016/j.buildenv.2005.01.013

Alsaad, H., Hartmann, M., Hilbel, R., Voelker, C., 2022. The potential of facade greening in mitigating the effects of heatwaves in Central European cities. Build. Environ. 216. https://doi.org/10.1016/j.buildenv.2022.109021

Améglio, T., Archer, P., 1996. Représentativité du potentiel de base sur sols à humidité hétérogène 11.

Angeniol, C., Dianoux, C., 2023. Étude de la croissance des arbres grâce aux données de dendrochronologie. Info-Etudes Div. Expert. Sol Végétal Ville Paris 58, 28–36.

APUR, 2023a. Les arbres d'alignement à Paris en 2022 [WWW Document]. APUR. URL https://www.apur.org/fr/geo-data/arbres-alignement-paris-2022 (accessed 5.16.23).

APUR, 2023b. La canopée des arbres plantés sur les espaces publics parisiens. Etude comparative de 8 essences principales.

Armson, D., Rahman, M.A., Ennos, A.R., 2013. A Comparison of the Shading Effectiveness of Five Different Street Tree Species in Manchester, UK. ResearchGate.

Armson, D., Stringer, P., Ennos, A.R., 2012. The effect of tree shade and grass on surface and globe temperatures in an urban area. Urban For. Urban Green. 11, 245–255. https://doi.org/10.1016/j.ufug.2012.05.002

Arnfield, A.J., 2003. Two decades of urban climate research: a review of turbulence, exchanges of energy and water, and the urban heat island. Int. J. Climatol. 23, 1–26. https://doi.org/10.1002/joc.859

Arnold, C.L., Gibbons, C.J., 1996. Impervious Surface Coverage: The Emergence of a Key Environmental Indicator. J. Am. Plann. Assoc. 62, 243–258.

ASHRAE, 2020. (American Society of Heating, Refrigerating and Air-Conditioning Engineers) Standard 55-2020: Thermal Environmental Conditions for Human Occupancy.

Atger, C., 2015. Le système racinaire des arbres. Jard. Fr. URL https://www.jardinsdefrance.org/le-systeme-racinaire-des-arbres/ (accessed 12.22.21).

AURAV, 2020. L'arbre en Ville.

Bamdad, K., 2023. Cool roofs: A climate change mitigation and adaptation strategy for residential buildings. Build. Environ. 236. https://doi.org/10.1016/j.buildenv.2023.110271

Bastin, J.-F., Clark, E., Elliott, T., Hart, S., Hoogen, J. van den, Hordijk, I., Ma, H., Majumder, S., Manoli, G., Maschler, J., Mo, L., Routh, D., Yu, K., Zohner, C.M., Crowther, T.W., 2019. Understanding climate change from a global analysis of city analogues. PLOS ONE 14, e0217592. https://doi.org/10.1371/journal.pone.0217592

Basu, R., Samet, J.M., 2002. Relation between Elevated Ambient Temperature and Mortality: A Review of the Epidemiologic Evidence. Epidemiol. Rev. 24, 190–202. https://doi.org/10.1093/epirev/mxf007

Bernard, J., 2017. Signature géographique et météorologique des variations spatiales et temporelles de la température de l'air au sein d'une zone urbaine.

Bernard, J., Gros, A., Rodler, A., Morille, B., Musy, M., Kéravec, P., Guernouti, S., 2022. COOLPARKS: Observation du rafraîchissement d'un parc nantais au-delàa de son enceinte. Presented at the 35ème colloque annuel de l'Association Internationale de Climatologie, Toulouse, France.

Bernard, J., Kérazec, P., Morille, B., Bocher, E., Musy, M., Calmet, I., 2019. Outdoor Air Temperature Measurement: A Semi-Empirical Model to Characterize Shelter Performance. Climate 7.

Blankenship, R.E., 2021. Molecular Mechanisms of Photosynthesis. John Wiley & Sons.

Bonnardot, A., 2020. Carnet de conseils pour les plantations et l'entretien d'arbres en zones urbaines. CAUE 77.

Bournez, E., 2018. Etude du rôle de la végétation dans la création de microclimats urbains : approche combinée de mesures et de modélisations à différentes échelles.

Bouthier, A., Scheurer, O., Seger, M., Lagacherie, P., Beaudoin, N., Deschamps, T., Sauter, J., Fort, J.-L., Cousin, I., 2022. Réservoir en eau du sol utilisable par les cultures, Editions ARVALIS. ARVALIS.

Bouvard, C., Brender, P., Ducos, G., 2018. Objectif "zéro artificialisation nette" : Eléments de diagnostic, THEMA. Commissariat général au développement durable.

Bouyer, J., 2009. Modélisation et simulation des microclimats urbains - Étude de l'impact de l'aménagement urbain sur les consommations énergétiques des bâtiments (phdthesis). Université de Nantes.

Bowler, D.E., Buyung-Ali, L., Knight, T.M., Pullin, A.S., 2010. Urban greening to cool towns and cities: A systematic review of the empirical evidence. Landsc. Urban Plan. 97, 147–155.

Bozonnet, E., Allard, F., Musy, M., Chazelas, M., Guarracino, G., 2006. URBAT : Approche méthodologique de la construction durable en milieu urbain : le microclimat urbain et son impact environnemental sur les constructions.

Bréda, N., Cochard, H., Dreyer, E., Granier, A., 1993. Field comparison of transpiration, stomatal conductance and vulnerability to cavitation of Quercus petraea and Quercus robur under water stress. Ann. For. Sci. 50, 571–582.

Brendel, O., Cochard, H., 2011. Comment les espèces végétales s'adaptent au stress hydrique, in: L'Eau pour les Forêts et les Hommes en Région Méditerranéenne : un équilibre à trouver, What Science Can Tell Us.

Britton, C.M., Dodd, J.D., 1976. Relationships of photosynthetically active radiation and shortwave irradiance. Agric. Meteorol. 17, 1–7. https://doi.org/10.1016/0002-1571(76)90080-7

Bröde, P., Fiala, D., Błażejczyk, K., Holmér, I., Jendritzky, G., Kampmann, B., Tinz, B., Havenith, G., 2012. Deriving the operational procedure for the Universal Thermal Climate Index (UTCI). Int. J. Biometeorol. 56, 481–494. https://doi.org/10.1007/s00484-011-0454-1

Bröde, P., Jendritzky, G., Fiala, D., Havenith, G., 2010. The Universal Thermal Climate Index UTCI in Operational Use. Presented at the Adapting to Change: New Thinking on Comfort.

Brooke Anderson, G., Bell, M.L., 2011. Heat Waves in the United States: Mortality Risk during Heat Waves and Effect Modification by Heat Wave Characteristics in 43 U.S. Communities. Environ. Health Perspect. 119, 210–218. https://doi.org/10.1289/ehp.1002313

Burgess, S.S.O., Dawson, T.E., 2008. Using branch and basal trunk sap flow measurements to estimate wholeplant water capacitance: A caution. Plant Soil 305. https://doi.org/10.1007/s11104-007-9378-2

Burton, A., 2016. Les rues « canyons », des hotspots locaux de pollution de l'air [WWW Document]. URL https://www.sante-environnement.be/Les-rues-canyons-des-hotspots-locaux-de-pollution-de-l-air (accessed 5.12.20).

Callahan, C.W., Mankin, J.S., 2022. Globally unequal effect of extreme heat on economic growth. Sci. Adv. 8. https://doi.org/10.1126/sciadv.add3726

Cannavo, P., Guénon, R., Galopin, G., Vidal-Beaudet, L., 2018. Technosols made with various urban wastes showed contrasted performance for tree development during a 3-year experiment. Environ. Earth Sci. 77. https://doi.org/10.1007/s12665-018-7848-x

Canonne, D., Demotes-Mainard, S., Saudreau, M., Thierry, J., Dubuc, B., Ledroit, L., Cesbron, D., Lebras, C., Brialix, L., Lemesle, D., Herpin, S., Bournet, P.E., 2023. Impacts of water restriction on the development of urban trees and their associated climate services. Presented at the 2nd World Forum on Urban Forests, 16 - 20 October 2023mate services, Washington DC (USA).

Cantat, O., 2004. L'îlot de chaleur urbain parisien selon les types de temps. Norois Environ. Aménage. Société 191. https://doi.org/10.4000/norois.1373

Carlosena, L., Ruiz-Pardo, Álvaro, Rodríguez-Jara, E. Ángel, Santamouris, M., 2023. Worldwide potential of emissive materials based radiative cooling technologies to mitigate urban overheating. Build. Environ. 243. https://doi.org/10.1016/j.buildenv.2023.110694

Caspari, H.W., Green, S.R., Edwards, W.R.N., 1993. Transpiration of well-watered and water-stressed Asian pear trees as determined by lysimetry, heat-pulse, and estimated by a Penman-Monteith model. Agric. For. Meteorol. 67, 13–27. https://doi.org/10.1016/0168-1923(93)90047-L

Cassel, D.K., Nielsen, D.R., 1986. Field Capacity and Available Water Capacity, in: Methods of Soil Analysis: Part 1 Physical and Mineralogical Methods. Arnold Klute.

Castellani, B., 2021. Application of retro-reflective materials in urban canyon at different geographical locations. Build. Environ. 193. https://doi.org/10.1016/j.buildenv.2021.107676

CAUE 77, 2022. Plantations d'arbres et changement climatique - 36e Arborencontre 2022 [WWW Document]. URL (accessed 10.12.22).

CEREMA, 2023. Services EcoSystémiques rendus par les Arbres Modulés selon l'Essence - Déclinaison de l'outil Sesame sur le territoire Parisien.

CESER Pays de la Loire, 2016. Impacts des changements climatiques et mesures d'adaptation en Pays de la Loire [WWW Document]. URL http://ceser.paysdelaloire.fr/images/etudes-publications/environnement/2016_02_23_Rapport_Etude_Climat.pdf (accessed 6.15.20).

Chen, L., Zhang, Z., Li, Z., Tang, J., Caldwell, P., Zhang, W., 2011. Biophysical control of whole tree transpiration under an urban environment in Northern China. J. Hydrol. 402, 388–400. https://doi.org/10.1016/j.jhydrol.2011.03.034

Chen, S., Chen, Z., Feng, Z., Kong, Z., Xu, H., Zhang, Z., 2023. Species difference of transpiration in three urban coniferous forests in a semiarid region of China. J. Hydrol. 617, 129098. https://doi.org/10.1016/j.jhydrol.2023.129098

Chen, T., Meili, N., Simone, F., Hang, J., Tan, P.Y., Yuan, C., 2023. Effects of tree plantings with varying street aspect ratios on the thermal environment using a mechanistic urban canopy model. Build. Environ. 111006. https://doi.org/10.1016/j.buildenv.2023.111006

Chen, Y., Shan, B., Yu, X., 2022. Study on the spatial heterogeneity of urban heat islands and influencing factors. Build. Environ. 208. https://doi.org/10.1016/j.buildenv.2021.108604

Cheung, P.K., Fung, C.K.W., Jim, C.Y., 2020. Seasonal and meteorological effects on the cooling magnitude of trees in subtropical climate. Build. Environ. 177. https://doi.org/10.1016/j.buildenv.2020.106911

City of Paris, 2018. Paris Climate Action Plan. City of Paris.

Civiate, M., Mandel, F., 2008. L'abri météorologique. Météo-France.

Cochard, H., Granier, A., 1999. Fonctionnement hydraulique des arbres forestiers. Rev. For. Fr.

Comité pour l'économie verte, 2019. Les enjeux de l'artificialisation des sols : diagnostic.

Convertino, F., Vox, G., Schettini, E., 2021. Evaluation of the cooling effect provided by a green façade as nature-based system for buildings. Build. Environ. 203. https://doi.org/10.1016/j.buildenv.2021.108099

Corell, M., Girón, I.F., Galindo, A., Torrecillas, A., Torres-Sánchez, R., Pérez-Pastor, A., Moreno, F., Moriana, A., 2014. Using band dendrometers in irrigation scheduling Influence of the location inside the tree and comparison with point dendrometer. Agric. Water Manag. 142.

Coutts, A.M., White, E.C., Tapper, N.J., Beringer, J., Livesley, S.J., 2016. Temperature and human thermal comfort effects of street trees across three contrasting street canyon environments. Theor. Appl. Climatol. 124, 55–68.

CSTB, Météo France, 2012. Etude Pluridisciplinaire des Impacts du Changement climatique à l'Echelle de l'Agglomération parisienne.

Dahech, S., Charfi, S., Madelin, M., 2020. Représentativité des températures mesurées dans la station météorologique Paris-Montsouris. Climatologie 17.

Daudet, F.-A., Ameglio, T., Cochard, H., Archilla, O., Lacointe, A., 2005. Experimental analysis of the role of water and carbon in tree stem diameter variations. J. Exp. Bot.

De Dear, R., Brager, G.S., Reardon, J., Fergus, N., 1998. Developing an adaptive model of thermal comfort and preference. ASHRAE Trans. 104.

De Swaef, T., De Schepper, V., W. Vandegehuchte, M., Steppe, K., 2015. Stem diameter variations as a versatile research tool in ecophysiology. Tree Physiol. 35, 1047–1061.

Demotes-Mainard, S., Herpin, S., Boukouya, A., Mballo, S., Dubuc, B., Ledroit, L., Le Lebras, C., Lemesle, D., Bournet, P.E., 2022. Impacts of the urban environment on well-watered tree architectural development and tree climate services. Presented at the 31st International Horticultural Congress, Angers, France.

Deng, J., Pickles, B.J., Smith, S.T., Shao, L., 2020. Infrared radiative performance of urban trees: spatial distribution and interspecific comparison among ten species in the UK by in-situ spectroscopy. Build. Environ. 172. https://doi.org/10.1016/j.buildenv.2020.106682

Dervishi, V., Fleckenstein, C., Rahman, M.A., Pauleit, S., Ludwig, F., Pretzsch, H., Rötzer, T., 2023. Trees in planters – Growth, structure and ecosystem services of Platanus x

hispanica and Tilia cordata and their reaction to soil drought. Urban For. Urban Green. 86, 128024. https://doi.org/10.1016/j.ufug.2023.128024

Dietrich, L., Zweifel, R., Kahmen, A., 2018. Daily stem diameter variations can predict the canopy water status of mature temperate trees. Tree Physiol. 38, 941–952.

Dobbs, R.C., Scott, D.R.M., 1971. Distribution of diurnal fluctuations in stem cirumference of Douglas-fir. Can. J. For. Res. 1.

Doulos, L., Santamouris, M., Livada, I., 2004. Passive cooling of outdoor urban spaces. The role of materials. Sol. Energy 77, 231–249. https://doi.org/10.1016/j.solener.2004.04.005

Du, K., Ning, J., Yan, L., 2020. How long is the sun duration in a street canyon? —— Analysis of the view factors of street canyons. Build. Environ. 172. https://doi.org/10.1016/j.buildenv.2020.106680

Dubreuil, V., Foissard, X., Nabucet, J., Thomas, A., Quénol, H., 2020. Fréquence et intensité des îlots de chaleur à Rennes : bilan de 16 années d'observations (2004-2019). Climatologie 17, 6. https://doi.org/10.1051/climat/202017006

Ebel, R.C., Mattheis, J.P., Buchanan, D.A., 1995a. Drought stress of apple trees alters leaf emissions of volatile compounds. Physiol. Plant. 93, 709–712. https://doi.org/10.1111/j.1399-3054.1995.tb05120.x

Ebel, R.C., Proebsting, E.L., Evans, R.G., 2001. Apple Tree and Fruit Responses to Early Termination of Irrigation in a Semi-arid Environment. HortScience 36, 1197–1201. https://doi.org/10.21273/HORTSCI.36.7.1197

Ebel, R.C., Proebsting, E.L., Evans, R.G., 1995b. Deficit Irrigation to Control Vegetative Growth in Apple and Monitoring Fruit Growth to Schedule Irrigation. HortScience 30, 1229–1232. https://doi.org/10.21273/HORTSCI.30.6.1229

Ebel, R.C., Proebsting, E.L., Patterson, M.E., 1993. Regulated Deficit Irrigation May Alter Apple Maturity, Quality, and Storage Life. HortScience 28, 141–143. https://doi.org/10.21273/HORTSCI.28.2.141

Elgheznawy, D., Eltarabily, S., 2021. The impact of sun sail-shading strategy on the thermal comfort in school courtyards. Build. Environ. 202. https://doi.org/10.1016/j.buildenv.2021.108046

Esperon-Rodriguez, M., Power, S.A., Tjoelker, M.G., Marchin, R.M., Rymer, P.D., 2021. Contrasting heat tolerance of urban trees to extreme temperatures during heatwaves. Urban For. Urban Green. 66, 127387. https://doi.org/10.1016/j.ufug.2021.127387

Fan, H., Sailor, D.J., 2005. Modeling the impacts of anthropogenic heating on the urban climate of Philadelphia: a comparison of implementations in two PBL schemes. Atmos. Environ. 39, 73–84. https://doi.org/10.1016/j.atmosenv.2004.09.031

FAO, Allen, R.G., Pereira, L.S., Raes, D., Smith, M., 2006. Crop evapotranspiration (guidelines for computing crop water requirements), FAO Irrigation and Drainage Paper.

Fiala, D., Havenith, G., Bröde, P., Kampmann, B., Jendritzky, G., 2012. UTCI-Fiala multi-node model of human heat transfer and temperature regulation. Int. J. Biometeorol. 56, 429–441. https://doi.org/10.1007/s00484-011-0424-7

Fiala, D., Psikuta, A., Jendritzky, G., Paulke, S., Nelson, D.A., van Marken Lichtenbelt, W.D., Frijns, A.J.H., 2010. Physiological modeling for technical, clinical and research applications. Front. Biosci.-Sch. 2, 939–968.

Fini, A., Frangi, P., Comin, S., Vigevani, I., Rettori, A.A., Brunetti, C., Moura, B.B., Ferrini, F., 2022. Effects of pavements on established urban trees: Growth, physiology, ecosystem services and disservices. Landsc. Urban Plan.

Fisher, J.B., Baldocchi, D.D., Misson, L., Dawson, T.E., Goldstein, A.H., 2007. What the towers don't see at night: nocturnal sap flow in trees and shrubs at two AmeriFlux sites in California. Tree Physiol. 27, 597–610.

FISRWG, 1998. Stream Corridor Restoration: Principles, Processes and Practices. Federal Interagency Stream Restoration Working Group.

Fleck, R., Gill, R.L., Saadeh, S., Pettit, T., Wooster, E., Torpy, F., Irga, P., 2022. Urban green roofs to manage rooftop microclimates: A case study from Sydney, Australia. Build. Environ. 209. https://doi.org/10.1016/j.buildenv.2021.108673

Frei, A., 2023. Thermal properties of green, white and other building roof materials and solar insolation: A case study in New York City. Build. Environ. 244. https://doi.org/10.1016/j.buildenv.2023.110842

Gandemer, J., Guyot, A., 1976. Intégration du phénomène vent dans la conception du milieu bati. CSTB Sci. Batiments Nantes.

Garcia-Nevado, E., Duport, N., Bugeat, A., Beckers, B., 2021. Benefits of street sun sails to limit building cooling needs in a mediterranean city. Build. Environ. 187. https://doi.org/10.1016/j.buildenv.2020.107403

Ge, J., Wang, Y., Akbari, H., Zhou, D., Gu, Z., Meng, X., 2023. Cooling energy saving by vegetation planting in high-density districts: Evaluation using the coupled simulation. Build. Environ. 232. https://doi.org/10.1016/j.buildenv.2023.110054

Gebauer, R., Volařík, D., Houšková, K., Matoušková, M., Paschová, Z., Štykar, J., Vitásek, R., Urban, J., Plichta, R., 2023. Sensitivity of physiological traits to different short-term drought events and subsequent recovery at the sapling stage in European white elm (Ulmus laevis Pall.). Environ. Exp. Bot. 214, 105469. https://doi.org/10.1016/j.envexpbot.2023.105469

Geletič, J., Lehnert, M., Resler, J., Krč, P., Middel, A., Krayenhoff, E.S., Krüger, E., 2022. High-fidelity simulation of the effects of street trees, green roofs and green walls on the distribution of thermal exposure in Prague-Dejvice. Build. Environ. 223. https://doi.org/10.1016/j.buildenv.2022.109484

Gholami, M., Middel, A., Torreggiani, D., Tassinari, P., Barbaresi, A., 2023. A hybrid Python approach to assess microscale human thermal stress in urban environments. Build. Environ. 111054. https://doi.org/10.1016/j.buildenv.2023.111054

Gillner, S., Vogt, J., Tharang, A., Dettmann, S., Roloff, A., 2015. Role of street trees in mitigating effects of heat and drought at highly sealed urban sites. Landsc. Urban Plan. 143, 33–42. https://doi.org/10.1016/j.landurbplan.2015.06.005

Girona, J., Behboudian, M.H., Mata, M., Del Campo, J., Marsal, J., 2010. Exploring six reduced irrigation options under water shortage for Golden Smoothee apple: Responses of yield

components over three years. Agric. Water Manag. 98, 370–375. https://doi.org/10.1016/j.agwat.2010.09.011

Gräf, M., Immitzer, M., Hietz, P., Stangl, R., 2021. Water-Stressed Plants Do Not Cool: Leaf Surface Temperature of Living Wall Plants under Drought Stress. Sustainability 13. https://doi.org/10.3390/su13073910

Grimmond, C.S.B., 1992. The suburban energy balance: Methodological considerations and results for a mid-latitude west coast city under winter and spring conditions. Int. J. Climatol. 12, 481–497. https://doi.org/10.1002/joc.3370120506

Grimmond, C.S.B., Oke, T.R., 1991. An evapotranspiration-interception model for urban areas. Water Resour. Res. 27, 1739–1755. https://doi.org/10.1029/91WR00557

Hajat, S., Kovats, R.S., Atkinson, R.W., Haines, A., 2002. Impact of hot temperatures on death in London: a time series approach. J. Epidemiol. Community Health 56, 367–372. https://doi.org/10.1136/jech.56.5.367

Hang, J., Chen, G., 2022. Experimental study of urban microclimate on scaled street canyons with various aspect ratios. Urban Clim. 46.

Hang, J., Wang, D., Zeng, L., Ren, L., Shi, Y., Zhang, X., 2022. Scaled outdoor experimental investigation of thermal environment and surface energy balance in deep and shallow street canyons under various sky conditions. Build. Environ. 225. https://doi.org/10.1016/j.buildenv.2022.109618

Havenith, G., Fiala, D., Błazejczyk, K., Richards, M., Bröde, P., Holmér, I., Rintamaki, H., Benshabat, Y., Jendritzky, G., 2012. The UTCI-clothing model. Int. J. Biometeorol. 56, 461–470. https://doi.org/10.1007/s00484-011-0451-4

Heisler, G.M., 1986. Effects of individual trees on the solar radiation climate of small buildings. Urban Ecol. 9, 337–359.

Hendel, M., 2015. Pavement-Watering in Cities for Urban Heat Island Mitigation and Climate Change Adaptation : A Study of its Cooling Effects and Water Consumption in Paris. Sorbonne Paris Cité.

Herpin, S., Mballo, S., Manteau, M., Lemesle, D., Boukouya, A., Dubuc, B., Ledroit, L., Cannavo, P., Demotes-Mainard, S., Bournet, P.-E., 2024. Dataset for a reduced-scale canyon street to study tree climate benefits: summer 2020 data with well-watered apple trees - V1. https://doi.org/10.57932/29a2ba8b-87e8-4a5d-aba6-ebf6a8faa2c6

Herpin, S., Mballo, S., Thierry, J., Lemesle, D., Brialix, L., Rodriguez, F., Demotes-Mainard, S., Bournet, P.-E., 2022. Benefits of well-watered trees on street microclimate: what is the influence of meteorological conditions? Presented at the 35ème colloque annuel de l'Association Internationale de Climatologie.

Höppe, P., 1990. The physiological equivalent temperature – a universal index for the biometeorological assessment of the thermal environment. Int. J. Biometeorol. 43, 71–75.

Howard, L., 1833. The Climate of London: Deduced from Meteorological Observations Made in the Metropolis and at Various Places Around it. Harvey and Darton, J. and A. Arch, Longman, Hatchard, S. Highley [and] R. Hunter.

Huang, J., Cedeño-Laurent, J.G., Spengler, J.D., 2014. CityComfort+: A simulation-based method for predicting mean radiant temperature in dense urban areas. Build. Environ. 80, 84–95. http://dx.doi.org/10.1016/j.buildenv.2014.05.019

Hudişteanu, S.V., Popovici, C.G., Cherecheş, N.-C., 2018. Wind tunnel study of natural ventilation of building integrated photovoltaics double skin façade. E3S Web Conf. 32, 01020. https://doi.org/10.1051/e3sconf/20183201020

IPCC, 2023. Synthesis report of the IPCC sixth assessment report (AR6) 36.

Jackson, R.D., Idso, S.B., Reginato, R.J., Pinter Jr., P.J., 1981. Canopy temperature as a crop water stress indicator. Water Resour. Res. 17, 1133–1138. https://doi.org/10.1029/WR017i004p01133

Jamei, E., Rajagopalan, P., Seyedmahmoudian, M., Jamei, Y., 2016. Review on the impact of urban geometry and pedestrian level greening on outdoor thermal comfort. Renew. Sustain. Energy Rev. 54, 1002–1017. https://doi.org/10.1016/j.rser.2015.10.104

Konarska, J., Lindberg, F., Larsson, A., Thorsson, S., Holmer, B., 2014. Transmissivity of solar radiation through crowns of single urban trees—application for outdoor thermal comfort modelling. Theor. Appl. Climatol. 117, 363–376. https://doi.org/10.1007/s00704-013-1000-3

Konarska, J., Uddling, J., Holmer, B., Lutz, M., Lindberg, F., Pleijel, H., Thorsson, S., 2016. Transpiration of urban trees and its cooling effect in a high latitude city. Int. J. Biometeorol. 60, 159–172. https://doi.org/10.1007/s00484-015-1014-x

Kotzen, B., 2003. An investigation of shade under six different tree species of the Negev desert towards their potential use for enhancing micro-climatic conditions in landscape architectural development. J. Arid Environ. 55, 231–274.

Kuchcik, M., 2021. Mortality and thermal environment (UTCI) in Poland—long-term, multi-city study. Int. J. Biometeorol. 65, 1529–1541.

Kuglitsch, F.G., Toreti, A., Xoplaki, E., Della-Marta, P.M., Zerefos, C.S., Türkeş, M., Luterbacher, J., 2010. Heat wave changes in the eastern Mediterranean since 1960. Geophys. Res. Lett. 37. https://doi.org/10.1029/2009GL041841

Laaidi, K., 2012. Rôle des îlots de chaleur urbains dans la surmortalité observée pendant les vagues de chaleur. Institut de veille sanitaire.

Lacombe, M., 2011. Results of the WMO Intercomparison of thermometer screens / shields and hygrometers in hot desert conditions. World Meteorol. Organ., WMO/TD- No. 1579.

Lacombe, M., Bousri, D., Leroy, M., Mezred, M., 2011. WMO Field Intercomparison of Thermometer Screens/Shields and Humidity Measuring Instruments: Ghardaïa, Algeria, November 2008 – October 2009. World Meteorol. Organ. 515.

Landsberg, H.E., 1981. The Urban Climate. Academic Press.

Lecoeur, J., 2007. Influence d'un déficit hydrique sur le fonctionnement d'un couvert végétal cultivé.

Les Décodeurs, 2016. A quelles températures peut-on parler de canicule ? Le Monde.

Ling, S.L., Sanny, J., Moebs, W., 2016. University Physics: Volume3, openstax. Houston, Texas, USA.

Litvak, E., McCarthy, H.R., Pataki, D.E., 2017. A method for estimating transpiration of irrigated urban trees in California. Landsc. Urban Plan. 158, 48–61. https://doi.org/10.1016/j.landurbplan.2016.09.021

Liu, H., Huang, B., Cheng, X., Yin, M., Shang, C., Luo, Y., He, B.-J., 2023. Sensing-based park cooling performance observation and assessment: A review. Build. Environ. 245. https://doi.org/10.1016/j.buildenv.2023.110915

Liu, H., Lim, J.Y., Thet, B.W.H., Lai, P.-Y., Koh, W.S., 2022. Evaluating the impact of tree morphologies and planting densities on outdoor thermal comfort in tropical residential precincts in Singapore. Build. Environ. 221. https://doi.org/10.1016/j.buildenv.2022.109268

Liu, M., Pietzarka, U., Meyer, M., Kniesel, B., Roloff, A., 2022. Annual shoot length of temperate broadleaf species responses to drought. Urban For. Urban Green. 73. https://doi.org/10.1016/j.ufug.2022.127592

Marigo, M., Carnieletto, L., Moro, C., Arcelli, T., Ciloni, C., Turchi, G.P., De Carli, M., Di Bella, A., 2023. Thermal comfort and productivity in a workplace: An alternative approach evaluating productivity management inside a test room using textual analysis. Build. Environ. 245. https://doi.org/10.1016/j.buildenv.2023.110836

Matzarakis, A., Muthers, S., Rutz, F., 2015. Application and comparison of UTCI and PET in temperate climate conditions. Finisterra vol. 49 n.º 98 (2014). https://doi.org/10.18055/FINIS6453

Mballo, S., 2022. Quantification et modélisation des services climatiques rendus par les arbres dans une rue canyon.

Mballo, S., Herpin, S., Manteau, M., Demotes-Mainard, S., Bournet, P.E., 2021. Impact of well-watered trees on the microclimate inside a canyon street scale model in outdoor environment. Urban Clim. 37, 100844. https://doi.org/10.1016/j.uclim.2021.100844

Meili, N., Acero, J.A., Peleg, N., Manoli, G., Burlando, P., Fatichi, S., 2021. Vegetation cover and plant-trait effects on outdoor thermal comfort in a tropical city. Build. Environ. 195. https://doi.org/10.1016/j.buildenv.2021.107733

Mestayer, P.G., Anquetin, S., 1995. Climatology of Cities, in: Gyr, A., Rys, F.-S. (Eds.), Diffusion and Transport of Pollutants in Atmospheric Mesoscale Flow Fields, ERCOFTAC Series. Springer Netherlands, Dordrecht, pp. 165–189. https://doi.org/10.1007/978-94-015-8547-7_7

Météo-France, 2023. Ressource en eau, sécheresses et changement climatique [WWW Document]. Météo-Fr. URL https://meteofrance.com/changement-climatique/observer/changement-climatique-eau-et-secheresses (accessed 4.3.23).

Météo-France, 2022a. Vagues de chaleur et changement climatique [WWW Document]. Météo-Fr. URL https://meteofrance.com/changement-climatique/observer/changement-climatique-et-vagues-de-chaleur (accessed 4.3.23).

Météo-France, 2022b. Bulletin climatologique mensuel régional - Pays de la Loire - Juillet 2022.

Météo-France, 2022c. Bulletin climatologique mensuel régional - Pays de la Loire - Août 2022.

Météo-France, 2021. Bulletin climatique - Paris - Année 2021. Météo-France.

Météo-France, 2020. Planète : le changement climatique observé [WWW Document]. Météo-Fr. URL https://meteofrance.com/changement-climatique/observer/le-changement-climatique-observe-dans-le-monde (accessed 4.3.23).

Migliari, M., Babut, R., De Gaulmyn, C., Chesne, L., Baverel, O., 2022. The Metamatrix of Thermal Comfort: A compendious graphical methodology for appropriate selection of outdoor thermal comfort indices and thermo-physiological models for human-biometeorology research and urban planning. Sustain. Cities Soc. 81.

Moreno, R., Zamora, R., Moreno-García, N., Galán, C., 2023. Effects of composition and structure variables of urban trees in the reduction of heat islands; case study, Temuco city, Chile. Build. Environ. 245. https://doi.org/10.1016/j.buildenv.2023.110859

Musy, M., 2014. L'étude des microclimats urbains: champ de recherche à l'interface entre climatologie, urbanisme et génie-civil. VertigO- Rev. Électronique En Sci. Environ.

Naor, A., 2000. Midday stem water potential as a plant water stress indicator for irrigation scheduling in fruit trees. Acta Hortic. 447–454. https://doi.org/10.17660/ActaHortic.2000.537.52

Nortes, P.A., Pérez-Pastor, A., Egea, G., Conejero, W., Domingo, R., 2005. Comparison of changes in stem diameter and water potential values for detecting water stress in young almond trees. Agric. Water Manag., Special Issue on Land and Water Use: Environmental Management Tools and Practices 77, 296–307. https://doi.org/10.1016/j.agwat.2004.09.034

Oke, T.R., 1988. The urban energy balance. Prog. Phys. Geogr. Earth Environ. 12, 471–508. https://doi.org/10.1177/030913338801200401

Oke, T.R., 1987. Boundary Layer Climates, 2nd ed. Routledge, London. https://doi.org/10.4324/9780203407219

Oke, T.R., 1978. Boundary Layer Climates, 1st ed. Routledge, London.

Oke, T.R., 1973. City size and the urban heat island. Atmospheric Environ. 1967 7, 769–779. https://doi.org/10.1016/0004-6981(73)90140-6

Osroosh, Y., Peters, R.T., Campbell, C.S., 2016. Daylight crop water stress index for continuous monitoring of water status in apple trees. Irrig. Sci. 34, 209–219. https://doi.org/10.1007/s00271-016-0499-3

Ouyang, W., Morakinyo, T.E., Ren, C., Ng, E., 2020. The cooling efficiency of variable greenery coverage ratios in different urban densities: A study in a subtropical climate. Build. Environ. 174. https://doi.org/10.1016/j.buildenv.2020.106772

Ouzeau, G., Déqué, M., Jouini, M., Planton, S., Vautard, R., 2014. Le climat de la France au XXIe siècle. Rapp. Dir. Générale L'énergie Clim. Www Dev.-Durable Gouv Fr.

Peel, M.C., Finlayson, B.L., McMahon, T.A., 2007. Updated world map of the Köppen-Geiger climate classification. Hydrol. Earth Syst. Sci. 11, 1633–1644.

Plate, E.J., Kiefer, H., 2001. Wind loads in urban areas. J. Wind Eng. Ind. Aerodyn., Bluff Body Aerodynamics and Applications 89, 1233–1256. https://doi.org/10.1016/S0167-6105(01)00159-3

Priya, U.K., Senthil, R., 2021. A review of the impact of the green landscape interventions on the urban microclimate of tropical areas. Build. Environ. 205. https://doi.org/10.1016/j.buildenv.2021.108190

Rahman, M.A., Armson, D., Ennos, A.R., 2015. A comparison of the growth and cooling effectiveness of five commonly planted urban tree species. Urban Ecosyst. 18, 371–389. https://doi.org/10.1007/s11252-014-0407-7

Rahman, M.A., Ennos, A.R., 2016. What we know and don't know about the cooling benefits of urban trees. Trees Des. Action Group. https://doi.org/10.13140/RG.2.1.5122.2645

Rahman, M.A., Smith, J.G., Stringer, P., Ennos, A.R., 2011. Effect of rooting conditions on the growth and cooling ability of Pyrus calleryana. Urban For. Urban Green. 10, 185–192. https://doi.org/10.1016/j.ufug.2011.05.003

Rahman, M.A., Stratopoulos, L.M.F., Moser-Reischl, A., Zölch, T., Häberle, K.-H., Rötzer, T., Pretzsch, H., Pauleit, S., 2020. Traits of trees for cooling urban heat islands: A meta-analysis. Build. Environ. 170, 106606. https://doi.org/10.1016/j.buildenv.2019.106606

Rapoport, H.F., Costagli, G., Gucci, R., 2004. The Effect of Water Deficit during Early Fruit Development on Olive Fruit Morphogenesis. J. Am. Soc. Hortic. Sci. 129, 121–127. https://doi.org/10.21273/JASHS.129.1.0121

Renard, M., 2020. La dendrochronologie pour mieux connaître les arbres parisiens : étude de l'âge et de la croissance de tilleuls dans les parcs et en alignement. Info-Etudes Div. Expert. Sol Végétal Ville Paris 52, 34–43.

Ringenbach, N., 2004. Bilan radiatif et flux de chaleur en climatologie urbaine : Mesures,modélisation et validation sur Strasbourg (These de doctorat). Université Louis Pasteur (Strasbourg) (1971-2008).

Ritchie, H., Rodés-Guirao, L., Mathieu, E., Gerber, M., Ortiz-Ospina, E., Hasell, J., Roser, M., 2023. Population Growth [WWW Document]. Our World Data. URL https://ourworldindata.org/population-growth (accessed 1.16.24).

RTE, 2021. Futurs Energetiques 2050 - Principaux resultats.

Salvati, A., Kolokotroni, M., Kotopouleas, A., Watkins, R., Giridharan, R., Nikolopoulou, M., 2022. Impact of reflective materials on urban canyon albedo, outdoor and indoor microclimates. Build. Environ. 207. https://doi.org/10.1016/j.buildenv.2021.108459

Santamouris, M., Asimakopoulos, D., 1996. Passive Cooling of Buildings. Earthscan.

Santé Publique France, 2022. Bulletin de santé publique - Canicule et santé - Ile de France - Eté 2022.

Santé Publique France, 2020. Bulletin de santé publique - Canicule et santé - Ile de France - Eté 2020.

Santé Publique France, 2019. Bulletin de santé publique - Canicule et santé - Ile de France - Eté 2019.

Sass, R.L., n.d. It's not cool to be hot in Houston. Rice Univ. Programm Study Clim. Change Sci. Policy Public Underst. URL https://www.ruf.rice.edu/%7Esass/UHI.html (accessed 1.28.24).

Schütt, A., Becker, J.N., Gröngröft, A., Schaaf-Titel, S., Eschenbach, A., 2022. Soil water stress at young urban street-tree sites in response to meteorology and site parameters. Urban For. Urban Green. 75. https://doi.org/10.1016/j.ufug.2022.127692

Serbin, S.P., Townsend, P.A., 2020. Scaling Functional Traits from Leaves to Canopies, in: Cavender-Bares, J., Gamon, J.A., Townsend, P.A. (Eds.), Remote Sensing of Plant Biodiversity. Springer International Publishing, Cham, pp. 43–82. https://doi.org/10.1007/978-3-030-33157-3_3

Shahidan, Mohd.F., Shariff, M.K.M., Jones, P., Salleh, E., Abdullah, A.M., 2010. A comparison of Mesua ferrea L. and Hura crepitans L. for shade creation and radiation modification in improving thermal comfort. Landsc. Urban Plan. 97, 168–181.

Sharmin, M., Tjoelker, M.G., Pfautsch, S., Esperon-Rodriguez, M., Rymer, P.D., Power, S.A., 2023. Tree crown traits and planting context contribute to reducing urban heat. Urban For. Urban Green. 83, 127913. https://doi.org/10.1016/j.ufug.2023.127913

Shashua-Bar, L., Rahman, M.A., Moser-Reischl, A., Peeters, A., Franceschi, E., Pretzsch, H., Rötzer, T., Pauleit, S., Winters, G., Groner, E., Cohen, S., 2023. Do urban tree hydraulics limit their transpirational cooling? A comparison between temperate and hot arid climates. Urban Clim. 49, 101554. https://doi.org/10.1016/j.uclim.2023.101554

Souch, C.A., Souch, C., 1993. The effect of trees on summertime below canopy urban climates: a case study. Bloomington, Indiana. J. Arboric. 19, 303–312.

Staiger, H., Laschewski, G., Matzarakis, A., 2019. Selection of Appropriate Thermal Indices for Applications in Human Biometeorological Studies. Atmosphere 10, 18. https://doi.org/10.3390/atmos10010018

Stirbet, A., Lazár, D., Guo, Y., Govindjee, G., 2020. Photosynthesis: basics, history and modelling. Ann. Bot. 126, 511–537. https://doi.org/10.1093/aob/mcz171

Sun, C., Lian, W., Liu, L., Dong, Q., Han, Y., 2022. The impact of street geometry on outdoor thermal comfort within three different urban forms in severe cold region of China. Build. Environ. 222. https://doi.org/10.1016/j.buildenv.2022.109342

Syndicat intercommunal de la vallée de l'Orge Aval, n.d. Le fonctionnement de l'arbre.

Tabatabaei, S.S., Fayaz, R., 2023. The effect of facade materials and coatings on urban heat island mitigation and outdoor thermal comfort in hot semi-arid climate. Build. Environ. 243. https://doi.org/10.1016/j.buildenv.2023.110701

Taha, H., 1997. Urban climates and heat islands: albedo, evapotranspiration, and anthropogenic heat. Energy Build. 25, 99–103. https://doi.org/10.1016/S0378-7788(96)00999-1

Taiz, L., Zeiger, E., 2002. Plant Physiology, 3rd ed. Sinauer Associates.

Tan, P.Y., Wong, N.H., Tan, C.L., Jusuf, S.K., Schmiele, K., Chiam, Z.Q., 2020. Transpiration and cooling potential of tropical urban trees from different native habitats. Sci. Total Environ. 705, 135764. https://doi.org/10.1016/j.scitotenv.2019.135764

Teshnehdel, S., Akbari, H., Di Giuseppe, E., Brown, R.D., 2020. Effect of tree cover and tree species on microclimate and pedestrian comfort in a residential district in Iran. Build. Environ. 178. https://doi.org/10.1016/j.buildenv.2020.106899

Teskey, R., Wertin, T., Bauweraerts, I., Ameye, M., Mcguire, M.A., Steppe, K., 2015. Responses of tree species to heat waves and extreme heat events. Plant Cell Environ. 38, 1699–1712. https://doi.org/10.1111/pce.12417

Thierry, J., Herpin, S., Maturana, L., Demotes-Mainard, S., Rodriguez, F., Cannavo, P., Bournet, P.-E., 2022. Impact of a moderate water stress on the microclimatic services provided by street trees: an experimental study inside an outdoor canyon street scale model. Presented at the 35th annual congress of the International Association of Climatology, Toulouse, France.

Ueda, M., Yoshikawa, K., Okitu, J., 1996. Measurement of diurnal changes in stem and branch diameters using strain gauges. J. For. Res. 1.

Unger, J., 2006. Modelling of the annual mean maximum urban heat island using 2D and 3D surface parameters. Clim. Res. 30, 215–226.

United Nations Department of Economic and Social Affairs, 2018. World Urbanization Prospects: The 2018 Revision - Keyfacts. New-York.

United Nations Department of Economic and Social Affairs, Population Division, 2022. World Population Prospects 2022: Summary of Results (No. UN DESA/POP/2022/TR/NO. 3). New-York.

USDA Natural Resources Conservation Service, n.d. Soil Texture Calculator [WWW Document]. URL https://www.nrcs.usda.gov/resources/education-and-teaching-materials/soil-texture-calculator

Vachon, B., 2015. Comment le plan national canicule fonctionne-t-il ? Le Monde.

Vailshery, L.S., Jaganmohan, M., Nagendra, H., 2013. Effect of street trees on microclimate and air pollution in a tropical city. Urban For. Urban Green. 12, 408–415.

Vialet-Chabrand, S., 2013. Modélisation des variations journalières de la conductance stomatique: apport d'une approche dynamique et conséquences sur l'efficience intrinsèque d'utilisation de l'eau chez le chêne (PhD Thesis). Université de Lorraine.

Vidal-Beaudet, L., Grosbellet, C., Forget-Caudel, V., Charpentier, S., 2012. Modelling long-term carbon dynamics in soils reconstituted with large quantities of organic matter. Eur. J. Soil Sci. 63, 787–797. https://doi.org/10.1111/j.1365-2389.2012.01494.x

Ville de Paris, 2024a. Paris pour le climat [WWW Document]. URL https://www.paris.fr/pages/paris-pour-le-climat-2148 (accessed 1.19.24).

Ville de Paris, 2024b. Tout savoir sur l'arbre à Paris [WWW Document]. URL https://www.paris.fr/pages/l-arbre-a-paris-199 (accessed 1.19.24).

Ville de Paris, 2023. Guide des essences de Paris - Mode d'emploi.

Wang, X., Liu, G., Zhang, N., Liu, H., Tang, X., Lyu, M., Meng, H., 2023. Effects of cooling roofs on mitigating the urban heat island and human thermal stress in the Pearl River Delta, China. Build. Environ. 245. https://doi.org/10.1016/j.buildenv.2023.110880

Wang, Z., Li, Y., Song, J., Wang, K., Xie, J., Chan, P.W., Ren, C., Di Sabatino, S., 2022. Modelling and optimizing tree planning for urban climate in a subtropical high-density city. Urban Clim. 43, 101141. https://doi.org/10.1016/j.uclim.2022.101141

Wardeh, Y., Kinab, E., Escadeillas, G., Rahme, P., Ginestet, S., 2022. Review of the optimization techniques for cool pavements solutions to mitigate Urban Heat Islands. Build. Environ. 223. https://doi.org/10.1016/j.buildenv.2022.109482

Whiting, D., Roll, M., Vickerman, L., 2023. Plant Physiology: Photosynthesis, Transpiration, and Respiration.

Wright, A., Young, A., Natarajan, S., 2005. Dwelling temperatures and comfort during the August 2003 heat wave. Build. Serv. Eng. Res. Technol. 26, 285–300. https://doi.org/10.1191/0143624405bt136oa

Yan, C., Guo, Q., Li, H., Li, L., Qiu, G.Y., 2020. Quantifying the cooling effect of urban vegetation by mobile traverse method: A local-scale urban heat island study in a subtropical megacity. Build. Environ. 169. https://doi.org/10.1016/j.buildenv.2019.106541

Yu, K., Van Geel, M., Ceulemans, T., Geerts, W., Ramos, M.M., Sousa, N., Castro, P.M.L., Kastendeuch, P., Najjar, G., Ameglio, T., Ngao, J., Saudreau, M., Honnay, O., Somers, B., 2018. Foliar optical traits indicate that sealed planting conditions negatively affect urban tree health. Ecol. Indic. 95, 895–906. https://doi.org/10.1016/j.ecolind.2018.08.047

Zander, K.K., Botzen, W.J.W., Oppermann, E., Kjellstrom, T., Garnett, S.T., 2015. Heat stress causes substantial labour productivity loss in Australia. Nat. Clim. Change 5, 647–651.

Zare, S., Hasheminejad, N., Shirvan, H.E., Hemmatjo, R., Sarebanzadeh, K., Ahmadi, S., 2018. Comparing Universal Thermal Climate Index (UTCI) with selected thermal indices/environmental parameters during 12 months of the year. Weather Clim. Extrem. 19, 49–57. https://doi.org/10.1016/j.wace.2018.01.004

Zhang, T., Hong, B., Su, X., Li, Y., Song, L., 2022. Effects of tree seasonal characteristics on thermal-visual perception and thermal comfort. Build. Environ. 212. https://doi.org/10.1016/j.buildenv.2022.108793

Zhang, Y., Yang, Y., Zhang, L., Zhao, C., Yan, J., Liu, M., Zhao, L., 2022. Seasonal variation in leaf area index and its impact on the shading effects of vertical green facades in subtropical areas. Build. Environ. 225. https://doi.org/10.1016/j.buildenv.2022.109629

Zhao, Y., Zhao, K., Zhang, X., Zhang, Y., Du, Z., 2024. Assessment of combined passive cooling strategies for improving outdoor thermal comfort in a school courtyard. Build. Environ. 111247. https://doi.org/10.1016/j.buildenv.2024.111247

Zheng, S., Guldmann, J.-M., Wang, Z., Qiu, Z., He, C., Wang, K., 2021. Experimental and theoretical study of urban tree instantaneous and hourly transpiration rates and their cooling effect in hot and humid area. Sustain. Cities Soc. 68, 102808. https://doi.org/10.1016/j.scs.2021.102808

Zuckerman, N., Lensky, I.M., 2023. Thermal performance of vertical greenery systems (VGS) in a street canyon: A real-scale long-term experiment. Build. Environ. 244. https://doi.org/10.1016/j.buildenv.2023.110750

Zweifel, R., Steppe, K., Sterck, F.J., 2007. Stomatal regulation by microclimate and tree water relations: interpreting ecophysiological field data with a hydraulic plant model. J. Exp. Bot. 58, 2113–2131.

7. Appendices

7.1. Reduced Scale Canyon Street (RSCS)

7.1.1. Optical and thermal properties of the materials

Table 23 summarizes the main characteristics of the materials used to build the reduced scale canyon street including some optical and thermal properties. These properties were published online together with the dataset associated with the measurement campaign performed in 2020 with the present reduced scale canyon street (Herpin et al., 2024). Emissivity was measured through non-direct infrared reflectometry (THEMACS EM-4) by E. Bozonnet from the LASIE research unit based at La Rochelle University and thermal conductivity of the concrete walls was measured by N. Issaadi and M. Muanda from GEM research unit based at Ecole Centrale Nantes. Other characteristics such as thermal capacity and albedo were not yet known when writing the present manuscript.

Table 23: Main properties and characteristics of the materials used to build the Reduced Scale Canyon Street (RSCS).

Material	Reference	Location in the street	Density	Thermal conductivity	Emissivity (hemispheric)	Emissivity (directionnal-normal)	Moisture properties
Expanded polystyrene *(12 cm thick)*	PRB ISOL BD	Inner side of buiding walls (walls next to the street)		Manufacturer: 0.0375 $W.m^{-1}.K^{-1}$ (NF EN 13163 : 2013)	0.64	0.66	
Concrete *(approx. 10 cm thick)*	CONSOLIS BONNA SABLA STOC'L and STOC'T	Building walls (walls next to the street)		2.398 $W.m^{-1}.K^{-1}$ (Hot disk measurement in GEM lab)			
OSB wood pannel *(approx 12 mm thick)*	OSB 3 KRONOPLY	Building roof and walls (walls next to outer environment)	Between 616 $kg.m^{-3}$ and 700 $kg.m^{-3}$	Manufacturer: 0.13 $W.m^{-1}.K^{-1}$ (NF EN 13986 : 2004 : A1 2015)	0.86	0.91	μ=50 (dry) ; μ=30 (humid)
Polycarbonate plate		Street ground, on tree pits					
Bituminous felt		street ground, on tree pits			0.89	0.94	

Material	Reference	Location in the street	Density	Thermal conductivity	Emissivity (hemispheric)	Emissivity (directionnal-normal)	Moisture properties
White steel pan *(0.75 mm thick)*	SPO SPONDINE 980 RAL 9010	Building roof and walls (walls next to outer environment)			0.79	0.83	
Gravel		Floor inside the building			0.87	0.92	
Weather barrier in polypropylene	HPV Delta Neovent	Building roof and walls (walls next to outer environment)					Sd=0.02m (EN ISO 12572), waterproofness W1 (EN 1928)
Black asphalt *(approx 4 cm thick)*		Street ground			0.88	0.93	
White plaster		Street walls (walls next to the street)			0.87	0.92	
Lawn		Outside the street, next to north mast			0.89	0.94	

7.1.2. Microclimate differences between the two vegetated zones at different positions inside the street

In addition to the evolution of the AH, T_a, T_{mrt} and UTCI presented in sections 3.2.3.2.3 to 3.2.3.2.6 at different positions inside the street for the 3 typical sunny days, the differences calculated for these four variables between the WR and the WW zone are presented hereinafter.

7.1.2.1. Air absolute humidity

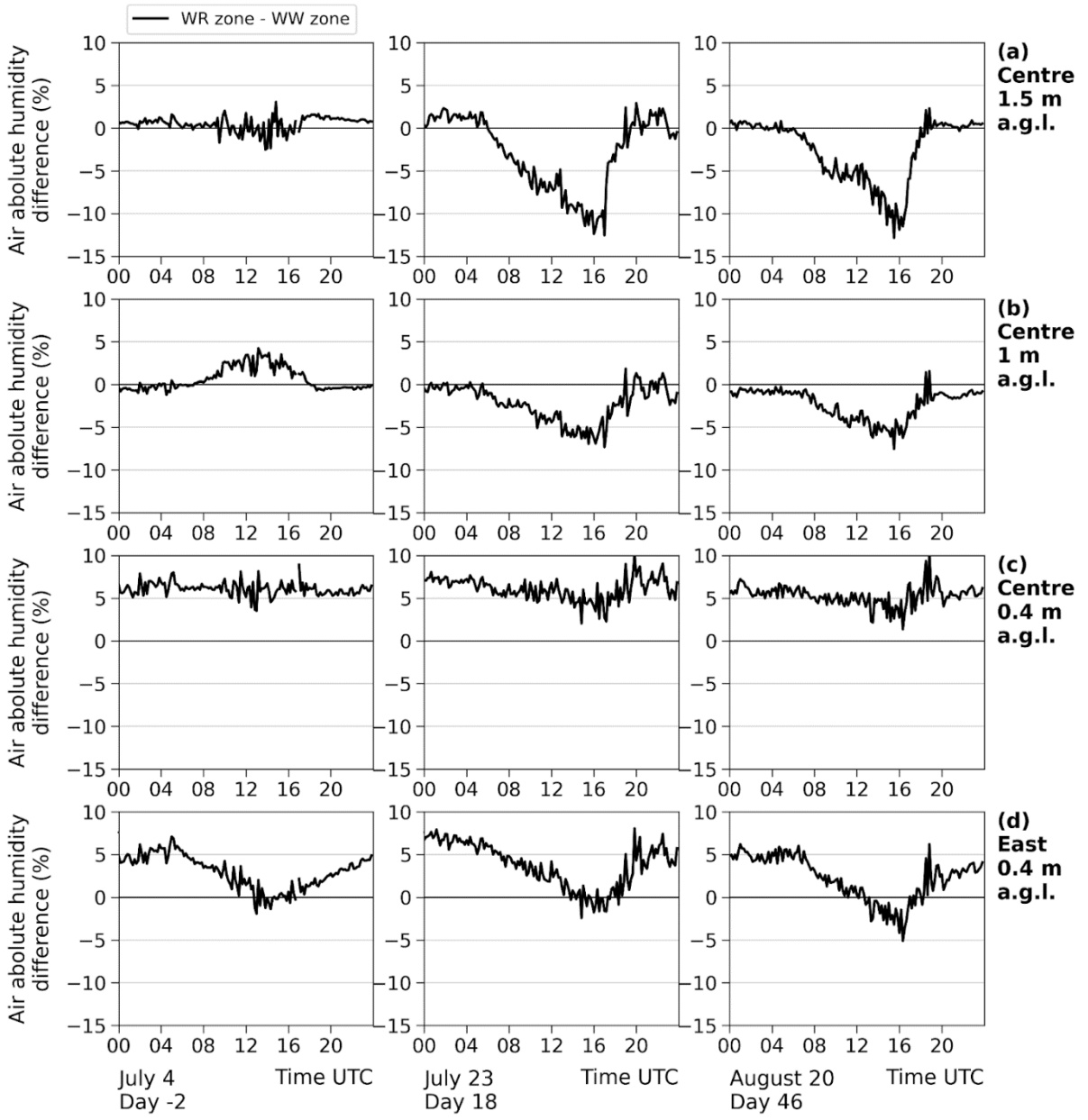

Figure 91: Evolution of the air absolute humidity difference between both vegetated zones (WR zone - WW zone) calculated at 4 different positions for the 3 typical sunny days of summer 2022.

7.1.2.2. Air temperature

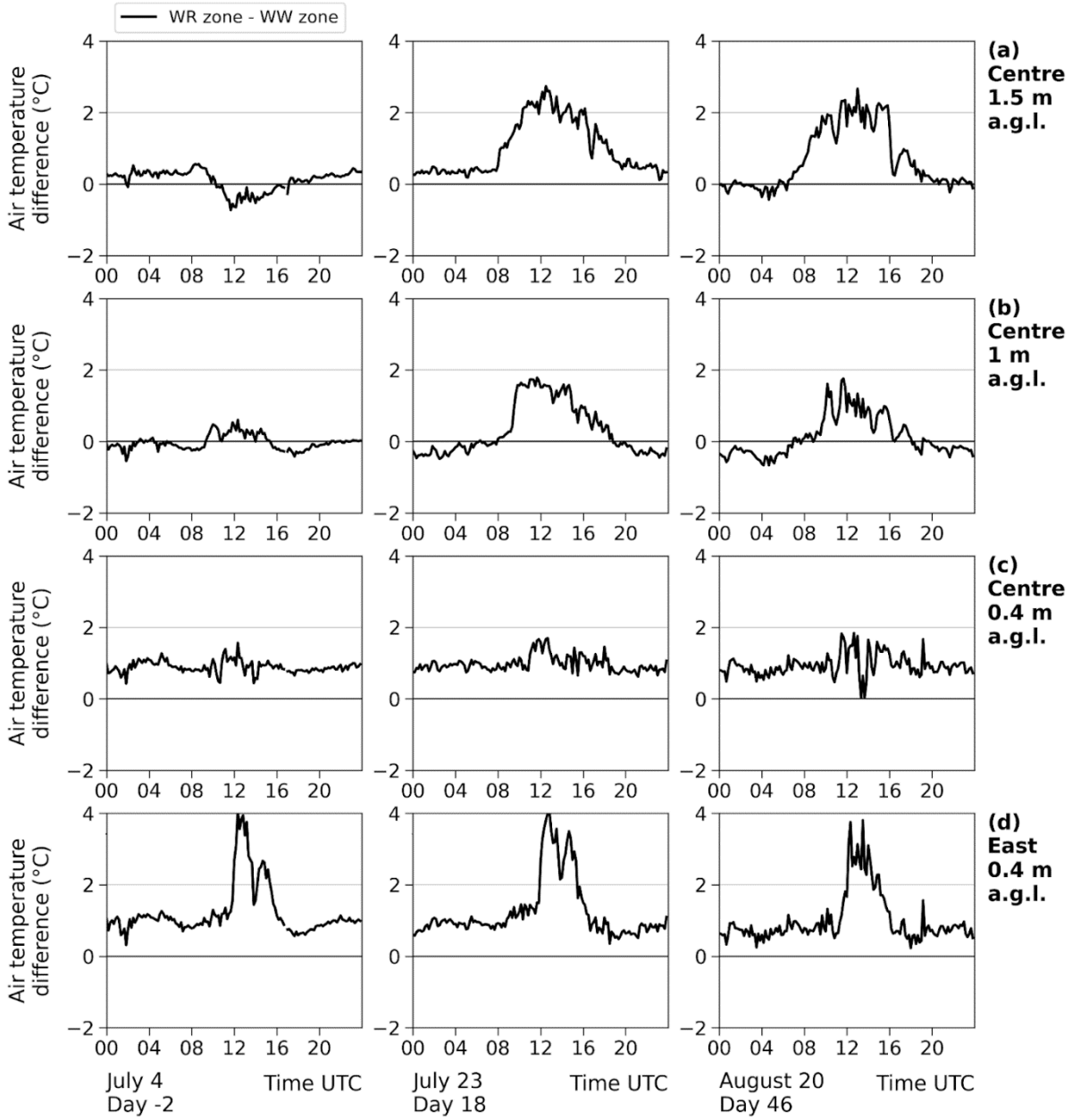

Figure 92: Evolution of the air temperature difference between both vegetated zones (WR zone - WW zone) calculated at 4 different positions for the 3 typical sunny days of summer 2022.

7.1.2.3. Mean radiant temperature

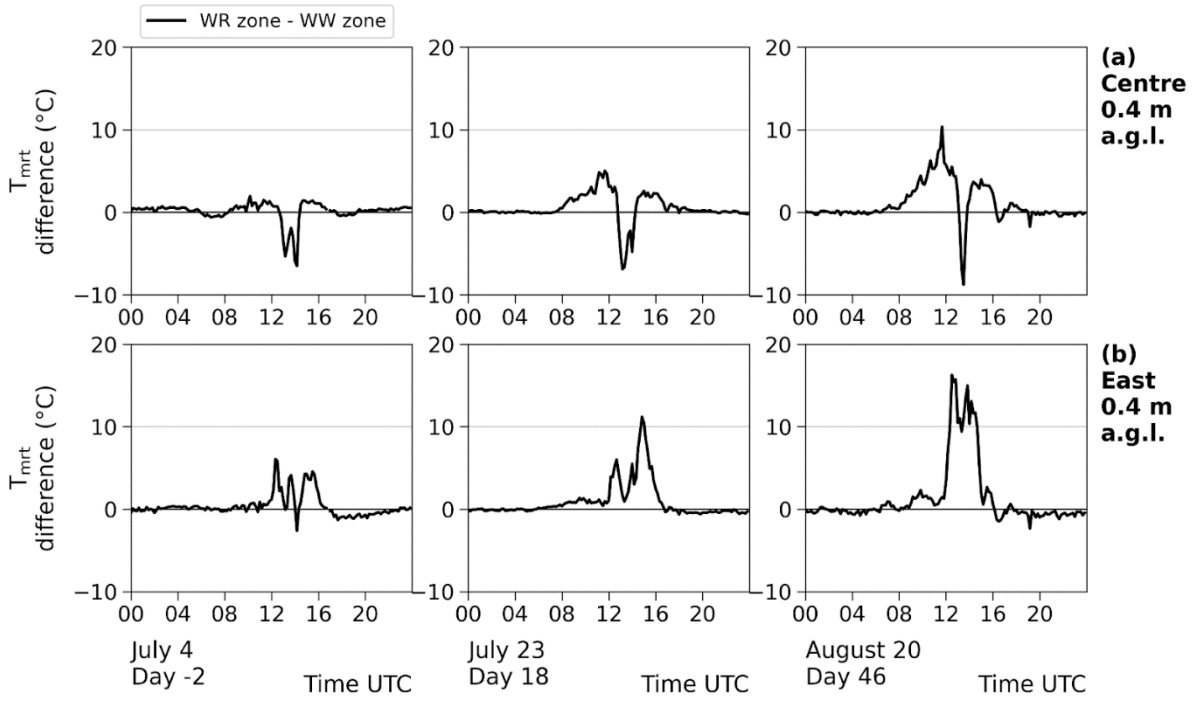

Figure 93: Evolution of the mean radiant temperature (T_{mrt}) difference between both vegetated zones (WR zone - WW zone) calculated at 4 different positions for the 3 typical sunny days of summer 2022.

7.1.2.4. UTCI

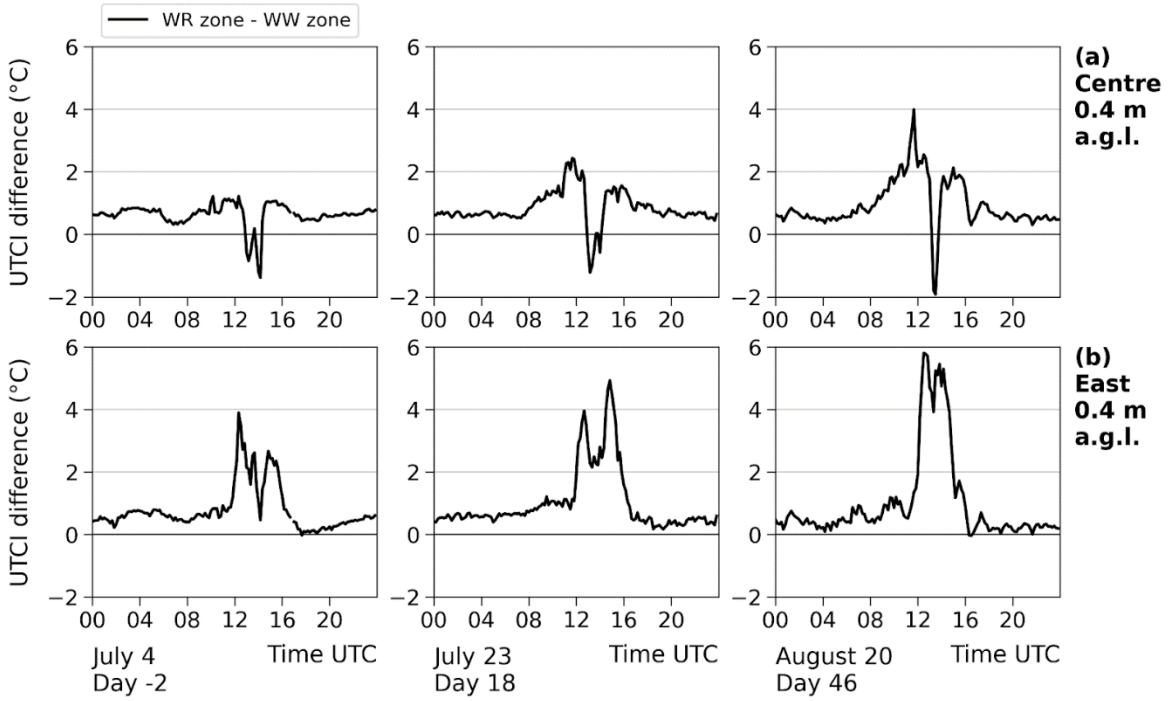

Figure 94: Evolution of the UTCI difference between both vegetated zones (WR zone - WW zone) calculated at 4 different positions for the 3 typical sunny days of summer 2022.

7.1.3. Air temperature and relative humidity sensors check

During the monitoring campaign performed in the reduced scale canyon street of Angers in summer 2022, an unexpected offset was noticed for T_a and RH measurements at 0.4 m a.g.l. on the central axis of the street when comparing both vegetated zones of the street. This offset was noticed even when focusing on night-time periods or periods before the water restriction. A focus on data acquired earlier in spring 2022 (data not shown in the present manuscript) also revealed that this offset was present even when the studied trees were still leafless. Such offset therefore has to be taken into account when comparing the measurements performed under the tree crowns of both vegetated zones.

In order to know more about the impact of this offset on the analyses and to provide a potential correction, the sensors used for T_a and RH measurements at 0.4 m a.g.l. on the central axis were compared after the end of the summer 2022 monitoring campaign.

7.1.3.1. Materials and methods

The sensors used for T_a and RH measurements at 0.4 m a.g.l. on the central axis of the street in the 2022 measurement campaign were placed in mechanically ventilated white painted cylindrical shelters and mounted next to each other on the roof of the eastern building of the canyon street as shown on Figure 95. The three zones of the street were equipped with slightly different sensors as reported in Table 2. The WW zone was equipped with HMP110 (Vaisala, Finland) while the WR and the NV zone were equipped with HMT330 (Vaisala, Finland). T_a and RH were monitored from October 4th to 7th 2022 at 10-min time step intervals.

Figure 95: Picture of the air temperature and relative humidity sensors placed in mechanically ventilated white painted cylindrical shelters, initially mounted at 0.4 m a.g.l. on the central axis of the street in the NV, WW and WR zones, being compared on the roof of the eastern building of the canyon street. The additional sensor appearing on the picture was not studied in the frame of the present project.

7.1.3.2. Results

T_a measured by the WW zone sensor appeared to be lower than the ones measured by both other sensors almost all the time. T_a was on average 0.7 °C higher in the WR zone sensor at night (from 18:00 to 06:00 UTC) compared to the WW zone one (Figure 96). During the day, this difference increased especially around noon and reached on average 1.2 °C from 10:00 to 14:00 UTC.

T_a was on average 0.5 °C higher in the NV zone sensor compared to the WW one at night (from 18:00 to 06:00 UTC). However, the difference of T_a between the NV and the WW zone sensor was highly variable. It was generally higher than 0.5 °C during the night of October 4th while it was very close to 0 °C during the night of October 7th. During the day, this difference increased especially around noon and reached on average 1.9 °C from 10:00 to 14:00 UTC with important daily contrasts as this difference barely exceeded 2 °C on October 5th but approached 4 °C on October 7th.

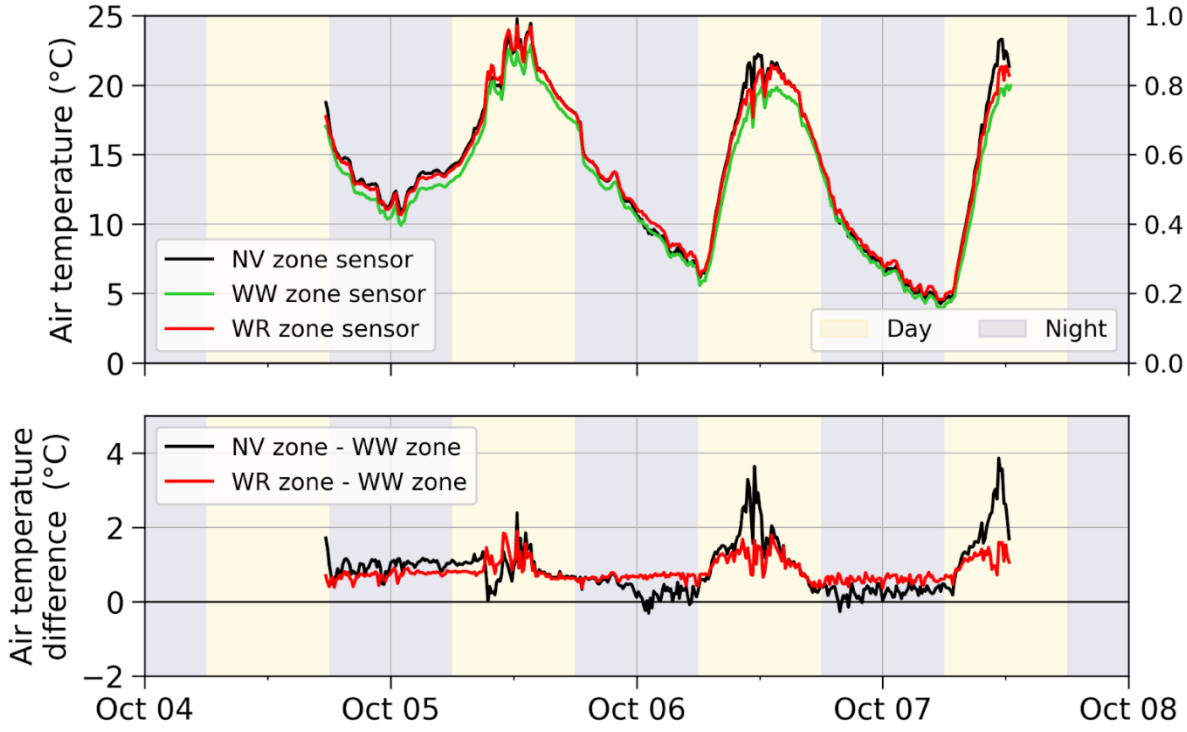

Figure 96: Evolution of the air temperature measured by the sensors initially placed in the three zones of the street and of the difference between pairs of sensors from October 4th to 7th, 2022.

RH measured with the WR zone sensor was slightly higher at night (1.5 pt% from 18:00 to 06:00 UTC) but slightly lower during the day, especially around noon (-0.7 pt%) compared with RH measured with the WW zone sensor (Figure 97).

RH measured with the NV zone sensor was generally lower than the one measured with the WW zone sensor but a strong variability was reported when comparing daytime and night-time. As for T_a, contrasted results were found during the night of October 4th (difference lower than -5 pt%) and during the nights of October 6th and 7th (average difference close to 0 pt%). During the day, RH measured with the NV zone sensor was up to 8.7 pt% lower and on average 4.5 pt% lower than RH measured with the WW zone sensor from 10:00 to 14:00 UTC.

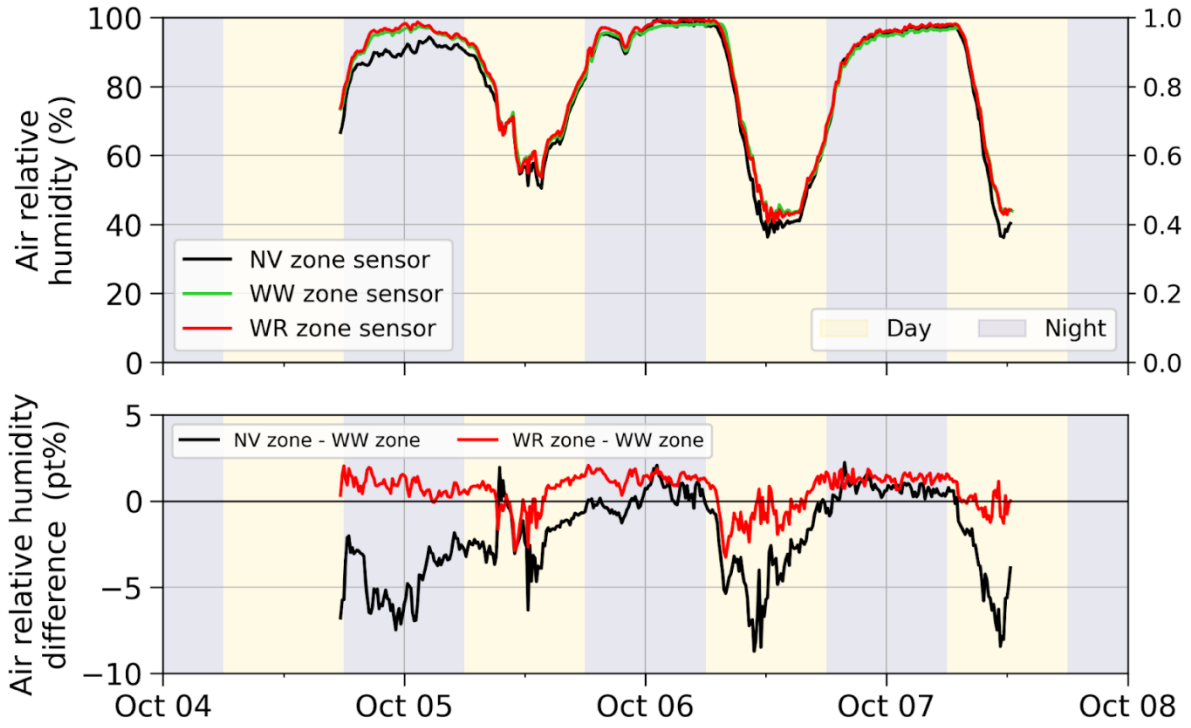

Figure 97: Evolution of the air relative humidity measured by the sensors initially placed in the three zones of the street and of the difference between pairs of sensors from October 4th to 7th, 2022.

7.1.3.3. Conclusion

The present comparison only lasted 3 days but it enabled to highlight noticeable differences of T_a and RH measured by the three sensors used in the 2022 summer campaign. The T_a differences were high regarding the platinum probes accuracy (± 0.2 °C, see Table 2 presented in section 3.1.2.1.3). RH differences were comparable to the capacitive probes accuracy (± 1.5 %, Table 2 presented in section 3.1.2.1.3) when comparing the WR and WW zone sensors but they were higher than the capacitive probes accuracy when comparing the NV and WW zone sensors.

Such results however need to be analyzed in the frame of the characteristics of the present experiment. The sensors (and shelters) were placed on top of the white painted roof of the eastern building of the canyon street. Compared to their previous location at 0.4 m a.g.l.

inside the street, they were then subject to a much higher SVF and were placed over a more reflective surface. Thereby, the shelters were exposed to a much higher amount of downward radiation (induced by the higher SVF) and upward radiation (reflected on the white painted roof of the eastern building) which may have reduced their efficiency. Moreover, the two types of sensors used have different lengths (7.7 cm long for both T_a and RH sensors of HMP110 and 13.5 cm long and 9.9 cm long respectively for T_a and RH sensors of HMT 330) which may induce different shelter efficiencies for the different probes when considering a same given shelter.

Finally, the highlighted differences are subject to a strong temporal variability which makes them difficult to predict and correct. The results presented in the body of the present manuscript were therefore not corrected but they can still be exploited especially as the effect of the water restriction can be evaluated by comparing measurements performed with the same sensor before and after the beginning of the water restriction.

7.1.4. Irrigation

In addition to the information reported in section 3.1.2.2.1 regarding the irrigation strategy used during the measurement campaign of summer 2022, Figure 98 indicates the daily amount of water poured to each WW and WR tree from July 1st to August 31st, 2022.

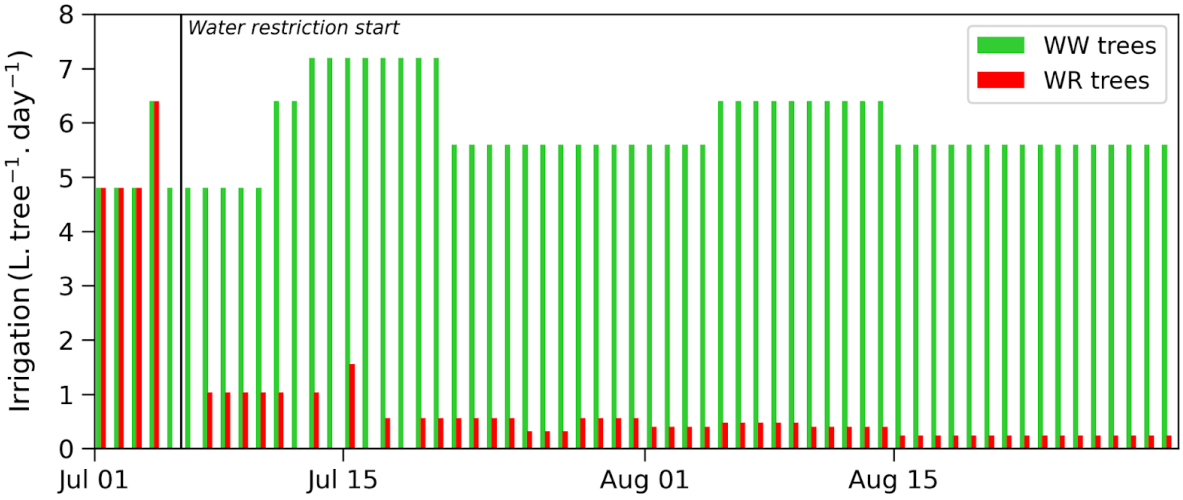

Figure 98: Daily amount of water poured to each WW and WR tree from July 1st to August 31st, 2022.

7.2. Trees & Climate study (T&C)

7.2.1. Characteristics of the studied trees

The main characteristics of the studied trees, mentioned in section 4.1.1.3 are presented in Table 24.

Table 24: Main characteristics of the studied trees.

Site	Species	Name	ID	Time since plantation (years)	Development stage	Phytosanitary status	Trunk circumference in 2019 (cm)	Branch circumference in 2019 (mm)	Sensors' height (m)
FLANDRE	Lamp post	CANDFlandre1							6,8
FLANDRE	Lamp post	CANDFlandre2							6,8
FLANDRE	Lamp post	CANDFlandre3							6,9
FLANDRE	Celtis australis	celtis_1	211818		JA	good	63	190	4,6
FLANDRE	Celtis australis	celtis_2	211789	24	JA	good	78	253	4,3
FLANDRE	Celtis australis	celtis_3	211915		JA	good	80	208	4,5
FLANDRE	Platanus x hispanica	platanus_1	256681	25	A	good	115	240	6,7
FLANDRE	Platanus x hispanica	platanus_2	256643		JA	good	77	250	6,6
FLANDRE	Platanus x hispanica	platanus_3	256782		JA	good	73	268	5,2
FLANDRE	Sophora japonica	sophora_1	232304		JA	good	75	254	6,2
FLANDRE	Sophora japonica	sophora_2	232236		JA	moderately damaged	75	209	7,3
FLANDRE	Sophora japonica	sophora_3	232254		A	good	86	230	6,2
FLANDRE	Tilia cordata	tilia_1	234855		JA	good	65	192	5,2
FLANDRE	Tilia cordata	tilia_2	234797		JA	good	67	169	6,5
FLANDRE	Tilia cordata	tilia_3	234850		JA	good	73	220	5,4
FLANDRE	Ulmus resista	ulmus_1	2022571	11	J	moderately damaged	53	218	3,6
FLANDRE	Ulmus resista	ulmus_2	2016467	11	JA	moderately damaged	60	210	4,2
FLANDRE	Ulmus resista	ulmus_3	2016465	11	JA	moderately damaged	63	254	4,3

Site	Species	Name	ID	Time since plantation (years)	Development stage	Phytosanitary status	Trunk circumference in 2019 (cm)	Branch circumference in 2019 (mm)	Sensors' height (m)
NOHAIN	Lamp post	CANDNohain							7
NOHAIN	Quercus cerris	qcerris_1	229285	26	JA	good	71	205	6,1
NOHAIN	Quercus cerris	qcerris_2	300300		JA	moderately damaged	80	277	6,3
NOHAIN	Quercus cerris	qcerris_3	300233		JA	moderately damaged	78	195	5,4
ORDENER	Lamp post	CANDOrdener							6,9
ORDENER	Gleditsia triacanthos	gleditsia_1	284161	31	JA	good	80	287	8
ORDENER	Gleditsia triacanthos	gleditsia_2	283753	31	JA	good	85	240	8,2
ORDENER	Gleditsia triacanthos	gleditsia_3	283645	24	JA	good	80	200	8
TEMPLE	Lamp post	CANDTemple							6,5
TEMPLE	Celtis australis	celtis_4	212274	13	JA	good	65	198	4,3
TEMPLE	Celtis australis	celtis_5	212277	13	JA	good	72	212	5,6
TEMPLE	Celtis australis	celtis_6	212255	15	JA	good	73	223	4,9
TEMPLE	Platanus x hispanica	platanus_4	225800	14	JA	good	60	194	5,8
TEMPLE	Platanus x hispanica	platanus_5	225801	14	JA	good	78	165	5,9
TEMPLE	Platanus x hispanica	platanus_6	274637		JA	good	53	169	5,7
TEMPLE	Quercus ilex	qilex_1	229455	14	JA	good	55	166	3,9
TEMPLE	Quercus ilex	qilex_2	229457	14	JA	good	57	220	4,5
TEMPLE	Quercus ilex	qilex_3	229459	14	JA	good	60	225	3,7
VICTOR	Lamp post	CANDVictor							6,4
VICTOR	Platanus x hispanica	platanus_7	249737	23	JA	good	71	230	6,7
VICTOR	Platanus x hispanica	platanus_8	249701		JA	moderately damaged	74	190	7
VICTOR	Platanus x hispanica	platanus_9	258406		JA	good	63	187	7,2
VICTOR	Zelkova serrata	zelkova_1	258466	14	JA	good	62	240	4,3
VICTOR	Zelkova serrata	zelkova_2	236612	19	JA	good	57	209	4,5
VICTOR	Zelkova serrata	zelkova_3	259224		JA	good	80	158	4,2

7.2.2. Overview of the data availability

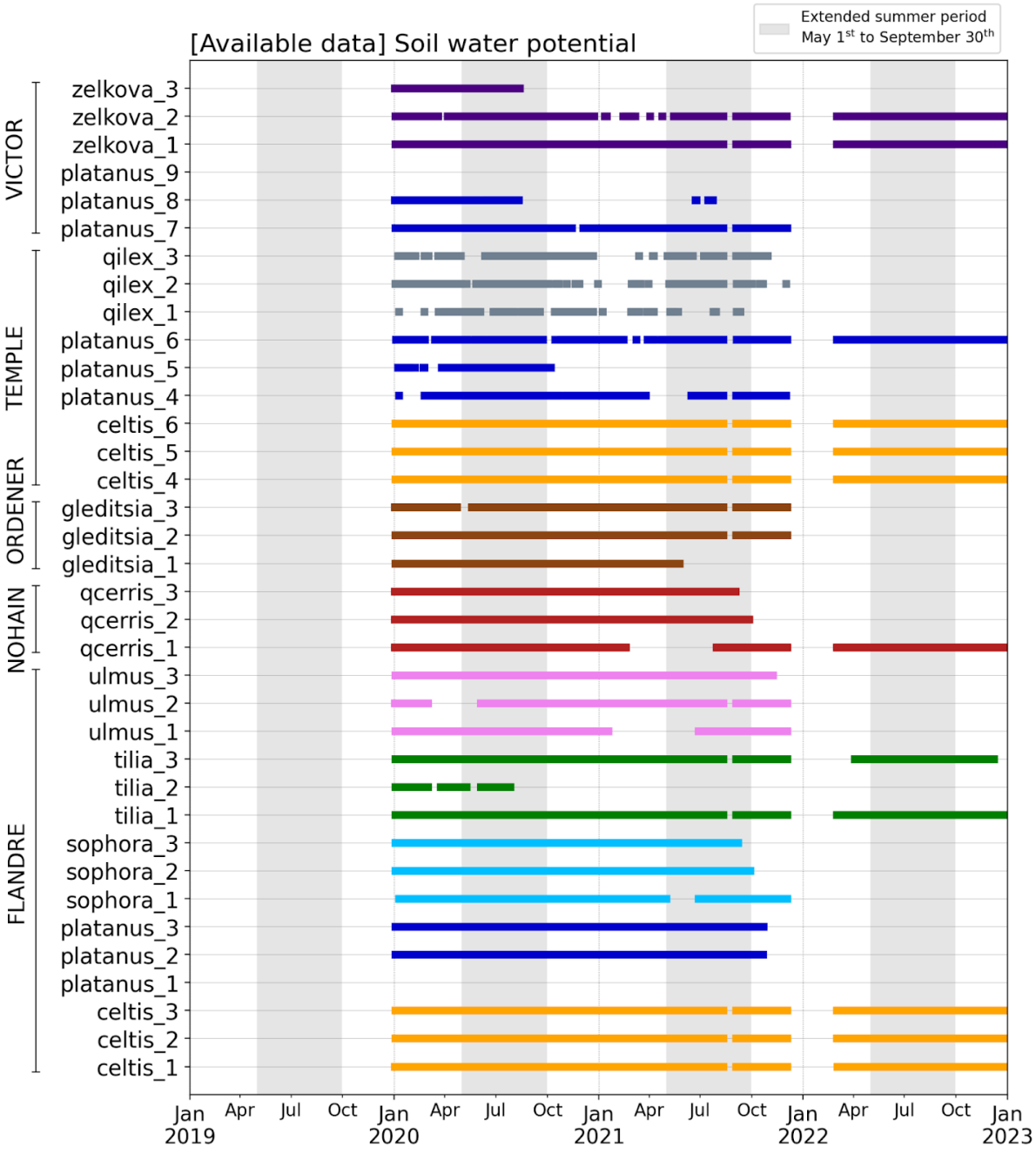

Figure 99: Availability of the soil water potential data for the 36 studied trees over the years 2019 to 2022.

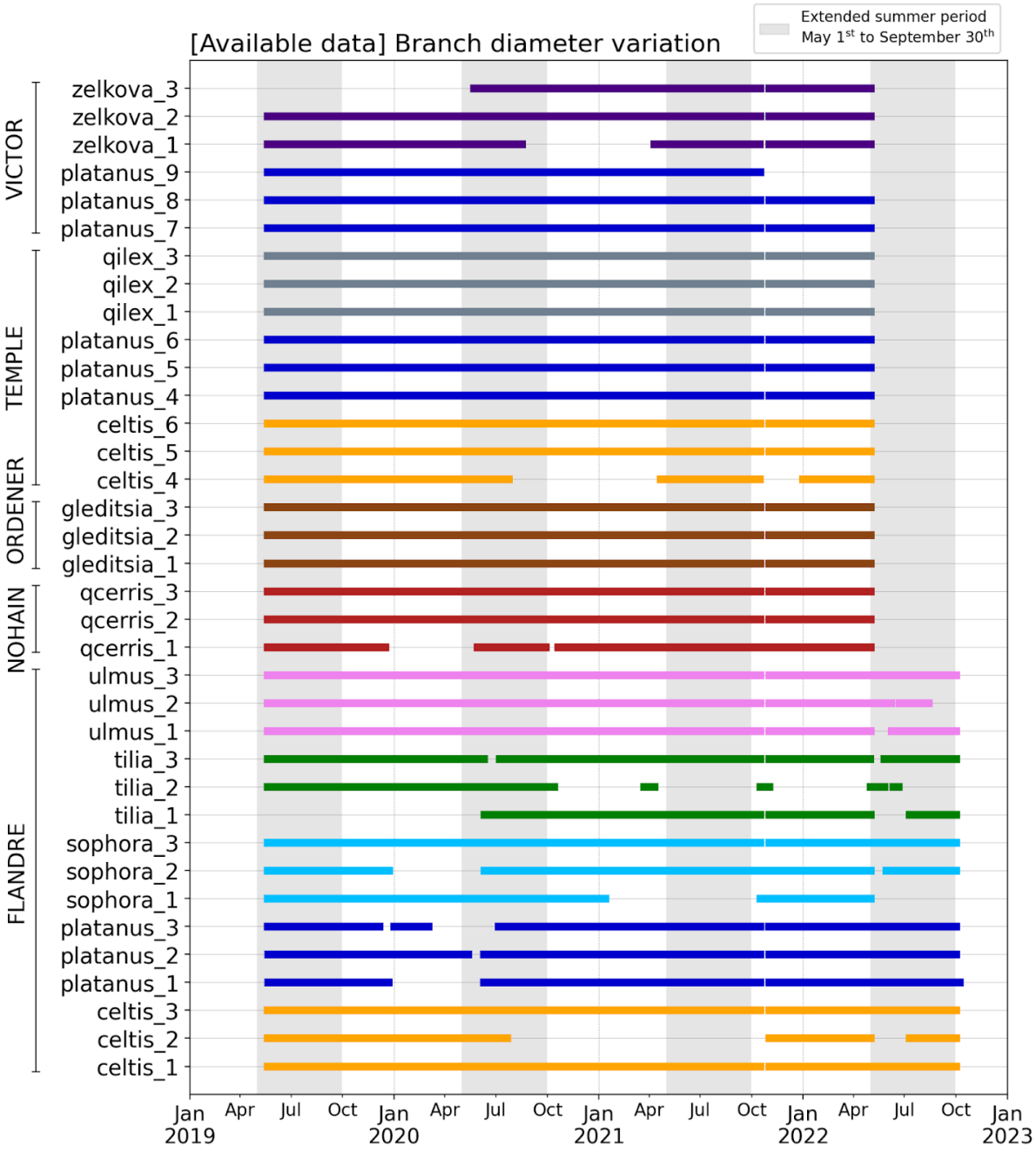

Figure 100: Availability of the branch diameter variation data for the 36 studied trees over the years 2019 to 2022.

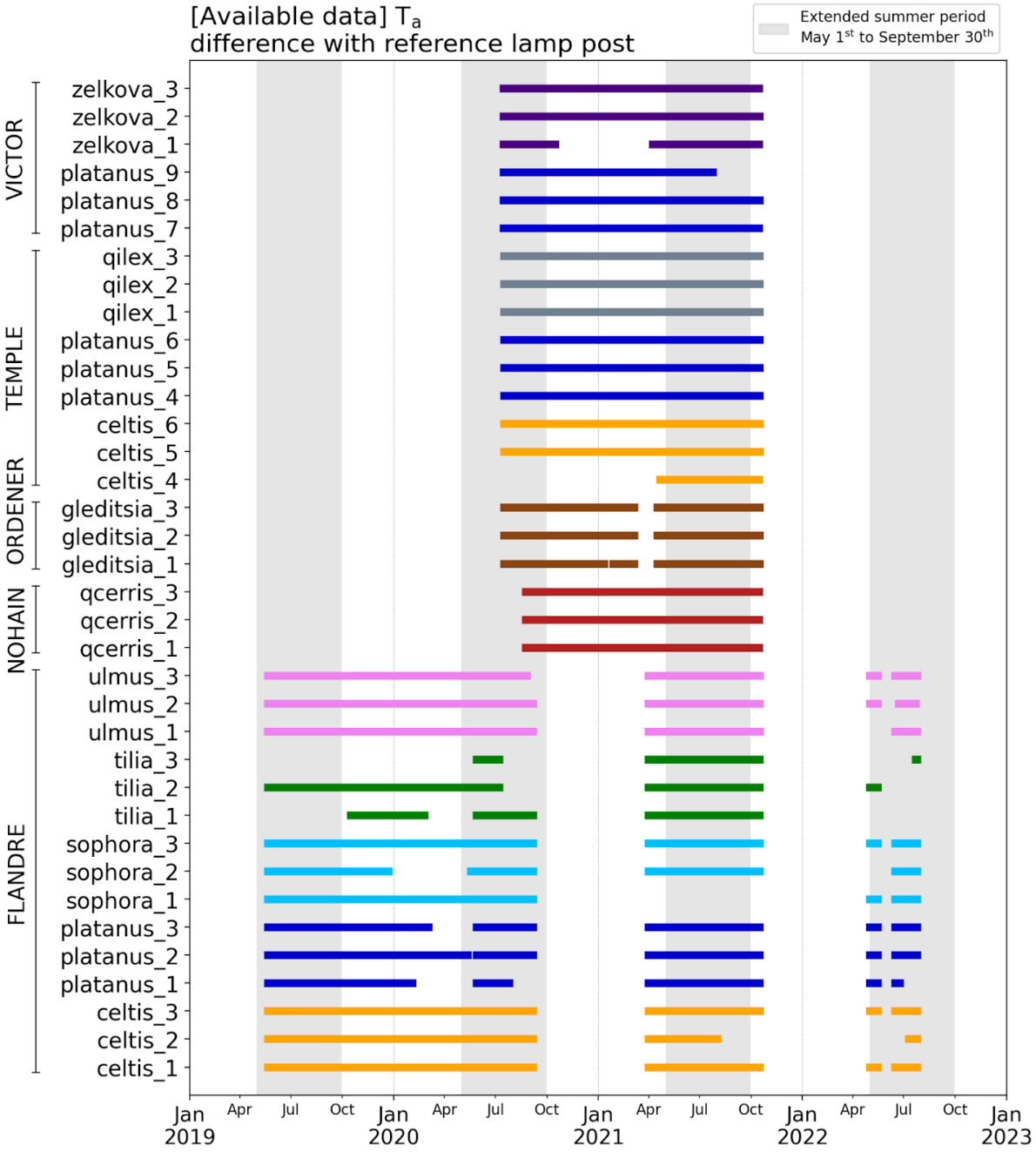

Figure 101: Availability of the difference of air temperature (ΔT_a) data for the 36 studied trees compared to their reference lamp post over the years 2019 to 2022.

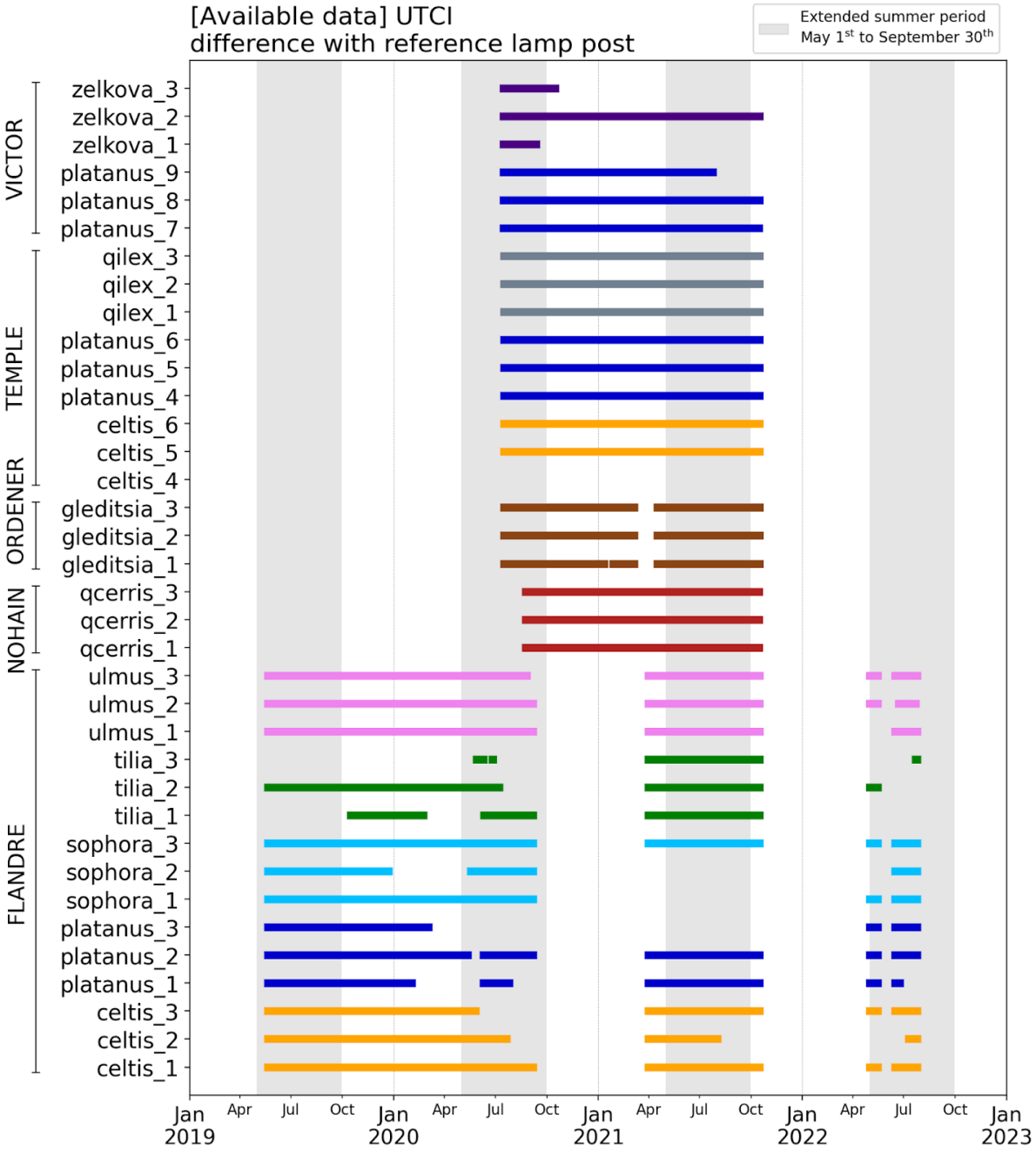

Figure 102: Availability of the difference of UTCI (ΔUTCI) data for the 36 studied trees compared to their reference lamp post over the years 2019 to 2022.

7.2.3. Representation of warm and dry periods

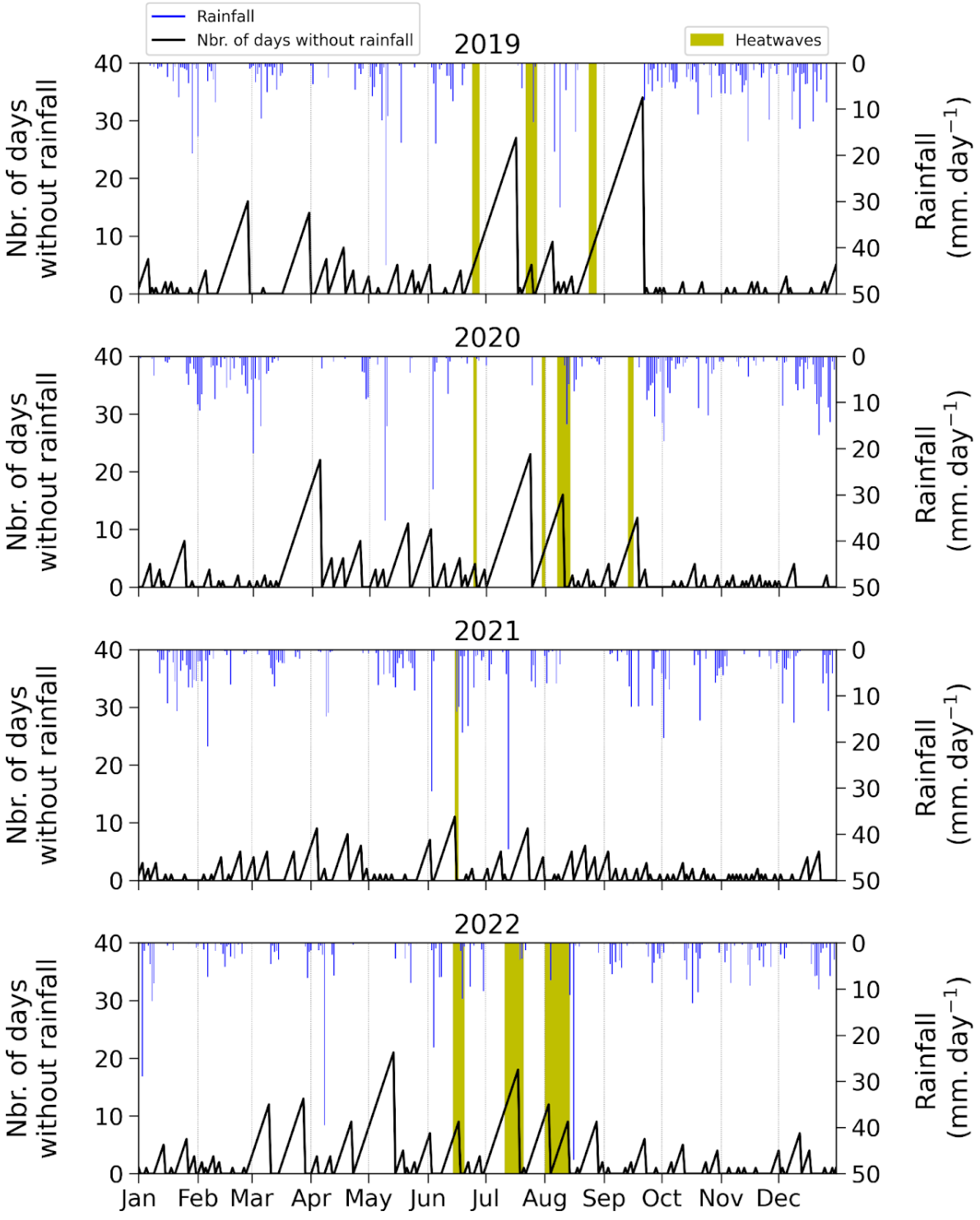

Figure 103: Evolution of the daily rainfall and the elapsed number of days since the last rain event from 2019 to 2020. The heatwaves identified by Météo-France are highlighted with yellow areas.

7.2.4. Pictures and 3D point clouds of the studied trees

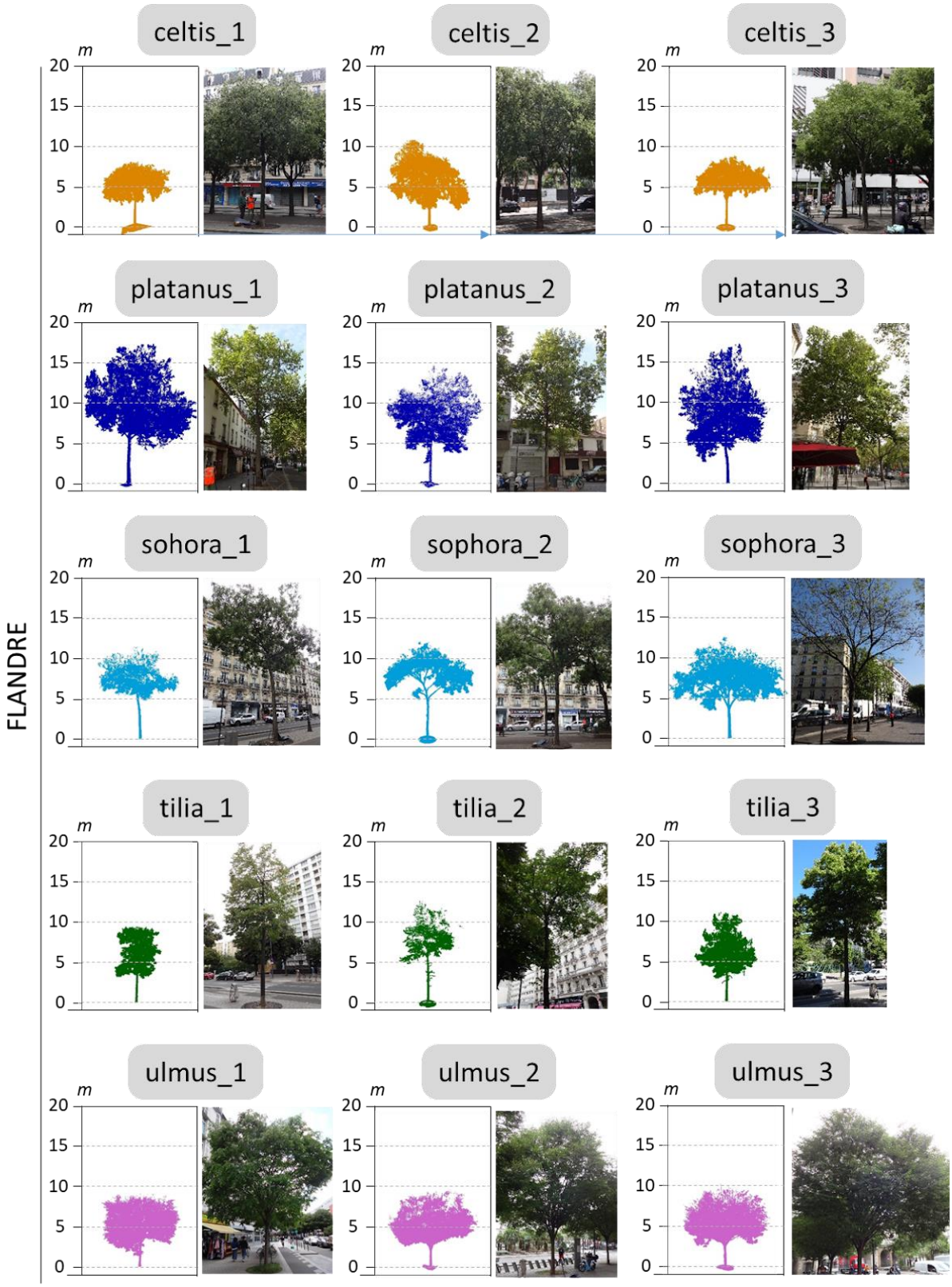

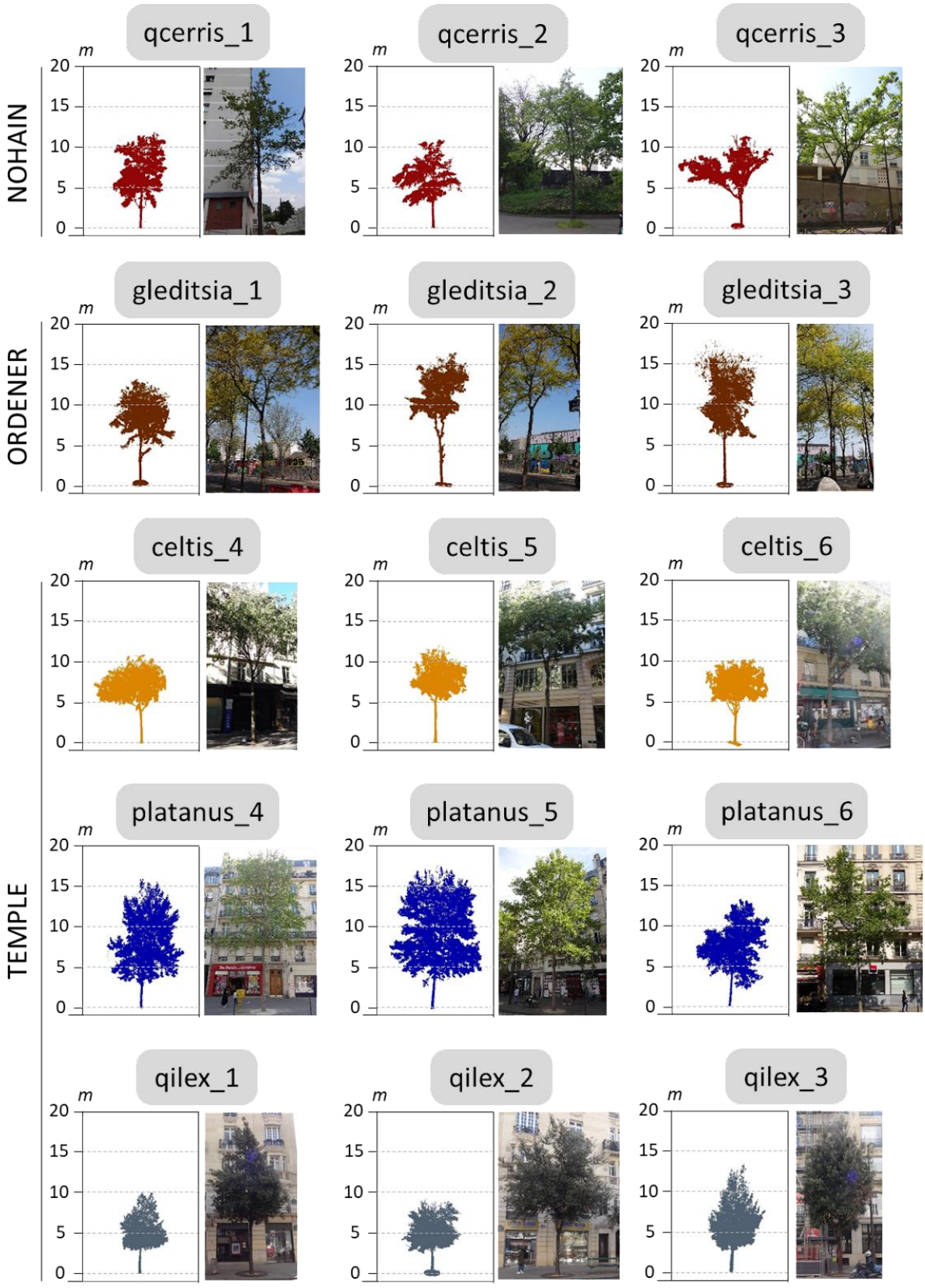
NOHAIN
ORDENER
TEMPLE
qcerris_1
qcerris_2
qcerris_3
gleditsia_1
gleditsia_2
gleditsia_3
celtis_4
celtis_5
celtis_6
platanus_4
platanus_5
platanus_6
qilex_1
qilex_2
qilex_3
m
20
15
10
5
0

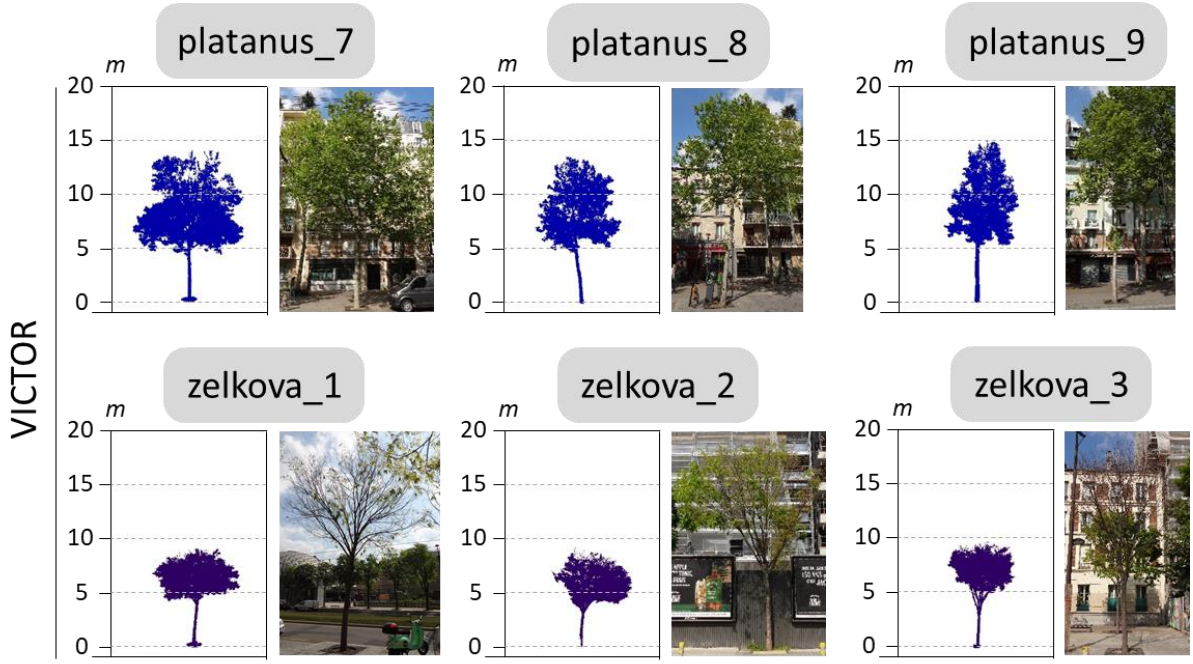
VICTOR
platanus_7
platanus_8
platanus_9
zelkova_1
zelkova_2
zelkova_3
m
20
15
10
5
0

7.2.5. Morphological variables calculated through the LiDAR scanning campaign

The detailed results of the calculation of the morphological characteristics of the studied trees, mentioned in section 4.2.1 are presented in Table 25.

Table 25: Morphological variables calculated on the basis of the LiDAR scanning campaign performed in August 2022. The definition and unit of the different parameters are provided in section 4.1.3.2.

Site	Species	Name	ID	Sensors' height (m)	Hbase	Hsurf_max	Htot	Hcrown	Vpoly	Vvox	Density	Sproj
FLANDRE	Lamp post	CANDFlandre1		6,8								
FLANDRE	Lamp post	CANDFlandre2		6,8								
FLANDRE	Lamp post	CANDFlandre3		6,9								
FLANDRE	Celtis australis	celtis_1	211818	4,6	3,2	4,7	8,2	5	85,1	39,6	0,46	23,1
FLANDRE	Celtis australis	celtis_2	211789	4,3	2,2	5,1	9,4	7,2	143,3	59,9	0,42	27,3
FLANDRE	Celtis australis	celtis_3	211915	4,5	2,8	5	8,6	5,8	98,4	42,5	0,43	26,8
FLANDRE	Platanus x hispanica	platanus_1	256681	6,7	3,7	9,1	17,4	13,7	338,1	115	0,34	36,9
FLANDRE	Platanus x hispanica	platanus_2	256643	6,6	3,7	8,7	13,4	9,7	212,6	76,9	0,36	33
FLANDRE	Platanus x hispanica	platanus_3	256782	5,2	2,9	9,5	15,1	12,2	290,5	83,7	0,29	35
FLANDRE	Sophora japonica	sophora_1	232304	6,2	4,2	6,5	11,2	7	131,1	32,5	0,25	30,4
FLANDRE	Sophora japonica	sophora_2	232236	7,3	5	7,8	11,3	6,3	130,9	37,9	0,29	30,3
FLANDRE	Sophora japonica	sophora_3	232254	6,2	3,2	7,4	11,1	8	205,2	73,5	0,36	38,4
FLANDRE	Tilia cordata	tilia_1	234855	5,2	2	8	9	7	78,7	28,5	0,36	16,9
FLANDRE	Tilia cordata	tilia_2	234797	6,5	4,4	8,8	11,6	7,2	84	16,3	0,19	21,4
FLANDRE	Tilia cordata	tilia_3	234850	5,4	2,8	5	10,3	7,6	107,9	39,5	0,37	21,5
FLANDRE	Ulmus resista	ulmus_1	2022571	3,6	2,1	5,3	8,4	6,3	137,9	75,4	0,55	27,4
FLANDRE	Ulmus resista	ulmus_2	2016467	4,2	2,4	6,3	9,3	6,9	163,8	76	0,46	34,7
FLANDRE	Ulmus resista	ulmus_3	2016465	4,3	1,8	6,2	9,6	7,8	174,7	85,6	0,49	32,7

Site	Species	Name	ID	Sensors' height (m)	Hbase	Hsurf_max	Htot	Hcrown	Vpoly	Vvox	Density	Sproj
NOHAIN	Lamp post	CANDNohain		7								
NOHAIN	Quercus cerris	qcerris_1	229285	6,1	1,4	4,8	10,6	9,1	117,9	34,1	0,29	25,1
NOHAIN	Quercus cerris	qcerris_2	300300	6,3	2,4	5,2	10,5	8,1	113,2	28,6	0,25	23,8
NOHAIN	Quercus cerris	qcerris_3	300233	5,4	4,9	8	10,6	5,7	107,3	28,7	0,27	30,9
ORDENER	Lamp post	CANDOrdener		6,9								
ORDENER	Gleditsia triacanthos	gleditsia_1	284161	8	4,1	8,6	12,2	8,1	166,8	50	0,3	29,9
ORDENER	Gleditsia triacanthos	gleditsia_2	283753	8,2	7,4	9,5	12,9	5,4	104,2	24,3	0,23	28,6
ORDENER	Gleditsia triacanthos	gleditsia_3	283645	8	5,3	9,9	15,3	10	187,1	40,5	0,22	30,1
TEMPLE	Lamp post	CANDTemple		6,5								
TEMPLE	Celtis australis	celtis_4	212274	4,3	4,4	6,7	10,2	5,8	100,9	38,7	0,38	24,4
TEMPLE	Celtis australis	celtis_5	212277	5,6	4,4	7,1	10,9	6,4	97	36,5	0,38	23
TEMPLE	Celtis australis	celtis_6	212255	4,9	4,3	6,3	9,5	5,2	90,3	36	0,4	23,2
TEMPLE	Platanus x hispanica	platanus_4	225800	5,8	3,4	6,5	14,7	11,3	197,9	59,3	0,3	26,8
TEMPLE	Platanus x hispanica	platanus_5	225801	5,9	2,8	7,3	15,8	13	290	84,1	0,29	33,9
TEMPLE	Platanus x hispanica	platanus_6	274637	5,7	2,6	6,9	12,6	9,9	169	54,1	0,32	26,7
TEMPLE	Quercus ilex	qilex_1	229455	3,9	3	5,4	9,9	6,9	77,7	31,1	0,4	17,5
TEMPLE	Quercus ilex	qilex_2	229457	4,5	2,9	4,4	8,9	6	102,1	52,3	0,51	23,2
TEMPLE	Quercus ilex	qilex_3	229459	3,7	2,6	6,1	12,3	9,7	117,4	45,4	0,39	19,2
VICTOR	Lamp post	CANDVictor		6,4								
VICTOR	Platanus x hispanica	platanus_7	249737	6,7	4,2	7,4	14,2	10	206,2	76,5	0,37	31,7
VICTOR	Platanus x hispanica	platanus_8	249701	7	4	6,2	13	9	153	44	0,29	26,4
VICTOR	Platanus x hispanica	platanus_9	258406	7,2	4,7	7,6	14,5	9,8	147	43,9	0,3	23,9
VICTOR	Zelkova serrata	zelkova_1	258466	4,3	3,9	6,4	8,6	4,7	85	42,6	0,5	24,4
VICTOR	Zelkova serrata	zelkova_2	236612	4,5	3,4	6,5	8,7	5,3	75,5	31,7	0,42	21,3
VICTOR	Zelkova serrata	zelkova_3	259224	4,2	4,4	7	8,8	4,4	61,7	29,4	0,48	19,6

7.2.6. Branch section variation

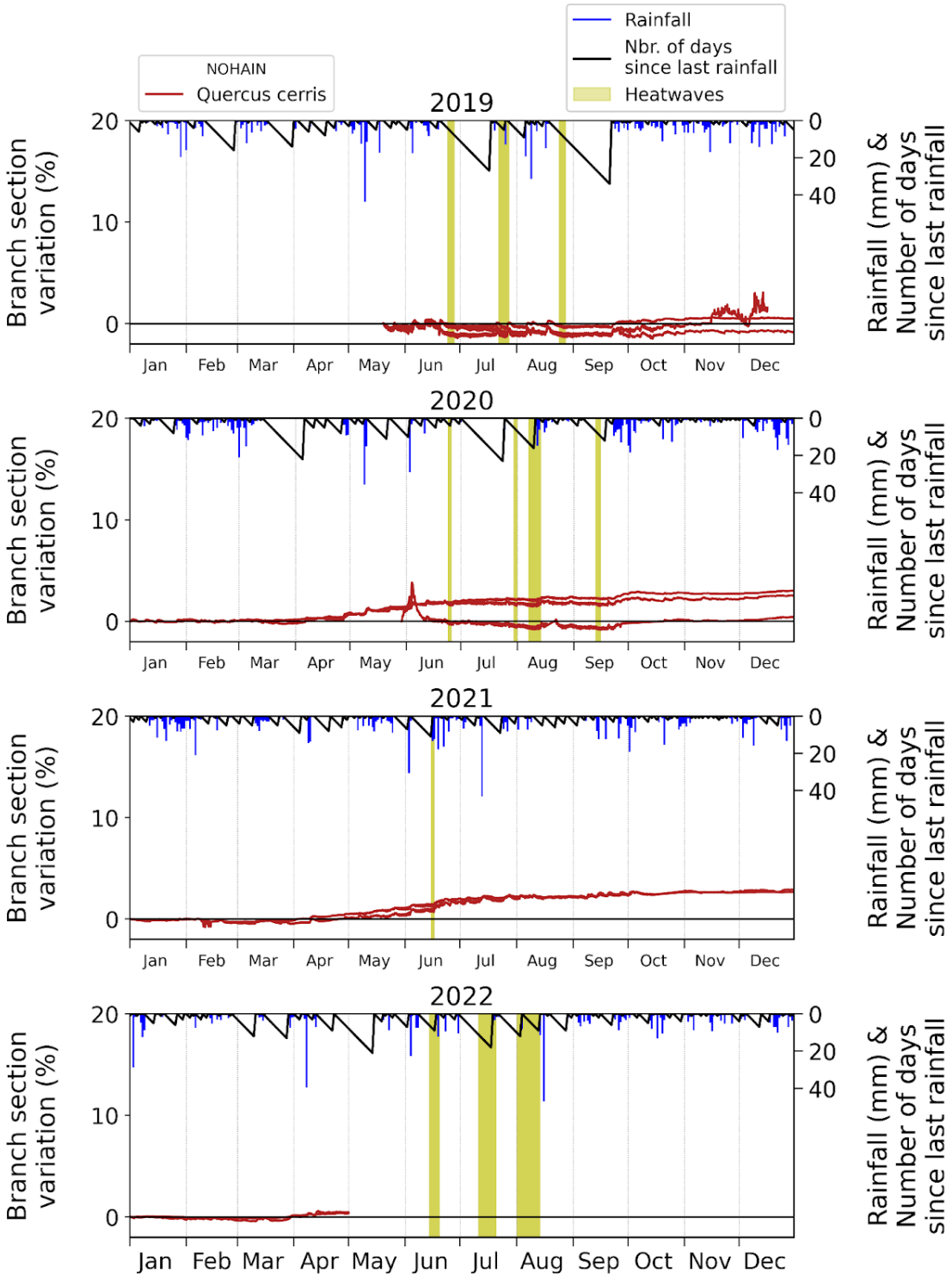

Figure 104: Evolution of the branch section variation on the basis of the initial branch section calculated at the beginning of each year for the trees located in NOHAIN, of the daily rainfall and of the elapsed number of days since the last rain event from 2019 to 2020. The heatwaves identified by Météo-France are highlighted with yellow areas.

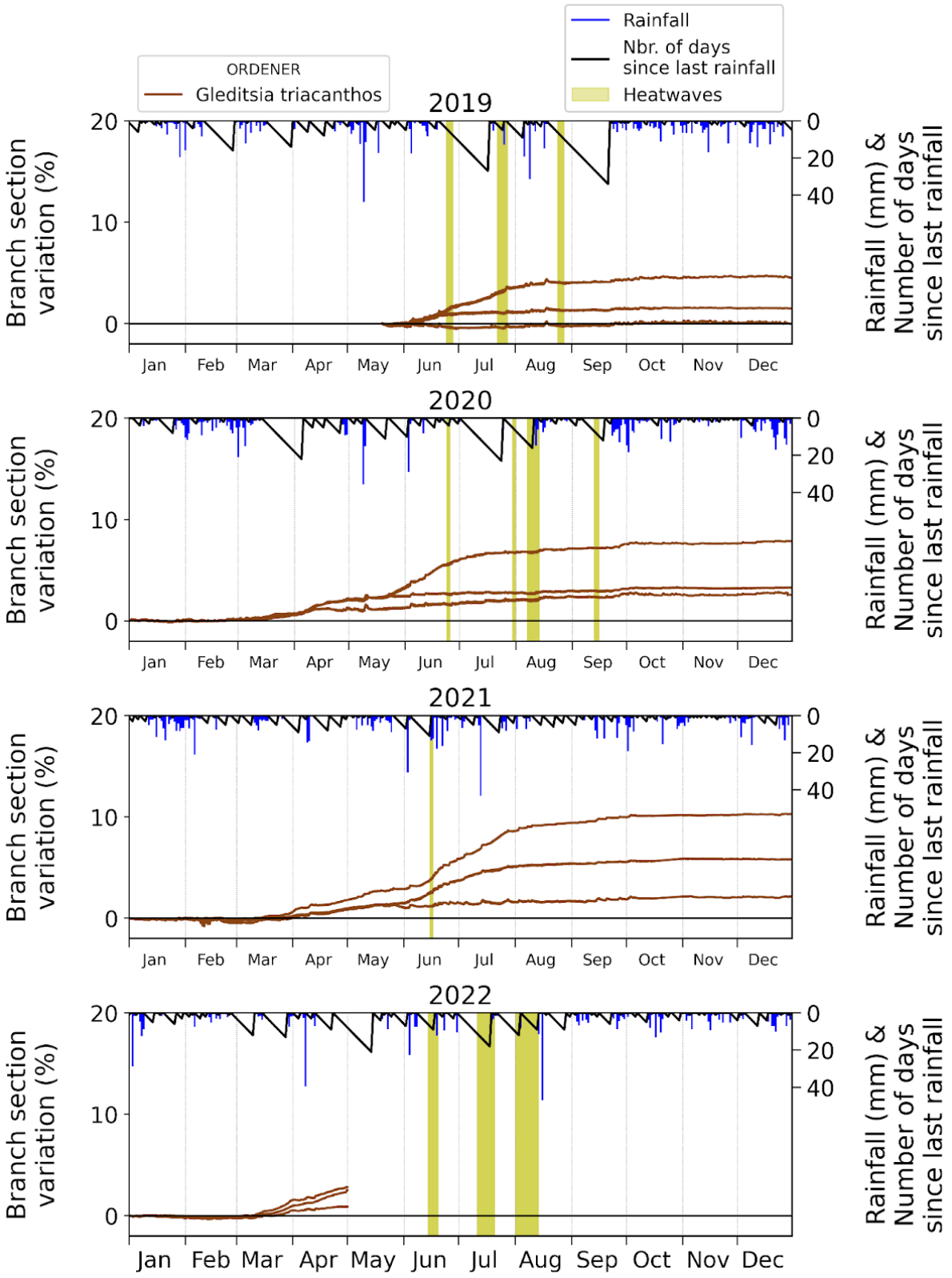

Figure 105: Evolution of the branch section variation on the basis of the initial branch section calculated at the beginning of each year for the trees located in ORDENER, of the daily rainfall and of the elapsed number of days since the last rain event from 2019 to 2020. The heatwaves identified by Météo-France are highlighted with yellow areas.

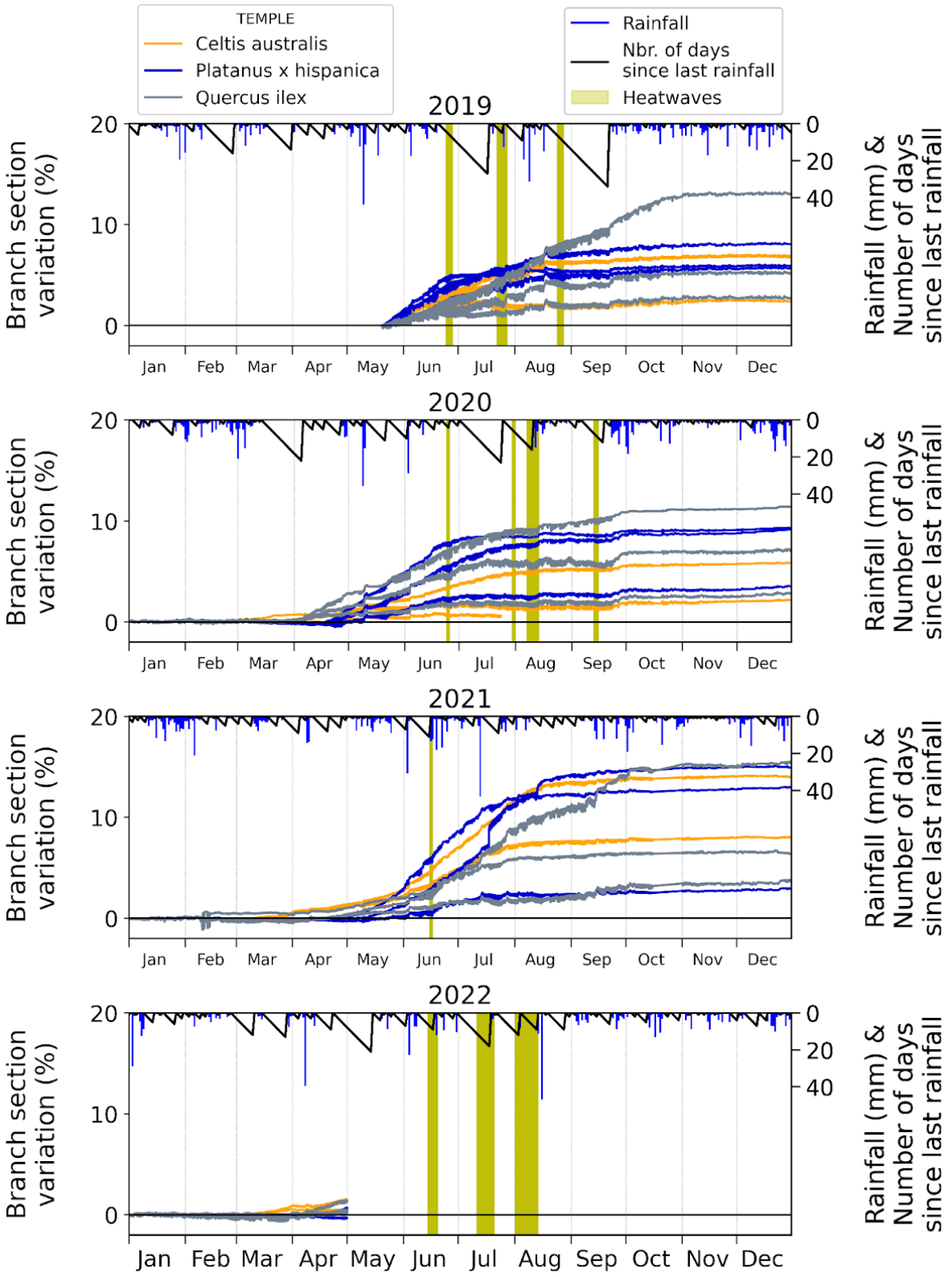

Figure 106: Evolution of the branch section variation on the basis of the initial branch section calculated at the beginning of each year for the trees located in TEMPLE and of the daily rainfall and the elapsed number of days since the last rain event from 2019 to 2020. The heatwaves identified by Météo-France are highlighted with yellow areas.

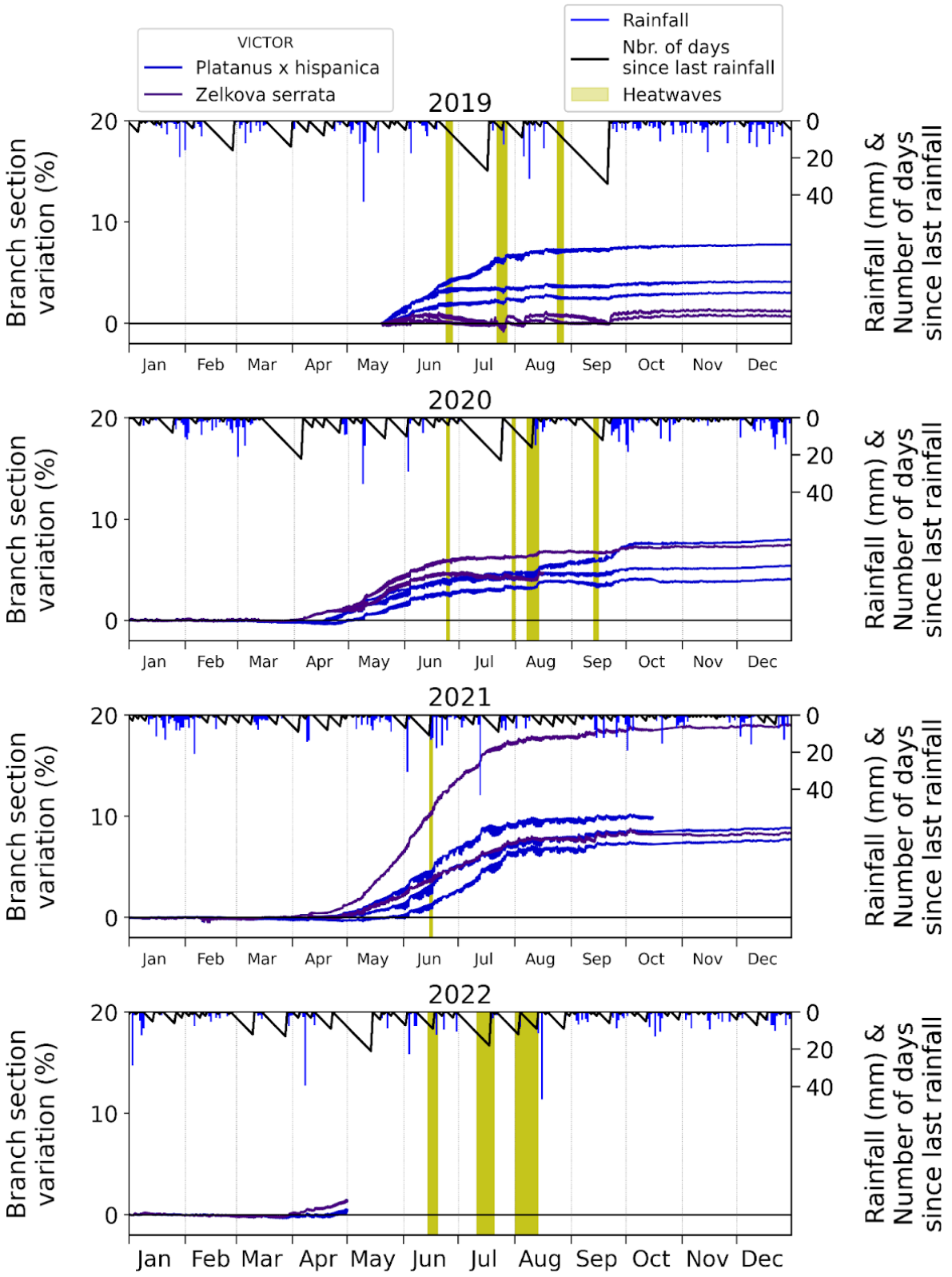

Figure 107: Evolution of the branch section variation on the basis of the initial branch section calculated at the beginning of each year for the trees located in VICTOR, of the daily rainfall and of the elapsed number of days since the last rain event from 2019 to 2020. The heatwaves identified by Météo-France are highlighted with yellow areas

7.2.7. Soil water potential of celtis_1

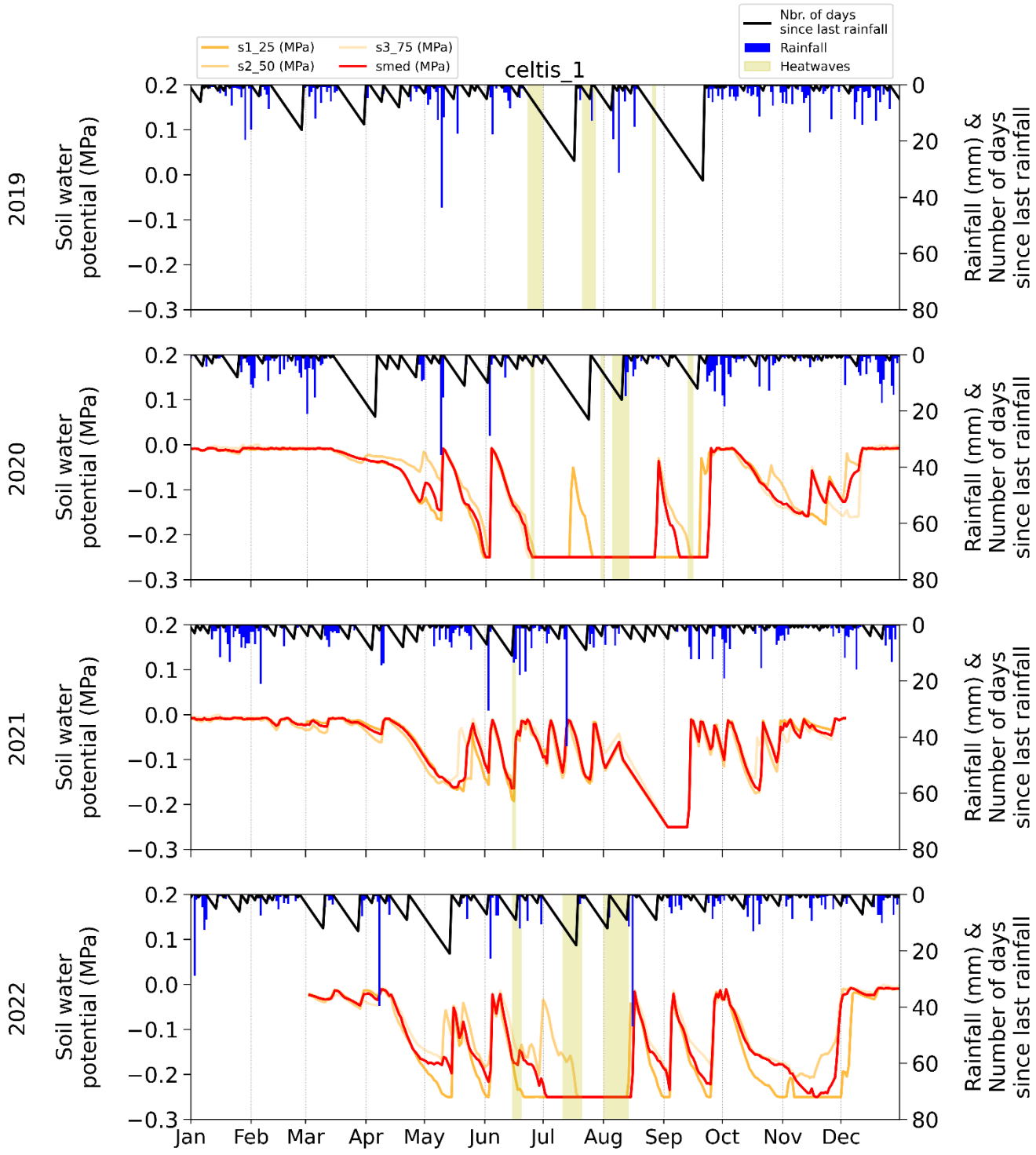

Figure 108 : Evolution of: the daily average soil water potential measured in the pit of celtis_1 from 2019 to 2020 at 25 cm depth (s1_25), 50 cm depth (s2_50) and 75 cm depth (s3_75), of the daily median soil water potential (smed) calculated among the values measured at the three depths, of the daily accumulated amount of rainfall measured at Paris-Montsouris and of the daily elapsed number of days since the last rain event.

7.2.8. Correction of air temperature and relative humidity measurements

Air temperature (T_a) and relative humidity (RH) measurements are generally carried out inside screens which are meant to protect the sensors from direct insolation and from the rainfall which could alter significantly the measurements. Some studies have already shown that the different existing designs of screens (Civiate and Mandel, 2008) may have contrasted efficiencies (Bernard et al., 2019; Lacombe, 2011; Lacombe et al., 2011). A screen is expected to reflect the majority of incoming solar radiation while not disturbing the air flow around the sensor in order to prevent the sensor from overheating. However, some low quality screens can sometimes absorb part of the incoming radiation and/or reduce the air flow around the sensor, which is likely to lead to an overheating of the air contained inside the screen and then an overestimation of T_a and underestimation of RH.

In the T&C study, the calculation of the climatic benefits provided by the trees relies on the comparison of Ta and RH measurements carried out in the shade of the tree crowns and in the complete sunlight (measurements at the lamp posts). Thereby, if ever the screens used in the T&C study are not perfect, T_a is very likely to be overestimated at the lamp posts but not inside the tree crowns where the screens are already shaded by the tree foliage.

In order to verify this aspect and, if needed, to try to correct the data, the efficiency of the screens used in the T&C study was performed during summer 2023. The air temperature and relative humidity were measured on the same site simultaneously inside the T&C screen as well as inside a Davis® screen which is reknowed and widely used in the literature (Bernard, 2017; Dubreuil et al., 2020).

7.2.8.1. Materials and methods

The measurements were carried out in an open area of the campus of Institut Agro Rennes-Angers, Angers, France (47°28’47’’ N, 0°36’33’’ W). T_a and RH were measured simultaneously with HMP110 (Vaisala) sensors placed inside two types of screens mounted at 1.5 m a.g.l. T_g was also measured at the same position using platinum probes mounted inside black painted copper spheres of 15 cm diameter. ↓SW radiation was measured nearby at 2 m a.g.l. Data-loggers were used to scan all sensors every 10 seconds and record average values every 10 minutes from August 9th to October 31st, 2023. The main characteristics of the sensors and of the compared screens are presented in Table 26 and Table 27 respectively and a picture of the mast bearing the different sensors is proposed in Figure 109.

Table 26: Characteristics of the screens compared.

Form of the screen	**Ventilation**	**Reference, Manufacturer**	**Dimensions** *width x length x height*
Overlapping cups	Naturally ventilated	7714, Davis®	191 x 215 x 152 mm
Overlapping cups	Naturally ventilated	TFA Dostmann®	95 x 102 x 180 mm

Table 27: Characteristics of the sensors used for the comparison (n.c. = not communicated).

Measured variable	**Sensor type**	**Measurement range**	**Accuracy**	**Reference, Manufacturer**
Air temperature	Platinum	-40 to +60 °C	± 0.2 °C	HMP110, Vaisala
Air relative humidity	Capacitive	0 to 100 %	± 1.5 % for HR ≤ 90%	HMP110, Vaisala
Globe temperature	Platinum	-5 to +95 °C	± 0.15+0.002*T (°C)	PT100, RS Pro
↓SW radiation	4 components Net radiometer	n.c.	± 10 % on daily sum	CNR4, Kipp&Zonen

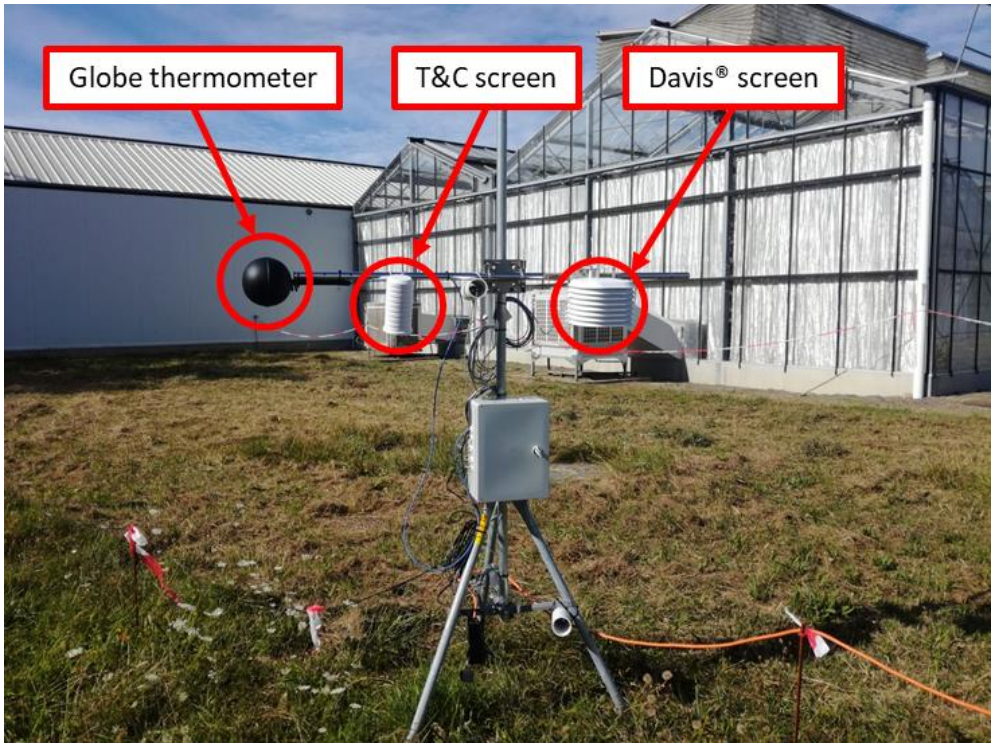

Figure 109: Picture of the mast bearing the globe thermometer as well as the thermohygrometers placed inside the T&C screen and the Davis® screen.

T_a and RH measured inside both screens were first graphed over a few days with varying climatic conditions in order to highlight the eventual differences. Then, the relationship between incident radiation and the eventual difference observed between both screens was investigated by plotting the T_a and RH differences as a function of the ↓SW, T_g and the difference between T_g and T_a (measured inside the Davis® screen). Indeed, while ↓SW gives a direct measurement of the incoming SW, T_g is also highly influenced by the different SW and LW fluxes. Moreover, it also takes into account the eventual SW fluxes reflected by the soil and other surrounded surfaces lower than 2 m a.g.l. which may reach the screens. However, T_g is also influenced by T_a as permanent convective heat exchanges exist between the globe and the atmosphere. Therefore, the difference between T_g and T_a was computed and used as an explanatory variable as it enables to take into account only the effects of the SW and LW exchanges on T_g.

7.2.8.2. Results

Strong differences can easily be noticed when comparing the measurements carried out inside both screens. A focus on a 10-day period lasting from August 23rd to August 31st 2023 is presented for T_a and RH respectively in Figure 110 and Figure 111. The difference between both screens was highly variable over a single day. At night, T_a was lower inside the T&C screen by up to 0.9 °C and on average by 0.2 °C compared to the one measured inside the Davis® screen. During the day, it was on average higher by 1.2 °C with a maximum difference of 3.6 °C recorded on August 30th at 16:00 UTC. As expected, opposite observations were reported for the RH. At night, RH was higher inside the T&C screen by up to 4.4 pt% and on average by 1 pt% compared to the one measured inside the Davis® screen. During the day, it was on average lower by 4.2 pt% with a maximum difference of 14.8 pt% recorded on August 30th at 08:50 UTC. The T&C screen then appeared to overheat and to provide very biased T_a and RH records.

The hourly variability of the difference between both screens also appears to be very close to the hourly variability of ↓SW as illustrated in both Figure 110 and Figure 111, which may explain why the difference is much higher during the day than at night when there is no ↓SW.

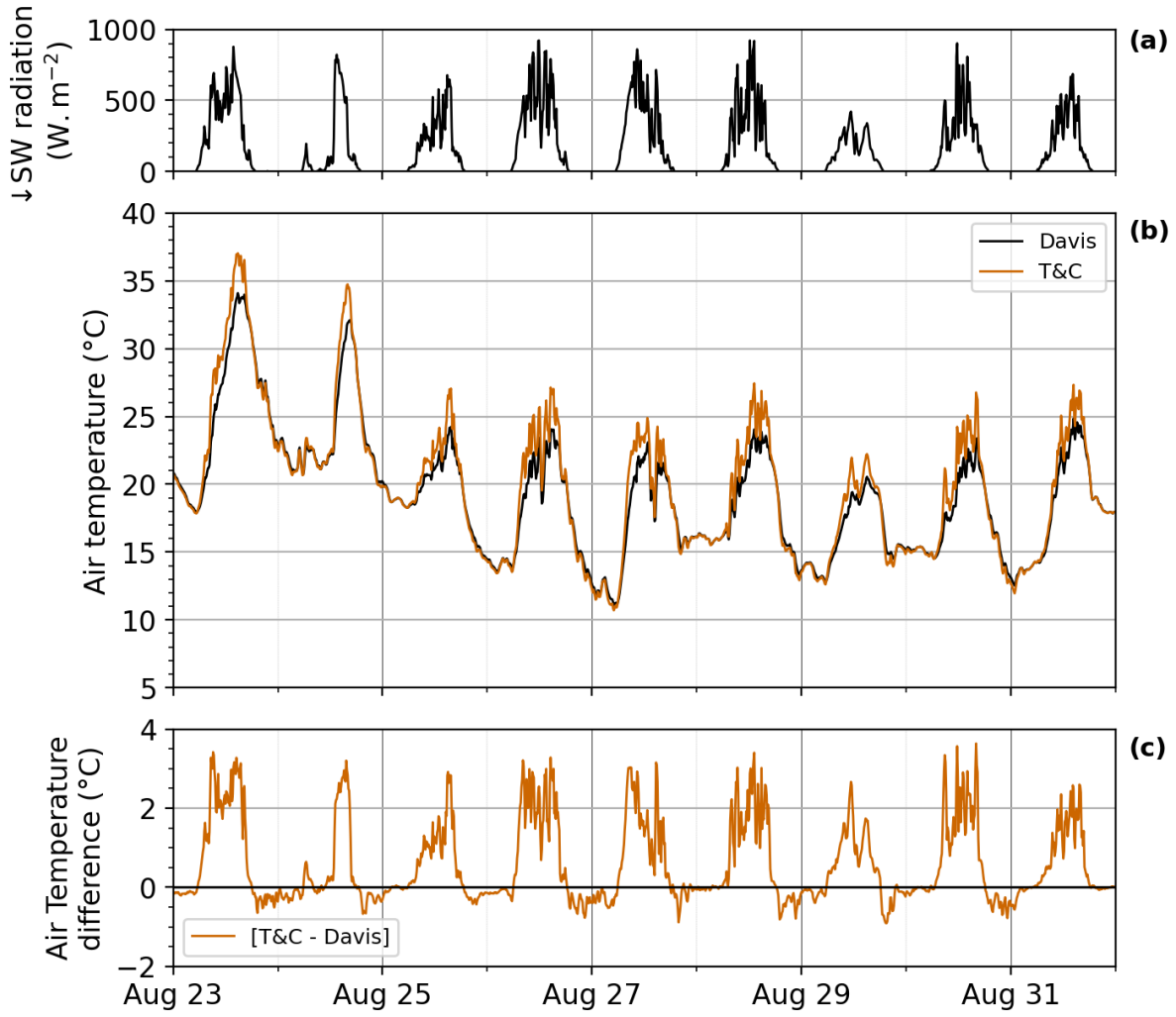

Figure 110: Evolution of (a) the ↓SW at 2 m a.g.l., (b) the air temperature measured inside the T&C screen and the Davis® screen at 1.5 m a.g.l. and (c) the resulting air temperature difference [T&C-Davis®] from August 23rd to August 31st 2023.

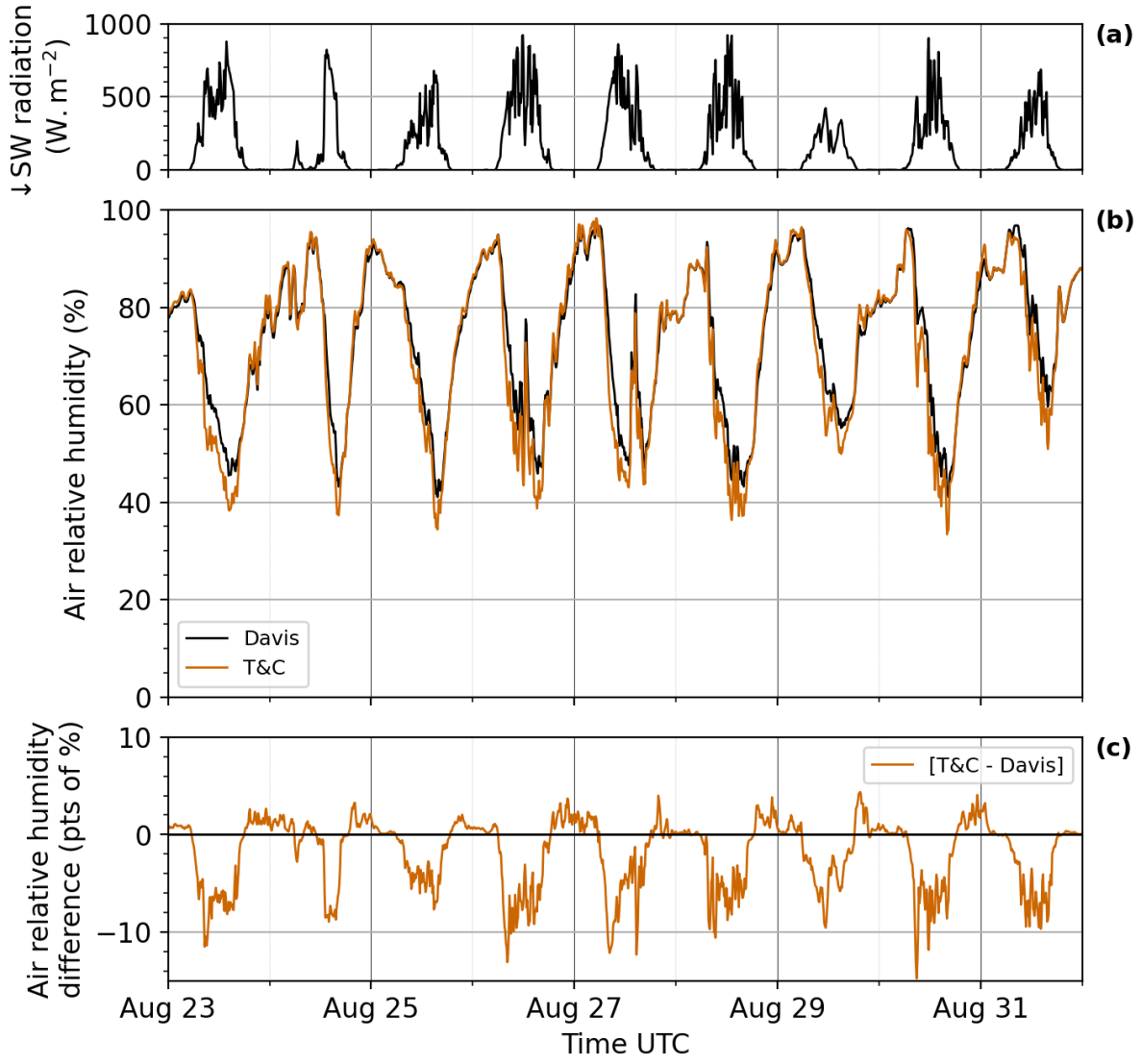

Figure 111: Evolution of (a) the ↓SW at 2 m a.g.l., (b) the air relative humidity measured inside the T&C screen and the Davis® screen and (c) the resulting air relative humidity difference [T&C-Davis®] from August 23rd to August 31st 2023.

The T_a and RH differences calculated between both screens were graphed as a function of ↓SW (Figure 112), T_g (Figure 113) and the difference between T_g and T_a (Figure 114). Positive and negative correlations were found respectively with T_a difference and RH difference in the three cases. The difference between T_g and T_a appeared to be the most effective explanatory variable (R^2 equals 0.94 and 0.84 respectively for T_a and RH differences), followed by ↓SW (R^2 equals 0.85 and 0.74 respectively for T_a and RH differences) and T_g alone (R^2 equals 0.69 and 0.54 respectively for T_a and RH differences).

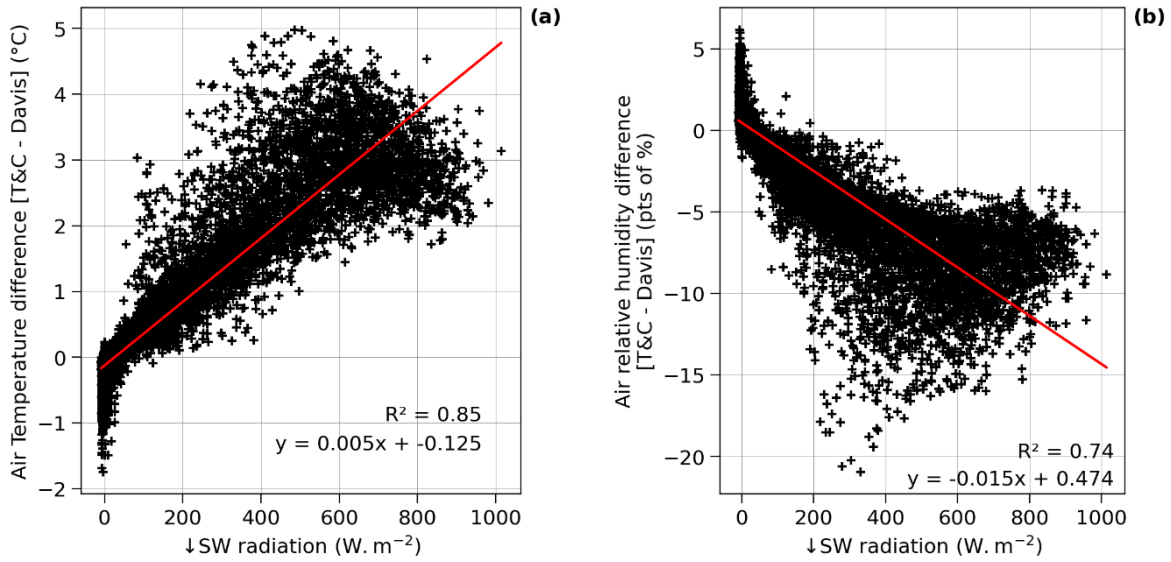

Figure 112: (a) Air temperature and (b) air relative humidity difference [T&C-Davis®] as a function of ↓SW at 2 m a.g.l. from August 23rd to August 31st 2023.

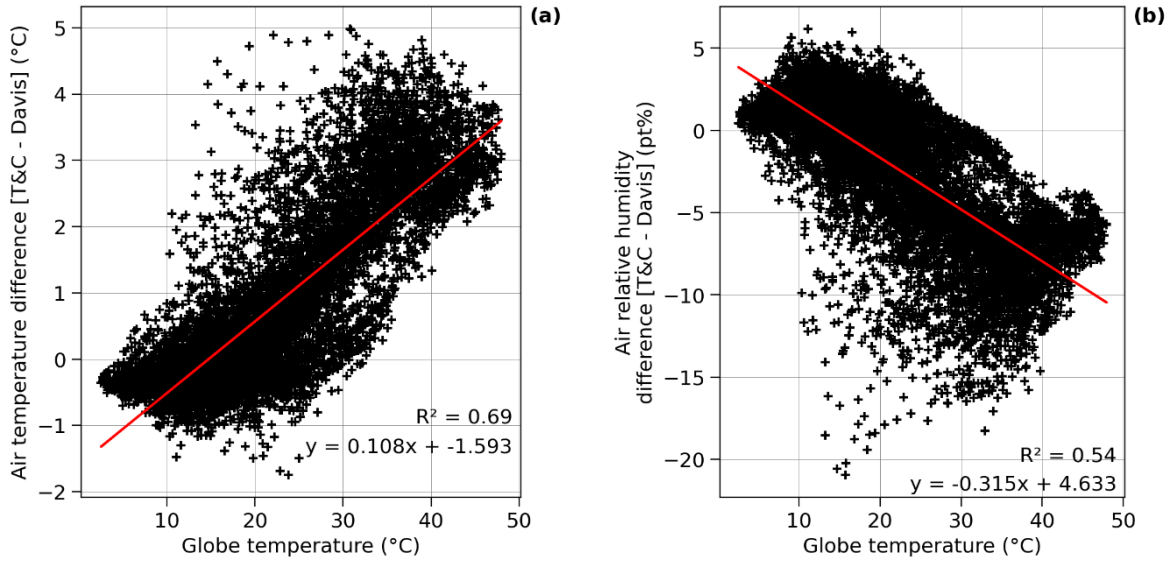

Figure 113: (a) Air temperature and (b) air relative humidity difference [T&C-Davis®] as a function of the globe temperature measured at 1.5 m a.g.l. from August 23rd to August 31st 2023.

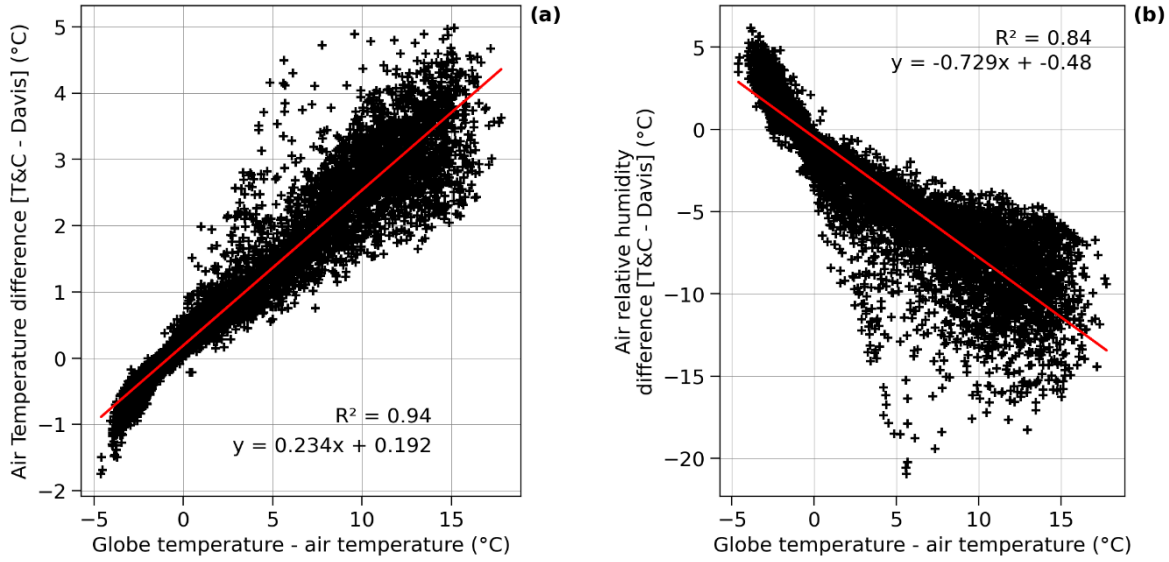

Figure 114: (a) Air temperature and (b) air relative humidity difference [T&C-Davis®] as a function of the difference between the globe temperature and the air temperature measured at 1.5 m a.g.l. in the Davis® screen from August 23rd to August 31st 2023.

7.2.8.3. Conclusions

The comparison of the T_a and RH measurements carried out in two different screens highlighted strong differences which appeared to be driven by the amount of radiation received by the screens. This study suggests that a correction should be applied to the T_a and RH measurements carried out in the frame of the T&C study to avoid biased conclusions. Although the ↓SW radiation and the difference between globe and air temperature appeared to be better explanatory variables, we propose to apply a correction to T&C measurements on the basis of the T_g for the following reasons:

- ↓SW radiation is not measured in the T&C study;
- There is no unbiased reference measurement of T_a performed close to the T&C screens;
- T_g is measured close to every T&C screen.

The following corrections are then proposed to correct the T_a and RH measurements performed in the T&C study:

$$T_a^{corrected} = T_a^{T\&C} - 0.108 * T_g^{T\&C} + 1.593$$

$$RH^{corrected} = RH^{T\&C} - 0.315 * T_g^{T\&C} - 4.633$$

The slopes coefficients were found to be significant ($p < 0.01$) for both T_a and RH and the RMSE calculated for both variables were 0.5 °C and 8 pt%.

7.2.9. Representativity of the branch diameter variation measurements

The branch diameter variations of the 36 trees of the Trees and Climate study were measured with microdendrometers mounted on one branch of each tree. The equipped branches were chosen to have diameters higher than 2 cm and lower than 15 cm as the microdendrometers could not fit branches with diameters out of this range. Also, the studied branches were chosen to ensure a low standard deviation of the population of branch diameters. However, the representativity of these measurements has been questioned according to various results found in the literature as cited in section 2.1.2.6. Indeed, although some studies reported comparable diameter variations depending on the location of the measurements on a same tree, others could highlight differences between the branches of a same tree and even on a same trunk, between measurements carried out close to the collar and close to the first branches. Indeed, the sap fluxes are very likely to be driven by the photosynthetic activity of each branch and thus the total leaf area they bear as well as their respective solar exposure. The trunk of the tree should normally be representative of the behavior of the entire tree crown as it bears all the branches, thereby, the microdendrometer should be mounted on the trunks to avoid any error caused by the eventual variability that may exist between branches. In the T&C study, the trunks of the studied trees could not be equipped with the microdendrometers, first because they were too wide to fit in the selected microdendrometers and then because it was decided to mount all sensors up inside the tree crowns in order to avoid any damages.

Also, the axis diameter variation may be highly related to the water holding capacity of each axis which may depend on the proportion of the different tissues. This proportion may vary for different tree species and may also vary for axes of different age in a same tree. Thus, it appeared to be important to evaluate the influence of the location of the measurement on the axis diameter variations and more precisely to understand whether the axis diameter variations measured on one branch could be representative of the whole crown behavior especially during dry conditions.

Therefore, two trees studied in the T&C project were equipped with 4 microdendrometers each from March to November 2023 in order to compare the diameter variations of branches bearing leaves with contrasted solar exposure and also branches with different hierarchical insertion in the crown structure.

7.2.9.1. Materials and methods

Given that only two trees could be studied, it was decided to focus on two trees of the same species to have at least 2 replicates although the assessment of the species-specific variability would also be of high interest. Two *Cetlis australis* (celtis_2 and celtis_3) were selected on the basis of the following criteria:

- 4 years of branch diameter variation measurements with very few lacks of data were already collected from 2019 to 2022 as both trees were located on the Flandre site;
- their DBH measured at the beginning of the T&C project (May 2019) were very close (78 cm for celtis_2 and 80 cm for celtis_3);
- preliminary analyses of the T&C data set reported contrasted branch diameter variation responses during summer 2020 with an important branch shrinkage for celtis_2 compared to an almost uninterrupted branch growth for celtis_3 although the Ψ_{soil} measured in the tree pits of both trees were close ;
- both trees were located quite close on the FLANDRE site on a central alignment of trees and had similar solar exposure.

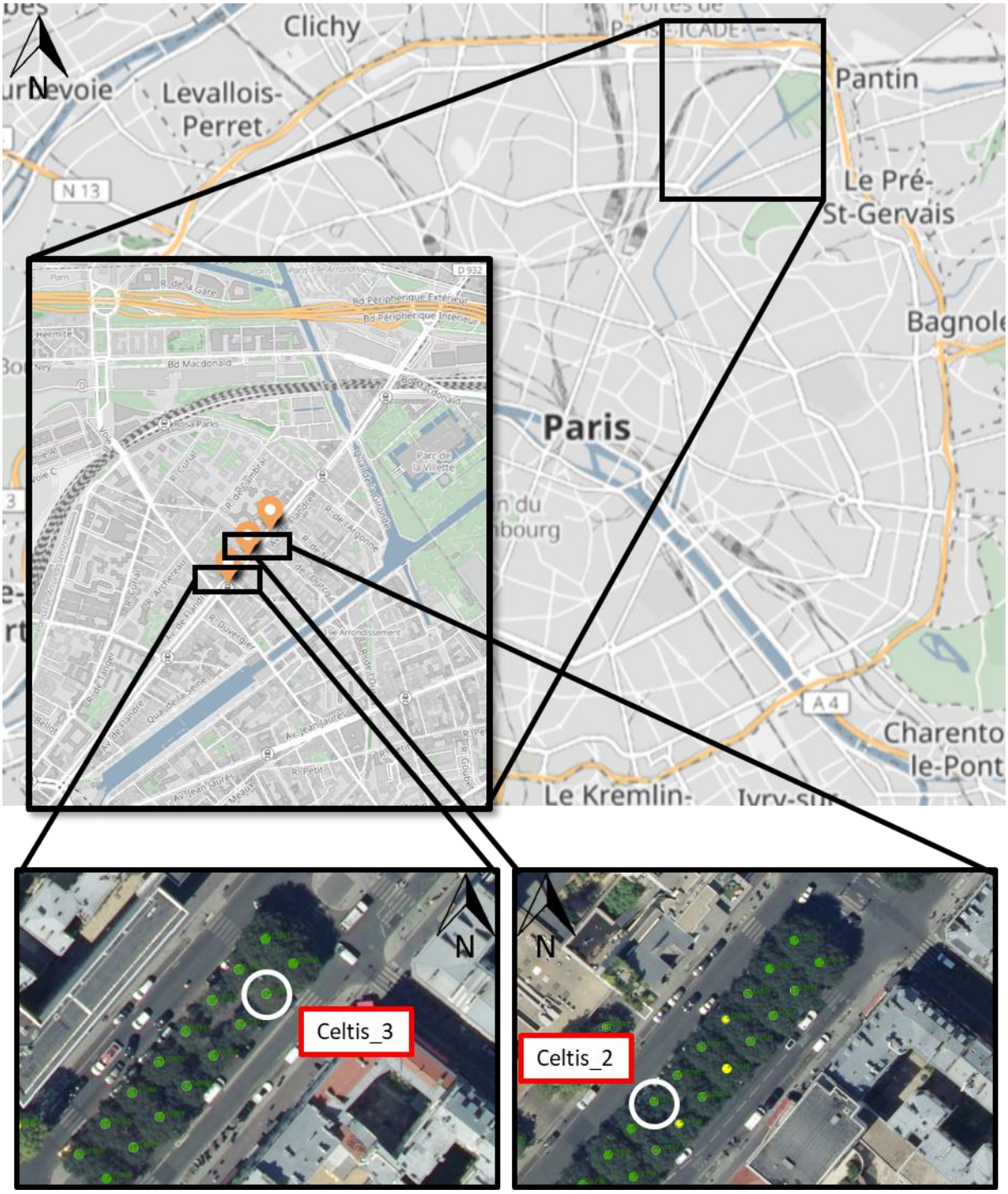

Figure 115: Location of the FLANDRE site in Paris and of the two studied *Celtis australis* in the FLANDRE site (OpenStreetMap and airborne photograph).

Table 28 also gathers some information regarding the two studied trees.

Table 28: Characteristics of the two studied trees.

	Celtis_2	Celtis_3
ID	211789	211915
Address	131 avenue de Flandre	102 avenue de Flandre
DBH measured in May 2019 (cm)	78	80

For each tree, four branches were selected for the experiment on the basis of their solar exposure and diameters. First, two branches with a low axis order (2 or 3) bearing leaves contrastingly exposed to the sun were selected. Then, one branch with a higher axis order was selected on both previously selected branches. For each tree, the branch which was previously equipped with a microdendrometer in the T&C study was one of the four branches studied in the previous experiment. Table 29 gathers some information about the 8 studied branches. The initial circumference of each branch was measured with a tape measure at the exact location of the microdendrometer just before installing it.

Table 29: Characteristics of the studied branches. *: branches equipped with microdendrometers from 2019 to 2022 during the T&C study.

Tree	Branch ID	Axis order[3]	Solar exposure	Initial circumference (cm)
celtis_2	celtis2_shade_2*	2	shaded	26.5
	celtis2_shade_3	3	shaded	13.8
	cletis2_sun_4	4	sunny	13.5
	celtis2_sun_3	3	sunny	23.4
celtis_3	celtis3_sun_3*	3	sunny	21.5
	celtis3_sun_4	4	sunny	16
	celtis3_shade_4	4	shaded	18.5
	celtis3_shade_3	3	shaded	20.5

Branches with contrasted diameters may grow at different rates. Thus, the comparison of the diameter increments between different branches and different trees is not trivial. Also, the diameter may not be the best estimate of the axis growth as it only considers one radius while it is the entire circumference of the axis which is growing. To deal with this issue, the diameter increment was transformed to the axis section area increment and standardized for each branch on the basis of its initial section (Figure 116). The sections of the studied branches

[3] axis order: hierarchical position of the considered axis in the tree architecture. The axis order of the trunk is 1, the axis order of all the branches born by the trunk is 2, the axis order of all the branches born by the axis of order 2 is 3, etc.

were very contrasted but the variability of branch sections is much higher for celtis_2 than for celtis_3. Also, axes of the same order may have very contrasted sections. Considering celtis_2 for instance, the section of celtis_2_sun_3 (43.6 cm^2) is three times higher than the one of celtis_2_shade_3 (15.1 cm^2) although both branches are from the same axis order.

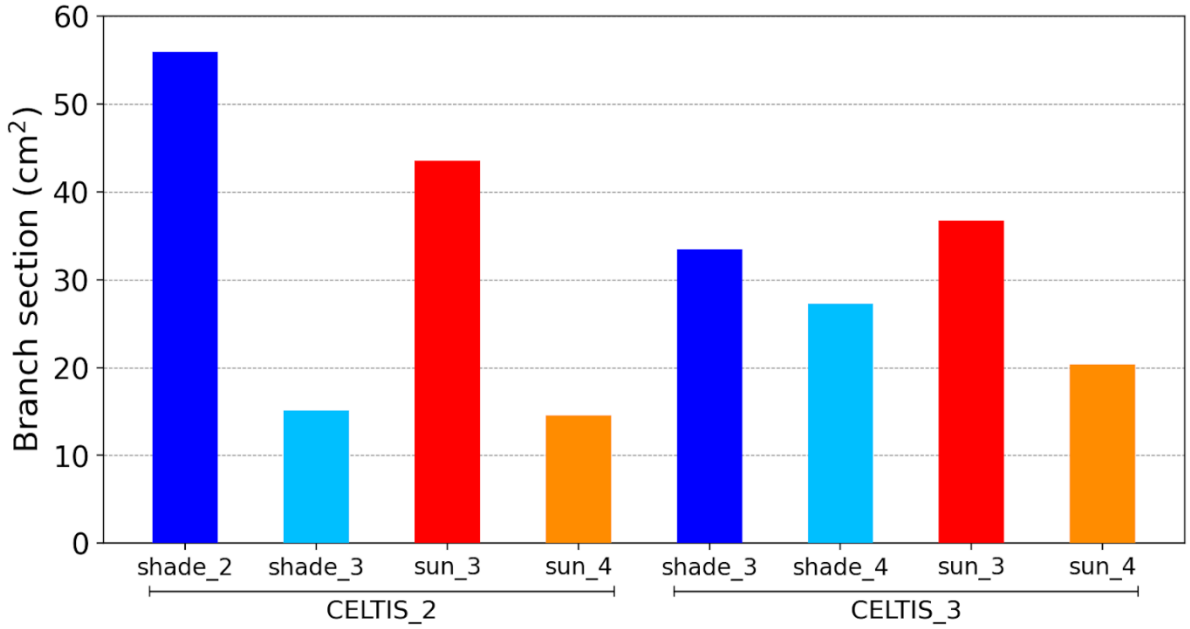

Figure 116: Area of the branch section of each branch at the location of the microdendrometer measured on March 30th, 2023.

The studied branches were then compared on the basis of their total growth and of the dynamic of their growth. To do so, the signal of branch section variation was divided into five daily indicators introduced previously in section 3.2.2.2 of chapter 3. Then, the influence of the initial diameter and axis order of the studied branches on their growth dynamics was assessed by comparing the maximum value of their Maximum Daily Shrinkage (MDS, expressed as a percentage of the maximum branch section recorded) and the number of days with a null Daily Growth (DG) both computed during the entire monitoring period.

7.2.9.2. Results

The section area variations of all the studied branches during the whole studied period are presented in Figure 117. It should be noted however that the signal recorded for the axis celtis3_shade_3 was noisy and could not be used for the analyses.

7.2.9.2.1. Total growth

The studied branches showed very contrasted total growths. First, the branches of celtis_2 grew more (minimal total growth reported was 0.35 % for this tree) than the branches of celtis_3 (maximal total growth reported was 0.29 % for this tree) but the variability of total growth between the different branches was higher for celtis_2 than for celtis_3. For celtis_2, the two branches with the highest solar exposure grew almost twice more than the two other branches characterized by a lower solar exposure. For celtis_3, the only one shaded branch with exploitable signal had a slightly lower total growth compared with that of the sunny branches but, the difference between sunny and shaded branches was much lower than that observed for celtis_2 (Figure 117).

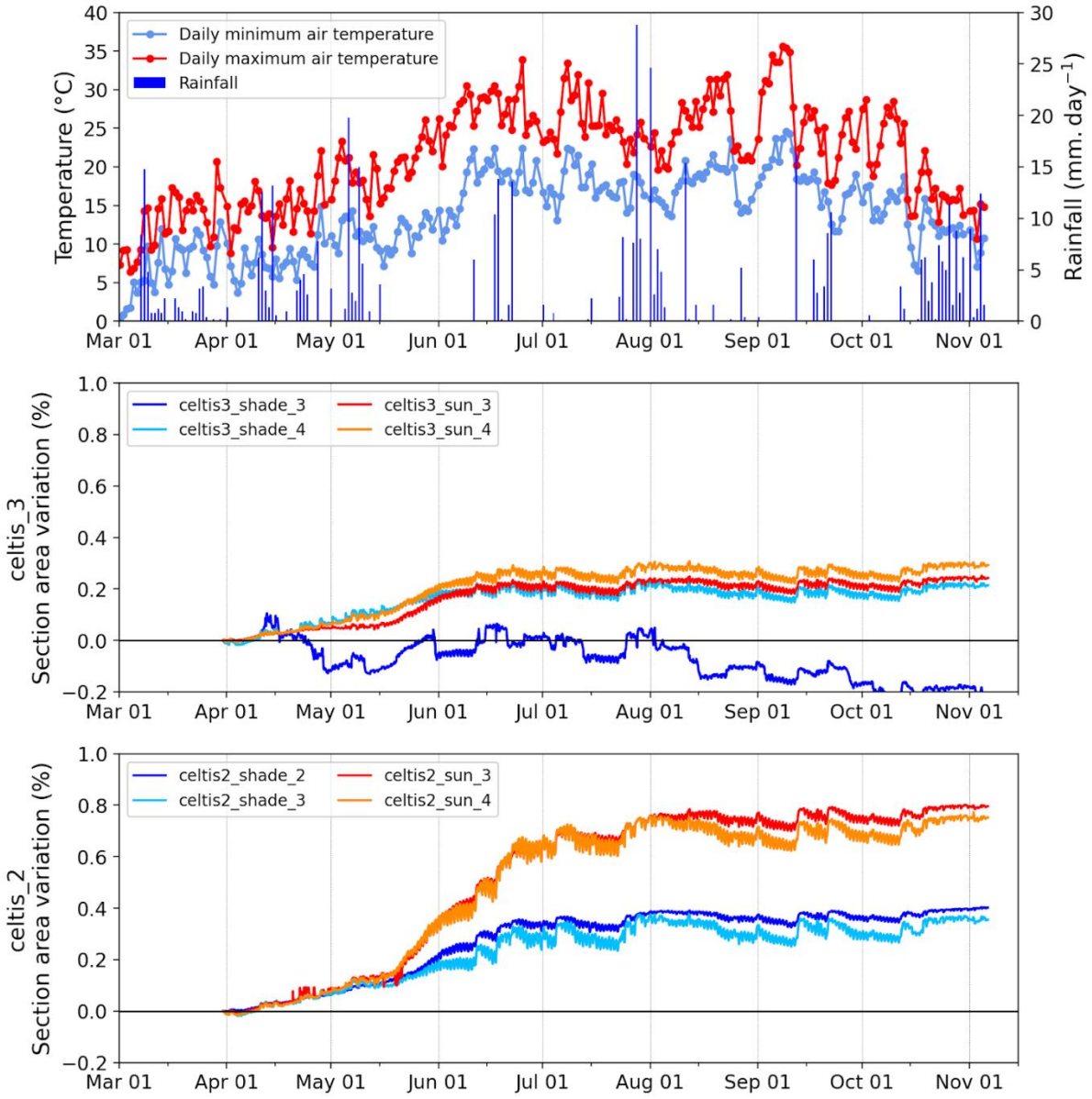

Figure 117: Evolution of the daily rainfall and minimum and maximum air temperature measured in Paris and of the branch section area variation for the 8 studied branches starting from March 30th, 2023.

When comparing the total growth measured and the different sizes and axis order, no general trend can be highlighted (Figure 118). There is no evidence that the branches with higher initial section could grow more than the thinner ones. Indeed, the branches of celtis_3 experienced very close total growth in spite of their contrasted initial section (ranging from 20 cm^2 to 37 cm^2). For this tree, the axis order also did not appear to influence the total growth. For celtis_2, there was also no relation between the branch initial section and its total growth as two pairs of branches with close total growth could be identified and the two branches of each pair had very different initial branch section. The variability of total growth between the

branches of a same tree then appears to be comparable or even higher than the one observed between the two different trees.

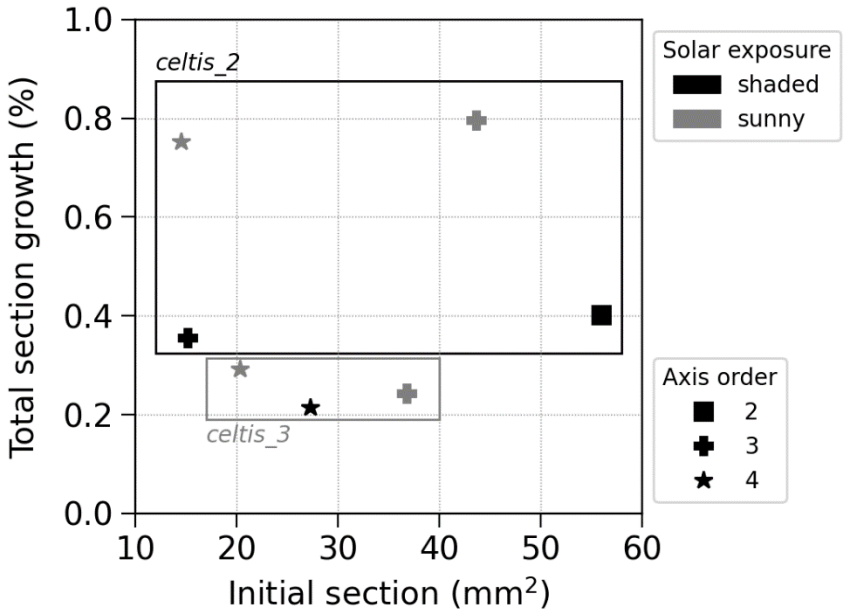

Figure 118: Scatter plot of the total growth of the branch section (expressed as a percentage of the initial branch section) against the initial branch section.

7.2.9.2.2. Dynamic of the growth

For each tree, the trend of the section area variations was the same for all the studied branches (Figure 117). More precisely, the different branches of a given tree appeared to experience branch shrinkage at the same time but with varying intensities. All branches reached their maximum shrinkage on September 10th, 2023 (except for celtis_3_sun_4 which reached it on September 11th, 2023). The thinner branches of celtis_2 experienced a greater shrinkage (in proportion of their initial section) and their growth was also stopped longer throughout the studied period compared to the thicker branches. A similar trend, although less visible, could be observed for celtis_3 considering the maximum branch shrinkage but not for the number of days without growth, maybe because the variability of the initial branch sections is lower for this tree.

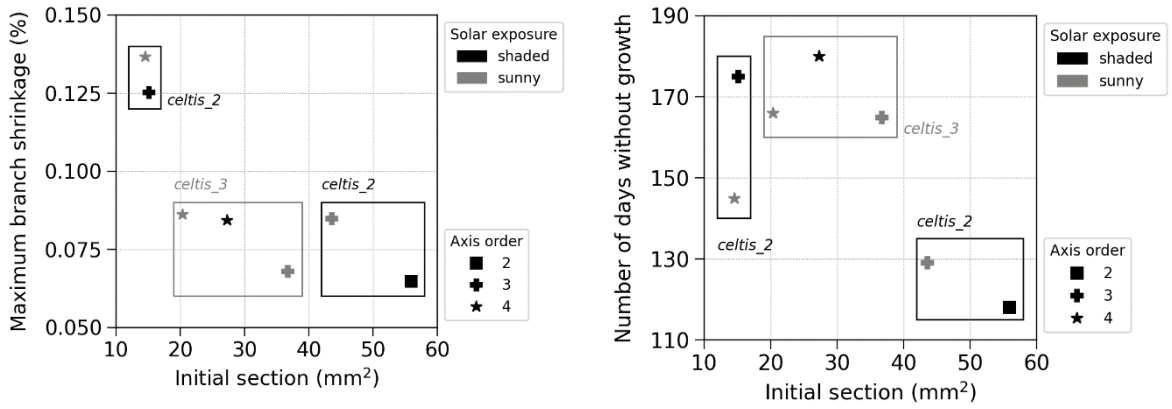

Figure 119: Scatter plot of (left) the maximum branch shrinkage (expressed as a percentage of the initial branch section) against the initial branch section and (right) the number of days without branch growth against the initial branch section.

7.2.9.3. Discussion and conclusion

Even though the evolution of the branch section of celtis_2 suggests that the branches having an important solar exposure grew more, this result was not confirmed with celtis_3. The signal of the branch celtis_3_shade_3 was of course not exploitable, but the other shaded branch only grew slightly lower than the two other ones. It is then not possible to draw a strong conclusion on the effect of solar exposure.

Although very similar trends of branch section area variation were reported for all the studied branches, a noticeable variability appeared when comparing the maximum value of their MDS as well as the number of days without growth that they experience. Although a slight influence of the initial branch section seems to exist, the present study shows that the variability among the branches of a single tree is likely to be comparable to the one existing between two different trees. The branch section variations measured in the frame of the T&C study must therefore be compared with precaution.

7.3. Summary of the publications and communications

The work described in the present manuscript was shared with the scientific community and society through the following publications and presentations.

7.3.1. Publications in peer-reviewed journals

One research article was submitted to a peer-reviewed journal on November 26th, 2023 and accepted for publication on June 4th, 2024:

Thierry, J., Herpin, S., Levi, R., Canonne, D., Demotes-mainard, S., Cannavo, P., Lemesle, D., Brialix, L., Rodriguez, F., Bournet, P.E., 2024. Impact of a water restriction on the summer climatic benefits of trees inside an outdoor street canyon scale model. Building and Environment 111722. https://doi.org/10.1016/j.buildenv.2024.111722

7.3.1. Other publications

Thierry, J., Debord, G., Angeniol, C., Gantois, M., 2022. Etude Arbres et Climat : Focus sur neuf essences d'arbres d'alignement à Paris. Info-Etudes, Division Expertises Sol et Végétal de la Ville de Paris, 56, 6–17.

Thierry, J., Debord, G., Angeniol, C., Gantois, M., 2024 Etude Arbres et Climat : Bilan - bénéfices climatiques des arbres d'alignement pendant les canicules et sécheresses. Info-Etudes, Division Expertises Sol et Végétal de la Ville de Paris, 59.

7.3.2. Presentations in international conferences

Thierry, J., Herpin, S., Maturana, L., Demotes-Mainard, S., Rodriguez, F., Cannavo, P., Bournet, P.-E., 2022. Impact of a moderate water stress on the microclimatic services provided by street trees: an experimental study inside an outdoor canyon street scale model. Presented at the 35th annual congress of the International Association of Climatology, Toulouse, France.

Herpin, S., Mballo, S., **Thierry, J.**, Lemesle, D., Brialix, L., Rodriguez, F., Demotes-Mainard, S., Bournet, P.-E., 2022. Benefits of well-watered trees on street microclimate: what is the influence of meteorological conditions? Presented at the 35th annual congress of the International Association of Climatology.

Thierry, J., Herpin, S., Rodriguez, F., Renard, M., Gantois, M., Bournet, P.-E., 2022. Climatic benefits of street trees on the microclimate and thermal comfort: an in-situ experiment in Paris. Presented at the 31st International Horticultural Congress, Angers, France.

Thierry, J., Herpin, S., Rodriguez, F., Renard, M., Gantois, M., Bournet, P.-E., 2022. A research methodology to select tree species able to meet the challenge of climate change

adaptation in cities: case study on street tree monitoring in Paris [POSTER]. Presented at the 31st International Horticultural Congress, Angers, France. → **Award of the best poster presentation at II International Symposium on Greener Cities: Improving Ecosystem Services in a Climate-changing World (GreenCities2022)**

Thierry, J., Herpin, S., Rodriguez, F., Gantois, M., Bournet, P.-E., 2023. An in-situ experiment in Paris to monitor street trees physiological response and climatic benefits during heatwaves and drought spells. Presented at the 11th International Conference on Urban Climate, Sydney, Australia.

Canonne, D., Demotes-Mainard, S., Saudreau, M., **Thierry, J.**, Dubuc, B., Ledroit, L., Cesbron, D., Lebras, C., Brialix, L., Lemesle, D., Herpin, S., Bournet, P.E., 2023. Impacts of water restriction on the development of urban trees and their associated climate services. Presented at the 2nd World Forum on Urban Forests, 16 - 20 October 2023, Washington DC (USA).

7.3.3. Presentation in seminars and workshops

Thierry, J., Herpin, S., Maturana, L., Demotes-Mainard, S., Rodriguez, F., Cannavo, P., Bournet, P.-E., 2022. Impact d'un stress hydrique modéré sur les bénéfices climatiques d'arbres d'alignement dans une rue canyon à échelle réduite. Presented at the IRSTV, Réunion d'axe MUE du 17 mars 2022, Nantes, France.

Thierry, J., Gantois, M., 2022. Présentation et discussion sur les premiers résultats de l'étude Arbres et Climat. Presented at the Comité Scientifique étude « Arbres et Climat » 2022, Paris.

Thierry, J., Herpin, S., Rodriguez, F., Gantois, M., Bournet, P.-E., 2022. A study of the climatic benefits of street trees under warm and dry conditions based on both reduced scale and in situ monitoring approaches. Presented at the EGAAL Scientific Days 2022, Rennes, France.

Thierry, J., Herpin, S., Rodriguez, F., Renard, M., Gantois, M., Bournet, P.-E., 2022. Climatic benefits of street trees on the microclimate and thermal comfort: impact of heatwaves and droughts. Focus on an in-situ experiment in Paris. Presented at the IRSTV, Plénière annuelle du 1er décembre 2022, Nantes, France.

Thierry, J., Gantois, M., 2023. Présentation et discussion sur les résultats et analyses en cours de l'étude Arbres et Climat. Presented at the Comité Scientifique étude « Arbres et Climat » 2023, Paris.

Thierry, J., Herpin, S., Rodriguez, F., Gantois, M., Bournet, P.-E., 2023. A study of the climatic benefits of street trees under warm and dry conditions based on both reduced scale and in-situ monitoring approaches. Presented at the SFR QuaSaV PhD student's Day, Angers, France. → **Award of the best presentation and video teaser (2 prizes, 8 challengers)**

Thierry, J., Herpin, S., Rodriguez, F., Bournet, P.-E., 2023. Impact of a water restriction on the summer climatic benefits of trees inside an outdoor canyon street scale model. Presented at the Les rôles de l'évapotranspiration en milieu urbain, Paris, France.

Résumé en français

Introduction

Le changement climatique en cours, en plus d'entraîner une augmentation de la température d'air moyenne à la surface du globe (IPCC, 2023), est responsable d'une multiplication et d'une intensification des vagues de chaleur. En France, 9 vagues de chaleur ont par exemple été recensées entre 1947 et 1986 alors que l'on en compte 37 sur la période 1989-2022 (Météo-France, 2022a). Les citadins, dont le nombre ne cesse de croître à travers le monde (United Nations Department of Economic and Social Affairs, 2018), sont particulièrement exposés à ces vagues de chaleur car les villes sont caractérisées par un phénomène de surchauffe causé entre autres par le remplacement des surfaces naturelles par des surfaces revêtues par des matériaux à faible albédo et forte inertie favorisant le stockage de la chaleur, ainsi que par une faible infiltration de l'eau. Des températures plus élevées de plusieurs degrés par rapport aux campagnes environnantes ont ainsi été mesurées dans de nombreuses villes notamment la nuit lors de journées peu venteuses et au ciel dégagé : 7 °C à Rennes (Dubreuil et al., 2020), 10 °C à Paris (Cantat, 2004).

Les vagues de chaleur, additionnées à l'effet d'îlot de chaleur urbain exposent ainsi le corps humain à un stress thermique croissant qui n'est pas sans danger pour la santé en particulier car les surchauffes urbaines se manifestent notamment la nuit, empêchant ainsi les villes de se rafraîchir et les corps de se reposer. De nombreux travaux ont en effet mis en évidence la surmortalité causée par les épisodes de chaleur extrêmes (Basu and Samet, 2002; Brooke Anderson and Bell, 2011). Etant donnés les enjeux sanitaires en cause, les pouvoirs publics se sont rapidement emparés du sujet en équipant les villes de systèmes de mesures et en lançant des campagnes de surveillance des épisodes caniculaires et de sensibilisation du grand public aux risques liés à la chaleur ainsi que des stratégies visant à adapter le milieu urbain aux fortes chaleurs.

Différentes solutions passives existent pour limiter le surchauffe en ville, elles reposent par exemple sur le recours à des matériaux à fort albédo, à la mise en place de toiles d'ombrage, à l'arrosage de la chaussée ou encore à la végétalisation (Bowler et al, 2010; Jamei et al., 2016). La végétation présente de nombreux intérêts. Elle permet de limiter les surchauffes localement

en interceptant le rayonnement solaire via le phénomène d'ombrage et en réduisant la température de l'air via l'évaporation de l'eau issue de la transpiration des plantes. De plus, elle offre d'autres services écosystémiques particulièrement recherchés comme la séquestration de CO2, la préservation de la biodiversité ou encore la gestion des eaux pluviales via l'infiltration (AURAV, 2020). La végétation peut être intégrée en ville via la création de parcs, de façades et toitures végétalisées, de pelouses et strates basses ou encore via la plantation d'arbres d'alignement. Les arbres d'alignement semblent particulièrement intéressants car ils permettent de combiner l'effet rafraîchissant de leur transpiration avec un ombrage efficace au plus proche des citadins, ils font l'objet de la présente étude.

Toutefois, le changement climatique s'accompagne également d'une modification de la disponibilité de l'eau. Bien que l'évolution future de la répartition spatiale et temporelle des précipitations soit difficile à prédire (IPCC, 2023), l'augmentation des températures pourrait entraîner une augmentation du déficit de vapeur d'eau dans l'air augmentant ainsi l'évaporation de l'eau et favorisant l'assèchement des sols. D'autre part, les épisodes de sécheresse se multiplient ce qui entraîne notamment des restrictions d'usage de l'eau. En France, 30 % du territoire métropolitain a été placé en restriction d'usage de l'eau chaque année entre 2017 et 2020 (Météo-France, 2023). Or, les arbres ont besoin d'eau pour assurer leur fonctionnement et notamment leur activité photosynthétique. De plus, les arbres, en milieu urbain, sont plantés dans des fosses de plantation au volume limité et entourées de surfaces imperméabilisées ce qui limite l'infiltration des eaux de pluie dans le sol ainsi que l'étendue de la prospection racinaire. Dans ce contexte, il apparaît que la pérennité du patrimoine arboré urbain et des bénéfices climatiques qu'ils fournissent est en jeu. Il apparaît également pertinent d'évaluer la capacité des différentes espèces d'arbre à résister aux conditions chaudes et sèches en milieu urbain tout en conservant des bénéfices climatiques importants. Le présent projet s'intéresse donc à la question suivante :

Comment les arbres d'alignement peuvent-ils fournir des bénéfices climatiques importants dans un contexte de réduction des apports en eau tout en préservant leur développement ?

Les bénéfices climatiques fournis par les arbres sont soumis à différentes sources de variabilité, premièrement liées aux conditions climatiques différentes chaque jour qui conditionnent d'une part le stress thermique humain mais influencent également l'ombrage et la transpiration, les deux mécanismes impliqués dans les bénéfices. Ces deux mécanismes sont directement influencés par la morphologie des arbres (forme du houppier, densité foliaire, etc.) et par leur comportement physiologique qui inclut les mécanismes impliqués dans la croissance

des arbres comme la photosynthèse, la respiration et la transpiration. Finalement, la disponibilité de l'eau du sol, qui varie notamment avec les conditions climatiques, conditionne le fonctionnement physiologique des arbres et in fine leurs caractéristiques morphologiques. Plusieurs phénomènes se déroulant aux interfaces du continuum sol-arbre-atmosphère sont donc impliqués dans les bénéfices climatiques fournis par les arbres.

De nombreux travaux se sont déjà intéressés aux interactions entre les arbres et leur environnement (sol et atmosphère) dans différents milieux dont le milieu urbain. Diverses études ont ainsi déjà proposé des quantifications des bénéfices climatiques fournis par les arbres, cependant, la compréhension globale du fonctionnement des bénéfices n'est pas simple vu le grand nombre de variables impliquées, la forte hétérogénéité des configurations urbaines et la diversité des caractéristiques morphologiques et des réponses physiologiques des arbres. Seule une partie des variables d'intérêt est donc généralement étudiée et il n'a généralement pas été possible de distinguer les contributions respectives de la transpiration des arbres et de l'interception du rayonnement solaire par leurs feuilles. Les densités d'instrumentation généralement utilisées sont faibles, elles ne permettent pas toujours d'évaluer la dispersion spatiale des bénéfices. De plus, le suivi en continu des bénéfices n'est pas toujours possible sur de longues périodes, ce qui n'a pas permis d'étudier en profondeur leur variabilité temporelle. Certaines études ont essayé de relier les bénéfices climatiques à certaines variables morphologiques comme le Leaf Area Index (LAI), mais des analyses approfondies de l'influence des caractéristiques morphologiques sur un plus grand nombre de variables impliquées dans les bénéfices restent nécessaires. Enfin, bien que les effets des stress hydrique et thermique sur la physiologie des plantes aient déjà été largement abordés dans différents contextes, les conséquences physiologiques et morphologiques de ces stress abiotiques sur les bénéfices climatiques fournis par les arbres restent largement inexplorées. En effet, la plupart des travaux abordant les bénéfices climatiques fournis par les arbres n'ont jusqu'à maintenant par pris en compte la disponibilité de l'eau du sol car ils ne pouvaient ni la contrôler dans les expérimentations in-situ, ni la mesurer avec un suivi suffisant.

Ainsi, le présent travail cherche à augmenter l'état des connaissances à ce sujet en se concentrant sur les objectifs suivants :

- Evaluer les sources de variabilité des bénéfices climatiques fournis par les arbres d'alignement;
- Quantifier l'impact de vagues de chaleur et de sécheresses sur la physiologie et la morphologie des arbres d'alignement;

- Quantifier l'impact de vagues de chaleur et de sécheresses sur les bénéfices climatiques fournis par les arbres d'alignement.

Deux dispositifs expérimentaux complémentaires

Pour remplir ces objectifs, une démarche de recherche basée sur la mesure des interactions le long du continuum sol-arbre-atmosphère dans deux dispositifs expérimentaux complémentaires est proposée. Dans les deux cas, des mesures du microclimat ont été menées à bien pour évaluer le stress thermique humain à proximité d'arbres ainsi que dans des zones non arborées. L'indicateur UTCI (Universal Thermal Climate Index) a été calculé et la disponibilité de l'eau dans le sol ainsi que certaines variables morphologiques et physiologiques des arbres ont été évaluées afin d'étudier les facteurs qui influencent le stress thermique humain. Les caractéristiques propres à ces deux dispositifs sont présentées dans le Tableau 1.

D'un côté, une rue canyon à échelle 1/5ème (appelée par la suite RSCS) partiellement végétalisée avec des jeunes pommiers d'ornement (*Malus Coccinella*® 'Courtarou') en pots et irrigués, située à Angers (France), a été instrumentée pour quantifier les effets sur le microclimat d'arbres soumis à différentes disponibilités en eau (Fig. 1). Bien que ne s'intéressant qu'à une seule espèce d'arbre, ce dispositif a permis de contrôler et mesurer la teneur en eau dans le sol des pots, d'estimer la transpiration des arbres et de calculer la quantité de rayonnement intercepté par leurs houppiers. Une campagne de mesures de deux mois menée en juillet et août 2022 a permis de comparer les bénéfices climatiques fournis par des arbres confortablement irrigués (well-watered -WW- trees), la teneur en eau dans leurs pots étant maintenue à la capacité au champ, et des arbres en restriction hydrique (water-restricted -WR- trees), la teneur en eau dans leurs pots étant maintenue proche du point de flétrissement permanent, dans la réserve difficilement utilisable. Pendant ces deux mois, deux vagues de chaleur ont été identifiées, la première durant deux jours, marquée par une température d'air (Ta) dépassant 40 °C, et la seconde durant 4 jours, affichant des températures d'air comprises entre 35 et 40 °C.

De l'autre côté, une campagne de mesures in-situ (appelée par la suite T&C) du microclimat dans et autour de la couronne de 36 arbres d'alignement adultes de 9 essences différentes répartis sur 5 sites dans Paris (France) a été menée (Fig. 2). Ce dispositif a permis l'étude des bénéfices climatiques fournis par des arbres en conditions réelles tant pour l'environnement urbain dans lequel ils évoluent que pour la disponibilité de l'eau dans le sol

qui n'est pas contrôlée et est soumise aux aléas climatiques. Bien que ce dispositif soit caractérisé par une hétérogénéité des configurations étudiées et une faible densité d'instrumentation, il a permis l'acquisition de mesures pendant 4 années (2019 à 2022) constituant ainsi un important jeu de données sur les bénéfices climatiques fournis par les arbres en été. Pour évaluer l'effet des périodes sèches, les analyses se sont concentrées sur la comparaison des mois de juillet 2020 et 2021, marqués par des cumuls de précipitations très contrastés, ainsi que sur l'évolution des différentes variables étudiées au cours d'une période sèche de l'été 2020. L'effet des vagues de chaleur n'a pas pu être étudié car il n'a pas été possible de trouver une période chaude pour laquelle l'ensemble des arbres étudiés pouvaient être considérés comme étant dans des conditions de confort hydrique.

Tableau 1 : Caractéristiques des deux dispositifs expérimentaux utilisés. Ta : température de l'air, AH : humidité absolue de l'air, Tmrt : température moyenne radiante, UTCI : Univseral Thermal Climate Index, ↓SW et ↑SW : rayonnement courte longueur d'onde descendant et ascendant, ↓LW et ↑LW : rayonnement grande longueur d'onde descendant et ascendant, LAI : Leaf Area Index, Hot : hauteur totale du houppier, Vpoly : volume du houppier par la méthode des polygones, Vvox : volume du houppier par la méthode des voxels, Density : densité du houppier, Hbase : hauteur de la base du houppier, Hsurf_max : hauteur de l'étendue horizontale maximale du houppier.

Caractéristiques	**Rue canyon à échelle réduite (RSCS)**	**Etude Arbres et Climat (T&C)**
Echelle	1:5	Real scale
Typologies des sites	Rue canyon orientée nord-sud Rapport d'aspect = 1	5 sites Orientations variables Rapports d'aspect variables
Arbres étudiés	2 alignements de 5 arbres	36 arbres
Référence minérale	zone non végétalisée dans la rue canyon	1 candélabre par site
Référence non-urbaine	Mât nord en dehors de la rue canyon	Station Météo-France de Paris-Montsouris
Variables météorologiques	<u>Dans chaque alignement d'arbres + dans la zone non végétalisée :</u> T_a *(4 positions)* AH *(4 positions)* T_{mrt} *(2 positions)* UTCI *(2 positions)* ↓SW, ↑SW *(sous + au-dessus de la couonne)* ↓LW, ↑LW *(sous + au-dessus de la couonne)* Wall temperature *(1 position)*	<u>Dans le houppier de chaque arbre + sur chaque candélabre :</u> T_a AH T_{mrt} UTCI *(All at 1 position)*

Caractéristiques	Rue canyon à échelle réduite (RSCS)	Etude Arbres et Climat (T&C)
Morphological measurements	Surface foliaire totale Surface du houppier projetée au sol LAI	Htot Sproj (Surface du houppier projetée au sol) Vpoly Vvox Density Hbase Hsurf_max
Mesures physiologiques	Transpiration Conductance stomatique Croissance radiale du tronc Température de feuille	Croissance radiale de branche
Disponibilité de l'eau	Controlée (irrigation par goutteurs) Mesurée (teneur en eau volumique)	Non controlée (conditions naturelles) Partiellement mesurée (potentiel hydrique du sol)
Essences d'arbres étudiées	*Malus Coccinella*® 'Courtarou'	*Celtis australis* *Gleditsia triacanthos* *Platanus x hispanica* *Quercus cerris* *Quercus ilex* *Sophora japonica* *Tilia cordata* *Ulmus resista* *Zelkova serrata*
Pas de temps de mesure	10 minutes	1 heure
Durée de la campagne de mesure	2 mois	4 années

Fig. 1 : Photographies de la rue canyon à échelle 1/5ème. En haut à gauche : vue de dessus. En bas à gauche : vue depuis le sud. A droite : zone non végétalisée de la rue au premier plan vue depuis le sud.

Fig. 2 : Photographies du dispositif expérimental de l'étude Arbres et Climat. En haut à gauche : capteurs dans le houppier d'un arbre. A droite : capteurs montés sur un candélabre de référence. En bas à gauche : carte des sites instrumentés et localisation de la station Météo-France Paris-Montsouris.

Principaux résultats

Différentes sources de variabilité des bénéfices

Le dispositif RSCS, bien qu'étant à échelle réduite, a permis de mesurer des bénéfices climatiques comparables à ceux mesurés in-situ dans le dispositif T&C ainsi qu'à ceux rapportés dans la littérature. Des réductions de T_a allant de 0,5 à 3 °C et d'UTCI allant de 4 à 11 °C ont été mesurées dans les houppiers des arbres du dispositif T&C tandis que les arbres du dispositif RSCS ont induit une réduction de T_a de 1,8 °C à l'intérieur de leur houppier (à

1 m du sol) ainsi qu'une réduction de T_a de 3,3 °C et une réduction de l'UTCI de 7,4 °C sous leur houppier (à 0,4 m du sol soit l'équivalent hauteur d'homme à échelle 1/5ème) en moyenne de 11h à 13h UTC lors de la journée ensoleillée du 4 juillet 2022, lorsque les arbres étaient tous en confort hydrique.

Le dispositif RSCS, qui comporte une densité d'instrumentation supérieure, a permis de mettre en évidence une variabilité spatiale des bénéfices. D'une part, la grande étendue spatiale de l'ombrage a pu être observée au travers des réductions de température moyenne radiante (T_{mrt}) mesurées à 0,4 m du sol sous les houppiers et proche du mur est de la rue canyon ainsi qu'à travers la réduction de température de façade mesurée sur le mur est de la rue canyon à 1 m de hauteur. D'autre part, il est apparu que l'étendue spatiale de l'impact microclimatique de la transpiration semblait plutôt restreinte car l'effet de la transpiration a semblé essentiellement visible dans les houppiers des arbres (à 1 m et 1,5 m de hauteur).

Les deux dispositifs ont également mis en évidence la forte variabilité temporelle des bénéfices, tout d'abord au cours d'une journée. La nuit, T_a est identique dans/sous et en dehors des houppiers mais il est parfois observé une T_{mrt} et un UTCI légèrement supérieurs dans ou sous les houppiers des arbres induits par le faible facteur de vue du ciel sous les arbres comme déjà mis en évidence dans la littérature (Coutts et al., 2016). De jour, les réductions de T_a et d'UTCI varient fortement au cours de la journée en fonction de la position du soleil, de la position des mesures et de la position des arbres au sein des sites étudiés et ce, dans les deux dispositifs expérimentaux. Dans le dispositif RSCS, la réduction maximale d'UTCI à 0,4 m du sol est par exemple observée autour de 12h UTC sur l'axe central de la rue et autour de 14h UTC proche du mur est. Dans le dispositif T&C, il apparaît clairement que les différents arbres, notamment en fonction du site sur lequel ils se trouvent, ne fournissent pas le maximum de réduction de T_a et d'UTCI au même moment de la journée. De plus, le caractère très local des mesures les soumet également à la forte hétérogénéité du feuillage des houppiers. Un globe noir, bien qu'installé sous ou dans un houppier, peut par exemple être momentanément exposé directement au soleil en présence d'éventuels trous dans le houppier ce qui peut conduire à de fortes et soudaines variations de la T_{mrt} et de l'UTCI qui en dépendent. Aussi, une forte variabilité des bénéfices d'un jour à l'autre a pu être mise en évidence et l'influence de l'ensoleillement sur cette variabilité a été soulignée, la réduction d'UTCI maximale journalière étant fortement liée à rayonnement global incident journalier.

Les variabilités spatiale et temporelle citées ci-dessus illustrent bien la complexité de mesurer les bénéfices climatiques fournis par les arbres, la diversité des variables impliquées et des approches possibles. Toutefois, ces premières analyses conduisent également à supposer

que l'ombrage pourrait avoir un effet prépondérant sur les bénéfices par rapport à la transpiration. Cette hypothèse a pu être confortée par l'évaluation dans le dispositif RSCS des quantités d'énergie dissipées quotidiennement respectivement par l'évaporation de l'eau transpirée par les arbres et par l'interception du rayonnement par leur houppier. Il s'est avéré que d'un point de vue énergétique, l'ombrage était alors responsable d'environ 70 % de l'énergie dissipée quotidiennement par des arbres en confort hydrique, la transpiration étant responsable des 30 % restant, confirmant ainsi les résultats obtenus par Mballo et al. (2021).

Enfin, des différences notables de réduction de la T_a et de l'UTCI ont pu être rapportées parmi les arbres étudiés dans le dispositif T&C (Fig. 3). Des tendances par site ont semblé se dégager car les réductions les plus importantes ont toutes été observées à FLANDRE et TEMPLE quand des réductions bien plus faibles ont été observées à NOHAIN, ORDENER et VICTOR. En particulier, les *Platanus x hispanica*, présents dans trois sites, ont fourni des bénéfices plus faibles à VICTOR et qu'à FLANDRE et TEMPLE. Cet effet de site qui semble se dessiner pourrait expliquer en partie pourquoi les bénéfices mesurés pour chaque espèce ne sont pas forcément cohérents avec les bénéfices attendus selon la littérature. En effet, selon le guide des essences de la Ville de Paris (2023), les essences *Gleditsia triacanthos*, *Sophora japonica* et *Quercus ilex*, sont toutes trois caractérisées par une note faible concernant l'indicateur "Régulation du climat local" calculé sur la base de leurs caractéristiques morphologiques et transpirations théoriques. Bien que les *Gleditsia triacanthos* aient effectivement affiché de faibles bénéfices dans le dispositif T&C, cela n'a pas été le cas des *Sophora japonica* et *Quercus ilex* qui ont induit de fortes réductions de la T_a et de l'UTCI. Toutefois, les arbres du dispositif T&C présentent des morphologies bien différentes des caractéristiques morphologiques théoriques considérées dans le guide des essences. En effet, les arbres du dispositif T&C sont encore jeunes et n'ont pas forcément atteint leur développement maximal. De plus, ils sont soumis aux contraintes du milieu urbain, notamment aux opérations de taille, qui impliquent des développements morphologiques différents de ceux qui pourraient être attendus en milieu naturel. Finalement, il s'est avéré que les caractéristiques morphologiques propres à chaque individu ne permettaient pas d'expliquer les écarts de bénéfices mesurés entre les différents arbres alors que la densité du houppier était envisagée comme une variable explicative intéressante pour expliquer la réduction de T_{mrt}. La densité du houppier calculée dans le dispositif T&C n'était cependant pas comparable au LAI classiquement utilisé dans la littérature pour expliquer les différentes quantités de rayonnement intercepté par différents arbres. Aussi, il est possible que les arbres étudiés dans T&C aient présenté une gamme de densité de houppier trop restreinte pour induire des effets forts sur

l'interception du rayonnement. L'impact du LAI sur l'interception du rayonnement a toutefois pu être abordé à l'aide du dispositif RSCS dont la campagne de restriction hydrique a permis de comparer, en fin de campagne, des arbres d'une même espèce avec des LAI contrastés. Ces aspects sont abordés plus en détails dans les sections suivantes qui traitent de l'impact du manque d'eau sur la physiologie, la morphologie et les bénéfices climatiques fournis par les arbres d'alignement.

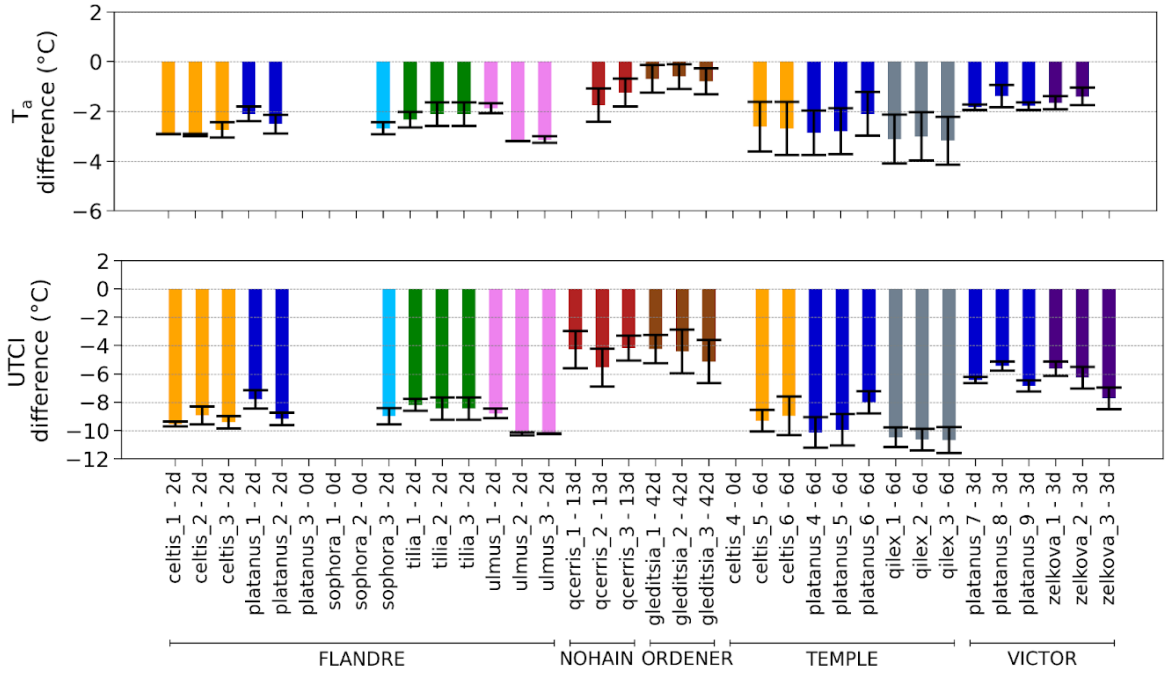

Fig. 3 : Moyennes des différences maximales journalières de température d'air (haut) et d'UTCI (bas) [arbre - candélabre] calculées pour chaque arbre du dispositif T&C par rapport à son candélabre de référence. Le nombre de jours de mesure considéré pour chaque arbre est indiqué au-dessus du nom de chaque arbre. Ce nombre est identique pour chaque arbre au sein d'un même site à l'exception des arbres qui ont été retirés de l'analyse par manque de données (0 jour considéré pour ces arbres).

Effet des vagues de chaleur et des sécheresses sur la physiologie et la morphologie des arbres

Dans le dispositif RSCS, la campagne de mesure comparant des arbres confortablement irrigués à des arbres en restriction hydrique a montré que la restriction hydrique induit une forte diminution de la résistance stomatique. En conséquence, la transpiration des arbres en restriction s'est très fortement et très rapidement réduite. Cette réduction s'est manifestée dès le deuxième jour de restriction et les arbres en restriction ont affiché une transpiration 81 % plus faible que celle des arbres en confort hydrique en moyenne sur toute la période de restriction. Ainsi, alors que la transpiration des arbres en confort hydrique évoluait en cohérence avec l'ET_{ref}, celle des arbres en restriction hydrique était totalement décorrélée de l'ET_{ref} et a

semblé limitée par la faible teneur en eau du sol. La décroissance de la transpiration s'est aussi accompagnée de l'apparition d'un écart de température de feuille entre les deux modalités végétalisées, les feuilles de la modalité en restriction devenant progressivement légèrement plus chaudes.

En parallèle, le dispositif RSCS a mis en évidence un fort effet de la restriction hydrique sur la croissance radiale des arbres étudiés. Alors que les arbres en confort hydrique n'ont cessé de croître tout au long de l'été 2022, la croissance radiale des arbres en restriction hydrique s'est interrompue dès le début de la restriction et ce jusqu'à la fin de la période de mesure. Un rétrécissement du diamètre des troncs a même pu être observé pour les arbres en restriction hydrique, ce qui pourrait indiquer la mobilisation d'eau contenue dans leurs tissus pour subvenir aux besoins transpiratoires des arbres. Cette éventuelle quantité d'eau mobilisée n'a toutefois pas pu être quantifiée. La restriction hydrique a ainsi entraîné un arrêt de la croissance foliaire pour les arbres en restriction. L'élongation des axes semble s'être arrêtée car la surface projetée au sol du houppier est restée constante contrairement à celle des arbres en confort. De plus, une réduction de la surface foliaire totale a été mise en évidence ce qui implique qu'une défoliation a eu lieu. Les dynamiques de cet arrêt de l'élongation, de la formation de nouvelles feuilles et de la défoliation n'ont toutefois pas pu être mises en évidence.

Dans le dispositif T&C, des croissances radiales de branche très contrastées ont pu être observées entre les différents arbres même au cours de l'été 2021 alors que le potentiel hydrique était assez élevé pour la majorité des arbres étudiés. La croissance des *Tilia cordata*, *Quercus cerris* et *Sophora japonica* a par exemple été fortement interrompue contrairement à celles des *Platanus x hispanica*, *Ulmus resista* et *Zelkova serrata*, ce qui pourrait suggérer des sensibilités différentes au manque d'eau. Ensuite, au cours de la période sèche de l'été 2020, bien que tous les arbres étudiés aient connu une interruption de leur croissance, des comportements assez contrastés ont été observés. La croissance des *Sophora japonica* et *Tilia cordata* était par exemple déjà interrompue au début de la période sèche étudiée, sans redémarrer tout au long de la période et même longtemps après ce qui suggère une forte sensibilité au manque d'eau pour ces espèces. Les *Gleditsia triacanthos*, *Platanus x hispanica* des sites TEMPLE et VICTOR, *Qercus ilex* et *Zelkova serrata* ont aussi semblé assez sensibles au manque d'eau car leur croissance a été rapidement interrompue et ce pour la majeure partie de la période d'étude, mais la croissance a repris rapidement grâce aux épisodes pluvieux qui ont suivi la période sèche étudiée. Ces espèces, également assez sensibles au manque d'eau, semblent donc avoir été plus résilientes. Enfin, les *Platanus x hispanica* de FLANDRE et les *Ulmus resista* ont continué à croître plus longtemps que les autres pendant la période sèche ce qui pourrait indiquer une

moindre sensibilité au manque d'eau. Toutefois, les différences observées pour les *Platanus x hispanica* entre les sites de FLANDRE, TEMPLE et VICTOR pourraient venir du fait que les individus de FLANDRE semblaient être exposés à un potentiel hydrique légèrement supérieur à ceux de TEMPLE et VICTOR au cours de la période étudiée.

Ces différents comportements se sont finalement avérés peu cohérents avec les informations initiales concernant les capacités de résistance à la sécheresse des différentes espèces étudiées issues de la littérature et capitalisées dans le guide des essences de la ville de Paris (2023). D'une part, le faible nombre d'individus, le manque de données ainsi que le non contrôle du potentiel hydrique dans le sol des fosses rendent compliquée la mise en évidence d'un effet "espèce" fort. D'autre part, les informations trouvées dans la littérature concernant la résistance des différentes espèces, notamment en milieu urbain, sont encore peu fournies et semblent donc devoir être confrontées à de plus amples campagnes de mesure.

Au regard des observations faites grâce au dispositif RSCS, il se pourrait également que l'arrêt de la croissance ou le rétrécissement du diamètre de branche observés chez les arbres du dispositif T&C indiquent une forte réduction de leur activité synthétique et donc de leur transpiration. Toutefois, les oscillations journalières des diamètres de tronc dans le dispositif RSCS n'ont pas semblé corrélées au flux de transpiration pour les arbres en restriction hydrique ce qui n'a pas permis d'utiliser cette variable comme un indicateur de la transpiration chez les arbres du dispositif T&C. Il est donc probable que l'élongation de leurs axes et la formation de nouvelles feuilles aient été ralenties mais aussi que des chutes de feuilles se soient produites pour les arbres du dispositif T&C mais ces hypothèses n'ont pas pu être vérifiées.

Les vagues de chaleur identifiées en juillet et août 2022 au niveau du dispositif RSCS ont été marquées par de fortes T_a, de fortes ET_{ref} et de forts ensoleillements et ont été associées à des transpirations journalières élevées pour les arbres en confort qui n'ont toutefois pas dépassé les transpirations journalières calculées pour d'autres journées moins chaudes et caractérisées par une ET_{ref} plus faible. Les journées chaudes semblent avoir induit des oscillations du diamètre de tronc plus importantes pour les arbres en confort hydrique ce qui pourrait indiquer une mobilisation de l'eau dans les tissus pour subvenir à la demande transpiratoire plus élevée au cours de ces journées. La transpiration réelle des arbres en confort pourrait donc être supérieure à celle calculée par le bilan hydrique centré sur le compartiment sol. Cette hypothèse n'a toutefois pas pu être vérifiée avec le dispositif RSCS.

Effet des vagues de chaleur et des sécheresses sur les bénéfices climatiques fournis par les arbres

Dans le dispositif RSCS, la forte réduction de transpiration pour les arbres en restriction s'est accompagnée d'une réduction de l'humidité absolue au sein des houppiers, mettant en évidence la réduction de la dispersion de vapeur d'eau au niveau des feuilles. Aussi, la réduction de la surface foliaire a induit une diminution de l'interception du ↓SW. Toutefois, les arbres en restriction continuaient de projeter une ombre efficace en interceptant 91 % du ↓SW lors d'une journée ensoleillée en fin de restriction hydrique contre 95 % pour les arbres en confort. Ainsi, la restriction n'a pas eu d'effet notable sur les composantes du bilan radiatif autres que le ↓SW mesuré sous les houppiers malgré la forte réduction de la surface foliaire, ainsi que la légère augmentation de la température de leurs feuilles illustrée plus haut. La forte relation entre la réduction maximale d'UTCI et l'ensoleillement journalier semble avoir été conservée pour les arbres en restriction hydrique ce qui confirme une fois encore leur capacité à intercepter efficacement le rayonnement ↓SW. Finalement, aucun impact notable de la restriction hydrique sur la T_a mesurée sous les houppiers (0,4 m de hauteur) n'a été rapporté dans le dispositif RSCS alors que la T_{mrt} et l'UTCI ont légèrement augmenté sous les arbres en restriction hydrique par rapport aux arbres en confort, certainement à cause de la légère diminution de l'interception du rayonnement solaire mise en évidence ci-dessus (Fig. 4).

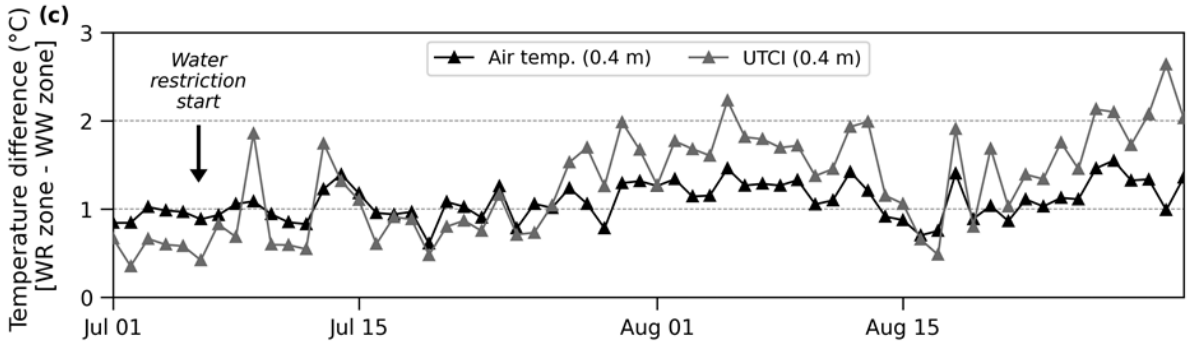

Fig. 4 : Evolution des différences de température d'air et d'UTCI entre la modalité en restriction hydrique (WR zone) et la modalité en confort hydrique (WW zone) moyennée quotidiennement de 10h à 14h UTC à 0,4 m du sol au cours de l'été 2022 dans le dispositif RSCS.

Dans le dispositif T&C, le calcul de la réduction de T_a et d'UTCI au cours de journées ensoleillées aux conditions climatiques proches, au début, pendant et à la fin de la période sèche étudiée, a également montré que les bénéfices ne semblaient pas être impactés (Fig. 5). La variabilité des bénéfices liée aux conditions climatiques changeantes d'un jour à l'autre a donc semblé être plus importante que l'éventuelle dégradation des bénéfices qui aurait pu être causée par le manque d'eau. Ainsi, bien que les arbres du dispositif T&C qui ont subi un arrêt de

croissance aient pu probablement voir leur transpiration s'arrêter ou bien fortement diminuer, ils semblent avoir conservé une capacité importante à intercepter le rayonnement solaire ce qui a permis le maintien des bénéfices importants.

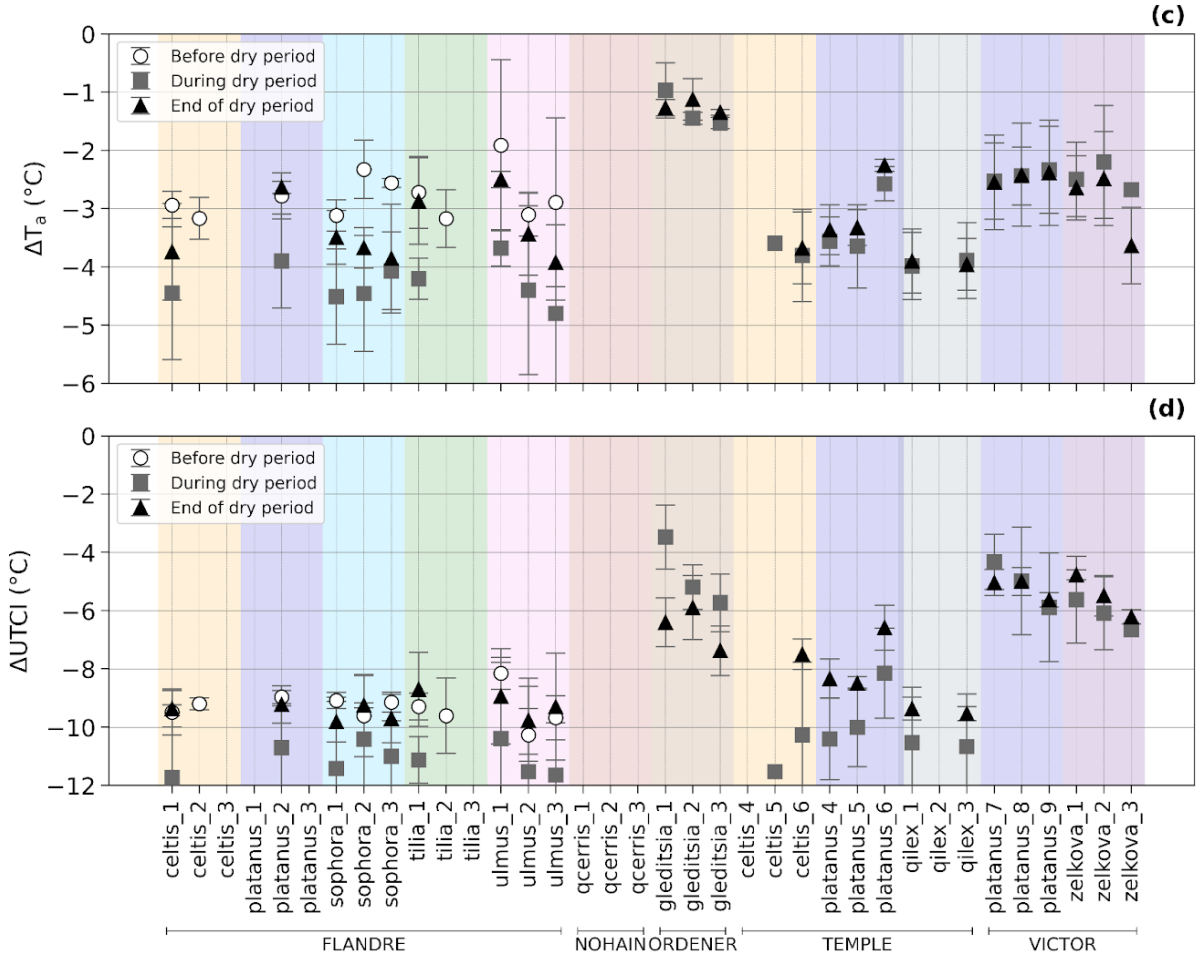

Fig. 5 : Pour chaque arbre étudié dans le dispositif T&C : (c) différence de température d'air et (d) différence d'UTCI maximales journalières calculées entre le houppier et le candélabre moyennées avant (before = 24 et 25 juin 2020), pendant (during = 30 juillet et 1er août 2020) et à la fin (end = 5 et 6 août 2020) de la période sèche étudiée.

Limites des deux dispositifs

Les deux dispositifs expérimentaux sur lesquels repose ce projet comportent quelques limites qu'il convient de garder en mémoire pour garantir une analyse éclairée des résultats présentés.

Tout d'abord, le dispositif RSCS est une maquette à échelle réduite qui permet de reproduire correctement une partie des transferts thermiques à l'œuvre mais qui de par son facteur de réduction ne permet pas de reproduire parfaitement le régime de convection naturelle

sur le champ vertical de température quand la vitesse d'écoulement de l'air est faible. Aussi, la rue canyon étudiée, bien que permettant de reproduire le phénomène de surchauffe à l'échelle d'une rue, se trouve dans un environnement ouvert non urbanisé et n'est donc pas soumise au phénomène global d'ilot de chaleur urbain caractéristique d'un centre-ville. Concernant le dispositif T&C, la localisation des arbres et candélabres de références est très hétérogène d'un site à l'autre mais aussi au sein d'un même site. Les arbres étudiés sont plus ou moins éloignés des arbres voisins, des bâtiments environnants mais aussi des candélabres de référence.

Ensuite, les capteurs utilisés dans les deux dispositifs sont généralement très localisés et ils ne peuvent par exemple pas être totalement représentatifs des conditions climatiques de l'ensemble du houppier, ou de la zone sous ou à proximité du houppier. Ils sont ainsi soumis à l'hétérogénéité des houppiers qui induit une forte variabilité de leur ensoleillement. Aussi les mesures de teneur en eau du sol réalisées dans le dispositif RSCS et en particulier les mesures de potentiel hydrique du sol réalisées dans le dispositif T&C ne sont pas forcément représentatives de l'ensemble du volume de sol prospecté par les racines des arbres.

Enfin, les thermo-hygromètres utilisés dans le dispositif T&C étaient montés dans des abris peu performants qui induisent de fortes surchauffes une fois placés en plein soleil. Une correction a donc été appliquée aux valeurs de température et humidité relative de l'air mais cette correction n'est pas parfaite et une incertitude résiduelle existe. Aussi, la mesure des variables météorologiques au sein des houppiers, qui avait pour but d'éviter la dégradation des capteurs installés en milieu ouvert sans surveillance pendant 4 années, n'est probablement pas totalement représentative des conditions réelles à hauteur d'homme. Il convient également de noter que la disponibilité partielle des données a parfois conduit à mener certaines analyses avec un faible nombre de journées et d'individus ce qui, additionné à la forte hétérogénéité des configurations, rend délicate la recherche d'un éventuel effet espèce concernant les comportements physiologiques comme les bénéfices climatiques.

Conclusion

De manière à étudier la capacité des arbres d'alignement à fournir des bénéfices climatiques importants pendant des périodes chaudes et sèches, le présent projet s'appuie sur deux dispositifs expérimentaux complémentaires : une rue canyon à échelle 1/5ème partiellement végétalisée avec des jeunes pommiers d'ornement (*Malus Coccinella*® 'Courtarou') irrigués et en pots (RSCS) et une campagne de mesures in-situ du microclimat dans et autour de la couronne de 36 arbres d'alignement adultes de 9 essences différentes répartis sur 5 sites dans Paris (T&C).

L'analyse croisée de ces deux dispositifs aux caractéristiques contrastées fournit une vue d'ensemble des sources de variabilité des bénéfices climatiques et propose d'illustrer les liens qui peuvent exister entre les réponses physiologiques et morphologiques des arbres d'alignement face aux épisodes chauds et secs ainsi que les bénéfices climatiques qu'ils fournissent.

En particulier, il est apparu que la contribution de l'interception du rayonnement solaire aux bénéfices climatiques fournis par les arbres était plus importante que celle de la transpiration. Aussi, les différentes espèces d'arbres étudiées via le dispositif T&C présentaient toutes des bénéfices climatiques notables mais les différences entre espèces ou au sein d'une même espèce n'ont pas pu être expliquées en l'état par les caractéristiques morphologiques propres aux espèces ou bien aux arbres eux-mêmes. Le dispositif RSCS a permis de montrer que la diminution de la disponibilité de l'eau dans le sol a induit une réaction physiologique forte et rapide via la réduction de la conductance stomatique, de la transpiration et l'arrêt de la croissance radiale. En parallèle, la surface foliaire des arbres en restriction a été nettement réduite mais ceux-ci ont continué à assurer une forte interception du rayonnement solaire ce qui a finalement conduit à un maintien de bénéfices climatiques importants, aucun impact n'ayant été rapporté sur la T_a et une légère augmentation de l'UTCI ayant été observée (UTCI supérieur de 1 °C sous les arbres en restriction par rapport aux arbres en confort). Le maintien des bénéfices pendant une longue période sèche a également été illustré in-situ grâce au dispositif T&C malgré la mise en évidence de réactions physiologiques contrastées entre les différents individus étudiés.

Finalement, et en perspective, la comparaison de différentes espèces d'arbres en conditions plus contrôlées comme celles offertes par le dispositif RSCS semble pertinente pour évaluer finement les effets du manque d'eau sur leur réponses physiologiques et morphologiques respectives ainsi que leur capacité à réduire le stress thermique. Aussi, bien

que des effets à court terme de la faible disponibilité de l'eau dans le sol sur la physiologie et la morphologie des arbres ont pu être mis en évidence, les effets à moyen et long terme n'ont pas pu être étudiés. Il semble toutefois capital d'évaluer la capacité des arbres d'alignement à se développer durablement en milieu urbain malgré les changements climatiques en cours pour assurer une continuité des services qu'ils fournissent dans le temps. En ce sens, la capitalisation d'informations sur le patrimoine arboré urbain (morphologie, état phytosanitaire, opérations de taille, etc.) telle que mise en place il y a quelques années par la Direction des Espaces Verts et de l'Environnement de la Ville de Paris semble être un outil puissant qui gagnerait à être enrichi et généralisé.